

Chapter 3-4. Mineralogy and geochemistry of the open-space secondary deposits from fractures and lithophysal cavities in the ESF

By S.Z. Smirnov and Y.V. Dublyansky

Table of contents

Chapter 3-4. Mineralogy and geochemistry of the open-space secondary deposits from fractures and lithophysal cavities in the ESF	180
3.4.1. Materials and Methods	182
3.4.2. Basics of the ontogenetic mineralogy	183
3.4.3 Major and accessory minerals	187
3.4.3.1. Major minerals	187
3.4.3.1.1. Calcite	187
3.4.3.1.2. Minerals of silica	196
3.4.3.2. Accessory minerals	200
3.4.3.2.1. Minerals of silica	201
3.4.3.2.2. Fluorite	201
3.4.3.2.3. Zeolites	206
3.4.3.2.4. Strontianite	207
3.4.3.2.5. Mn-oxides	208
3.4.3.2.6. Rare minerals and minerals of uncertain origin	208
3.4.4. Paragenetic assemblages: compositional, spatial, and temporal interrelationships	209
3.4.4.1. Relationships between assemblages	211
3.4.4.2. Repository block-scale and mineral crust-scale zonation of secondary mineralization	212

3.4.5. Mechanisms and history of secondary mineral deposition based on the textural evidence	213
3.4.5.1. Textures: key to deciphering the history of calcite deposition	213
3.4.5.2. Pinacoidal calcite	215
3.4.5.3. The relationships between platelet and blocky morphology	216
3.4.5.4. Sequence and mechanism of silica deposition	217
3.4.5.5. Colloids in the Yucca Mountain mineral forming system	218
3.4.5.5.1. Textures indicative of the colloidal mineralization	218
3.4.5.5.2. Evidence on the colloidal mineralization at Yucca Mountain	219
3.4.5.6. The history of accessory mineral deposition	221
3.4.5.7. Scepter morphology	222
3.4.5.7.1. Scepter calcite	222
3.4.5.7.2. Scepter quartz	224
3.4.5.8. Mineralogic and textural evidence: Summary	225
3.4.6. Discussion: Alternative models of mineral deposition	226
3.4.6.1. "Rainwater" concept	226
3.4.6.2. Hydrothermal upwelling concept	227
3.4.6.3. Major minerals and major-element geochemistry of mineral-forming fluids	228
3.4.6.4. Accessory minerals and minor-element geochemistry	229
3.4.6.4.1. Fluorite	229
3.4.6.4.2. Zeolites	230
3.4.6.4.3. Mn-minerals	231
3.4.6.4.4. Strontium	231
3.4.6.4.5. Magnesium	240
3.4.6.4.6. Rare Earth Element geochemistry of secondary minerals	242
3.4.6.4.7. Uranium in the silica minerals	259
3.4.6.5. Summary on mineralogy and geochemistry	264
3.4.6.6. Textures of secondary deposits	265
3.4.6.6.1. Geopetal appearance of the crusts	265
3.4.6.6.2. Euhedral crystals	268
3.4.6.7. Summary on the mineral textures	270
3.4.7. Summary	271

Chapter 3-4. Mineralogy and geochemistry of the open-space secondary deposits from fractures and lithophysal cavities in the ESF

By S.Z. Smirnov and Y.V. Dublyansky

Epigenetic mineralization at Yucca Mountain is not restricted to the bulk-rock alteration described in Chapter 3-1 of this book. It is also present as mineral crusts, lining walls of open fractures and lithophysal cavities. Deposits in fractures and lithophysal cavities consist of two distinct generations of minerals. The earliest generation comprises minerals deposited during the vapor-phase diagenetic alteration of tuffs. These minerals are mostly confined to lithophysal cavities and thin fissures in welded ash-flow tuffs but also appear in some wide-aperture fractures. Minerals of the second, epigenetic generation occur in lithophysal cavities and in fractures. The secondary minerals overgrew earlier vapor-phase alteration minerals, indicating that mineralized fluids with complex chemistry moved through what is now the vadose zone of Yucca Mountain after solidification and cooling of the tuffs.

The later generation of the open space-crystallized minerals is undoubtedly epigenetic. Nevertheless, the origin of these minerals is a subject of heated debate with two drastically different interpretations being championed by different research groups. One of these groups is comprised of the authors of this book and their associates; the other group is comprised of employees of the USGS, the DOE, and DOE contractors. The representatives of the federal government are grouped for purposes of discussion as the Yucca Mountain Project researchers. Collectively, their hypotheses have prevailed to date in providing a limited rationale for a favorable site suitability determination made by the Secretary of Energy in February 2002.

At early stages of the Yucca Mountain characterization studies, it was demonstrated that fracture- and open cavity-lining calcite from the unsaturated (vadose) zone is different in terms of its stable and radiogenic isotope compositions from calcite that occurs in the deeper phreatic (saturated) zone. At the same time, its isotopic properties were found to be similar to those of the micritic calcite veins and slope-parallel deposits developed at the surface of Yucca Mountain. Since the hydrothermal origin of the saturated-zone calcite was known with certainty (e.g., Bish and Aronson, 1993), and the "pedogenic" origin of the surface calcite-silica deposits was by that time vigorously publicized (e.g., Quade and Cerling, 1990; Stuckless et al. 1991; Whelan and Stuckless, 1992; Peterman et al., 1992), these isotopic observations were used to assign the vadose-zone calcite and silica phases a non-hydrothermal origin. It was hypothesized that these minerals crystallized from the meteoric (rain) water that percolated through

the interconnected fractures in the vadose zone and carried dissolved material from the overlying soil environment (e.g., Szabo and Kyser, 1990, Whelan and Stuckless, 1991; Peterman et al., 1992; Vaniman, 1993; Roedder et al., 1994; Whelan et al., 1994, and many others). This concept has won official endorsement of the U.S. DOE, and presently serves as one of the cornerstones of the Yucca Mountain safety case (U.S. DOE, 1998; 2001).

The official line of reasoning presented above, which has influenced other researchers in their acceptance of the non-hydrothermal origin of the vadose-zone calcite, contains an obvious logical flaw. The fact that the vadose-zone calcite is different from calcite produced in the course of the deep-seated magma chamber-based hydrothermal circulation means that the former calcite is, most probably, unrelated to this particular hydrothermal circulation. It does not necessarily mean, however, that the vadose-zone calcite is not hydrothermal. Hydrothermal circulations in nature are caused by a multitude of processes; therefore, some processes other than the residual heat of the cooling magma chamber could have been responsible for the hot water movement and the formation of the vadose-zone calcite.

On the other hand, the isotopic similarity between the vadose-zone calcite and the surface deposits cannot be viewed as a strong argument favoring the "rainwater" origin of the former. First, the pedogenic origin, assigned to the surface deposits is contentious and the assignment, in our opinion, is in error (see Chapter 3-3 for discussion). Second, later finer scale studies have demonstrated that the spectrum of isotopic properties of the vadose-zone calcite is much wider than that of the surface calcite, and in many instances isotopic values of the vadose-zone and the phreatic-zone calcite overlap (see, for example, Figure 3-4-30 in this chapter for Sr isotopes and Figures 3-5-8 and 3-5-9 in Chapter 3-5 for stable isotopes of C and O).

Among the arguments, used in support of the non-hydrothermal origin of calcite from the vadose zone were, for example, the following: "... (1) the lack of any visible fluid inclusions that often form in calcite at high temperatures; (2) the absence of minerals in the tuffaceous wall rocks that would indicate the fluids were hydrothermal; ..." (Szabo and Kyser, 1990, p. 1717). Ironically, both of these contentions were later proven to be wrong. For instance, secondary quartz, calcite and fluorite (all typical hydrothermal minerals) sampled in the ESF were found to contain two-phase fluid inclusions, indicating elevated temperatures of fluids that moved through the vadose zone in the past (up to 85°C; Dublyansky and Reutsky, 1995; Dublyansky et al., 1996, Dublyansky and Mazurova, 2000; Wilson et al., 2000; Whelan et al., 2000). The complex mineralogy, atypical of the low-temperature processes, elevated temperatures of crystallization, and complex chemistry of gases trapped in fluid inclusions has led a number of researchers to the conclusions that the minerals in question were formed from thermal fluids

that ascended into the vadose zone from great depth (Harmon, 1993; Dublyansky et al. 2001; Smirnov and Dublyansky, 2001).

In Chapter 3-4 we present the results of mineralogic and geochemical studies of secondary minerals from the underground ESF-ECRB complex. In our analysis of the publications dealing with the secondary minerals from the Yucca Mountain vadose zone, we have found, to our great surprise, that the extent of the mineralogical studies carried out over the last decade is appallingly meager. A thorough investigation of fracture zeolites and manganese oxides performed by Carlos with, co-authors (1993, 1995-a, 1995-b) is the only exception. Although much work was done on the trace-element geochemistry, radiogenic (Sr, U) and stable (C, O) isotopes and radiometric dating (U-Th and U-Pb) of secondary minerals, mineralogical information published between 1990 and 2001 is remarkably scarce. The results that will be reported below are intended to fill (at least partly) this gap and provide mineralogical context to the more-sophisticated studies, such as fluid inclusions and stable isotopes, discussed in subsequent chapters. We also report some data and interpretations of the geochemistry of secondary minerals.

The inventory of minerals, reported from the Yucca Mountain vadose zone compiled by Smirnov and Dublyansky (2001) is provided as Appendix 3.4.1 to this chapter.

3.4.1. Materials and Methods

This chapter is based mostly on the database and author's observations of secondary minerals in fracture and lithophysal cavity linings from the Exploratory Studies Facility (ESF) and the east-west cross-drift (ECRB), supplemented, where appropriate by the analysis of the data published in the literature. The work was commissioned by the State of Nevada (Smirnov and Dublyansky, 2001).

Observations were performed in hand specimens, thin and thick sections by means of optical microscopy, as well as on crystals and fragments of mineral aggregates by means of scanning electron microscopy (SEM) with energy-dispersive X-ray spectrometer (EDS). The chemistry of the minerals was studied by means of electron microprobe (EMP) with special focus on the compositional variations in different growth zones of calcite and fluorite. Trace- and rare-earth elements in a number of fluorite samples from several ESF locations were studied by instrumental neutron activation analysis (INAA).

The core method of this study was ontogenetic mineralogy. This branch of mineralogy addresses the origin of mineral individuals and aggregates. The aim of the ontogenetic studies was to reconstruct the complete history of the development of a mineral – starting from the act of nucleation to the latest stages of its existence (Grigoriev and Zhabin, 1975; Krasnova and Petrov, 1997). The method is widely used for the reconstruction of the history of mineral deposition on the basis of principles of crystal growth (Kirkpatric, 1975; Sunagawa, 1982; and others).

3.4.2. Basics of the ontogenetic mineralogy

Experimental and theoretical investigations have established that the morphology of minerals and their textural relationships in aggregates reflect the conditions and mechanisms of the mineral forming process. The morphology of crystals is controlled by the growth mechanism and depends on a number of parameters, the major one being the supersaturation of the mineral-forming fluid (Sunagawa, 1982). Supersaturation reflects the "distance" from equilibrium or how much the actual concentration of the dissolved matter is greater than the equilibrium concentration. Supersaturation is proportional to the difference of chemical potentials between the dissolved and the crystalline states:

$$\sigma = \frac{\Delta\mu}{kT}, \quad (3-4-1)$$

where: σ - is the supersaturation, $\Delta\mu$ - is the difference of potentials, k - is the Boltzman constant, and T is the temperature (K). The equation above implies that supersaturation is controlled by two major factors: the temperature T and the chemistry of the fluid $\Delta\mu$.

At supersaturation values close to zero, the probability of the formation of a nucleus or the probability of the attachment of a particle to the growing crystal is so small, that crystal growth ceases. The system crystal-fluid is then said to be in the metastable state. This phenomenon, best studied for the case of the crystallization from melts is termed "nucleation delay" (Donaldson, 1985). Nuclei begin to form and crystals start growing only when supersaturation reaches some minimum threshold value (Chernov et al., 1980).

The interdependence of crystal morphology and supersaturation was addressed in detail in publications by Sunagawa (1982). Figure 3-4-1 shows that polyhedral (euhedral) crystals require relatively low saturations ($< \sigma'$) to form. The growth rate is controlled by the rates of surface

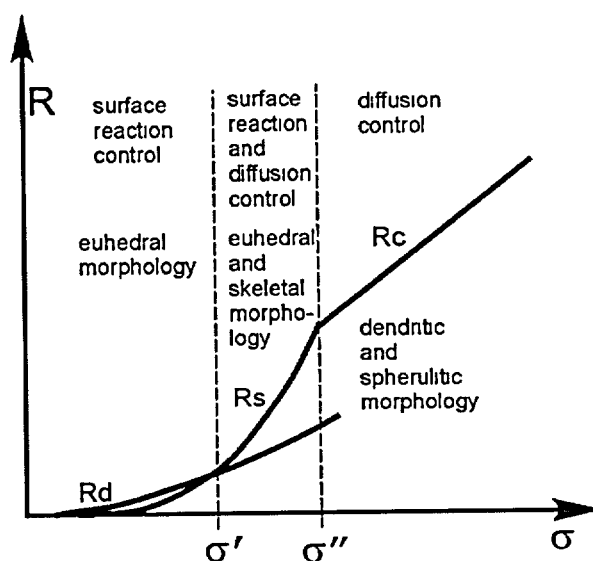


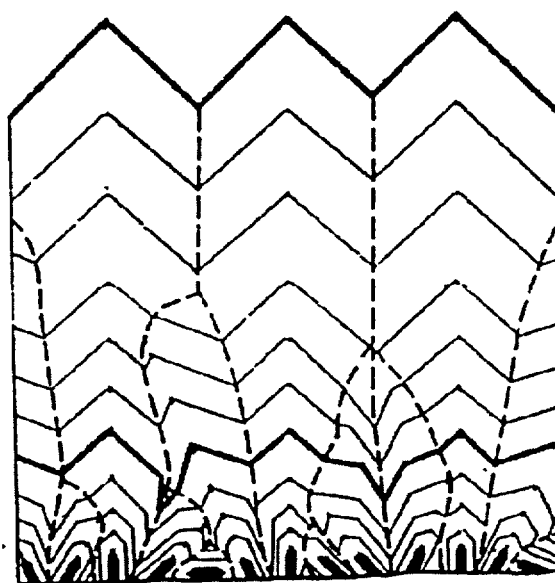
Figure 3-4-1. Interdependence between crystal morphology, growth controlling factors and supersaturation expressed through the interdependence of growth rate R and supersaturation σ . Curves R_d , R_s and R_c represent the $R(\sigma)$ functional dependences for the dislocation-controlled, the surface nucleation-controlled and the continuous growth mechanisms. Critical supersaturation values σ' and σ'' mark transitions from one growth mechanism to another. Based on Sunagawa (1984).

reactions, but variations of the conditions in this low-supersaturation region do not generally affect the perfect crystallographic shape of growing crystals. As the supersaturation approaches σ' , the crystal growth begins to outpace the diffusion supply of material to the growing crystal. This leads to the appearance of crystals with skeletal morphology, in which the growth mostly occurs at the edges and tips of crystals. At supersaturations greater than σ' , growth is predominantly diffusion-controlled. As a result, growing crystals acquire dendritic and/or spherulitic morphologies.

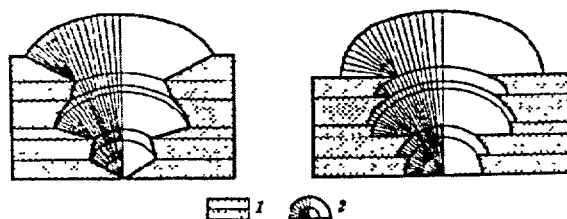
The numeric values of σ and σ' depend on the mineral and phase states of the mineral-forming medium (Sunagawa, 1982). Nevertheless, the very existence of transitions between polyhedral (euhedral), skeletal and dendrite morphologies in a studied aggregate allows for qualitative assessment of variations of the supersaturation in the mineral-forming fluid (and, therefore, of variations of the temperature and/or chemistry of the fluid, which are the major factors controlling supersaturation).

The interdependence of the crystal morphologies and the parameters of the mineral forming processes are commonly more complex than simple gradation from polyhedral, to skeleton and to dendrite morphologies delineated above. Calcite is one of the few minerals, for which this interdependence is fairly well documented (e.g., Kalb, 1929; Sunagawa, 1953; Aliev, 1966, Ikornikova, 1975, and many others).

In order to make meaningful physico-chemical reconstructions based on studies of mineral parageneses, one important prerequisite must be met: the studied minerals must be syngenetic (co-genetic). In order to establish that two studied minerals in a given sample are syngenetic, it is commonly



a



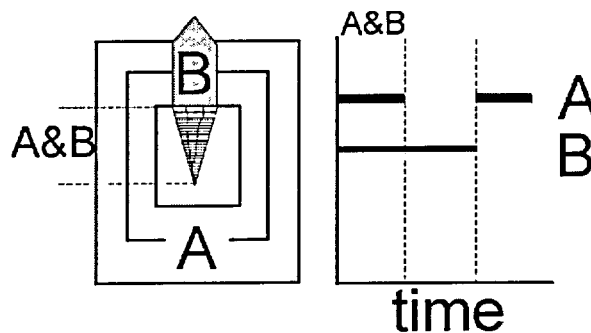
b

Figure 3-4-2. Compromise boundaries (surfaces of concurrent growth) between crystalline individuals in drusy aggregate (a, dashed lines) and between crystal and spherulite (b, 1-crystal, 2-spherulite). Based on Krasnova and Petrov, (1997).

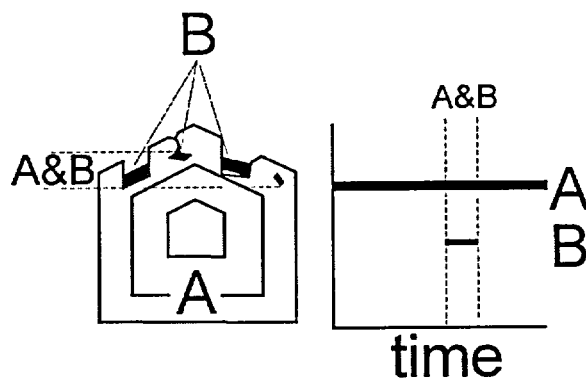
sufficient to demonstrate that they grew simultaneously. Simultaneous growth is normally established through the observations of the relationships between mineral individuals in aggregates. Chesnokov (1966) argued that the only reliable criterion for establishing simultaneous growth of the two mineral individuals is the presence of the compromise boundaries (also called boundaries of common growth) between them. Such boundaries develop between simultaneously growing crystals, as well as at the contact between the growing crystal and spherulitic aggregate (Figure 3-4-2).

In a section view of Figure 3-4-2, the compromise boundaries between crystalline individuals in drusy aggregate and between crystal and spherulite are shown to have an indented character and their orientation does not necessarily correspond to the crystallographic faces. One mineral may be included in another. The syngenetic character of the minerals may be established by finding surfaces of simultaneous growth (e.g., Figure 3-4-3-a). The absence of such surfaces indicates either a great difference in the growth rates of minerals (Figure 3-4-3-a), or spatially discontinuous (but simultaneous) growth (Figure 3-4-3-b). If it can be demonstrated that crystals of the mineral B are not detrital fragments and do not have the attachment sites on the crystal of mineral A, it may be concluded that crystals of mineral A were formed in fluid, which was not in contact with crystal B.

The absence of the common growth surfaces is readily explainable if the host mineral grows substantially faster than the included mineral. Mineral inclusions formed in such a way are interpreted as broadly synchronous with the mineral A, but non-synchronous with the specific growth zone in which they are trapped.



a.



b.

Figure 3-4-3. Evidence of the simultaneous growth of minerals. Episodes of common growth are denoted as A&B. A paragenetic schema, depicting temporal relationships between the two minerals, is given on the right of each drawing.

Note that there is a hiatus in growth of the mineral A on the drawing a (at the end of the A&B stage).

Table 3-4-1

Features of mineral assemblages originated from supergene and hypogene hydrothermal processes in the host rock represented by acidic volcanic rocks (based on Betekhtin, 1956 and Stankeev, 1986)

Feature	Supergene	Hypogene hydrothermal
Mechanism of formation	Interaction between host rocks and meteoric rain waters.	Crystallization from hydrothermal solution due to the decrease in temperature and reaction with the host rock
Specifics of the chemistry and mineral composition of the paragenetic assemblages	The features are controlled by the chemistry resulting from the water-rock interaction. The composition of secondary assemblages reflects chemistry of the host rock. Removal of components from the system, rather than input of components. Pronounced vertical zonation, reflecting increasing downward degree of interaction between water and rock (rock-to-water ratio)	The features are controlled by the initial chemistry of the fluid and the rate of its interaction with the host rock. The composition of the secondary assemblages does not correspond to the chemistry of the host rock. There might be both input and removal of components from the system. Complex vertical and lateral zonation.
Typomorphic minerals	Smectites, kaolinite, illites, oxides and hydroxides of Al, Fe, and Mn, silica (opal).	Quartz, chalcedony, opal, calcite, fluorite, zeolites, etc
Morphologic features of mineral individuals	Typically, small sizes and uniform morphology. Euhedral, anhedral and collomorph (oolites) morphology. Relatively large crystals may only form in local phreatic environment	Variety of sizes, large, well-shaped crystals are common. Variable morphology (euhedral, skeletal, and spherulitic).
Aggregates	Earthy masses, dense laminated flowstone-type deposits. Druzy aggregates only in local phreatic environment	Granular aggregates and druzes
Examples of natural assemblages	Weathering crusts upon silicate rocks of the bauxite and clayey types.	Low-temperature hydrothermal (epithermal) veins

The coeval character of minerals may be established by determining the common characteristic zonation in specific growth zones. Zonation may be expressed through the characteristic chemistry of the mineral in the growth zone, its color, the specific assemblage of inclusions, and a number of other features (Mineev and Rozenkova, 1962). This approach is particularly useful in analyzing the spatially separated occurrences of minerals.

The relationships between mineral individuals in aggregates reflect influences of gravity, fluid hydrodynamics, geometry of the growth space, interaction with neighboring individuals, etc., as well as the sequence of mineral crystallization (Table 3-4-1). For example, mechanisms of mineral depositions in the cases of the interaction of the descending meteoric and ascending hydrothermal waters with rhyolitic tuffs must be substantially different. This difference is expressed in the sets of typomorphic

(characteristic) minerals, composition and spatial distribution of mineral assemblages, morphology of mineral individuals and their relationships in aggregates. The differences are summarized in Table 3-4-1.

A brief description of the basics of the ontogenetic method presented above provides the justification for its selection as the methodology appropriate to this type of study. The ontogenetic method, supplemented by studies of the variations in chemical composition of secondary minerals, provides a basis for the reconstruction of the evolution of the mineral-forming system and the mechanisms of mineral deposition. The method, thus, provides a powerful tool for verification of the two competing hypotheses as to the origin of the secondary minerals at Yucca Mountain.

3.4.3 Major and accessory minerals

The mineral assemblages record and reflect the chemistry of the mineral forming solutions, which have circulated through the rocks. In this section we discuss the secondary mineral assemblages found in open cavities and fractures in the rhyolite tuffs in the vadose zone of Yucca Mountain. The term paragenesis has a number of definitions. In this text we define paragenetic assemblage as a set of minerals formed during the same period of time and reflecting the same mineral-forming process. This means that a paragenetic assemblage is composed of syngenetic minerals.

In this section we generalize the available data on the mineralogy of linings and fillings of the open cavities in the rhyolites of Yucca Mountain and describe the typomorphic minerals of the secondary assemblages. In order to delineate the overall evolutionary trends in the chemistry of the mineral forming fluids, we will distinguish major and accessory minerals. The term major minerals applies to minerals that absolutely dominate the paragenesis, while the term accessory minerals describes minerals present in subordinate amounts, on the basis of microscopic observations.

3.4.3.1. Major minerals

In the course of the previously described studies (e.g., Paces et al, 1996; Whelan et al, 1998; Smirnov and Dublyansky 2000; 2001; Wilson and Cline, 2001; see also summary in Fabryka-Martin et al., 2000) it was established that the major secondary minerals in the Yucca Mountain rhyolites are calcite and various varieties of silica.

3.4.3.1.1. Calcite

Calcite forms crusts, built up of 1 to 3 generations of mm- to cm-long crystals. Occurrences of calcite in most cases have a so-called geopetal appearance, which means that crystals and aggregates are confined to the floors of lithophysal cavities and footwalls of the low-angle fractures. The most striking feature of calcite in fractures at Yucca Mountain, by far, is that the secondary minerals are almost always

absent from the hanging walls. Very rarely, is calcite found lining both the walls of the near-vertical fractures. Occasionally it may be observed on the ceilings of lithophysal cavities. In the ESF, we have observed these unusual occurrences almost exclusively in the vicinity of the North Portal. In some instances calcite was found to fill small-aperture (less than $\cong 5$ mm) fractures in tuffs and fractured bases of lithophysal cavities. "Classic" veinlets, in which calcite completely fills the fractures, do exist (see, Figure 3-4-4-a), although they are not very common. Calcite commonly cements broken fragments of tuffs in large open, near-vertical, fractures at the bases of lithophysal cavities and in low-angle veinlets, forming peculiar breccias. Breccia shown in Figure 3-4-4b, for instance, has bedrock tuff fragments "floating" in the calcite matrix.

Secondary calcite shows a variety of morphologies, indicative of the varying conditions of crystal growth. In cementation and small fissure fillings calcite forms aggregates of anhedral (granular) crystals. Granular calcite was also found within crusts deposited in lithophysal cavities, as well as on the walls of the fractures. Grains in such

calcite do not have any specific orientation; boundaries between them represent the compromise boundaries of the concurrent growth. A relatively rare sub-variety of granular calcite is cellular calcite. Individual grains of such calcite have cavities inside and often contain all-gas inclusions. The sizes of these inclusions are commonly comparable to the sizes of the host grains, which indicate the primary origin of these inclusions (Roedder, 1984; Goldstein and Reynolds, 1994). At least in some cases, therefore, the cellular character of calcite crystals can be explained by the entrapment of large gas bubbles in the course of crystal growth from a heterogeneous (liquid + gas) fluid.

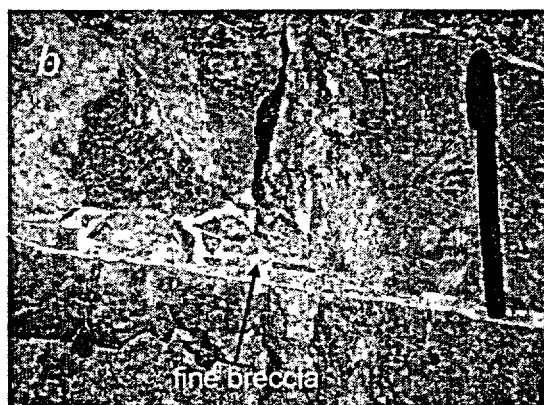
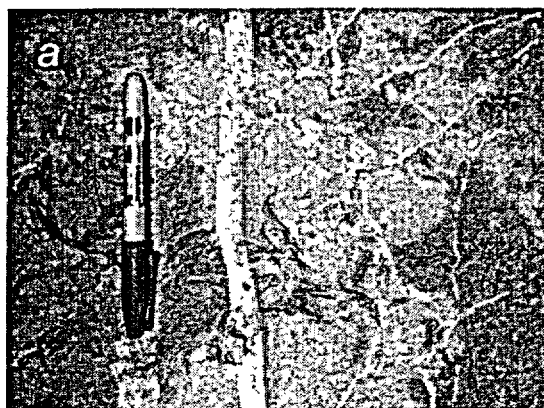


Figure 3-4-4. Uncommon occurrences of calcite in the ESF. *a* – "Classic" veinlet in the Topopah Spring welded tuff. Station ESF 67+81.0; Dune Wash fault zone. Sample 2210). *b* – Low-angle veinlet with breccia (ESF Station 37+37.0; Alcove #6 station 0+55.1. Northern Ghost Dance Fault zone. Sample 2222). Central segment of the veinlet shown in photograph *b* contains "micro-breccia" – numerous bedrock tuff fragments 0.5 to 5 mm in size embedded in authigenic calcite matrix. Note larger fragments of bedrock tuff "floating" in calcite.

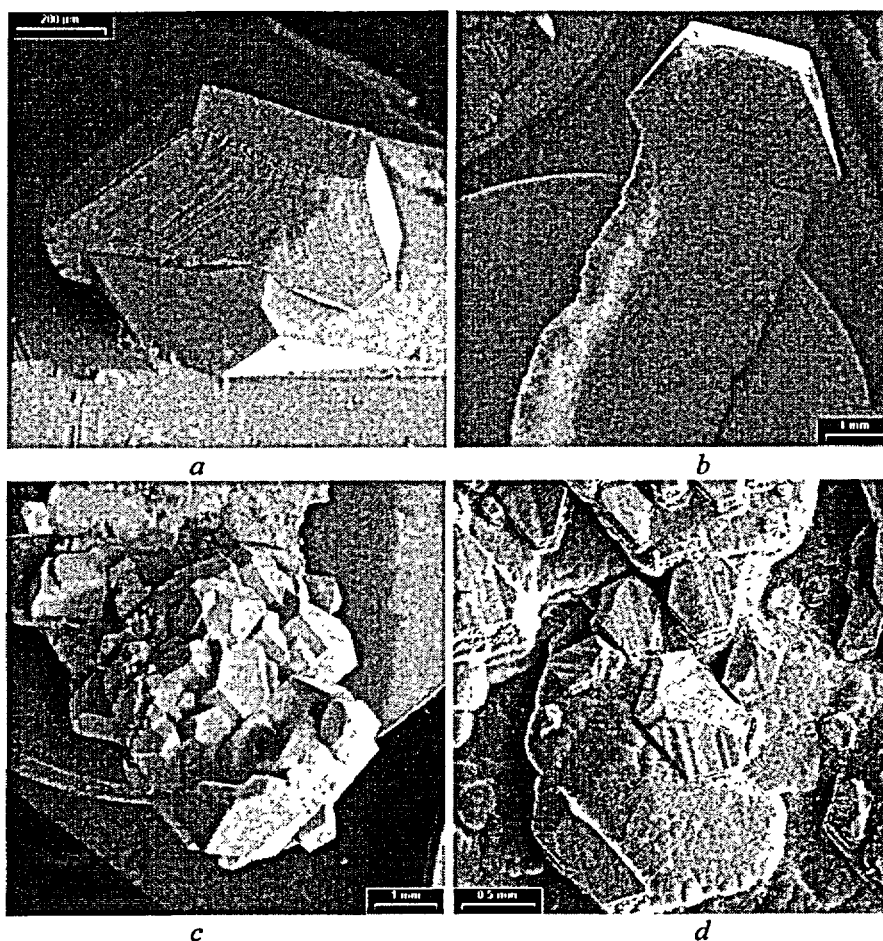


Figure 3-4-5. SEM micro-photographs showing crystal morphology of euohedral calcite from ESF: a - thin platelet (c+m) ESF station 14+75; b - bladed (c+m) ESF station 28+80; c - prismatic (m+ δ) ESF station 52+43; and d - rhombohedral (δ or δ +m) ESF station 38+80.

The outermost crystals of calcite crusts have euohedral morphologies, which means that their surface is constrained by various crystal faces. Euohedral crystals from the Yucca Mountain vadose zone may be subdivided into two broad morphologic types: platelet or bladed, and blocky.

A platelet or bladed morphology refers to crystals, two dimensions of which are greater than the third one. By contrast, blocky crystals have equant or sub-equant shapes. Some typical morphologies of calcite are shown in Figure 3-4-5; its morphologic varieties are described below.

Pinacoid $c\{0001\}$ is the habit face of thin-platelet calcite. The crystals are lens-shaped isometric (rounded or hexagonal in the plan view). Hexagonal crystals have faces of a prism $m\{10\bar{1}0\}$ (Figure 3-4-5-a and -b). The thin-platelet calcite does not typically form scepters.

Bladed is the most spectacular calcite morphology. In contrast to thin-platelet crystals, bladed calcite has an elongated rather than isometric shape in the plan view with a dominant pinacoid. Crystals are elongated parallel to $[11\bar{2}0]$ or $[10\bar{1}0]$. According to the crystal symmetry of calcite, its pinacoidal section is isotropic; nevertheless bladed calcite grows faster in one selected direction. This makes bladed crystals similar to skeletal formations. SEM and optical imaging has revealed that pinacoidal surfaces of bladed crystals carry stepped growth hillocks indicative of a dislocation-controlled growth. The growth steps propagate away from growth centers, both toward the crystal heads and toward the crystal bases. Bladed crystals show a characteristic growth zonation emphasized by the entrapment of chains of opaque inclusions parallel to the pinacoidal faces.

Bladed calcite commonly exhibits a scepter variety, which develops by a combination of two morphologies: tabular (or blade-shaped) "stem" with dominant pinacoid and blocky "head" with dominant rhombohedron $\delta\{01\bar{1}2\}$ and/or prism (Figures 3-4-5-b). Importantly, no indications of the hiatuses between the formation of the "stem" and the scepter head were found. Typically the heads have well-formed crystal faces. Sometimes, however, a head has the "swallow tail" morphology resulting from the preferential growth of the head edges.

In cases where the bladed crystals are located close to each other, scepter heads develop only on the end of the crystal, farthest from the substratum (cavity wall). On the less-densely distributed crystals, rhombohedral faces develop not only at crystal tips, but also overgrow the whole side of a blade. In the most advanced cases, this development leads to the complete overgrowth of a blade by calcite layer composed of numerous similarly oriented subindividuals with rhombohedral habit. The calcite in scepter heads commonly precipitates together with opal, forming rhythmically zoned calcite-opal crusts over the bladed calcite.

Characteristic growth zonation helps to establish the sequence of facing of the scepter calcite and to determine the relationships between platelet, bladed and blocky calcite types. Figure 3-4-6 schematically shows the growth zonation

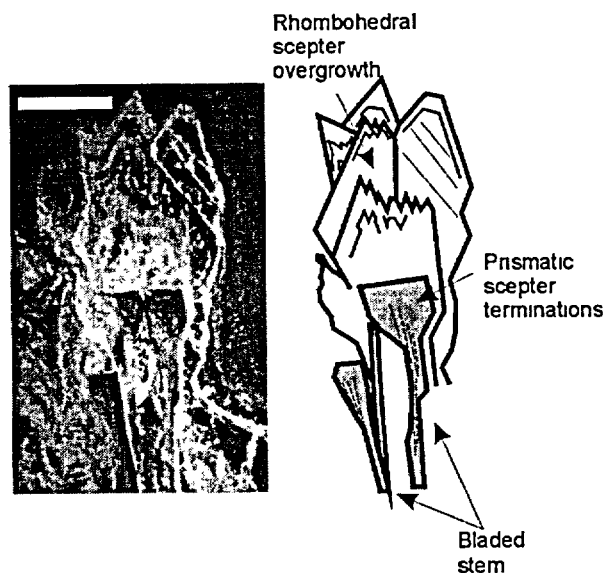


Figure 3-4-6. Micro-photograph and explanatory line-drawing of the section of scepter crystal, showing morphology of bladed crystals with scepter terminations and rhombohedral blocky heads. The latter are commonly cloudy due to the zones with opal. Scale bar is 5 mm.

Figure 3-4-6 schematically shows the growth zonation

of a scepter crystal. The crystal started growing as a platelet crystal without any clearly defined crystal faces and with the curved rough surface of a pinacoid. As growth continued, faces of a prism appeared on the tips of the platelets (i.e., at the growth front) to form the scepter head. At this time, the head of the crystal became thicker, indicating an activation of growth centers of prismatic faces and reducing activity of growth centers on the pinacoid surface. In cases where growth continued unperturbed, euhedral rhombohedral heads developed. Such heads acquired the overall blocky character. In some cases, dust-sized particles were entrapped on the prismatic faces of the growing scepter. As the edges of the scepter head continued to grow, the "swallow tail" morphology of the crystal head developed.

Figure 3-4-7 shows that the platelet, bladed and scepter morphologies are restricted to the north central part of the repository block. The restriction suggests that these morphologies could be atypical rather than common and may not be a universal part of the paragenetic sequence at Yucca Mountain. This is in contrast with the interpretation of Paces et al (1996), Whelan et al (1998), and Wilson and Cline (2001), who seem to be of the opinion that the absence of bladed and scepter morphologies at other locations indicates the incompleteness of the mineralogic record.

The best-developed platelet-type calcite was found near ESF stations 14+75 and 16+12.38. This distribution pattern shows a quite remarkable affinity with the paleo-temperature field determined by fluid inclusions (see Chapter 3-6, Figure 3-6-7), as well as with the distribution of U, Th and Pb in secondary opal associated with calcite (see Chapter 3-7, Appendix 3-7-1).

Blocky morphology (see Figure 3-4-5 *c* and *d*) dominates in the outer zones of crusts. Habit faces of the blocky calcite are: negative rhombohedron $\delta\{01\bar{1}2\}$ and prism $m\{10\bar{1}0\}$ plus optional pinacoid. Dominant habit forms are either rhombohedron or prism (see Figure 3-4-5 *c* and *d*). Crystals with rhombohedral habit ($\delta+m$) are most common. The prism-dominated habit ($m+\delta$ or $m+c$) is typical of late calcite that crystallizes with opal. The latest calcite crystals with Mg-enrichment (see below) have

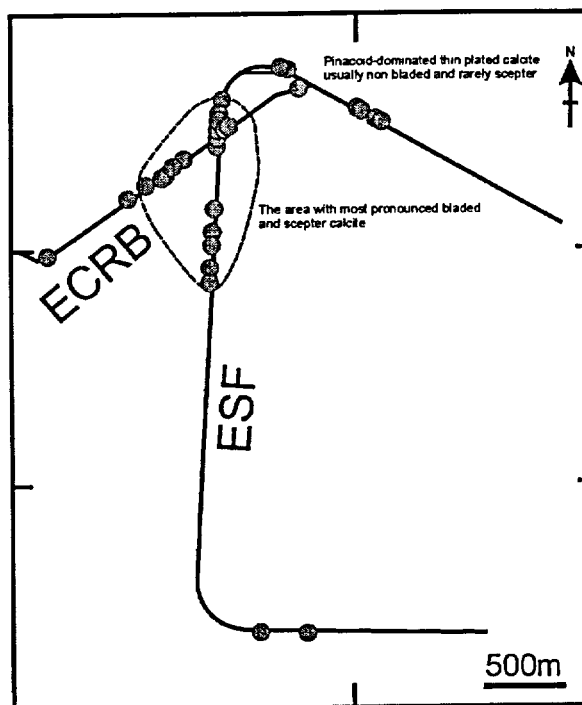


Figure 3-4-7. Distribution of bladed and thin-platelet calcite in the ESF and ECRB. Dashed line contours zone of the most abundant occurrences.

rhombohedral shapes without prismatic faces. Morphologies, that are extremely rare in the Yucca Mountain calcites, are sharp rhombohedron $\{02\bar{2}1\}$ and scalenohedron. The following three types of blocky crystals can be defined based on the character of the crystal zonation.

Type 1 - Non-zoned crystals. Crystals of this type do not exhibit any visible zonation.

Type 2 - Crystals with rhythmic rhombohedral zones highlighted by layers of opal. Crystals of this type are typically rhombohedral and are commonly the latest members of the paragenesis. Here, the growth zonation is emphasized by the deposition of extremely fine layers of co-genetic opal on the rhombohedral faces of the calcite. In some cases zonation indicates that, at early stages, the crystal was developing the faces of a prism, which become extinct at later stages of growth.

Type 3 - Crystals with complex zonation. Such crystals have domains with zonation parallel to pinacoid (characteristic of the bladed calcite), although pinacoid is absent from the set of external crystal faces. The outer parts of such crystals either do not exhibit any visible zonation (i.e., Type 1), or have growth zones parallel to the rhombohedron (Type 2).

The development of blocky crystals begins from the rhombohedral or from platelet/bladed crystals. Typically, the earliest blocky crystals do not have any visible zonation. Late generations exhibit growth zonation due to the synchronously depositing opal. The faces of a prism appear in such crystals. An interesting feature observed in the late calcite associated with opal is the epitaxial overgrowth of the prismatic calcite upon the rhombohedral one. The latest prismatic calcite typically has a cloudy appearance due to the abundance of tiny inclusions. This feature suggests that the growth of calcite may have occurred in the silica gel. Experimental studies show that calcite which grows in gels forms perfectly shaped crystals, which are commonly cloudy inside due to the presence of abundant inclusions of colloidal particles (Henisch, 1970).

Chemistry of calcite

Chemically, the calcite in fractures and lithophysal cavities of Yucca Mountain is relatively pure. In most cases, the contents of FeO, MnO, and SrO are below the detection limits for the electron microprobe (EMP) analysis (i.e., below 70 – 200 ppm). The only component found in somewhat elevated quantities (up to 1.2 wt. %) was MgO. Generally, chemically pure calcite is not typical of supergene deposits. According to Stankeev (1986), calcites with relatively low MnO+FeO contents are characteristic of either high-temperature skarn deposits or low-temperature (50-150°C) hydrothermal deposits.

A summary of the MgO contents in calcite of different morphologic types is presented in Figure 3-4-8. The contents of MgO are low (generally < 0.1-0.2 wt.%) in banded granular calcite (a rare variety of granular calcite appears at the bases of some crusts in fractures), platelet, and bladed calcites, as well as in

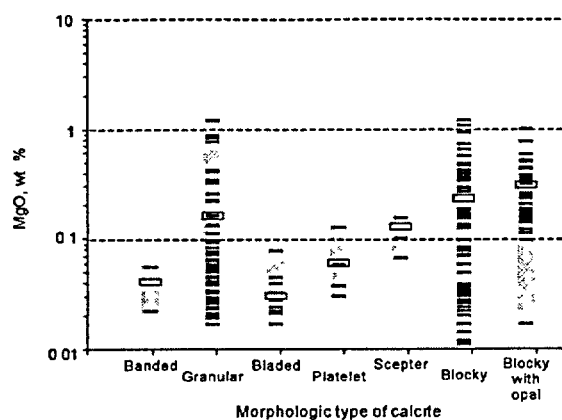


Figure 3-4-8. Contents of MgO in calcite of the different morphological types (EMP data). Morphological types shown along the x-axis are arranged to reflect the generalized growth sequence in mineral crusts from oldest to youngest. Horizontal bars show the mean values. Detection limit is approximately 0.01 wt.%.

those scepter overgrowths that do not have a zonation related to opal. In scepter overgrowths, the MgO contents are somewhat higher, reaching up to 0.2 wt.%. Contents of MgO in granular and blocky calcite are variable and range from below the detection limit to as much as 1.2 wt.%. As it is shown in Figure 3-4-9, granular and blocky calcite varieties with and without opal have similar overall MgO contents, with the paragenetically youngest blocky calcite having somewhat higher modal values (0.3 to 0.5 wt. % as opposed to 0.0 to 0.3 wt. % in blocky non-zoned calcite).

We studied the variations of MgO within the calcite crusts by electron microprobe (EMP) analyses along profiles intersecting the crusts from the base to the outer zones. Data from 13 profiles (about 160 microprobe points) were grouped into three distinct patterns of MgO change in the process of calcite growth. Some representative profiles are shown in Figures 3-4-10 through 3-4-12.

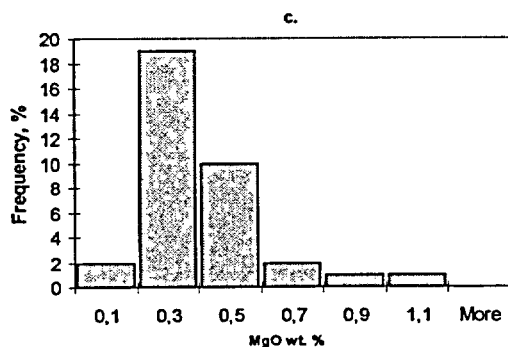
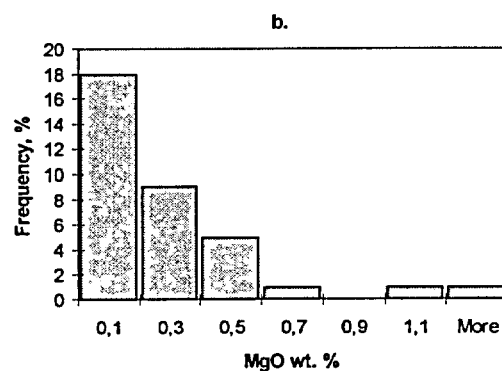
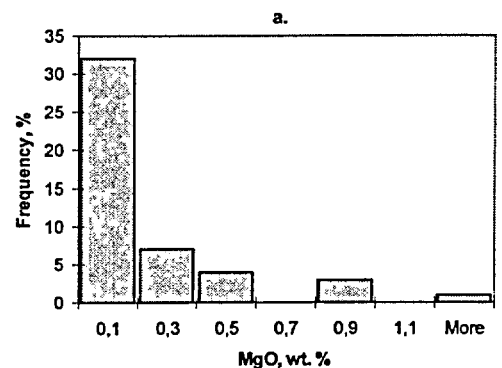


Figure 3-4-9. MgO contents in granular and blocky calcite (EMP data). *a* – granular calcite; *b* – blocky calcite without opal; and *c* – zoned blocky calcite with opal.

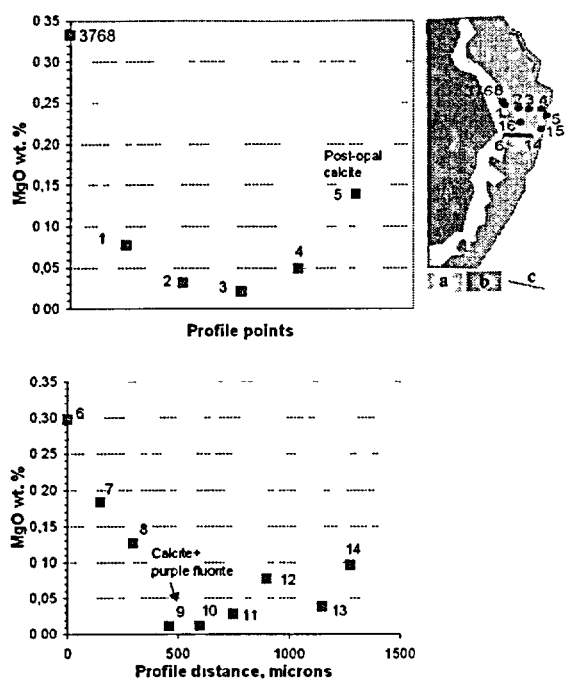


Figure 3-4-10. Pattern-1 compositional profiles of MgO in calcite from sample 3768 (ESF 38+80; lithophysal cavity). Two parallel EMP profiles across the same crust. Locations of analytical points are shown on the inset. Solid line on the inset indicates points 6 through 14. Inset: *a* – tridymite, *b* – blocky calcite, *c* – layers of bubbly transparent opal.

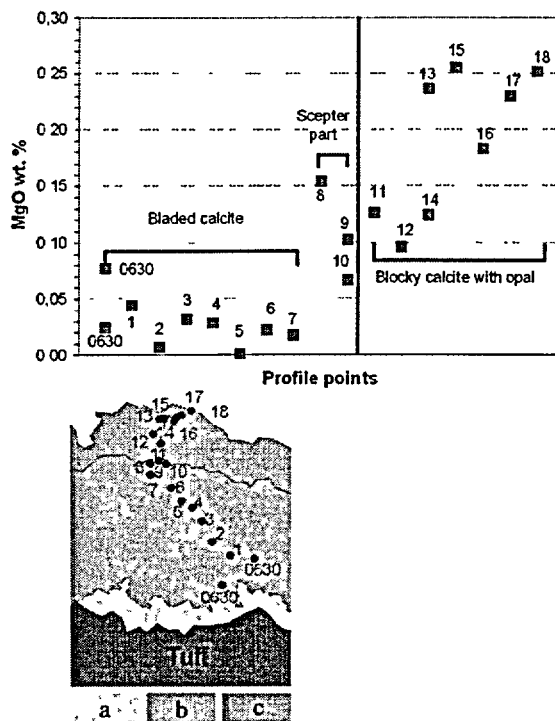


Figure 3-4-11. Pattern-2 compositional profiles of MgO in calcite from sample 0630 (ECRB 07+93; lithophysal cavity). EMP data. Locations of analytical points are shown on the inset. Inset: *a* – tridymite, *b* – bladed and scepter calcite, *c* – blocky calcite with tiny opal layers.

Note: Blades of calcite are oriented at an angle of approximately 50° to the substratum (tuff and tridymite). Analytical points shown on the inset are located along the growth axis of the individual blade crystal.

Pattern 1. The Mg content is high at the base of the crust and decreases toward the periphery. The contents might slightly increase again toward the outer part of the crust (Figure 3-4-10). *Pattern 2.* The Mg content is low at the base of the crust and increases outward (Figure 3-4-11). *Pattern 3.* The Mg contents vary, increasing and decreasing along the profile (Figure 3-4-12). Virtually all distributions of the Mg contents have a minimum in the middle part of the profile.

Figure 3-4-8 clearly shows that increased Mg-contents are associated with particular calcite morphologies: the paragenetically earliest granular and blocky calcite, and particularly paragenetically latest blocky variety containing opal.

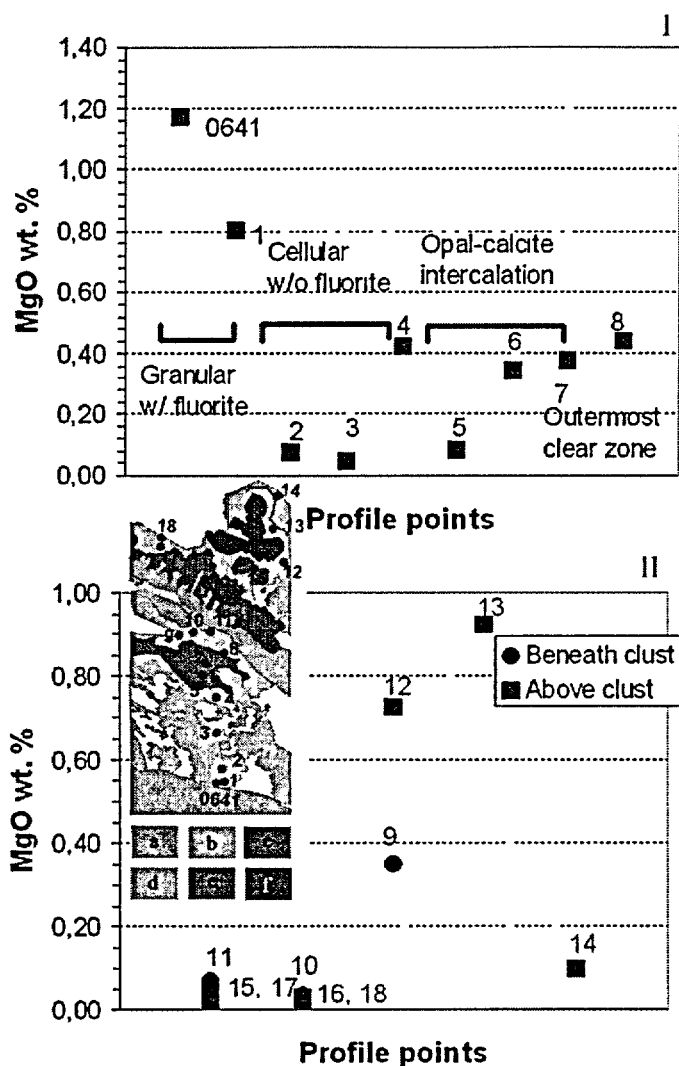


Figure 3-4-12. Combination of the pattern-1 and pattern-2 types of MgO profiles (pattern-3) in calcite sample 0641 (ECRB 25+30; lithophysal cavity). The crust is built up of two parts. The lower (profile *I*) consists of granular and cellular calcite and grows against the wall of cavity. The upper consists of blocky calcite, overgrowing the clust of tuff (profile *II*). EMP data. Locations of analytical points are shown on the inset. Inset: *a* – tuff, *b* – cellular and granular calcite with fluorite inclusions, *c* – calcite-opal intercalation, *d* – blocky calcite, *e* – spherulitic and euhedral purple fluorite overgrowth, and *f* – quartz and chalcedony.

It is in this late calcite that Wilson and Cline (2001) found oscillatory zonation expressed as alternating layers of calcite with varying degrees of Mg-enrichment (up to ~1.0 wt. % Mg). The nature of this zonation at present remains indeterminate. The formation of the oscillatory zonation pattern may be a consequence of local nonlinearities in the growth process, but the pattern details may be strongly affected by subtle changes (noise) in the external environment. In general, oscillatory mineral zonation is usually associated with crystal growth in a system, which may be driven sufficiently far from thermodynamic equilibrium to produce autonomous patterns by geochemical self-organization (Holten et al., 2000). Mathematic analysis of the zonation pattern may be helpful in determining the causes of the zonation (Wang and Merino, 1992, Halden and Hawthorne, 1993, Halden, 1996, Bryxina and Sheplev, 1997), but this analysis has not been done.

From the present data set, it is reasonable to conclude that the activity of Mg in the mineral-forming solutions varied through the time of the secondary calcite deposition. Samples presented in Figures 3-4-10 through 3-4-12 were collected from different locations in different parts of the potential repository zone. The figures demonstrate that the character of the Mg zonation in studied crusts is quite dissimilar from the characteristically rhythmic patterns of zonation typical of mineral deposits formed from descending meteoric waters, which "record" the climatic signal (e.g., Hill and Forti, 1997; Bryxina et al., 2000). This in turn, is at variance with the "rainwater" hypothesis, ascribing the leading role in deposition of calcite at Yucca Mountain to meteoric water (e.g., Peterman et al., 1992, Paces et al., 1996 and 2001, U.S. DOE, 1998 and 2001).

3.4.3.1.2. Minerals of silica

Minerals of silica in fractures and lithophysal cavities of Yucca Mountain are chalcedony, opal and quartz. These minerals form two types of crusts: (1) massive crusts with fine-grained, in places spherulitic, textures; and (2) zoned crusts with spherulitic or drusy textures. The thickness of both types of crusts may reach 1 cm.

Minerals of silica demonstrate two important features. **First**, their distribution within the repository block is zoned, showing an abundance, which decreases from the east to west. This distribution is opposite to the distribution of calcite (Figure 3-4-13). In the plane view, occurrences of silica minerals seem to show a concentration in the northeast corner of the repository zone (Figure 3-4-14). As will be demonstrated below, this distribution virtually "mimics" the distribution of the maximum fluid inclusions temperatures and the minimum $\delta^{18}\text{O}$ values measured in calcite samples from the ESF (see Section 3.5.2. and Chapter 3-6).

Second, the silica-dominated secondary crusts commonly show a non-geopetal appearance (the non-geopetal appearance means that the minerals occur on both ceilings and floors of cavities or on hanging walls and footwalls of the fractures). This contrasts the silica-dominated crusts with the calcite-dominated ones that are typically restricted to the floors of cavities and footwalls of fractures. The feature is most prominent at the northern ramp of the ESF (see Figure 3-4-14).

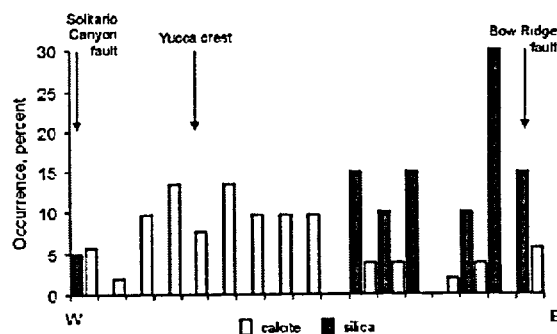


Figure 3-4-13. Distribution of carbonate and silica mineral assemblages across the northern part of the repository block. Diagram reflects the number of occurrences sampled in northern ramp of the ESF and in the ECRB. Percentage of occurrences is normalized to the 200 m-intervals.

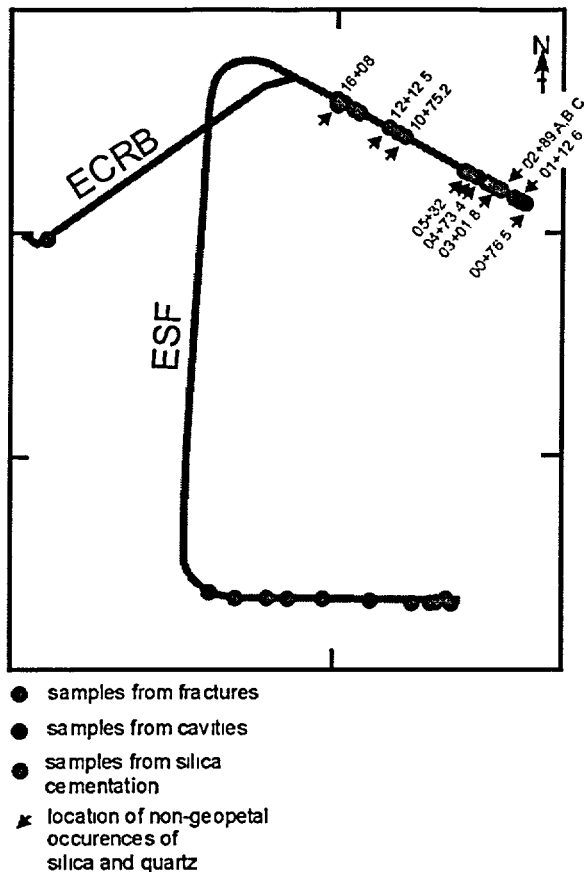


Figure 3-4-14. Distribution of minerals of the silica assemblage in the ESF and ECRB. Locations, where mineralization does not show the "geopetal" character (i.e., minerals are present on both floors and ceilings of cavities and foot- and hanging walls of fractures) are indicated by arrows, and for these locations numbers of the ESF stations are shown.

crystals were found growing over the latest chalcedony. In certain places, quartz forms monomineral crusts with drusy textures, or layers confined within calcite.

In contrast to calcite, which in most cases occurs on the floors of cavities and footwalls of fractures, quartz crystals grow on the walls and ceilings of the lithophysal cavities and on the hanging walls of fractures. Large quartz crystals almost always have scepter morphology (Figure 3-4-15).

Opals

In zoned silica-dominated crusts, opals form milky-white layers between the chalcedony-quartz layers. In the calcite-dominated crusts, opals occur as water-clear spherulites or botrioidal crusts embedded in the calcite crystals or deposited on the calcite surface.

We need to point out that this observation seems to be in conflict with the strong statements made by the Yucca Mountain Project researchers who claim that in the ESF tunnel, mineral coatings are never present on the cavity ceilings: *"The presence of mineral coatings only on fracture footwalls and cavity floors indicates that water only flowed downward on the lower surfaces and never filled the open space. Even the earliest mineral deposits consisting of massive silica and quartz largely are restricted to the same sites that continued to accumulate younger deposits..."* (Paces et al. 2001, p. 66). Locations of samples where secondary silica minerals were observed on the cavity ceilings and fracture hanging walls are shown in Figure 3-4-14.

Chalcedony and Quartz

Quartz forms crystals, with the largest individuals being as large as 1 cm. In massive silica layers, quartz may grade into chalcedony. In most instances, quartz is restricted to the stratigraphically lowermost (i.e., earliest) parts of the massive and zonal crusts, although some quartz

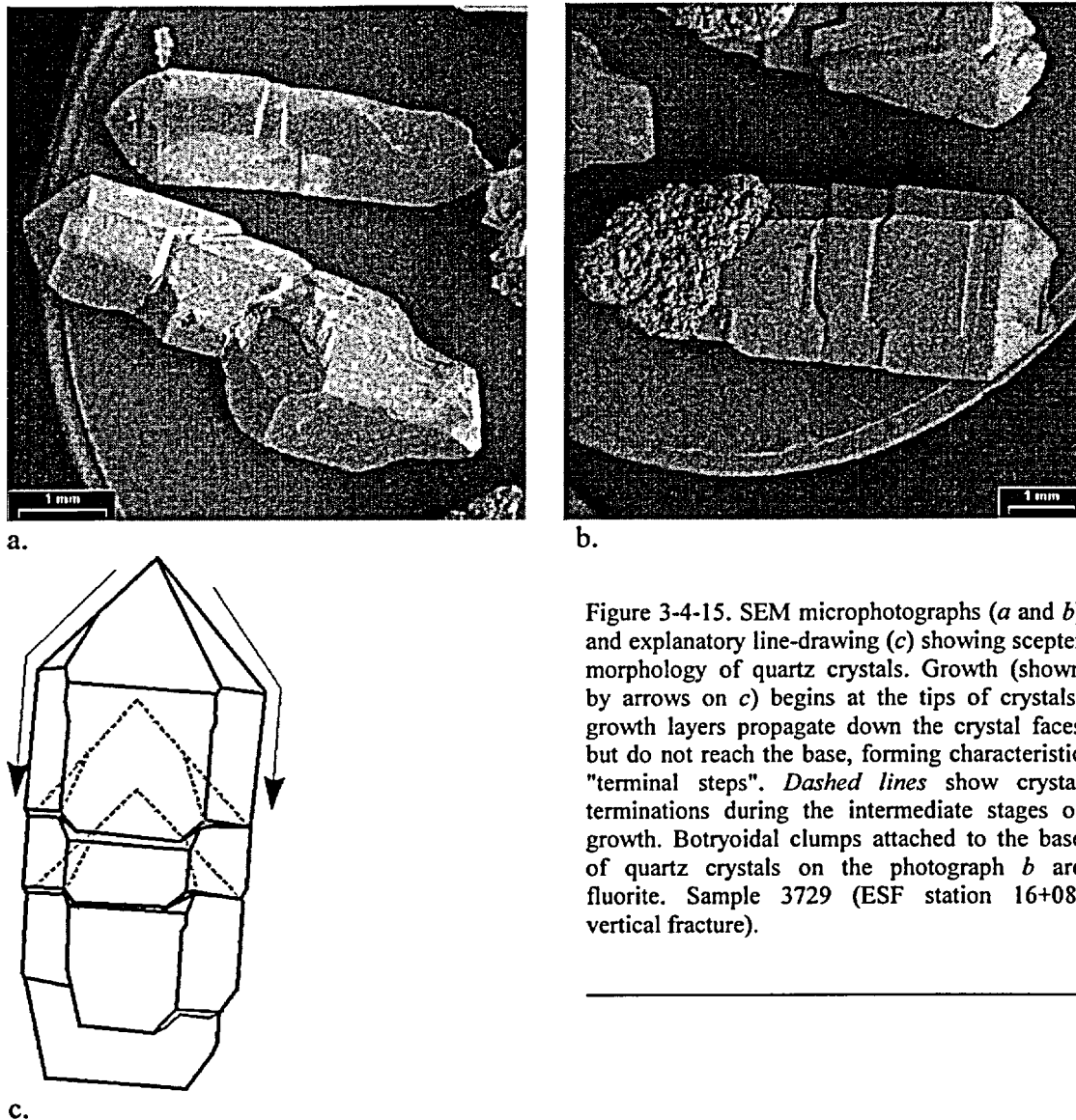


Figure 3-4-15. SEM microphotographs (*a* and *b*) and explanatory line-drawing (*c*) showing sceptor morphology of quartz crystals. Growth (shown by arrows on *c*) begins at the tips of crystals; growth layers propagate down the crystal faces but do not reach the base, forming characteristic "terminal steps". *Dashed lines* show crystal terminations during the intermediate stages of growth. Botryoidal clumps attached to the base of quartz crystals on the photograph *b* are fluorite. Sample 3729 (ESF station 16+08, vertical fracture).

The latest zones in the blocky calcite crystals, as well as the heads of sceptor crystals commonly represent rhythmic calcite-opal intercalations. In late chalcedony-opal crusts, opal is present in amounts, comparable to those of the chalcedony; and must be considered, therefore, as the major mineral of the assemblage. Meanwhile, opal inclusions and the thin layers in calcite and opal layers in zoned chalcedony-quartz crusts must be classed as accessory minerals. In this section we will discuss variants in the relationships between opals and other minerals.

According to the classification by Graetsch (1994), the Yucca Mountain opals are microcrystalline. Opals C, CT; late, colorless, translucent opal all belong to this category.

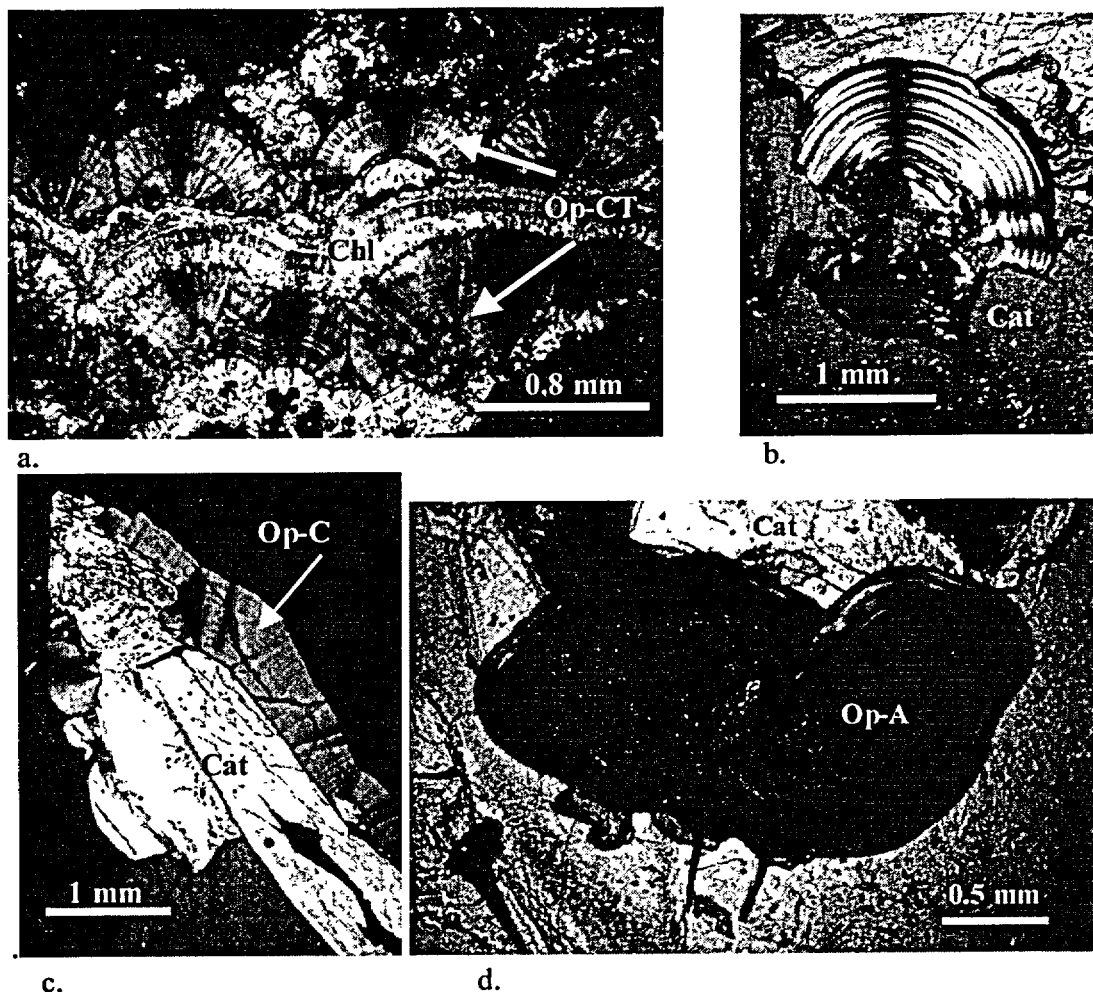


Figure 3-4-16. Three types of opals. *a* – layers of spherulitic opal-CT (opal 1; dark gray) within quartz-chalcedony layers (Chl; rainbow-colored); sample 3720, ESF station 05+56.9, fracture, cross-polarized light; *b* – spherulite of opal-CT (opal 2, first variety) within bladed calcite (Cat); sample 1230A, ESF station 28+80, low-angle fracture, cross polarized light, *c* – spherulitic crust of opal-C (opal 2, second variety) deposited over scepter calcite (Cat); sample 1230B, ESF station 28+80, low-angle fracture, cross polarized light, and *d* – bleb of opal-A (opal 3) included in the bladed calcite (Cat). Note gray layers of opal-CT at top right part of the bleb (sample 1230A, ESF station 28+80, low-angle fracture, cross-polarized light).

Based on their microscopic properties, we have defined three varieties of opals in the Yucca Mountain samples (Figure 3-4-16).

Opal 1 associates with both silica minerals and calcite. In most cases, Opal 1 occurs in the late parts of the massive silica crusts. It forms layers between the chalcedony-quartz layers. In places, layers of this opal laterally grade into the chalcedony; in some spherulites, it contains irregular patches composed of chalcedony. Such textures indicate partial or complete replacement of the metastable Opal 1 with the more stable chalcedony. In calcite-dominated crusts it commonly associates with accessory chalcedony.

In transmitted light Opal 1 commonly has a brownish color due to abundant inclusions and its length-slow fibrous character. A spherulitic texture becomes apparent in polarized light. These properties allow us to classify this opal as *lussatite* or CT-opal.

Opal 2 associates only with calcite. In polarized light, the inclusions of the opal in calcite and botryoidal crusts reveal a spherulitic character (Figure 3-4-16-b). In contrast to Opal 1, mineral individuals in the spherulitic Opal 2 are not optically discernible even at high magnification. There are two varieties of Opal 2 that have different optical characteristics. The *first variety* occurs as single spherulites and clusters of spherulites in calcite (Figure 3-4-16-b). This variety of opal also associates with accessory chalcedony. In polarized light, spherulites show a pronounced concentric zonation with each zone having significantly different birefringence. Individuals are length-slow. This variety of opal may also be classified as *lussatite* or CT-opal having a cryptocrystalline character. The *second variety* of Opal 2 is restricted to the rims of calcite crusts and typically associates with the latest Mg-enriched calcite (Figure 3-4-16-c). It forms single spherulites and layers of spherulites. In polarized light Opal 2 reveals its spherulitic texture and length-fast character. According to these optical properties we classify Opal 2 as *lussatine* or C-opal. Similarly to Opal 1, layers have a thickness of one spherulite. The compromise boundaries between adjacent spherulites indicate competitive growth.

Opal 3 in the secondary assemblages of the Yucca Mountain is the amorphous A-opal (Figure 3-4-16-d). This is the least common type of opal in the studied samples. It is found in association with opals C and opal CT. According to Graetsch (1994) A-opals have a gel structure, i.e. an irregular, voluminous framework composed of spherical silica particles. Typically these opals form from colloidal solutions.

3.4.3.2. Accessory minerals

Unlike the major minerals, accessory minerals did not attract any serious attention of the early students of the Yucca Mountain mineralogy. Mineralogical data from drill holes reported by (Carlos et al., 1993, 1995-a) do not allow for discrimination of the major and accessory minerals. Excavation of the ESF provided access to the great number of mineral occurrences and made it possible to collect large high-quality samples. This allowed, potentially, not only a determination of the complete set of secondary minerals, but also a characterization of their spatial and temporal relationships. None of the publications dealing with the secondary mineralization from the ESF, however, offers information in this regard. Some authors (e.g., Vaniman and Chipera, 1996; Whelan et al., 1998-b; Wilson and Cline, 2000, 2001) pay much attention to the sequence of major mineral deposition based on their micro-stratigraphic relationships and merely mention the presence of accessory minerals. The latest summary of the geochemical data on the vadose zone of Yucca Mountain (Fabryka-Martin et al., 2000) does not mention accessory minerals at all.

In this section we discuss accessory minerals of the secondary assemblages from the Yucca Mountain vadose zone with special emphasis on the indications of their syngenetic character relative to the major minerals. This will provide additional insight into the chemistry of the ancient mineral-forming solutions.

3.4.3.2.1. Minerals of silica

As we stated above, the only criterion that allows attribution of minerals to the accessory category, is their content in the rock or secondary formation (e.g., aggregate) that is established on the basis of the microscopic studies of thin sections and hand specimens. We have found that both calcite and quartz may be present in the same assemblage. In the assemblage, however, one of them will be a major mineral and the other one – an accessory mineral. Calcite rarely occurs in accessory quantities in association with minerals of silica. Conversely, chalcedony/quartz and opals are the most common accessory minerals in calcite-dominated assemblages, where they occur as individual spherulites embedded in calcite, or as fine crusts highlighting zonation of the calcite crystals or lining voids between them. The indented character of contacts between the spherulites and the host calcite indicate co-precipitation, whereas the incrustations of interstices between crystals and the healings of fractures in crystals indicate that deposition of some silica minerals post-dated the host mineral (typically, calcite). In places, the pitted character of the opal-calcite interface has been observed, suggesting that minor dissolution of calcite took place before the deposition of opal; the same opal, however, commonly exhibits indented compromise boundaries with calcite, indicative of co-precipitation.

3.4.3.2.2. Fluorite

Fluorite is a typical hydrothermal mineral (see Table 3-4-1) that, to the best of our knowledge, has not been reported to form in the course of interaction between surficial waters and rhyolitic or other igneous rocks. It is particularly important, therefore, to demonstrate the syngenetic relationships between fluorite and the major secondary minerals from the Yucca Mountain vadose zone. Bish and Vaniman (1984) first reported fluorite from the core of the USW GU-3 borehole. Later Bish and Vaniman (1985) reported abundant (up to 50 % on the basis of XRD data) fluorite in fracture-filling material in the core samples from USW GU-3 and UE-25 b#1 boreholes. Carlos et al. (1995-a) reported abundant fluorite in fractures from core samples of USW G-3 and UE-25 a #1 boreholes.

Figure 3-4-17 shows the locations of fluorite-bearing samples from the ESF and ECRB (based on the data of Whelan et al., 1998-b; Dublyansky and Reutsky, 1998; and Smirnov and Dublyansky, 2001). It is apparent from the figure that fluorite is present along the whole length of the ESF, as well as in the cross-drift (ECRB). Taking into account the common occurrence of fluorite found in the borehole cores (e.g. Bish and Vaniman, 1985; Carlos et al. 1995-a), it could be concluded that fluorite mineralization is

ubiquitous across the whole block of Yucca Mountain. The most abundant occurrences of fluorite were found between stations ESF 12+12.05 to 16+12.38 and ESF 37+62.9 to 39+38.7. In the ECRB, samples richest in fluorite were collected near the stations ECRB 24+80 and 25+38. Rare, but rich in fluorite, samples were also found close to the Bow Ridge fault. The richest occurrences of fluorite seemed to cluster near the intersections of the north trending faults with the northwest trending shear faults of the Walker Lane zone (Sundance fault and Drill Hole Wash fault).

Fluorite was found in association with both silica minerals and calcite. In a few samples, fluorite was found to form almost mono-mineral occurrences. Although the amount of the deposited fluorite was small (it typically forms thin films of powdery material with local patches of micro-crystalline fluorite), strictly speaking, it must be considered a major mineral.

Fluorite gives a variety of mono- and polycrystalline forms. Crystals are typically light lilac, pinkish or colorless. Late zones of fluorite commonly have a more intense violet color. Dark violet fluorite primarily occurs in association with calcite, whereas fluorite associated with the silica minerals is typically light-colored or colorless. Fluorite occurs as aggregates of anhedral crystals, single flat- and bent-faced euhedral crystals, and spherulites and concentrically zoned oolitic colloform segregations.

Anhedral fluorite forms aggregates commonly associated with quartz/chalcedony layers or with granular calcite.

Euhedral fluorite crystals mostly have cubic and rhombododecahedral habits, suggestive of the crystallization from relatively low-temperature hydrothermal solutions (<100°C) or from solutions with relatively low salinity (Glikin and Petrov, 1966). Euhedral fluorite occurs as single crystals or clusters, commonly included in calcite or quartz.

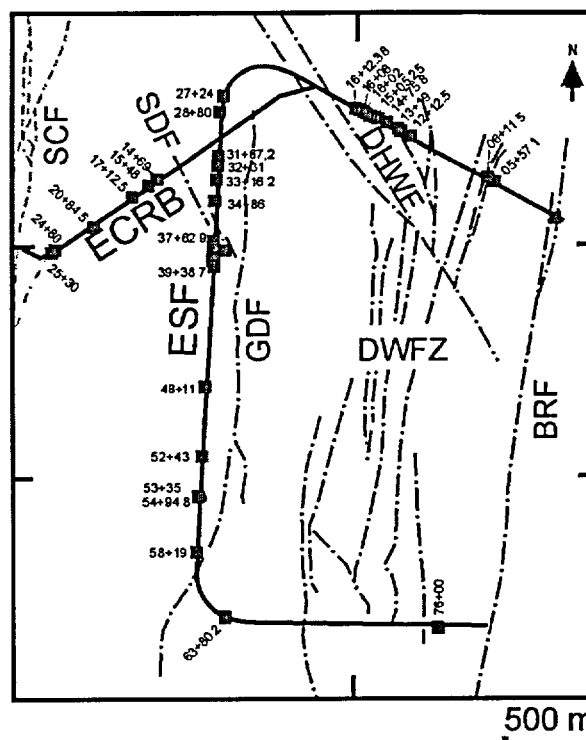


Figure 3-4-17. Distribution of fluorite in the ESF and ECRB. Dash-and-dot lines schematically show major fault structures of the repository area: North trending faults: SCF – Solitario Canyon fault; GDF – Ghost Dance fault; DWFZ – Dune Wash fault zone; BRF – Bow Ridge fault; Northwest trending faults of Walker Lane zone: SDF – Sun Dance Fault; DHWF – Drill Hole Wash fault. Numbers are the ESF and the ECRB sampling stations.

Table 3-4-2

Minor elements of fluorite from the ESF, Yucca Mountain, compared to the minor element composition of the two hydrothermal fluorspar deposits from Bare Mountain

ESF station	ESF 12+12 05		ESF 14+75 8	ESF 16+08		ESF 38+80		ESF 52+43		ESF 52+43	
Morphology	Colloform		Euhedral	Spherulitic		Spherulitic		Euhedral		Anhedral	
Assemblage	Silica		Silica	Silica		Carbonate		Carbonate		Carbonate	
	Avg	Std		Avg	Std	Avg.	Std	Avg	Std	Avg.	Std
Sr	900	190	1,120	920	90	1,150	130	1,130	140	990	140
Mg	690	20	590	660	50	590	80	540	80	610	40
P	910	90	330	340	10	360		300	10	220	
Si	1,680	680	70			2,240	1,860	60	40	120	50
n	5		1	10		5		5		4	
Sr (INAA)				229	90			184		172	
As (INAA)				208	63			338		243	
n				2				1		1	

ESF station or location	ESF 52+43		ESF 76+00		Daisy Mine, Bare mountain				Diamond Queen Mine, Bare Mountain		
Morphology	Spherulitic		Spherulitic		Euhedral				Aggregate		
Assemblage	Carbonate		Silica		Carbonate				Carbonate		
	Avg	Std	Avg	Std	DM1Y	DM2Y	DM3P	DM4V	DQ1G	DQ3YV	DQ4GV
Sr	890	160	1,430	510	1,040	1,000	810	880	1,100	1,200	740
Mg	700	130	660	130	640	690	760	670	750	600	610
P	340		410		nd	570	610	380	850	440	nd
Si	350	460	1,590	2,110	50	70	40	0	90	60	90
n	3		2		1	1	1	1	1	1	1

Note: All numbers are in ppm. The data were obtained by means of the Electron Microprobe technique, on the Camebax Micro microprobe at the Institute of Mineralogy and Petrography SB RAS except for those denoted as INAA (Instrumental Neutron Activation Analysis) obtained at the Analytical Center of the United Institute of Geology, Geophysics and Mineralogy SB RAS (analyst M. Melgunov).

Cathodoluminescence (CL) reveals concentric polygonal zonation of euhedral crystals and the absence of the allogenic cores. In most cases, euhedral crystals do not show attachment places and/or compromise surfaces, which suggests homogeneous nucleation in the bulk of the solution.

Spheroidal formations of fluorite may be subdivided into two types: spherulites and oolites. Spherulites have clearly distinguishable radiating individuals. CL patterns of these spherulites typically reveal distorted polygonal zonation, indicating that these spherulites are in fact splintered single crystals. Oolites have concentric layers built-up of micro-crystals. Other minerals (e.g., opal) sometimes serve as cores of spherulites and oolites, which provide an evidence of heterogeneous nucleation.

Within micro-cavities in the quartz-chalcedony crusts from ESF station 12+12.05 we found porous aggregates of fluorite, composed of randomly distributed oolites. Colorless euhedral cubic crystals sometimes develop at the periphery of these aggregates. We suggest that this fluorite aggregate was formed through the coagulation of a Ca- and F-rich colloid.

Different morphologic types of fluorite do not seem to show any systematic distribution within the repository block. When different morphologic types are found within the same mineral crust, spherulitic and anhedral forms tend to dominate at the crust's base, whereas euhedral crystals typically occur in the outermost parts of crusts.

Chemistry of fluorite

The results of the microprobe and INAA analyses of fluorite are given in Table 3-4-2. The analyzed samples of fluorite have low contents of impurities. The most important minor elements detected by the EMP analysis are Sr, Mg, Si, and P. Electron microprobe analyses have a relatively low accuracy at concentrations of impurities lower than 0.1 wt. %. The more-accurate INAA analyses confirmed the enrichment of the Yucca Mountain fluorite in Sr (up to 293 ppm) and revealed, additionally, an enrichment in As (up to 338 ppm).

Si and P contents were found to be higher in the spherulitic and colloform varieties of fluorite and very low in the euhedral and anhedral varieties. Since these elements cannot be incorporated into the fluorite lattice, their elevated amounts indicate, most probably, the presence of tiny allogenic (probably colloidal) particles, trapped between individuals in spherulites and oolites.

Relative age of the fluorite and its interrelationships with major minerals

Figure 3-4-18 illustrates certain interrelationships between fluorite and the major minerals of the secondary assemblages. In Figure 3-4-18-a the base of the fluorite spherulite is aligned along the buried crystal face of calcite. This provides an unequivocal indication of the co-genetic relationships between

these two minerals in the sample. Fluorite in Figure 3-4-18-*b* shows the compromise boundary (an indication of common growth) with late quartz. In the quartz-chalcedony crusts, the boundaries between the fluorite spherulites and the chalcedony are commonly indented, which again, indicates co-precipitation (Figure 3-4-18-*c*).

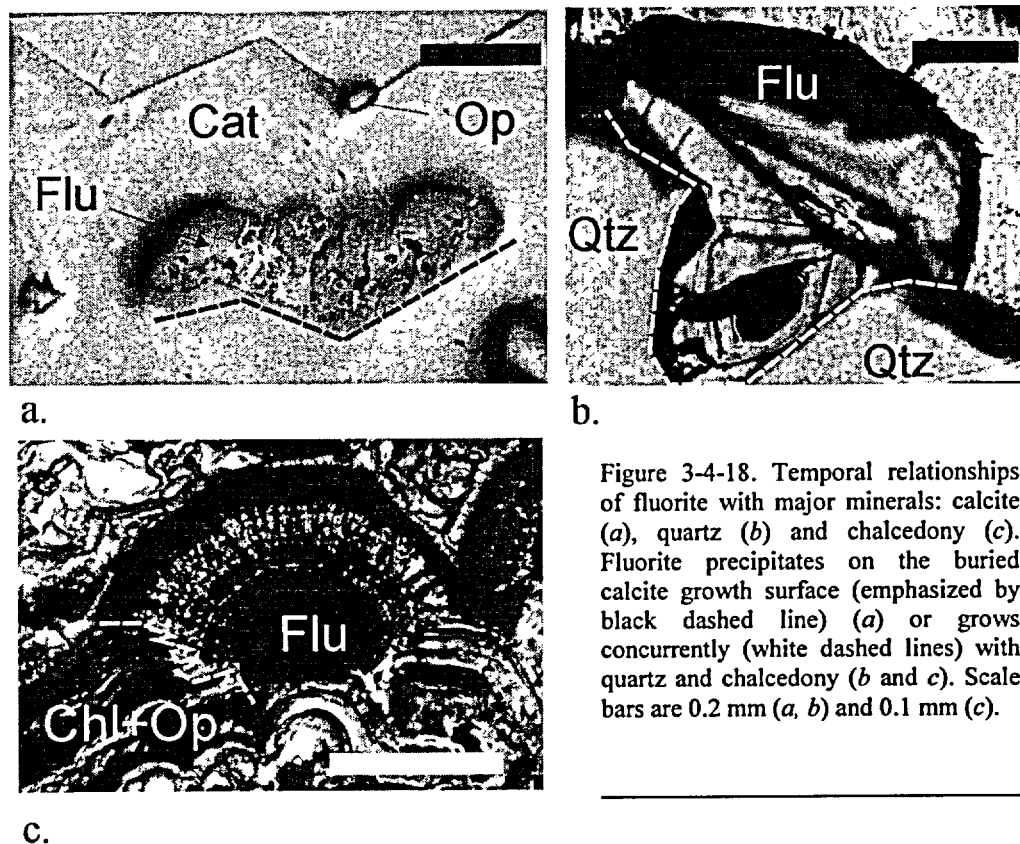


Figure 3-4-18. Temporal relationships of fluorite with major minerals: calcite (*a*), quartz (*b*) and chalcedony (*c*). Fluorite precipitates on the buried calcite growth surface (emphasized by black dashed line) (*a*) or grows concurrently (white dashed lines) with quartz and chalcedony (*b* and *c*). Scale bars are 0.2 mm (*a*, *b*) and 0.1 mm (*c*).

The position of the fluorite within the mineral crusts indicates both early and late development in the secondary mineral sequence. Early (old) fluorite forms layers at the bases of crusts or appears as inclusions in minerals from the basal parts of the crusts. In order to be classified as late (or young), an accessory mineral must be shown to have formed simultaneously with the latest major minerals in the paragenesis. Fluorites in the carbonate assemblage of Yucca Mountain were found in the outermost growth zones in association with bubbly translucent C-opal, which is, typically, one of the latest minerals to appear in the calcite crusts. It provides a strong indication of the relatively young age of the fluorite.

Fluorite has never been found in association with scepter or bladed calcite, either as inclusions or as an overgrowth. On the other hand, fluorite is commonly associated with blocky or granular calcite. Some researchers argue that this is evidence of its relatively old age because the blocky variety is believed to be the earliest variety of calcite (e.g., Whelan et al., 1998-b). It will be demonstrated below, however, that

blocky and bladed calcite from different parts of the repository block may well be coeval. Thus, we cannot view the association of fluorite with blocky calcite as an unequivocal indication of its old age.

Summarizing the data discussed in this section, we conclude that:

1. Fluorite is a common accessory mineral in the secondary assemblages from the Yucca Mountain vadose zone.

2. Fluorite occurs in association with both calcite and minerals of silica and shares the same origin with them.

3. Even though precipitation of fluorite was most active at the early stages of the secondary mineral crust formation, fluorite was also found in association with the latest growth layers of the paragenetically youngest calcite.

4. Fluorite, thus, is a typomorphic mineral of the secondary assemblages of Yucca Mountain and can be considered an indicator of the chemistry of the mineral-forming process.

3.4.3.2.3. Zeolites

An important role for zeolites, among the fracture-lining minerals, was established by Carlos et al. (1995-a). Studying samples from drill holes they determined that fracture-lining zeolites are present throughout the whole volcanic sequence penetrated by the drill holes. The most common zeolite species found in fractures and lithophysal cavities are heulandite, mordenite and stellerite. Unfortunately, Carlos et al. (1995-a) did not describe the fractures from which zeolites were studied, so the possible paragenetic relationships with other open-space secondary minerals remain unclear.

Early mineralogical observations in the ESF have revealed that zeolites are present throughout the repository block. Dublyansky and Reutsky (1995) reported euhedral zeolites at the base of the calcite crust sampled at ESF station 0+84.7, and identified them as heulandite. Whelan et al. (1998) mentioned the presence of zeolites in fractures and lithophysal cavities, but did not characterize them. Smirnov and Dublyansky (2001) demonstrated that zeolites are the second-most widespread accessory minerals after fluorite and identified them in a number of samples from the ESF as heulandite and “mordenite or erionite” on the basis of EMP and SEM analyses. If zeolites in secondary assemblages of Yucca Mountain are equilibrated, then according to Chipera and Bish (1997), heulandite could only associate with mordenite. Thus, fibrous zeolite reported by Dublyansky and Smirnov (2001) is, most likely, mordenite. The reported occurrences of zeolites in the ESF are localized along the north ramp and in the northwest sector of the repository block.

As it was shown in Sections 3.1.4.6 and 3.1.4.7, Sr and Mg are the most important impurities of the fracture-lining zeolites from both the drill core (Carlos et al., 1995-a) and the ESF samples (Smirnov and Dublyansky, 2001).

In the calcite-dominated crusts from the ESF, heulandite and mordenite were found in two positions: in the granular calcite at the bases of the crusts and overgrowing the bladed calcite. Heulandite was found to associate with accessory chalcedony and opal, which agrees with observations of Carlos et al. (1995-a) as to the core samples. This association indicates that the activity of silica sporadically increased during the crystallization of the calcite. Heulandite, included in or overgrowing calcite, typically forms well-developed euhedral crystals devoid of attachment sites. Sometimes heulandite crystals split at the contact with the surfaces of the accessory chalcedony spherulites, indicating that heulandite growth post-dates chalcedony. Accessory zeolite-chalcedony intergrowths, found to be included within bladed calcite crusts, further supports our conclusion that these zeolites are co-genetic with the bladed calcite. In the sample from ESF station 28+81, euhedral heulandite was found to overgrow the calcite blades, forming a drusy aggregate. The bladed calcite occupies an intermediate position in the secondary paragenesis; thus, we conclude that in addition to early stages, heulandite crystallization took place at the intermediate or late stages of calcite crystallization as well. In the silica-dominated crusts, heulandite and mordenite were found growing on the tops of the chalcedony spherulites, which indicates that the zeolites were deposited after the crystallization of silica minerals ceased. We have not observed heulandite or mordenite mineral inclusions within silica minerals, which lead us to conclude that zeolites typically post-date the silica-deposition stage in studied assemblages.

Summarizing the above observations, we conclude that zeolites are important accessory minerals co-genetic with the major secondary minerals from the Yucca Mountain vadose zone. Our observations demonstrate that zeolites preferentially formed in association with calcite, and, to a lesser extent, at late stages of the silica mineral deposition.

3.4.3.2.4. Strontianite

Even though it was found only in one sample, strontianite is a mineral that undoubtedly belongs to secondary mineralization. Numerous aggregates built up of radiating needles were found in granular calcite (sample 2300; station ESF 78+41; Figure 3-4-19).



Figure 3-4-19. Radiating needles of strontianite in the granular calcite. Sample 2300, ESF station 78+41. Scale bar is 100 μm .

Calcite hosting strontianite forms a base of the late zoned calcite with opal and, therefore, was most likely deposited at the intermediate stages of the calcite crust formation, shortly before the deposition of late opal-bearing calcite. Isotopic properties of the host calcite, $\delta^{18}\text{O} = 18.3$ to 19.7 ‰ SMOW and $\delta^{13}\text{C} = -6.4$ to -7.7 ‰ PDB, are consistent with this interpretation (see Section 3.5.2. for discussion of stable isotopic properties of calcite from the Yucca Mountain paragenesis). Based on the results of the EMP analyses, the chemical composition of the Yucca Mountain strontianite corresponds to the Ca-enriched strontianite (61.2 to 62.8 wt.% SrO, 6.5 to 7.0 wt.% CaO, and 0.02 to 0.05 wt.% MgO).

3.4.3.2.5. Mn-oxides

Carlos et al. (1993) identified various Mn-oxide minerals in fractures of the Yucca Mountain rhyolitic tuffs. Our studies of large-aperture fractures in the ESF indicate that Mn-oxides are present only as minor minerals. Most likely, they are restricted to thin fractures and are related to stages of the mineral forming process that preceded the deposition of the major secondary minerals exposed in the large-aperture fractures and lithophysal cavities in the ESF.

The most important geochemical feature of the Mn-oxide minerals observed in fractures of the Yucca Mountain rhyolites is the dominant role of Ba, Ca and K, serving as major channel cations. The deposition of Ba- and Ca-bearing Mn-oxides requires a high activity of these elements, which cannot be accounted for solely by the rhyolitic source rock (although the later could serve as a source of Mn). Additionally, minor elements in Mn-minerals are Mg, Sr, and Na; importantly, Pb- and Al-bearing Mn-oxides (hollandite and lithiophorite) have also been reported from fracture coatings Carlos et al. (1993).

3.4.3.2.6. Rare minerals and minerals of uncertain origin

Rare finds of apatite were reported in fracture mineralization studied in borehole samples (Carlos et al., 1995-a) and in samples from the ESF (Wilson, 2000 pers. comm.). Wilson also reported the presence of barite formed on the outer surface of chalcedony in one of the ESF samples. A cluster of tiny crystals of gypsum was found by Smirnov and Dublyansky (2001) on the surface of the tridymite crystal (sample 3741, station ESF 27+26). The origin of this gypsum is not clear; it may belong to the secondary mineralization, or, alternatively, it could have been formed recently, during the excavation of the ESF. The latter two mentioned minerals provide some tentative indications that the sulfate form of sulfur played some role in the geochemical system during the deposition of secondary minerals at Yucca Mountain.

Several other minerals were reported from samples of the secondary mineral crusts taken from the ESF and ECRB. Sanidine was found in sample 2201 (station ESF 72+31.3). It forms thin needle-like crystals and sheaf-like aggregates. Sanidine overgrows the vapor-phase tridymite and occurs as solid

inclusions in calcite. Aggregates of sanidine and tridymite are immersed in the calcite matrix. Sanidine occurs as unbroken crystals (no crystal fragments were found). Generally, crystallization of stable sanidine requires very high temperatures, which were not reached either during the diagenesis of the tuffs or during the deposition of the secondary minerals. Most probably, the Yucca Mountain sanidine is a metastable phase, belonging to the vapor-phase alteration stage that was preserved inside the calcite. One noteworthy feature of the secondary mineralization studied in the ESF and ECRB is the absence in the fractures and lithophysal cavities of any significant amounts of smectites and kaoline (see Appendix 3-4-1 for an inventory of minerals found in the vadose zone).

3.4.4. Paragenetic assemblages: compositional, spatial, and temporal interrelationships

As stated earlier in this chapter, we defined a paragenetic assemblage as a set of minerals formed during the same period of time and reflecting the same mineral-forming process. The ultimate goal of the paragenetic studies was to decipher the details of the evolution of the mineral-forming process by studying the spatial relationship between co-genetic minerals.

We repeat the paragenesis definition here in order to avoid confusion with the somewhat different use of the term by other students of the Yucca Mountain mineralogy. For instance, Wilson and Cline (2001) defined the paragenetic study as a determination of “...*the growth history of secondary minerals from across the site*”, whereas Paces et al. (2001) reduced the meaning of the paragenetic analysis to the establishment of the “microstratigraphic framework” of mineral deposition. This approach focuses on the sequence of mineral deposition as it is recorded in the spatial relationships of minerals, but omits the evolution of the physicochemical parameters of the mineral-forming solutions, which governed the history of the mineral deposition.

In the course of our studies we determined that the major minerals of the secondary fracture linings in the ESF are calcite and silica minerals – quartz, chalcedony and opal. In the most studied samples, chalcedony and quartz are the dominant silica minerals, while opal is volumetrically subordinate. We also note that the major assemblage-forming minerals, calcite and silica, are never present in a given sample in similar proportions: one of them is always dominant while the other is subordinate. We define, therefore, two chemically different crystallization environments, expressed as two paragenetic assemblages: one, the silica assemblage in which silica polymorphs are the dominant minerals and, two, the carbonate assemblage in which calcite is the major mineral.

A generalized deposition sequence, based on the observation reported in the previous section is presented in Figure 3-4-20.

Smirnov and Dublyansky (2001) reported a repository-scale zonation relative to the distribution of the silica and carbonate assemblages. The silica assemblage dominates in the eastern part of the repository and is most abundant at the North Portal of the ESF. The carbonate assemblage is present throughout the whole repository block, but absolutely dominates in its western part (see Figure 3-4-13). Relationships between the two assemblages are best seen in the eastern part of the repository block (North and South ramps of the ESF) where both assemblages are well developed. In the western parts of the ESF, where the carbonate assemblage dominates, minerals of the silica assemblage form continuous or discontinuous layers that separate different generations of calcite. We classify the opal that forms rhythmic inclusions in the late-stage calcite as an accessory mineral, because, by the time of its precipitation, the major mineral was calcite and its growth was not interrupted by precipitation of opal (although minor dissolution events did occur at this stage). Noteworthy, in the northeastern part of the ESF, fractures and/or cavities occupied by different assemblages (calcite and the silica) occur near to each other.

Secondary mineral crusts can be subdivided into three general groups:

1. Those composed of the silica assemblage only;

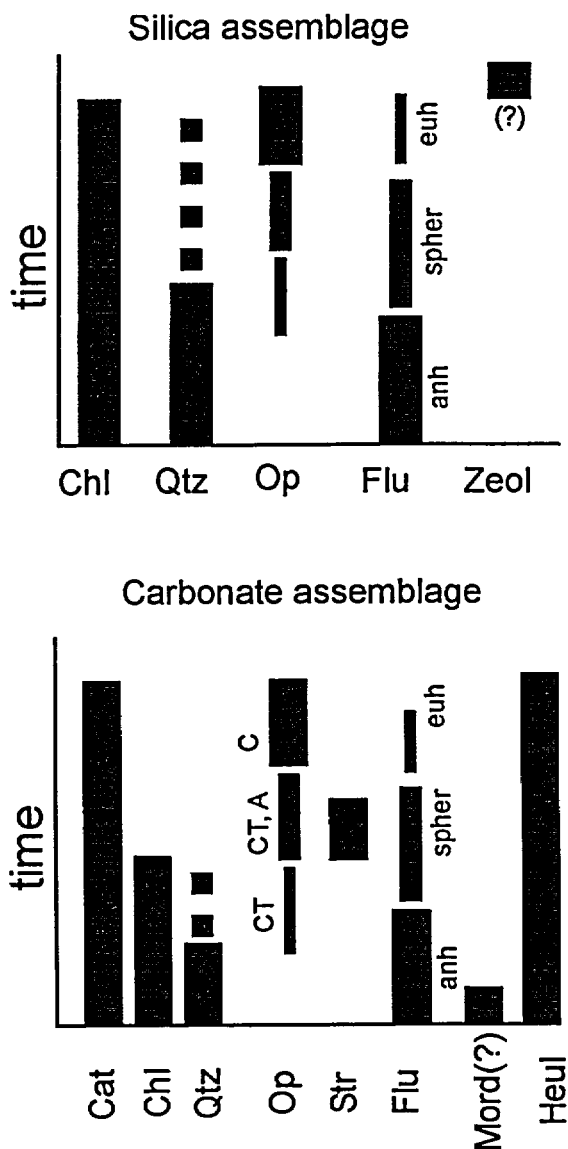


Figure 3-4-20. Generalized scheme of mineral composition and deposition sequences of the silica and the carbonate secondary assemblages of Yucca Mountain. Thickness of the bin reflects changes in relative abundance of the mineral variety (note that thickness of bins should not be compared between different minerals). Breaks indicate that several generations of a mineral might be present.

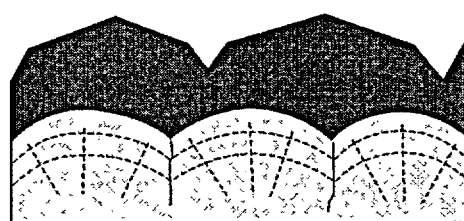
Cat – calcite, *Chl* – chalcedony, *Qtz* – quartz, *Op* – opals (*C*, *CT* and *A* – types of opal), *Str* – strontianite, *Flu* – fluorite (*anh* – anhedral, *spher* – spherulitic and oolitic, *euh* – euhedral), *Zeol* – zeolites, *Heul* – heulandite, and *Mord(?)* – mordenite.

2. Those composed of the carbonate assemblage only; and
3. Those composed of both assemblages.

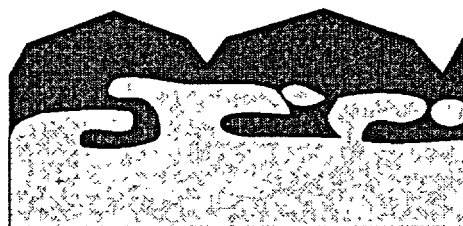
The crusts of the third group typically have a zoned texture. Smirnov and Dublyansky (2001-*a*) concluded that there is no single universal sequence or pattern of transition between the silica and the carbonate assemblages. This means that the minerals of the carbonate assemblage may overgrow those of the silica assemblage and, conversely, minerals of the silica assemblage may overgrow those of the carbonate assemblage. This observation is at variance with the opinion of Wilson and Cline (2001), who concluded that the secondary mineral parageneses across the repository block evolved in a consistent manner. We define two types of interrelationships between the silica and the carbonate assemblages within individual crusts: overgrowth and intercalation (Figure 3-4-21). Overgrowth is characterized by sharp boundaries between zones composed of silica and carbonate. The term intercalation describes a gradual transition from one assemblage to another with alternating layers and patches of calcite and silica minerals.

3.4.4.1. Relationships between assemblages

Figure 3-4-22 demonstrates that solubilities of calcite and silica have opposite dependencies on pH that persist throughout the whole range of temperatures expected for the Yucca Mountain secondary mineralization. The interplay of temperature and chemistry of the fluid (expressed through pH) causes a preferential deposition of either the silica or the carbonate assemblage. This is a logical explanation for the separate deposition of the silica-dominated and the calcite-dominated assemblages. However, at certain stages of the mineral crust formation, particularly at the final stage, conditions existed that favored coprecipitation of calcite and silica. According to the fluid inclusion data and isotopic studies, the late Mg-enriched calcite typically associated with opal was formed at temperatures of less than approximately 35-50°C. At these temperatures amorphous silica and calcite have comparable



a.



b.

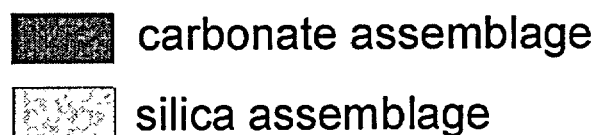


Figure 3-4-21. Two types of interrelationships between the silica and the carbonate assemblages in individual crusts: *a* – overgrowth; *b* – intercalation.

solubilities within the pH range from 7.5 to 8.0 (see Figure 3-4-22). Variations of pH in the system, tends to shift the equilibrium toward the preferential precipitation of either calcite or opal. The role of the temperature is more complex because it affects both the mineral solubility and the pH. The interplay of these two parameters may lead to the co-precipitation of the two minerals, as well as to the dissolution of one mineral preceding the deposition of the other. The consequences of the interplay between these parameters are observed in the complex interrelationships between the calcite and the opal in different crusts. Apparently, variations of pH were greater at higher temperatures (which is expressed as the deposition of chemically different assemblages), whereas at lower-temperature stages these variations were less intense, leading to the alternating deposition of calcite and silica minerals.

3.4.4.2. Repository block-scale and mineral crust-scale zonation of secondary mineralization

The repository block-scale zonation with respect to the distribution of secondary mineralization found in the ESF, i.e., the predominance of silica minerals in the eastern part of the block (close to the horst-bounding Paintbrush fault) and the predominance of calcite in the western part of the ESF (central part of the block) is quite uncommon for meteoric water deposits, but is typical for hydrothermal fields (so-called lateral zonation). It is to be noted that besides mineralogy, a similar trend is exhibited by a number of other geochemical parameters, e.g. maximum temperature of paleo fluids (determined by fluid inclusions, see Chapter 3-6), $\delta^{18}\text{O}$ in calcite (see Chapter 3-5), as well distribution of U, Th and Pb in silica minerals (see Chapter 3-7). The co-variation of these independently determined parameters allows us to conclude that the observed lateral zonation is real rather than apparent.

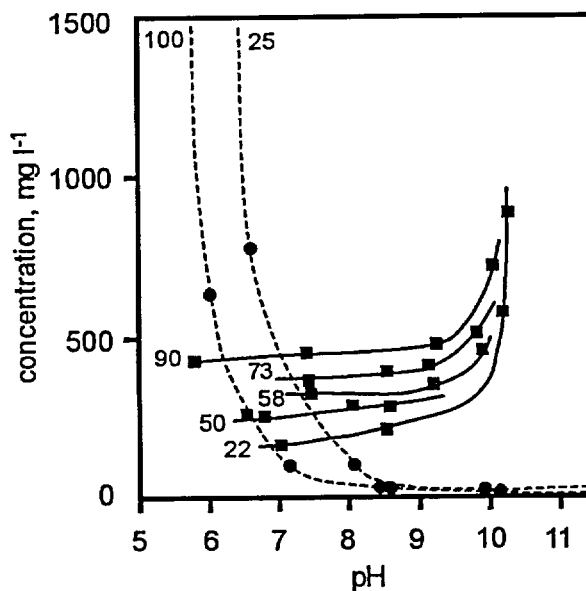


Figure 3-4-22. The temperature and the pH control of the solubility of calcite (*dashed lines*) and amorphous silica (*solid lines*) in water. Solubility of calcite was calculated from the solubility constant. Numbers at the curves show the temperature in °C. Solubility of amorphous silica is from the experimental data by Okamoto et al. (1963).

The Yucca Mountain Project researchers speculated that the observed differences in the compositions and the temperature of formation of the ESF minerals may reflect vertical rather than lateral zonation (Whelan, 2000, pers. comm.). This contention is based on the fact that the north and south ramps of the ESF have a west inclination, whereas the surface of the Yucca Mountain dips eastward. The ESF

ramps, thus, intersect stratigraphically higher Tiva Canyon tuffs near the portals, whereas the western parts of the ramps and the north-south drift run within the stratigraphically deeper Topopah Spring tuff. The depth from surface increases from the portals toward the north-south drift, reaching 250-280 m in the deepest part of the ESF.

We do not know of any evidence supporting the vertical zonation interpretation; in fact most of the evidence available to us argues against it. First, we do not see a reasonable explanation why silica minerals would be more abundant near the Earth's surface and become less abundant with depth, whereas the calcite does the opposite. Thermodynamic modeling (Palyanova et al. 2002, and Chapter 3-2) predicts exactly the opposite sequence of deposition for hypothetical fluids percolating from the topographic surface downward. Second, surficial calcretes, identified by the USGS researchers as the source of calcium carbonate for the subsurface calcite deposits, are much more abundant and voluminous at the base of the Yucca Mountain eastern slope (near the North Portal of the ESF); their abundance decreases significantly toward the ridge top of Yucca Mountain and the calcretes are practically absent on the steep western slope of the mountain. Thus, if the calcretes were indeed the source of the calcite in the ESF, one would expect to see abundant calcite near portals and much less calcite in the north-south drift and the ESF, located under the Yucca Mountain crest and western slope. The actual distribution of calcite and silica minerals is the opposite (see Figure 3-4-13).

The small-scale zonation described for individual mineral crusts indicates that, beside large-scale lateral variations in the chemistry of fluids, there have been temporal variations. Similar to the mountain-scale zonation, mineralogical and textural trends within individual crusts are accompanied by a systematic change in isotopic properties of calcite (see Section 3.5.2.). Except for the very latest calcite, this zonation is unidirectional rather than cyclic. Neither of these zonations, in our opinion can be rationally explained by the climate-induced changes in the chemistry of meteoric waters, as it would be required by the "rainwater" concept.

3.4.5. Mechanisms and history of secondary mineral deposition based on the textural evidence

Observations presented in the preceding sections serve as a basis for deciphering the mechanisms of deposition of the secondary minerals in the Yucca Mountain vadose zone.

3.4.5.1. Textures: key to deciphering the history of calcite deposition

The mechanism and the history of calcite crystallization is the major issue in debates regarding the origin of secondary minerals in the vadose zone of Yucca Mountain. Mineral textures change in response

to changing conditions of growth; these textures, therefore, can provide valuable information as to the mode of formation of the minerals. A summary of the characteristic sequences of the morphologic change in calcite crusts from the ESF is shown in Figure 3-4-23.

In many cases mineral crusts are built up of calcite having a single, simple morphology, e.g., granular, or blocky, or platelet (Figure 3-4-23 *a*, *d*, and *g*). The more-complex sequences are observed in thick crusts residing in lithophysal cavities. The typical sequence there comprises granular calcite at the base and blocky in the outer zones; bladed calcite may be present between these two morphologies (Figure 3-4-23-*a* through -*c*). In places, granular calcite is absent at the base and bladed calcite grows directly on the tuff substratum (Figure 3-4-23-*d* through -*f*). Blocky calcite nucleates at the tips of blades or platelets to form scepters (Figure 3-4-23-*b* and -*e*); at advanced stages crystals in such aggregates acquire blocky morphology (Figure 3-4-23-*c* and -*f*), preserving in the cores, a zonation typical of bladed crystals. This textural diversity indicates that the conditions of calcite growth have not been uniform through the time of crystallization.

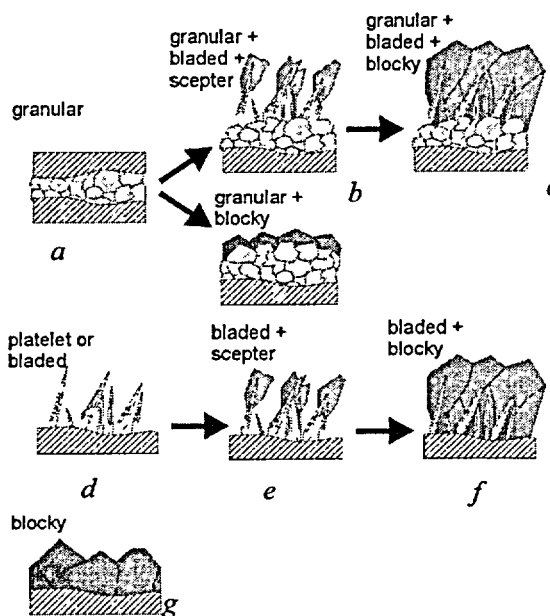


Figure 3-4-23. Typical patterns of the morphological change in the Yucca Mountain calcite crusts. Note that patterns involving platelet and bladed morphologies (*b*, *c*, *d*, *e*, and *f*) are spatially restricted to the north-central part of the repository block (see Figure 3-4-7).

Granular texture indicates that a large number of crystals nucleated and started growing virtually simultaneously. Such growth patterns indicate there was not enough free space in the zone where the crystals grew so that euhedral crystals could not form and anhedral crystals formed instead. Only the outermost crystals of the granular aggregates in cavities and fractures acquired crystallographic shapes. In contrast to granular calcite, the number of nucleation events that occurred at the inception of blocky and platelet crystals was relatively small, so that the forming crystals had enough free space to develop crystallographically defined faces.

The transition from granular to blocky/platelet morphology within an aggregate thus indicates the change in the nucleation rate (the number of nuclei forming in a unit of volume per unit of time). The nucleation rate is closely related to supersaturation in the system (Chernov et al., 1980). For crystallization, which proceeds in aqueous solutions at temperatures in excess of 20°C, the nucleation rate

increases with increasing supersaturation. This implies that in order to produce complex textures, such as those shown in Figure 3-4-23-*b*, -*c*, -*e*, and -*f* for example, the mineral-forming solutions must have experienced significant changes in their saturation states. A consistent overall pattern of textural changes, i.e., transition from granular through (in some samples) platelet/bladed to blocky euhedral textures, may be interpreted as indicating an overall decrease in the degree of supersaturation that accompanied the mineral growth. The systematic unidirectional overall character of the textural change, as well as the repository-scale textural zoning (restriction of the bladed calcite to the north-central part of the repository block) suggest that the change was caused by the overall evolution of the mineral-forming system (i.e., at a minimum on the spatial scale of the repository block), rather than by some local (cavity- or fracture-scale) controls, as Whelan et al. (2001) have suggested. This inference is further supported by the systematic unidirectional change in isotopic properties of calcite in mineral crusts, with calcite crystals of different morphologies showing similar patterns of change in isotopic properties (see Section 3.5.2.). The pattern suggests that crystals with different morphologies may be syngenetic. This inference is in complete contrast with conclusions made by Whelan et al. (2001) who believe that "*The observed mineralogical and paragenetic variability may reflect local depositional controls, such as ease of evaporative concentration of fluids, rather than chemical or temporal differences in fluid input.*"

It might be inferred that the simultaneous (or nearly simultaneous) growth of calcite crystals in different parts of the repository block occurred at substantially different supersaturations and thus acquired different morphologies. Such significant differences in supersaturation would also require significant differences in either the chemistry or temperature of the fluids. Substantial temperature gradients and supersaturations are typical of thermal solutions. Such gradients, however, cannot be accounted for in the hypothetical case of meteoric fluids percolating through the vadose zone.

3.4.5.2. Pinacoidal calcite

A very peculiar feature of the secondary calcite at Yucca Mountain is the abundance of crystals with well-developed pinacoidal faceting. Pinacoid is a pair of crystal faces oriented perpendicularly to the three-fold axis. This crystallographic form is not typical of calcite crystals formed in the vadose zone (e.g., Onac, 1997). It is not very common in hydrothermal associations, either, since the development of pinacoidal morphology requires specific environments. Experiments by Ikornikova (1975) on hydrothermal calcite growth have demonstrated that three parameters control the appearance of the pinacoidal morphology: the pressure of the CO₂, the alkalinity, and the content of LiCl.

Chlorides of lithium are not expected to be present in the geochemical system of the Yucca Mountain waters and were not observed in the course of the fluid inclusion studies (Dublyansky et al., 2001). Thus, the LiCl control of the pinacoidal morphology may safely be ruled out. In experiments by

Ikornikova, the rhombohedron was a stable morphologic form at CO_2 pressures less than 250 bar; pinacoid began to develop at CO_2 pressures of ~ 250 bar and become a dominant morphology at 300-350 bar. Such high pressures, corresponding to 3000 to 3500 m of hydrostatic pressure do not seem to be plausible for the geologic setting of Yucca Mountain. Thus, at this point we have to admit that the reason(s) of such abundant appearance of the pinacoidal morphology remain(s) unclear.

3.4.5.3. The relationships between platelet and blocky morphology

High supersaturation at elevated CO_2 pressure would result in vigorous nucleation should the total pressure in the system be released (e.g., as a response to the vibratory motion during an earthquake). Granular calcite would crystallize at this stage. Nucleation of calcite and removal of CO_2 from the system (e.g. through effervescence of gas bubbles) would decrease the overall supersaturation with respect to calcite. The latest calcite crystals would, therefore, acquire blocky (rhombohedral) morphology. If the elevated pressure of CO_2 in the system is not released for

some time (i.e., there is no degassing), platelet and blade-shaped crystals may form. As we noted above, the bladed morphology is determined by preferential growth of a crystal along one selected crystallographic direction. The bladed crystals, therefore, are similar to the skeleton crystals. The skeleton growth is realized only at high growth rates and high supersaturations, which is consistent with a model, which provides for the release of CO_2 at high pressure. The resulting decrease in the pressure of CO_2 caused by crystallization of the calcite would induce a transition from platelet and bladed into scepter and, finally, blocky morphologies, as shown in Figure 3-4-23-*b*, -*c*, -*e*, and -*f*.

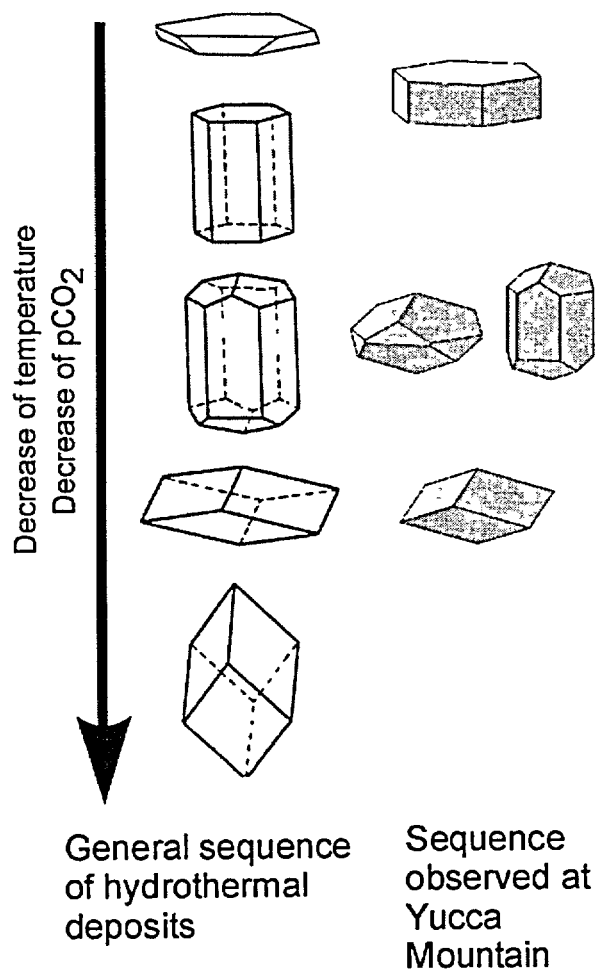


Figure 3-4-24. Morphological sequence of Yucca Mountain calcite compared to general trend of habit change reported for hydrothermal calcite. Compiled from (Kalb, 1929; Sunagawa, 1953; Aliev, 1966; and Ikornikova, 1975)

As it will be discussed below, the crystallization of late blocky calcite may reflect a substantial change in the chemistry of the mineral forming solution, which is reflected by the increase in Mg content as well as co-precipitation of opal. In those cases where blocky calcite is not associated with opal, its growth is caused, most probably, by decreasing CO₂ pressure.

It is well known that the vadose-zone calcite crystals growing in the ambient-temperature caves (speleothems) have a characteristic rhombohedral (with dominant sharp rhombohedron $\phi\{02\bar{2}1\}$) and scalenohedral morphology (Onac, 1997). Climate change or other variations of growth-controlling parameters are not known to cause substantial changes in crystal morphology of the calcites. By contrast, the calcite from Yucca Mountain exhibits a transition from platelet crystals with dominant pinacoid to the rhombohedral and prismatic crystals. Many researchers described the existence of such a morphologic sequence as a typical sequence found in hydrothermal deposits from around the world (e.g., Kalb, 1929; Sunagawa, 1953; Aliev, 1966). The morphologic trend shown in Figure 3-4-24 is thought to be a response to decreasing CO₂ pressure and the temperature (Krasnova and Petrov, 1997).

3.4.5.4. Sequence and mechanism of silica deposition

The major difference between silica and calcite minerals within individual crusts is the degree of their structural order. The ordering decreases according to the following sequence: quartz → chalcedony → opals. Among microcrystalline opals, structural ordering decreases from disordered cristobalite (lussatine or opal-CT) through lussatite or opal-C (indicating a high degree of the inter-stratal disordering), to A-opals (Graetsch, 1994). At Yucca Mountain, minerals of the silica assemblage form a sequence in which the structural order decreases with time (see Figure 3-4-20).

Most accessory silica minerals from the carbonate assemblage follow the same pattern. When all silica minerals are present within the same crust, chalcedony and quartz always crystallize earlier than opals. When only opals are present in the sample, the opal-CT, having a more fibrous texture, is typically located micro-stratigraphically deeper than the less-fibrous opal-C. Opal A, however, does not seem to follow the general pattern. In a number of samples it was forming earlier than some opal-C.

The spherulitic appearance is the most important feature of the majority of the secondary silica minerals at Yucca Mountain. Even when quartz forms relatively large crystals, they are combined into radially branching drusy clusters. According to Keith and Padden (1963), spherulitic textures are indicative of high supersaturation, high concentration of impurities, and low viscosity of fluids. This happens when the crystal growth rate substantially exceeds the diffusion rate (Keith and Padden, 1963; Cahn, 1967), which is typically observed in strongly supersaturated fluids. The accumulation of impurities at the growth front at high supersaturation further decreases the diffusional supply of matter and leads to the splitting of crystals and the formation of radiating textures. The presence of foreign

particles further facilitates the formation of spherulites. Godovikov et al. (1987) suggested that a spherulitic texture of chalcedony is indicative of crystallization from a supersaturated diluted colloidal solution. Grigoryev (1961) demonstrated that the spherulite growth is only possible in the submerged within parental fluid state to allow for the uniform bulk diffusion to its surface.

3.4.5.5. Colloids in the Yucca Mountain mineral forming system

Colloids exist as extremely disperse systems, intermediate between true (ionic) solutions and coarse disperse systems (suspensions and emulsions). The sizes of colloidal particles range from several nanometers to several hundred, or from 10^{-9} to 10^{-6} m (Bergna, 1994). Colloidal particles, therefore, are much larger than most inorganic molecules and ions, which have characteristic sizes of $<10^{-9}$ m (or <10 Å). For comparison, while the atomic mass of a molecule of silica is 55, the typical mass of a single particle of silica gel is about 50,000 (Chukhrov, 1955). The sizes of colloids are comparable to the sizes of crystal nuclei. In many cases, nuclei of micelles are represented by nanocrystals (e.g., clay colloids) or by aggregates of amorphous particles. It has long been recognized that under proper conditions virtually any substance may form a colloidal solution (Veimarn, 1906; Khmel'nitsky, 1988).

One important property of colloidal particles is their electrical charge. The same charge prevents similar colloidal particles from coalescing; conversely, the loss of this charge facilitates coagulation and the ensuing precipitation of colloidal particles. The charge of the same colloidal particles may be different in different fluids. For example, colloidal silica has a negative charge in acidic waters and a positive charge in alkaline waters (Chukhrov, 1955).

Colloids are well-recognized agents of mineral formation, particularly (but not exclusively) in the near-surface environment. They are common in low-temperature hydrothermal environments where they typically occur in the final stages of evolution of hydrothermal systems. Mineral colloids (silica, clay, fluoride, etc.) and gels were found in a variety of hydrothermal systems (e.g., Chukhrov, 1955; Lebedev, 1975, 1979). Silica and its derivatives (silicates) are among the most common natural colloid-producing chemicals. Gels of silica are known to be a parent medium for opals; a typical representative of such natural gels is A-opal. If silica transported in colloidal form enters a carbonate environment the latter serves as an efficient geochemical barrier, which causes coagulation of colloids and the precipitation of silica.

3.4.5.5.1. Textures indicative of the colloidal mineralization

The deposition of matter from colloidal solutions typically occurs through coagulation, i.e., the coalescent growth of smaller colloidal particles, and the precipitation of large particles under the force of gravity with the formation of an amorphous precipitate. The latter may subsequently become compact and crystallize. As early as the end of the 19-th century, it was demonstrated that crystalline minerals could

form from diluted colloidal solutions. Chrustschoff (1887) synthesized crystals of quartz from the sol of silica at 250 °C. Gels also represent a good crystallization medium, in which macroscopic crystals can form. These crystals may become large and perfectly shaped as the crystals grow from ionic solutions (Henisch, 1970), but they may trap abundant gel particles, which give these crystals a muddy or milky appearance. A spherulitic morphology is common for crystals formed in gels. Such morphology is explained by the crystallization in a supersaturated and relatively viscous medium (Keith and Padden, 1963) where the supply of matter occurs through diffusion (Grigoryev, 1961). Coagulation of colloidal particles in gels may produce massive cryptocrystalline or spherulitic aggregates. After precipitation, coagulated particles may continue to grow through the supply of material from ionic solution, or they may serve as nuclei for the crystallization of other minerals.

Two major factors controlling the textures of colloidal deposits are gravity and bulk diffusion. Colloidal crystallization produces massive aggregates or layers of near-spherical particles with concentric zonation or spherulitic structures. Crystals formed in gels may form porphyric textures, because in the course of growth, these crystals are suspended in a gelatinous medium.

3.4.5.5.2. Evidence on the colloidal mineralization at Yucca Mountain

Our observations and evaluation of the available data have led us to conclude that mineral-forming processes at Yucca Mountain occurred, at least partly, in presence of the colloidal solutions. Colloidal solutions, even dilute ones, may lead to substantial changes in the pattern of mineral deposition, and, more importantly, in the patterns of the uptake of minor- and trace elements. The latter elements, particularly U, Th and Pb are very important in the context of the Yucca Mountain geochemistry, since isotopes of these elements are used for geochronologic purposes (U-²³⁰Th and U-Pb methods of dating). Recognition of the presence of colloidal solutions, therefore, may prove important in interpreting the results of the geochronologic studies (see Chapter 3-7). Below we summarize the evidence regarding the presence of colloids in the mineral-forming system at Yucca Mountain.

Natural colloids have long been known in rhyolitic tuffs at Yucca Mountain. Natural gels of silica, smectite, and zeolites filling pores and fractures in tuffs were first studied at Yucca Mountain and Rainier Mesa by Levy (1992). Chepizhko and Dublyansky (1995) reported partly- to completely solidified mineral gels in fractures of Rainier Mesa tuff in Trench 14 on the eastern slope of Yucca Mountain. Some peculiar textures described for secondary minerals from the ESF also suggest crystallization in the presence of colloidal solutions. Figure 3-4-25 shows several examples of the colloform textures.

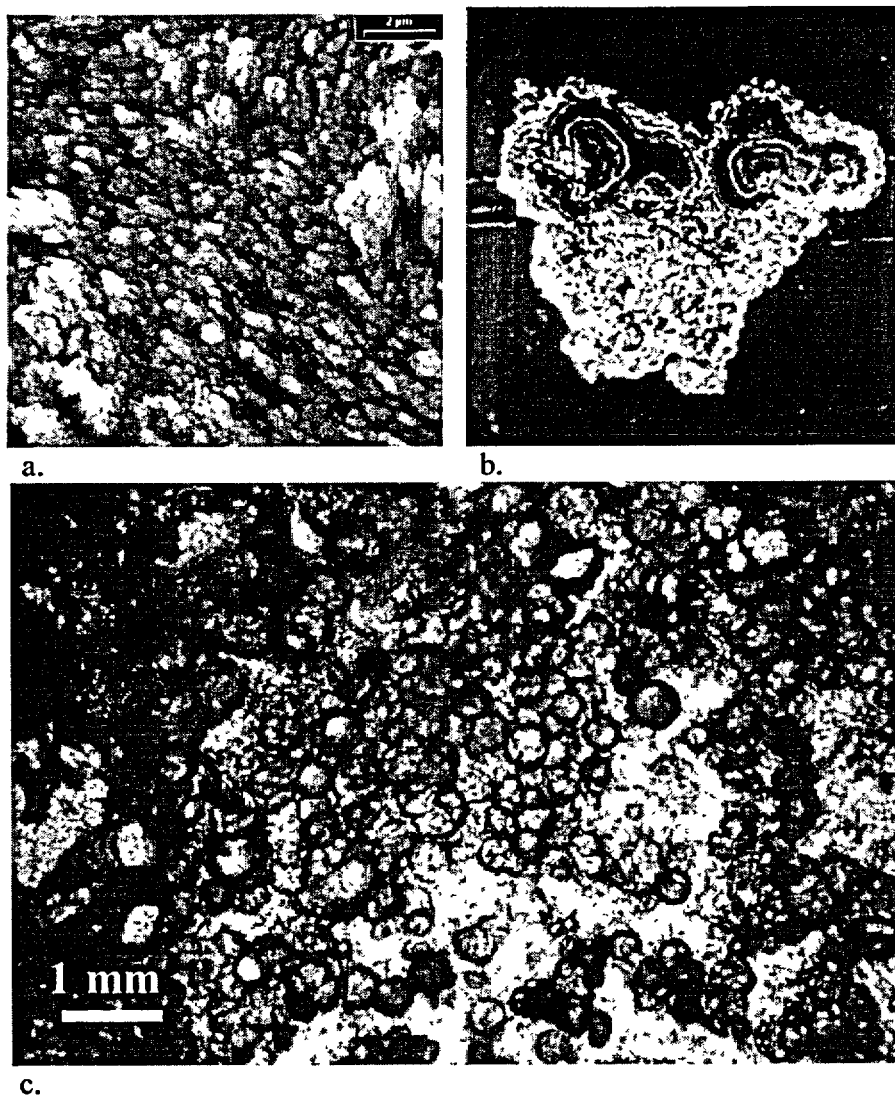


Figure 3-4-25 Mineral textures indicative of the crystallization in the presence of colloidal solutions. *a* - chalcedony/opal fibers composed of spherical particles $< 1 \mu\text{m}$ in size; *b* - oolitic character of fluorite; and *c* - aggregate of spherical chalcedony particles embedded in massive chalcedony.

A SEM image in Figure 3-4-25-*a* shows that fibers of chalcedony/opal spherulites are built up of tiny spherules with characteristic sizes less than $1 \mu\text{m}$. These particles are in the size range typical of colloidal particles. Colloform aggregates of fluorite (ESF station 12+12.05 and other parts of the tunnel) are composed of oolites (Figure 3-4-25-*b*). The silica layers always consist of spherulites of chalcedony and/or CT-opal. The spherulitic textures are also typical of the latest C-opal.

Irregularly distributed spherulitic particles are occasionally found embedded in massive chalcedony (Figure 3-4-25-*c*). These textures are interpreted to be a result of precipitation of coagulated particles and

their subsequent growth in porous gelatinous aggregate until the interstices are filled by silica, precipitated from synergetic liquid.

Calcite crusts in the northwestern part of the ESF sometimes host inclusions of A-opals. These opals typically have a gel structure, e.g., a voluminous disordered framework of silica particles (Graetch, 1994).

In order to produce characteristic colloform textures, colloidal particles must be given sufficient time for coagulation, sedimentation, and aggregation. This requires hydrologic conditions with a very low-level dynamic. Since the colloidal particles are relatively large it is extremely unlikely that such particles can be transported by films of water and colloform deposits formed from films of water. We are not aware of any reported examples of such a process. Quite the opposite, published studies of mineralization produced by natural colloids emphasize the stagnant character of waters in cavities where colloidal mineral deposition takes place (e.g., Mozgova, 1963).

Another indication of the colloidal nature of opals at Yucca Mountain is the elevated amounts of uranium hosted by these opals. Data reported by Paces et al. (1996) and Neymark et al. (2000 and 2002) indicate that opals from the ESF typically contain between 50 and 280 ppm U, whereas the contents of U in co-genetic calcite range between <0.01 and 0.5 ppm. Thus, opals demonstrate a substantial concentration of uranium relative to the co-genetic calcite. This topic will be discussed in more detail in the section 3.4.6.4.7 below.

3.4.5.6. The history of accessory mineral deposition

In the previous section we pointed out that fluorite is a genuine member of the secondary mineralization of Yucca Mountain. As in the case of calcite, the diversity of crystal morphologies of fluorite indicates that the environment of crystal growth evolved substantially during the formation of the fluorite-bearing crusts. Systematic unidirectional progression from anhedral crystals to spherulites and finally to euhedral crystals suggests that the overall evolution of the growth environment was similar on the spatial scale of the repository block. The character of the morphologic sequence indicates that the mineral forming solutions were substantially supersaturated with respect to fluorite. The degree of supersaturation gradually diminished with time, leading to the morphological evolutionary trend similar to one described for calcite. This trend is expressed through the decrease in the rate of nucleation (anhedral fluorite → spherulites), and the subsequent decrease in the crystal growth rate (spherulite → euhedral fluorite).

Fluorite spherulites commonly possess allogenic cores, composed of silica minerals and oolitic segregations. This indicates that the mineral forming fluid contained substantial amounts of chemical and

particulate impurities, which are known to foster the splitting of crystals. Oolitic segregations commonly form in relation with the coagulation and sedimentation of colloids. Euhedral fluorite crystals that overgrow oolitic aggregates crystallize from an ionic solution, which may represent the residual solution after the removal (precipitation) of the colloidal fluorite.

The data of Carlos et al. (1995-a) strongly suggest that a number of episodes of zeolite deposition took place during the formation of secondary minerals. This inference is supported by the data on K-Ar ages presented by WoldeGabriel et al. (1993). The chemistry of fluids, from which zeolites precipitated varied significantly and showed a gradual decrease in Sr and Ca contents, as well as an increase in Mg contents (see Section 3.1.4.7. for details).

3.4.5.7. Scepter morphology

Scepter morphology is a characteristic feature of two major secondary minerals at Yucca Mountain, calcite and quartz. Such morphology indicates a significant change in the conditions of crystal growth (Krasnova and Petrov, 1997). In most instances, scepter crystals represent two different stages of a mineral-forming process that are divided by a hiatus. This is not the case, however, for the Yucca Mountain secondary minerals. We were unable to identify any traces of the interrupted growth between “stems” and “heads” of scepter crystals. This means that the conditions of the growth had significantly changed within a single growth event.

3.4.5.7.1. Scepter calcite

Ontogenetic reconstruction of the process of growth of the scepter crystals has led us to two important inferences. **First**, a drastic change in the growth rate anisotropy is required in order to produce the drastic change in the pattern of growth “recorded” by the changing crystal morphology. Such change can only be caused by an equally drastic change in the conditions of mineral deposition. **Second**, preferential growth of the crystal edges in scepter heads, reflected in the “swallow tail” morphology, indicates that the process of the growth was controlled by diffusion. As we discussed at the beginning of this chapter, the diffusion-controlled growth of skeletal and dendritic crystals is only possible if the crystal growth rate exceeds the rate of the diffusional supply of the matter. This in turn requires elevated supersaturations and/or the absence of an effective mixing of the fluid.

Crystallization of the scepter calcite is associated with the transition from the pinacoidal habit to the rhombohedral one (see Figure 3-4-6), which constitutes a characteristic feature of the calcite growth in the Yucca Mountain vadose zone, as well as a typical feature of hydrothermal calcite in general (see Figure 3-4-24). The late stages of scepter crystallization occur at low supersaturations. This suggests that the absence of effective mixing along with a sharp drop in supersaturation, rather than high growth rates, were responsible for the scepter morphology.

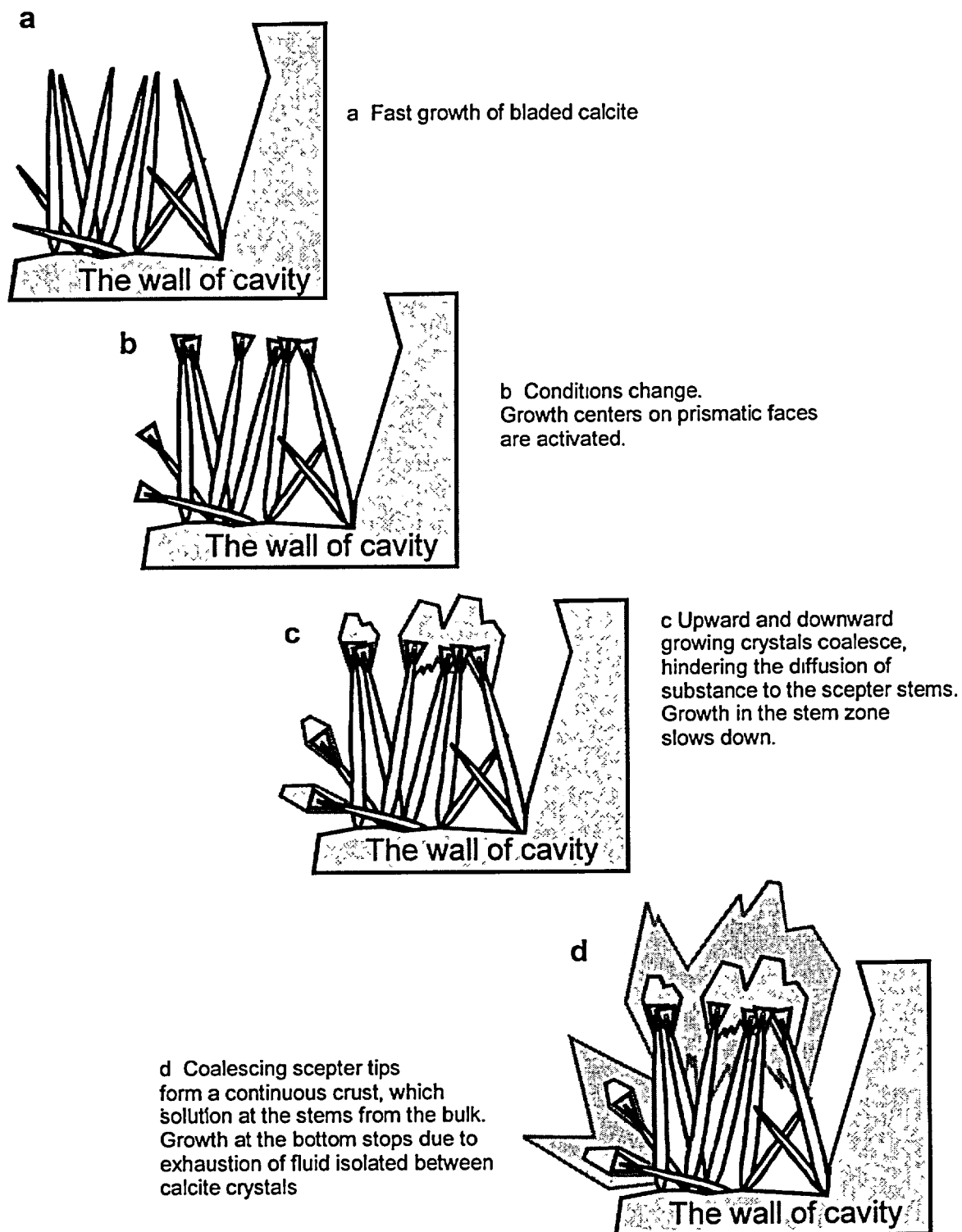


Figure 3-4-26. A conceptual model of the development of scepter aggregates in the lithophysal cavities and low-angle fractures in the Yucca Mountain vadose zone.

One important observation, in this regard, is that the scepter heads are best developed in those crystals that are located close to each other. In the less-densely spaced crystals, their whole surface may be re-grown. A model of the formation of scepter crystals is presented in Figure 3-4-26. The model requires a complete submergence of the crystalline aggregate in fluid during the entire time of its formation.

Figure 3-4-26-*a* shows the first stage in the stage of formation of the blade shaped crystals. Such crystals may grow over the vapor-phase alteration minerals or on the earlier granular calcite. The growth occurs at high supersaturation. The growth of the scepter crystal heads (Figure 3-4-26-*b*) begins without a hiatus and reflects a decreasing supersaturation of the fluid. This may be related to the decrease of CO₂ pressure and decrease of temperature, as well as the increase in the Mg content in the solution. Increasing contents of Mg slow down the calcite growth and may eventually completely stop it (Zhang and Dawe, 2000). The introduction of the Mg into the system also lowers the solubility of silica, and the relatively high ionic strength of the Mg-salt solutions promotes the stabilization of colloids. This explains both the change in the morphology of calcite and the co-precipitation of opal.

A further decrease in the growth rate leads to a transition from the tabular to the rhombohedral morphology and a change in location of the inception points of the growth layers. At this stage the inception of new layers takes place on the prismatic faces or on the edges of the blades. The character of growth anisotropy also changes: the three-fold axis becomes a preferred growth direction, so that the growth along the blade proceeds slower than perpendicularly to it. Consequently, the scepter tops of the crystals coalesce (Figure 3-4-26-*c*), hindering the diffusion exchange between the fluid at the bases of crystals and the bulk of the fluid. The fluid at the bases soon becomes depleted and the growth on the blade surfaces ceases.

In the advanced stage of growth (Figure 3-4-26-*d*), crystal heads may form continuous crusts of blocky crystals. When the aggregate of the bladed crystals is not dense, the developing scepter heads fail to merge fast enough so that the whole surface of the blades experiences re-faceting and the developing crystals may acquire the shape of single rhombohedrons.

3.4.5.7.2. Scepter quartz

Scepter morphology of quartz crystals reflects the transition from the long-prismatic form to the short-prismatic one. Such gradation toward the isometric shapes may also be related to decreasing supersaturation. The mechanism of the scepter growth of quartz crystals involves the inception of growth layers near the crystal tips and a slowing down of their development as they propagate toward the base of the crystal. Growth layers come to a complete stop forming terminal steps well before they reach the base of the crystal (see Figure 3-4-15).

Scepter morphology of quartz crystals also indicates a non-uniform supply of matter for crystal growth controlled by diffusion. The location of quartz crystals on ceilings of cavities and on hanging walls of fractures indicates that matter was supplied from the bulk of the fluid with the overall flux of the matter directed toward the walls of the voids. Such a growth mechanism may be realized only in cavities completely filled with fluid.

Summarizing, the scepter morphology of both major minerals of the Yucca Mountain secondary assemblages, calcite and quartz, provides unequivocal evidence of their growth in the submerged state by a diffusion-controlled mechanism. Importantly, the development of the scepter crystals conforms to the overall pattern of the morphologic change established for the textures of the calcite crusts. Thus, we believe that samples containing the scepter calcite represent a special case within the general pattern of the evolution of the calcite morphology, rather than the most complete expression of this evolution, as Paces et al. (2001) and Wilson and Cline (2001) seem to believe.

3.4.5.8. Mineralogic and textural evidence: Summary

Secondary mineralization in the Yucca Mountain vadose zone is represented by macro-crystalline drusy and spherulitic aggregates composed of calcite, quartz, and chalcedony with subordinate amounts of fluorite, zeolites and opals. The minerals form two clearly distinct assemblages with carbonate and silica compositions. The spatial distribution of these two assemblages within the ESF block is zoned with the silica assemblage dominating in its eastern part and the carbonate assemblage in the western part.

Ontogenetic observations have demonstrated that the minerals are mainly formed from concentrated (substantially supersaturated) aqueous solutions. Massive spherulitic aggregates, as well as the presence of euhedral mineral inclusions of accessory fluorite within major minerals suggest homogeneous nucleation in the bulk of the solution, which corroborates an inference regarding high supersaturations.

The morphologic trends observed for both major minerals and accessory fluorite indicate that the supersaturation of the mineral-forming fluids was decreasing, either gradually or abruptly, with time. The chemistry of the mineral-forming fluids also changed causing a sequential deposition of minerals of the two different assemblages.

A comparison of the established features of the Yucca Mountain secondary mineralization (i.e., the set of the typomorphic minerals, as well as the character of the mineral individuals and aggregates) with the typical characteristics of minerals forming within supergene and hypogene processes (see Table 3-4-1) makes it apparent that these features are most compatible with a low-temperature hydrothermal origin of the studied assemblages. The observations discussed above serve as a basis for the formulation of a hypothesis describing the origin of the Yucca Mountain secondary mineralization.

3.4.6. Discussion: Alternative models of mineral deposition

We acknowledge that the morphology of crystal aggregates, combined with their nearly exclusive appearance at the cavity floors and their absence from the cavity ceilings, makes the Yucca Mountain vadose zone deposits a truly unique mineralogical curiosity. We are not aware of any descriptions of similar deposits in the mineralogical literature. The Yucca Mountain Project scientists seem to share, at least in part, this opinion: "*The bladed calcite textures along with the presence of opal on crystal extremities ... are uncommon with respect to UZ [unsaturated (vadose) zone] calcite deposits in other environments.*" (Paces et al. 2001, p. 66). Apparently, this must reflect a very special environment involving particular mineral forming and crystalline growth processes. How this unusual environmental setting, that does not seem to have a strict analog among deposits studied by mineralogists, may be characterized is the subject of our next topic.

3.4.6.1. "Rainwater" concept

The Yucca Mountain Project scientists believe that this setting can be described as a crystallization produced from thin gravity-driven films of water moving along connected fractures from the surface to sites deep within the vadose zone (U.S. DOE, 2001). Such an environment, however, is not unique. In fact, it is rather common. Different types of cave deposits (speleothems) in hundreds of thousands of karst caves known on all continents are formed from gravity-driven water films (see e.g., Hill and Forti, 1997). The Yucca Mountain Project researchers attribute differences in the Yucca Mountain minerals crusts to the difference in the mineral growth rates. Paces et al. (2001) suggested in this regard: "*... rates of mineral growth are very different between deposits in the UZ environment at Yucca Mountain and in karst environments. The growth rates reported by Hill and Forti (1997, p. 286) commonly range from millimeters to centimeters of mineral per year. The slowest reported karst growth rates ranged from 0.007 to 0.042 mm/yr, which are more than three orders of magnitude greater than growth rates estimated from UZ calcite at Yucca Mountain.*" (p. 66). Setting aside, for the moment, our reservations regarding the estimates of the growth rates based on the radiometric dating of the Yucca Mountain samples (this issue will be discussed in detail in Chapter 3-7), we would, nevertheless, state that the proffered explanation does not appear satisfactory to us.

If it is presumed that the overall environment of mineral deposition in karst caves and in cavities of Yucca Mountain was the same (i.e., open space filled with air; water films flowing on the fracture and cavity surfaces; crystallization of minerals from the films, etc.) and, nevertheless, mineralization in the Yucca Mountain cavities is drastically dissimilar to the mineralization typical of the karst caves, an explanation must be provided as to what specific parameters of the environment were responsible for the

dissimilarity. The alleged "slow growth" does not serve the purpose, because it entails an immediate question: What were the parameters of the environment, then, that caused these abnormally low growth rates at Yucca Mountain?

Importantly, the parameters (or boundary conditions) of all processes involved in the hypothetical mineral growth from thin water films can be constrained by assigning them geologically (or physically) reasonable values. The Yucca Mountain Project scientists have not performed this relatively straightforward assignment of such values to their model. In all publications known to us, the slow growth rates are simply asserted, and no analysis of the possible mechanisms is provided.

3.4.6.2. Hydrothermal upwelling concept

If the concept of the hydrothermal upwelling of water into the hundreds of meters-thick vadose zone, introduced in the Parts I and II of this book, is correct, such upwelling would necessarily create a large-scale but transient hydrodynamic disturbance in the vadose zone. Mineral growth in the environment of the relatively short-lived dissipating hydraulic mound would be expected to be a dynamic process associated with unidirectional changes in the environment, such as, for example, the release of pressure, cooling of fluids, degassing of such fluids and the mixing with shallow oxidized waters, etc. It might be expected that these unidirectional changes could be "recorded" by the deposits of the mineral crusts – in their changing mineralogy, evolving textures, geochemical and isotopic properties, etc.

It must be born in mind that existing geologic knowledge provides little or no direct analogs of a system characterized by episodic upwelling water for at least three reasons. First, even though the record of the seismically induced discharges of waters on the Earth's surface does exist (see Part One and Part Two for details), these events, being rare, short-lived and largely unpredictable, present a challenging subject for scientific study. As a result, they have not been studied by hydrologists in sufficient detail. Second, mineralogists have had even less opportunities and incentives to study mineral deposits that may have been formed in the course of such seismically induced discharges. The deposits would not have potential in terms of the commercial value of such mineral resources. At the same time, the sampling of the deposits would likely require mining activities. Third, a combination of parameters responsible for the appearance of systems similar to those responsible for the deposition of secondary minerals at Yucca Mountain is quite unique by itself. Not many places on Earth possess an extensive (hundreds of meter-thick) vadose zone. Additionally, it is a vadose zone underlain by a mantle of instability, which produces time- and space variations in the fluxes of heat and matter (see Part I for discussion). We believe that the unique geologic setting of the Yucca Mountain region is the primary cause of the unusual patterns of secondary mineralization found there.

In studying objects where reliance cannot be placed on previous geological experience, the conservative approach is to test every hypothesis or conclusion against the principles of physics. In other words, every question must be answered positively for every hypothetical mechanism, which is advanced. We believe that any model or concept addressing the origin and modes of formation of the secondary minerals at Yucca Mountain, to be viable, must provide a rational and coherent explanation of all crucial features of these deposits. In the discussion below we will focus on the following key features:

1). Mineralogy (including accessory minerals) and major- and minor-element geochemistry of secondary deposits; and

2). Textures of secondary deposits, including (a) the geopetal character of the deposits; (b) the relatively large sizes of the crystals (up to 1 cm for quartz and 3 cm for calcite) and the euhedral shapes of the crystals; and (c) the scepter morphology of the major minerals (calcite and quartz).

It is our opinion that all of the observed mineralogic, geochemical and textural features of the Yucca Mountain secondary deposits are perfectly compatible with the model of deposition in the hydrologically saturated environment from heated waters that acquired dissolved components from deep in the crust and during their transport upward to the topographic surface. Below we evaluate the compatibility of these features with the competing "rainwater" model.

3.4.6.3. Major minerals and major-element geochemistry of mineral-forming fluids

Thermodynamic modeling (see Chapter 3-2) demonstrates that fluids produced by an interaction of percolating rainwater with surface calcretes and rhyolitic bedrock tuffs ("rainwater model") are incapable of precipitating the observed mineral assemblages. The requisite minerals do not form even if the modeled fluids-rock system is heated to 100°C (Palyanova et al., 2002). Minerals forming in such a system would be represented by silicates (kaoline, micas, etc.) as well as Fe-, Mn-, and Al-oxides – typical minerals evidenced by the weathering crusts of kaolinite and bauxite, which develop on the acidic volcanic rocks (Lebedev, 1979; Barsukov and Borisov, 1989; Palyanova et al., 2002). Even the saturation of rainwater with calcium carbonate entering the rhyolitic rocks does not result in the appearance of the observed set of minerals (see Chapter 3-2 for details). Thus, the deposition of the silica-carbonate crusts observed at Yucca Mountain requires a substantial input of Ca, CO₂ and SiO₂ into the system.

At Yucca Mountain the major element geochemistry of the mineral forming fluids is expressed through the development of two chemically distinct carbonate and silica assemblages.

An intrinsic feature of mineral assemblages formed through reaction of descending meteoric fluids with carbonaceous material in the soil zone and the bedrock tuff would be an overall similarity between the mineral- and chemical compositions of the secondary assemblages and those of the host- and

overlying rocks (see Table 3-4-1). Temporal variations in the chemistry of the mineral-depositing fluids, recorded in the mineral-scale zonation, are difficult to explain by the "rainwater" concept. Since both the carbonate and the silica assemblages are developed in rock of the same chemical composition, the major factor that could (hypothetically) control the chemistry of meteoric water percolating through the tuffs is the climate. We believe that "local depositional control" in individual crystallization cavities, suggested by Whelan et al. (2001) can be ruled out because of the consistent overall character of the intra-crust zonation throughout the repository block. It would be absurd, however, to claim that the climate-induced variations in the chemistry of rainwater could lead to shifts in the depositing minerals from calcite to quartz and then back to calcite.

It is equally difficult to explain, within the "rainwater" concept, the repository block-scale zonation in the distribution of calcite and silica minerals (see discussion above, section 3.4.4.2.).

3.4.6.4. Accessory minerals and minor-element geochemistry

The interpretational models developed for the deposition of the secondary minerals at Yucca Mountain as presented in the publications of the Yucca Mountain Project researchers (e.g., Fabryka-Martin et al., 2000; U.S. DOE, 2001; Paces et al., 1996; 2001) deal exclusively with the major minerals (calcite and silica). No attempt was made thus far to account for the co-genetic accessory minerals. Since we have established that accessory minerals such as fluorite, zeolite, strontianite and opals represent an integral part of the mineral-forming system at Yucca Mountain, we believe that a model of the process must explain the appearance of these minerals along with the major calcite and silica minerals.

The compositions of the accessory minerals at Yucca Mountain were controlled by the activity ratios of SiO_2 and CO_2 , as well as F^- , and probably SO_4^{2-} and PO_4^{3-} in the mineral-forming fluids. Although the anion composition of the fluids responsible for deposition of the accessory minerals at Yucca Mountain is quite diverse, the dominant cation is always Ca.

3.4.6.4.1. Fluorite

The data of Dublyansky and Mazurova (2000), and Smirnov and Dublyansky (2001) indicate that fluorine played an active role in mineral formation at elevated temperatures (~65 to 85°C). Fluorite was found in association with translucent opal. The latter is typically associated with the latest rhombohedral calcite, the temperature of formation of which is estimated to be less than approximately 35-50°C. The co-occurrence of fluorite and late translucent opal suggests that either this variety of opal could have formed at temperatures higher than 35-50°C (suggested by the presence of all-liquid inclusions), or that the activity of fluorine remained sufficiently high at low temperatures.

The common presence of fluorite indicates that the mineral-forming solutions were enriched in F. Chemical analyses and thermodynamic modeling show that neither rhyolitic tuffs nor the surface calcretes can provide the requisite amounts of fluorine. Meanwhile, limestones and dolomites of the Paleozoic Nopah formation, exposed 15 km to the west of Yucca Mountain in the tectonic block of Bare Mountain, host significant amounts of fluorine in the form of commercial grade hydrothermal fluor spar deposits. The data from drill hole UE-25 p#1 demonstrated that the same rocks underlying the Yucca Mountain tuffs host fluorite veinlets. Thus, the upwelling of hot, weakly acidic waters from the level of the fluorine-rich carbonates underlying Yucca Mountain, and their mixing with cool weakly alkaline meteoric waters may likely cause the decrease in fluorite solubility and its precipitation. This is thought to be a leading mechanism responsible for deposition of the fluorite in hot springs elsewhere (e.g., Mukherjee, 1986).

Also revealing is the extremely high content of As in the Yucca Mountain fluorites (up to 338 ppm). Arsenic is not a characteristic element of the rhyolite tuffs (at Yucca Mountain its average content is about 1 ppm; NBMG/UNR, 2000). Meanwhile, in the Great Basin, arsenic is a typical pathfinder or associated element for low-temperature hydrothermal precious metal deposits (Romberger, 1986).

3.4.6.4.2. Zeolites

The presence of zeolites indicates that quartz, chalcedony and opal are not the only chemical forms of silica that were stable in the Yucca Mountain mineral-forming system. The occurrence of zeolites implies conditions that favored the formation of an aluminosilicate structural framework instead of quartz or other silica polymorphs. At temperatures below $\sim 200^{\circ}\text{C}$ zeolites from the mordenite and heulandite groups are known to have very low aqueous solubilities. For example, in the temperature range $25\text{-}50^{\circ}\text{C}$, the logarithm of the solubility constant of heulandite and mordenite ranges between -26 and -25 (Benning et al., 2000).

Taking into account: (a) the extremely low solubility of heulandite; (b) an experimentally established impossibility of the synthesis of heulandite from low-mineralization solutions in the 25 to 50°C temperature interval (Senderov and Khitarov, 1970); and (c) the clearly co-genetic relationships of zeolites with the major minerals in the silica and the carbonate assemblages, we conclude that crystallization of zeolites most probably occurred from heated mineralized ionic solutions or from diluted colloidal solutions. This conclusion is in overall agreement with the data on the secondary calcite, fluorite and silica minerals from the Yucca Mountain vadose zone.

The results of the thermodynamic modeling indicate that in order for heulandite to play the dominant role among zeolites found in the ESF, the depositional temperature must have been higher than $\sim 70^{\circ}\text{C}$ (Palyanova et al., 2002). This conclusion is in good agreement with the thermodynamic modeling by Chipera and Bish (1997). Additionally, the formation of heulandite requires relatively low activities of

alkalis and silica. The latter should not exceed equilibrium values for quartz or cristobalite. These activities are lower than those expected in a system where the mineral-forming fluid acquires silica through interaction with rhyolite (in such a system the activity of silica will be determined by its reaction with glass and thus will be greater). Crystallization of heulandite after the bladed-scepter variety of calcite, intermediate in the paragenetic sequence, indicates that conditions delineated above could have persisted during a substantial part of the mineral-forming process.

3.4.6.4.3. Mn-minerals

The published data on the mineralogy of secondary minerals in fractures and lithophysal cavities in the Yucca Mountain unsaturated zone demonstrate that other chemical elements took part in the mineral-forming process. Carlos et al. (1993 and 1995-a) described secondary minerals of manganese. Even though these minerals were not found in the course of our studies in the ESF, their composition indicates that such elements as Ca, Ba and K, along with Mn, played an important role at certain stages of the mineralization.

The discussion above demonstrates that the formation of accessory minerals, together with the major minerals of the Yucca Mountain secondary assemblages, require elevated temperatures, mineralized fluids and sources of matter other than rhyolitic tuffs and calcretes. These properties make the formation of the accessory minerals incompatible with the "rainwater" model.

One characteristic feature of the mineral forming system at Yucca Mountain is that both the major and the accessory minerals have similar sets of minor elements - admixtures. These are Mg, Sr, and alkali metals (K and subordinate Na). Below we discuss the two most important minor elements of the Yucca Mountain secondary minerals – Sr and Mg.

3.4.6.4.4. Strontium

Strontium is one of the most important trace elements of both major and accessory secondary minerals at Yucca Mountain. Its abundance and isotopic composition may hold clues for determining the source of matter for the secondary minerals.

Sr abundances

The Yucca Mountain Project's "rainwater" model hypothesizes the acquisition of Sr by the mineral-forming fluid through the interaction of meteoric water with surficial carbonate deposits as well as soil and eolian carbonates (e.g., Paces et al., 1996 and 2001; DOE, 2000; Fabryka-Martin et al., 2000). The derivation of limited amounts of Sr from the host rhyolite tuff is not completely ruled out but is thought to be negligible (Vaniman et al., 2001). Paces et al. (1996 and 2001) and Denniston et al. (1997) demonstrated that the contents of Sr in calcite from the vadose zone vary substantially in individual

samples. In several samples from the ESF reported by Paces et al. (1996, 2001, see Figure 3-4-31) the abundance of Sr increased from early to late parts of the calcite crust. Paces et al. (1996) hypothesized that this behavior may be due to the continuously increasing amounts of slope carbonate accumulating on the topographic surface of Yucca Mountain over the last several million years: "*Strontium concentration would tend to be higher in the later calcite due to a more readily available source in calcretes, along with multiple dissolution and recrystallization events preceding shallow infiltration...*" (p. 32).

The increase of Sr in the mineral-forming fluids toward the latest stages of crystallization is further confirmed by an increase of Sr in late generation of zeolites reported by Carlos et al. (1995-a). In addition to Sr-enriched calcite and zeolites, fluorite at Yucca Mountain also shows a conspicuous enrichment in Sr ranging up to 200 ppm. Strontium, thus, must be considered a genuine component of the mineral-forming fluids during the fluorite crystallization. Finally, in the southern part of the repository block Smirnov and Dublyansky (2001) observed strontianite in association with granular calcite that preceded the opal-bearing late calcite. This indicates that, at times, the concentration of Sr in the mineral-forming solution was high enough to form a separate mineral phase. Strontianite is a common mineral in both the diagenetic and the hydrothermal environments. Rare occurrences of strontianite in speleothems, however, are always related to the action of thermal waters and require the presence of the primary celestite in the host rocks (Hill and Forti, 1997-a).

In contrast to the Yucca Mountain Project researchers, we are of the opinion that the surface deposits are daughters rather than parents with respect to the subsurface minerals (see Chapter 3-3 for discussion). Nevertheless, in the following text we evaluate the compatibility of the Sr geochemistry of secondary minerals from the ESF with the "rainwater" model.

There is presently no data on the chemical composition of waters that interacted with surface calcretes or soils and percolated through rhyolite. The possible contents of Sr in such waters may, nevertheless, be assessed on the basis of the knowledge of the solubility of calcite and the abundance of Sr in calcretes. Calcite exposed in Trench 14 and in the vicinity of Trench 14 on Exile Hill, on the east slope of Yucca Mountain, may be used to constrain the chemistry of the purported source of the carbonate. According to Vaniman et al. (1995), calcite from Trench 14 contains from 834 to 3019 ppm Sr. The greatest values are from outlying samples and may be related to secondary redistribution of Sr by plant activity. Vaniman et al. (1995) suggested 2100 ppm as the mean concentration of Sr in calcite. By using this value, one may calculate the formulae of the Sr-bearing calcite: CaO = 55.75 wt. %; SrO = 0.248 wt. %, and CO₂ = 44 wt. %, which yields Ca = 0.99 mole and Sr = 0.0024 mole (molar weight of Ca = 56.078 and Sr = 87.6). Such low contents of Sr do not change the molar weight of calcite, which may be taken as 100 g.

The solubility of CaCO_3 in water at $\text{pH} \cong 7$ and $T = 25^\circ\text{C}$ equals $7.73 \cdot 10^{-3}$ mole \cdot kg $^{-1}$ (see Figure 3-4-21). Thus, the amount of Sr in the solution, which is chemically equilibrated with the model calcite will be $X'_{\text{Sr}} = 1.88 \cdot 10^{-5}$ mole or $1.65 \cdot 10^{-3}$ g per 1000.775 g of the solution, or about 1.65 ppm. It is to be noted that the strontium-to-calcium ratio in the solution resulting from dissolution of slope calcretes in rainwater will be equal to that in the dissolving calcite, i.e., $\text{Sr}/\text{Ca} \cong 0.0024$. This will not be the case, however, for calcite depositing from such fluid.

Vaniman and Chipera (1996) correctly noted that the uptake of Sr into the calcite structure requires a specific environment (fast growth of calcite). This stems from the crystal chemistry of carbonates. Strontium carbonate, strontianite, has the structure of the aragonite type. This structural type is characterized by a higher cation coordination (9, as opposed to 6 in calcite). Therefore, the uptake of the large ion of Sr into the position of Ca in calcite would induce a distortion of the crystal lattice. This would result in an increase of internal energy, which would make the resulting mineral thermodynamically unstable. Therefore, during crystallization of the calcite-dominated assemblages, Sr must preferentially accumulate in the solution, form separate mineral phases, or enter into minerals that have suitable positions. In other words, not all strontium dissolved along with calcite from slope calcretes will be incorporated into the calcite crystallizing from the solution.

The maximum contents of Sr in calcite depositing from this hypothetical solution may be calculated. Assuming crystallization takes place in a closed system and that the volume of the crystallized calcite is significantly smaller than that of the mineral forming fluid, these assumption allow us to use the equation:

$$\left. \frac{m\text{Sr}}{m\text{Ca}} \right|_{\text{Cat}} = K_d \left. \frac{m\text{Sr}}{m\text{Ca}} \right|_{\text{Fl}} \quad (3-4-2)$$

where: $m\text{Sr}$ and $m\text{Ca}$ are molal concentrations of strontium and calcium in the calcite (Cat) and mineral forming fluid (Fl), and K_d is the equilibrium distribution coefficient for Sr. For $T = 25^\circ\text{C}$ $K_d \cong 0.1$ (Veizer, 1983; Tesoriero and Pankow, 1996; Rimstidt et al., 1998). Considering the solubility of calcite ($7.75 \cdot 10^{-3}$ mole kg^{-1}), in order to deposit calcite with a Sr content of 500 ppm, 1 kg of the mineral-forming fluid must carry $4.4 \cdot 10^{-5}$ mole or $3.85 \cdot 10^{-3}$ g or 3.85 ppm of Sr. The calculations thus show that fluid equilibrated with commonly encountered surficial calcretes does not seem to be capable of depositing calcite with the highest contents of Sr measured in the ESF samples (about 500 ppm), but could deposit calcite with relatively low Sr contents (50-100 ppm).

In carrying out a geologic interpretation of the calculations, one needs to consider the following auxiliary information.

- The actual distribution coefficients depend on the temperature, growth velocity and the presence of other admixtures in the solution.
- Calcite is not the only mineral that uptakes strontium from solutions. Strontium also partitions into fluorite and zeolites. In some cases, strontium even forms a separate mineral phase – strontianite.
- The distribution of calcretes, the hypothetical source for Sr, is non-uniform at the surface of Yucca Mountain. They are least abundant in the northern and central parts of the repository block, where calcites richest in Sr are found.

Lorens (1981), Rimstidt et al. (1998), Tesoriero and Pankow (1996) have demonstrated that the growth rates of calcite crystals exert a strong control on the distribution coefficient of Sr between calcite and fluid, particularly in the domain of low growth rates. The proponents of the "rainwater" concept have estimated that the long-term average growth rates of calcite at Yucca Mountain should be based on the results of the U-Pb and ^{230}Th -U dating at between 0.035 and 1.8 mm Ma^{-1} (Neymark et al., 2000)*. Figure 3-4-27 suggests that the K_d value of 0.03, rather than 0.1 would be a more realistic estimate of the distribution coefficient at such low growth rates.

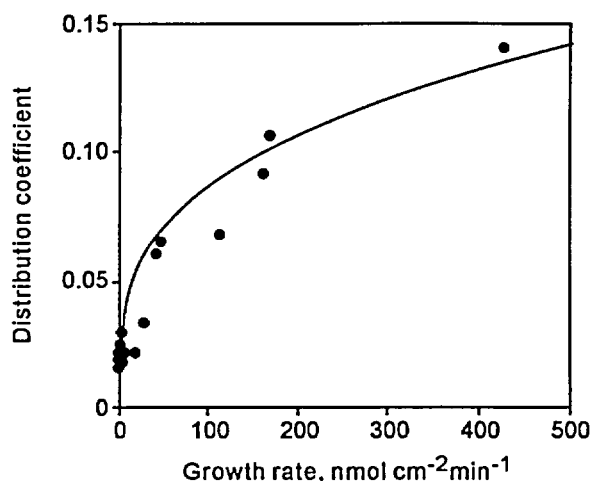


Figure 3-4-27. Distribution coefficients (K_d) for Sr as a function of the rate of calcite precipitation. From Rimstidt et al. (1998).

In order to deposit calcite containing 100 and 500 ppm of Sr a fluid must carry 23 and 116 ppm of Sr, respectively, (compare with 1.65 ppm in fluid equilibrated with the average for the surface calcretes).

* The authors of this monograph do not endorse these values of the growth rates. The problems with the radiometric dating of the Yucca Mountain samples will be discussed in Chapter 3-7.

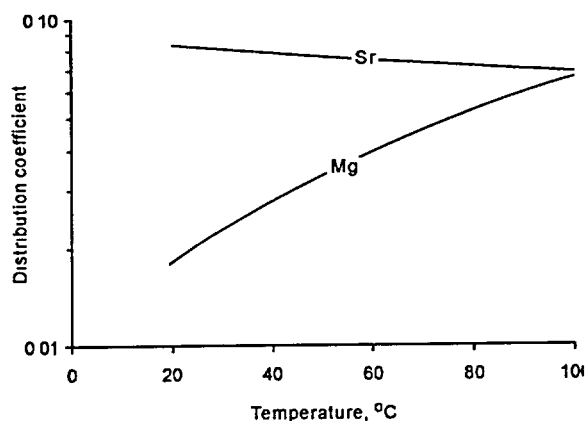


Figure 3-4-28. Estimated distribution coefficients for Sr and Mg in calcite at different temperatures. Calculated by using equations of Rimstidt et al. (1998).

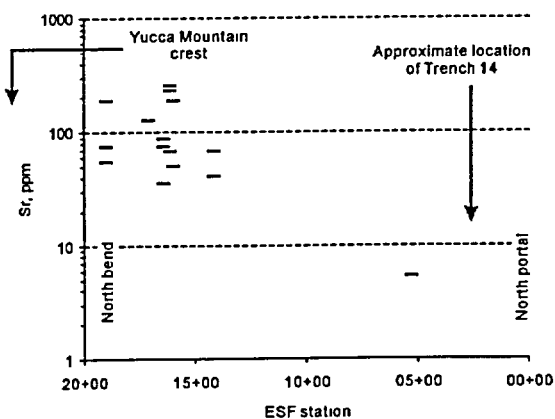


Figure 3-4-29. Distribution of strontium in calcite along the east-west transect across the northern part of the repository block. Diagram is based on the data by Paces et al. 1996.

The effect of temperature on the distribution coefficient of Sr was examined by Rimstidt et al. (1998). They measured the increase of K_d values from 0.069 at 100 °C to 0.1 at 25 °C (Figure 3-4-28). Earlier, Kinsman (1969) reported similar values of 0.08 at 100 °C and 0.14 at 25 °C. Even though the general trend suggests that calcites deposited from a fluid with decreasing temperatures should exhibit increasing contents of strontium, the increase in K_d between ~85 and ~35 °C (the temperature interval of mineral deposition at Yucca Mountain, see Chapter 3-6 for details) is too slight to provide a plausible explanation for the increase from ~100 to ~500 ppm observed in some Yucca Mountain samples (e.g., Paces et al. 1996).

The problem with the mismatch in the spatial distributions of the surface calcretes and the mineralogy of the secondary mineralization in the ESF was discussed above (see section 3.4.3 and Figure 3-4-13). Strontium geochemistry provides another insight for this discussion. The highest contents of strontium in the ESF calcites are found in the central part of the repository block, located under the Yucca Mountain crest. In this area calcretes are much less abundant than at the base of the eastern slope in the vicinity of Trench 14. Taking into account that most of the meteoric precipitation falling at the crest of Yucca Mountain should flow eastward as downslope surface run-off, the degree of chemical equilibration of meteoric waters with surface calcretes must increase from west to east. It is difficult to explain, therefore, why the least equilibrated (and thus containing the least Sr) waters percolating down in the area of the Yucca Mountain crest would deposit calcite with Sr contents greater than those that reacted with massive calcretes in the more easterly, Trench 14 area (Figure 3-4-29).

In the zone of mineral deposition, minerals such as fluorite and zeolites may also uptake strontium. This may further lower the apparent distribution coefficient for strontium in fluid and calcite. At the current state of knowledge regarding both distribution coefficients of strontium between the fluid and fluorite and zeolites and the relative amounts of calcite, fluorite and zeolites in individual crusts, it is difficult to numerically assess the significance of this mechanism.

In the southern part of the repository block we identified strontianite co-precipitated with calcite (see section 3.4.3). This finding is important since it reflects a very high activity of strontium in the mineral-forming solution. The question is: could this activity be associated with hypothetical rainwater percolating through slope calcretes?

As was pointed out above, the strontium-to-calcium ratio in the solution resulting from the interaction of rainwater with the slope calcretes will be equal to that in the dissolving calcite, i.e., $Sr/Ca \approx 0.0024$. By contrast, Helz and Holland (1965) have shown that solutions in equilibrium with both calcite and strontianite at 25 °C must have $Sr^{2+}/Ca^{2+} = 0.1$. Later work by Kinsman (1969) demonstrated that in the temperature interval between 25 and 100 °C the mSr^{2+}/mCa^{2+} values range between 0.1 and 0.5 (m stands for mole content). This clearly shows that the hypothetical rainwater must be strongly undersaturated with respect to strontianite.

The coefficient of distribution of Sr is higher for calcite enriched in Mg. Mucci and Morse (1983) have suggested that uptake of Mg, whose ionic radius is smaller than that of Ca ($r_{VI} = 0.72$ as compared to 1.0 for Ca; lower index VI indicates the six-fold coordination), causes the distortion (shrinkage) of crystal lattice near the replaced position. Strontium ($r_{VI} = 1.16$) compensates for the shrinkage, entering the lattice in the adjacent area of expansion. A comparison of the data on the evolution of Mg contents in calcite (see section 3.4.3.1.1 Calcite and Figures 3-SS-8 through 3-4-12) with the data on Sr contents across the calcite crusts (Paces et al., 1996 and 2001) shows that there seems to be a positive correlation between the two elements.

Summarizing, our analysis shows that the "rainwater" hypothesis does not offer a satisfactory explanation of two observed features: (a) crystallization of calcite with high, up to 500 ppm, contents of Sr and (b) crystallization of strontianite. Neither the host tuffs nor the surficial carbonate deposits could serve as adequate sources of Sr.

Sr isotopes

The isotopic composition of Sr has been interpreted as additional evidence in support of the interaction between meteoric waters and surficial and soil carbonate material (e.g., Marshall et al., 1998; Marshall and Whelan, 2000). Peterman et al. (1992) was the first to report that fracture-lining calcite

encountered in boreholes within the upper 400 m of the vadose zone has $^{87}\text{Sr}/^{86}\text{Sr}$ values similar to those of the surficial calcite and drastically dissimilar from the deep-seated (i.e., developed below the water table) hydrothermal calcite values. These data were interpreted as indicating a situation whereby "... *strontium is initially added to infiltrating water by dissolution of calcite in the soil zone.*" (Fabryka-Martin et al., 2000).

After the excavation of the ESF, when more calcite became available for studies, the range of the $^{87}\text{Sr}/^{86}\text{Sr}$ values of calcite was found to substantially overlap the values characteristic of both the deep-seated and the surficial calcites (Figure 3-4-30). Furthermore, in a number of samples, the $^{87}\text{Sr}/^{86}\text{Sr}$ ratio exhibited a pronounced increase from paragenetically early to late calcite (Figure 3-4-31).

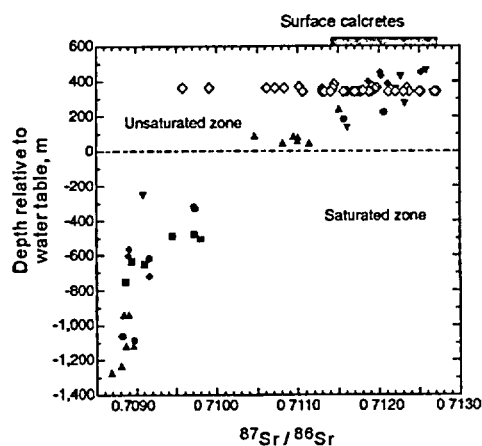


Figure 3-4-30. Sr isotope composition of fracture-lining calcite from the Yucca Mountain subsurface. *Filled symbols* – calcite from drill cores, *open diamonds* – calcite from ESF. The bar at the top of the diagram shows the range of $^{87}\text{Sr}/^{86}\text{Sr}$ values of surficial calcites (from Paces et al. 1996).

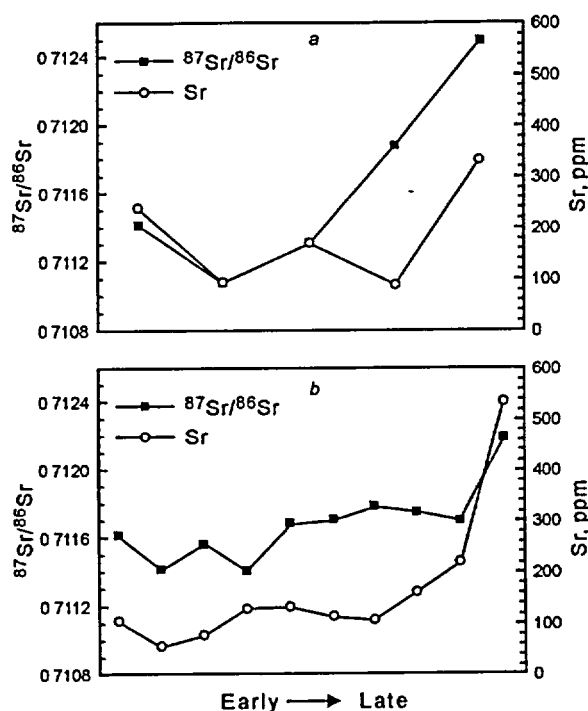


Figure 3-4-31. Variations of $^{87}\text{Sr}/^{86}\text{Sr}$ and Sr abundances in two calcite samples from ESF. *a* – sample 2019, ESF station 28+80; *b* – sample 2065, ESF station 33+16.2. From Paces et al. (1996).

These findings, nevertheless, did not change the essence of the Yucca Mountain Project scientist's concept. The concept was modified slightly and the Project scientists now consider that paragenetically early calcite incorporated strontium derived from bedrock tuff, whereas late calcite incorporated strontium that came from the surface calcretes.

Strontium isotopes do not fractionate in most natural physico-chemical reactions, such as dissolution and crystallization. Therefore, the systematically changing $^{87}\text{Sr}/^{86}\text{Sr}$ ratios in a mineral, similar to those apparent in Figure 3-4-31, may potentially be caused by two mechanisms: the *in situ* decay of ^{87}Rb and the crystallization of minerals from fluids with changing Sr isotope ratios. Since the $^{87}\text{Rb}/^{87}\text{Sr}$ ratio in the Yucca Mountain calcite is close to zero, the first possibility may safely be ruled out. Thus, any changes in $^{87}\text{Sr}/^{86}\text{Sr}$ values in the course of calcite growth must be the result of changing isotopic properties of the mineral-forming fluids.

Figure 3-4-32 summarizes the Sr isotope compositions of several potential sources (rocks, deposits) that could have supplied strontium in the ESF calcite. It also shows the Sr isotope compositions of waters in the Yucca Mountain region. In order to emphasize their respective roles in the two competing hypotheses of secondary mineral formation, the sources are provisionally subdivided into the *hypogene* and the *supergene* groups. It is important to note that the calcrete source is positioned in the *supergene* group only to make possible an examination of its role in supplying Sr for the subsurface calcite within the "rainwater" concept. This in turn requires an assumption that the calcretes were formed before the deposition of calcite in the subsurface. It is to be noted that such an assumption assigns the calcrete and the subsurface calcite a parent-daughter relationships whereas, as we argued in Chapter 3-3, their actual relationship is most likely the opposite.

Figure 3-4-32 demonstrates that all potential sources of Sr at the topographic surface are enriched in radiogenic ^{87}Sr . Calcites with low radiogenic compositions, encountered in the ESF cannot thus be accounted for by the surficial source of Sr.

As was mentioned above, the most recent version of the "rainwater" concept explains the low- $^{87}\text{Sr}/^{86}\text{Sr}$ values, typically found in microstratigraphically early calcite in the ESF, by preferential derivation of strontium from the tuff at early stages of calcite deposition. The evident flaw in this

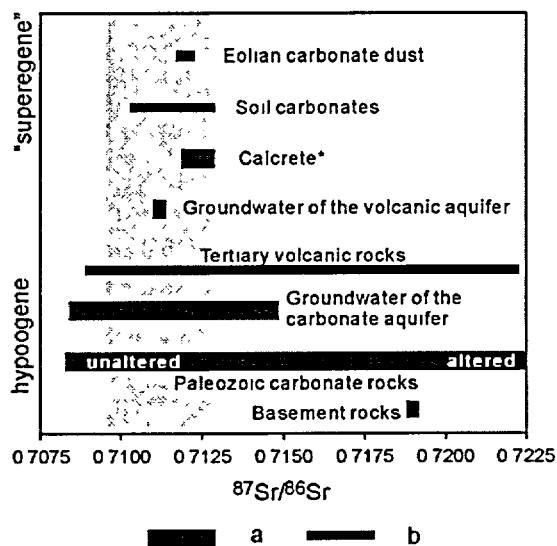


Figure 3-4-32. Sr isotope compositions of the possible sources of strontium in the calcite from ESF (gray field). Bars with different thickness indicate sources with abundant Sr or sources from which Sr may be derived readily (a) and less abundant Sr sources (b). The range of isotope compositions for Paleozoic carbonate rocks includes hydrothermally altered and unaltered varieties.

Based on the data of Marshal et al. (1991 and 1992); Peterman et al. (1992 and 1994); Zartman and Kwak (1993-a); Marshal and Mahan (1994); and Fabryka-Martin et al. (2000).

explanation is that even the quartz-latite tuff cannot provide enough Ca and Sr for deposition of calcite (e.g., Vaniman et al., 2001).

It has recently been suggested that the low values of $^{87}\text{Sr}/^{86}\text{Sr}$ in the ESF calcite may be due to the extraction of strontium from the non-welded Paintbrush tuff (e.g., Fabryka-Martin et al., 2000). There are two problems with this interpretation. First, the strontium isotope values of the non-welded Paintbrush tuff are quite variable ($^{87}\text{Sr}/^{86}\text{Sr} = 0.710$ to 0.716) and, overall, more radiogenic than the lowermost values measured in calcites. Second, the low $^{87}\text{Sr}/^{86}\text{Sr}$ ratios were measured in secondary calcite from the ESF not only at the bases of crusts, but also in the intermediate positions.

The detailed data on Sr composition of secondary calcite presented by Paces et al. (1996 and 2001) permits an evaluation of the evidence of mineral deposition from mixing fluids. If two fluids with different Sr contents and Sr isotope compositions mix in different proportions and minerals are deposited from these mixtures, the points on the $^{87}\text{Sr}/^{86}\text{Sr}$ vs. Sr plot for these minerals follow a hyperbola (Faure, 1986). The mixing hyperbola can be transformed into a straight line by plotting $^{87}\text{Sr}/^{86}\text{Sr}$ vs. $1/\text{Sr}$.

Figure 3-4-33 shows such plots for the two secondary crusts studied by Paces et al. (1996). Although general linear trends are apparent from the picture, there is also a conspicuous scatter of points around the trendlines (see, for example, point 2 of the sample HD2059). The most

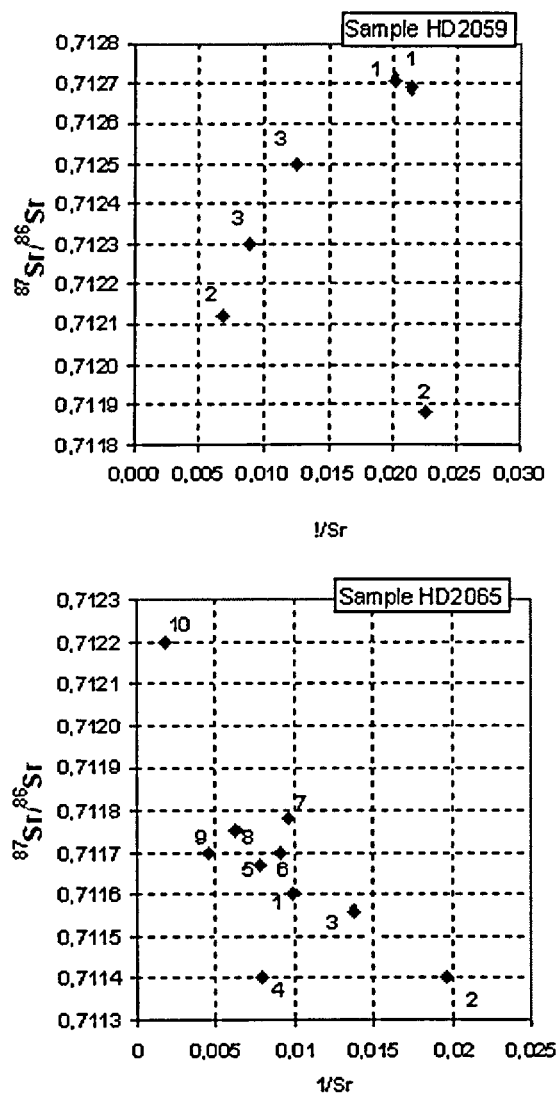


Figure 3-4-33. Sr isotope composition vs. Sr abundance cross-plots for two calcite crusts displaying mixing lines. Significant scatter of the data, opposite direction of trendlines, and the absence of regularity in the base-top direction strongly suggests the complex character of mixing and involvement of multiple sources. Numbers indicate the position of a subsample within the crust with smaller numbers corresponding to the subsamples collected closer to the base of the crust. Plotted from data reported in Paces et al. (1996). Sample HD2059 - ESF station 30+17.8, sample HD2065 - ESF station 33+16.2). $1/\text{Sr}$ is in ppm^{-1} .

reasonable explanation for such a complex pattern of Sr isotope composition is a multiple-source mixing. Another important observation is that the trends for the two samples shown in Figure 3-4-33 have the opposite directions. One trend suggests a mixing between the Sr- and ^{87}Sr -rich fluid and the Sr- and ^{87}Sr -poor fluid (3-4-33-a), whereas a second trend suggests mixing between the Sr-rich but ^{87}Sr -poor fluid and Sr-poor ^{87}Sr -rich fluid (3-4-33-b). The mixing of fluids deriving their Sr from surficial calcrete with those equilibrated with volcanic rocks would not explain the opposite directions of the $^{87}\text{Sr}/^{86}\text{Sr}$ vs. $1/\text{Sr}$ dependencies for samples taken from the same host-rock and located not too far from one another.

Summary on Sr geochemistry

It is evident that the "rainwater" concept fails to reasonably explain a number of features of the Sr geochemistry of the secondary calcite from the ESF. These features are: (1) the high contents of Sr in the fluids that deposited calcite in the Yucca Mountain subsurface; (2) the apparent systematic changes in the fluids, involving concurrently increasing with time Sr (and Mg) abundances as well as increasing $^{87}\text{Sr}/^{86}\text{Sr}$ ratios; (3) low-radiogenic $^{87}\text{Sr}/^{86}\text{Sr}$ values of early and intermediate calcite in secondary crusts; and (4) the complex pattern of Sr isotopic compositional change during calcite deposition.

The hydrothermal upwelling concept involves sources of Sr located beneath the Yucca Mountain rhyolite tuffs. These sources include the Paleozoic/Proterozoic carbonate rocks and probably deeper older basement rocks. The sources have highly variable Sr isotope compositions (Figure 3-4-32) and varying Sr contents. Figure 3-4-32 shows that the input of the low-radiogenic strontium might be accounted for by the incursion of groundwater from the carbonate aquifer. Peterman et al. (1994) demonstrated that Sr isotope composition of altered Paleozoic carbonates acquires more radiogenic character in the vicinity of the hydrothermal gold deposits in Bare Mountain. Elevated $^{87}\text{Sr}/^{86}\text{Sr}$ values (up to 0.7150) of some carbonate ground waters might reflect an interaction of these waters with hydrothermally altered carbonates or perhaps their mixing with hydrothermal solutions. Hydrothermal fluids equilibrated with altered Paleozoic carbonates strongly enriched in radiogenic ^{87}Sr would bring enough Sr to cause isotopic enrichment of calcite, fluorite and zeolites taken from the ESF. The pulse of these fluids during the crystallization of late calcite is probably responsible for both the Sr enrichment and the highly radiogenic Sr isotope composition. The change of Sr isotopic compositions during the calcite deposition would be determined by mixing between fluids of different pulses and meteoric waters, creating the complex patterns of the $^{87}\text{Sr}/^{86}\text{Sr}$ vs. $1/\text{Sr}$ dependences.

3.4.6.4.5. Magnesium

The contents of Mg in calcite vary substantially and the variations display pronounced patterns. The character of these patterns, however, is non-rhythmic, which contrasts them with rhythmic climate-induced zonation. The only possible exception is late calcite, which was found to possess oscillatory Mg-

enrichment zonation (Wilson and Cline, 2001). A determination of the origin of the oscillatory zonation may be achieved, potentially, by means of mathematical analyses. From the existing data set, it can be concluded that the activity of Mg in the mineral-forming solutions varied throughout the time frame in question. We note at the outset of this discussion that the "rainwater" concept does not and cannot provide a rational explanation for the source of Mg or for what caused the activities of Mg to vary so significantly during mineral deposition.

When considering possible sources for the Mg-enriched calcite, one should recognize that Mg enrichment is a geochemical feature that, at and around Yucca Mountain, is typically associated with minerals deposited at the ancient discharge sites, commonly from fluids with elevated temperatures. Vaniman et al. (1995) reported that Mg-enriched calcite commonly occurs at contemporary and fossil discharge sites of thermal waters in Death Valley (Travertine Point, Grapevine Spring, and Nevares Spring) and at the southern end of Yucca Mountain (USGS site #199). The Mg content varies between 1.53 and 2.63 wt. % MgO, for the Death Valley locations, and between 3.0 and 5.8 wt. % MgO, for site #199. Further, the Nye County well NC-EWPD-1S revealed that the USGS site #199 is underlain, at a depth of about 20 meters, by a ~100 meters tall hydraulic "mound", which is composed of thermal water with a Ca-Mg bulk composition (see Chapter 2-1 in Part Two of this report). Directly above this mound, there is a series of outcrops of warm-spring deposits, which in part are composed of diatomaceous earth. The site #199 deposits were found by Paces et al. (1993) to carry $^{230}\text{Th}/\text{U}$ ages ranging from 45.7 ± 4.9 (2 samples), through 30 ± 2.7 (2 samples), to 17.4 ± 2.9 (5 samples) Ka.

Thermodynamic calculations by Palyanova et al. (2002) demonstrated that Mg might precipitate from rainwater interacting with rhyolites at ambient temperatures (25 °C) in the form of dolomite if the rock-to-water ratio exceeds 10^3 . At higher temperatures (50°C) the solubility of carbonates increases and dolomite does not form. This leads to the conclusion that elevated contents of Mg in early blocky calcite cannot be accounted for by the percolation of the rainwater through tuffs. Importantly, the calcite of the surficial calcretes and bedrock veins contains low abundances of Mg (<1 wt.% MgO; EMP data on calcite from Trench 14; by Vaniman et al., 1995). The distribution coefficients for Mg in the solution-calcite system are very low (about 0.02-0.03 at $T = 20\text{-}40$ °C; Rimstidt et al., 1998; see Figure 3-4-28). Thus, calcite crystallizing from solution that acquired its Mg through dissolution of surface calcretes is expected to contain substantially less Mg than the "parent" calcretes. The actual situation, however, is the opposite, which makes surface calcretes an unsuitable source of Mg for subsurface calcite.

As for the increased abundances of Mg in late blocky calcite, reported by Wilson et al. (2000) and Wilson and Cline (2001), this feature is perfectly compatible with the hydrothermal upwelling concept.

Thermal waters injected into the vadose zone would necessarily lose heat and cool down; and could have deposited the Mg-enriched minerals at relatively low temperatures.

Detailed studies of fracture-lining minerals by Carlos et al. (1995-a) revealed that the Mg-enriched minerals include calcic zeolites, such as stellerite and heulandite. Their studies further revealed that prismatic heulandite crystals and rims of tabular heulandite crystals are enriched in Mg. Such crystals occur in the devitrified interior of the Topopah Spring ash-flow tuff. Thus, one can be reasonably certain that these zeolites were formed from ionic solutions, rather than through the hydration of aluminum and silica-bearing volcanic glasses. The results of the thermodynamic modeling by Chipera and Bish (1997) showed that precipitation of heulandite from Ca-bearing solutions requires an aqueous silica activity in equilibrium with cristobalite or quartz and a temperature between 35 and 100°C. WoldeGabriel (1993) reported that the clinoptilolite/heulandite fractions from the vadose zone at Yucca Mountain carry (mixed) K/Ar ages ranging between 1.0 and 7.5 Ma (see Section 3.1.5. for discussion). Thus, it is also reasonably certain that these fractions are broadly contemporaneous with the ESF coatings.

Unlike Sr, the distribution coefficient for Mg decreases with decreasing temperature (see Figure 3-4-27). The highest contents of Mg are commonly associated with the latest calcite, which formed at temperatures less than approximately 50-35 °C (see Chapter 3-6 for details). At these temperatures the distribution coefficients are lower than those in earlier, higher-temperature calcite. Thus, the Mg/Ca ratios in the mineral-forming solutions at late stages of mineral deposition must have been much greater than those at early stages.

Summarizing, it is reasonably certain that neither the rhyolite tuffs nor the surface calcretes could have served as an adequate source of Mg for the subsurface minerals at Yucca Mountain. The Paleozoic dolomite of the Roberts Mountain Formation is widely recognized as a source of Mg for the Mg-rich carbonates found in spring deposits of the region. At Yucca Mountain, the Roberts Mountain dolomite underlies the tuffs and occurs at a depth ranging between 1.2 and >3.5 km. It is perfectly compatible with the hydrothermal upwelling model that in addition to serving as the source of fluorine, this dolomite served as a source of the allogenic Mg.

It is entirely reasonable, in our opinion, to conclude from all of the observations presented above that warm or hot solutions, ascending from the basement, were responsible for introducing the allogenic Mg. This includes the altered tuffs (see Section 3.1.2.), the calcic zeolites, the Mg-enriched calcite, and the most recent blocky calcite possessing oscillatory Mg-zonation (Wilson and Cline, 2000).

3.4.6.4.6. Rare Earth Element geochemistry of secondary minerals

Lanthanide rare-earth elements (REE) are La and the row of chemically similar elements with atomic numbers between 57 and 71. The low-atomic-number members of the REE series, from

Lanthanum (La) to Samarium (Sm) are commonly called light rare-earth elements or LREE; similarly the high-atomic-number elements, from Erbium (Er) to Lutetium (Lu) are called heavy rare-earth elements or HREE. Having high charge and large ionic radii REE are relatively immobile and their ratios typically remain unchanged in the course of the water-rock interaction. Therefore REE compositions of hydrogenic minerals provide important information about the rocks with which water or hydrothermal fluid interacted along its flow path.

Most of the elements in the REE series invariably form stable 3+ ions. Two elements may also exist in two oxidation states: Ce (3+ and 4+) and Eu (3+ and 2+). They form larger and smaller ions respectively, relative to the 3+-oxidation state. These two elements commonly give "anomalies" (peaks or troughs) on the otherwise smooth chondrite- or shale-normalized REE abundance graphs.* Due to their ability to change the oxidation state, Ce and Eu may be used to probe into the redox environment of the mineral forming process.

The database

The REE composition of calcites, and some other minerals, from Yucca Mountain were studied by Vaniman (1993), Vaniman and Chipera (1996), and Denniston et al. (1997). It was demonstrated in the first two publications that REE in secondary calcite exhibits two major types of REE patterns: (1) a pattern with one negative Eu anomaly, and (2) a pattern with two negative Ce and Eu anomalies. More fine-scale analyses by Denniston et al. (1997) that employed SIMS method of analysis of secondary calcites revealed that the patterns are in fact more complex. They defined four general types of REE patterns: (1) depleted LREE ($La/Sm \sim 1$) with a pronounced negative Ce ($La/Ce \sim 200$) and Eu ($Sm/Eu \sim 10$) anomalies; (2) enriched LREE ($La/Sm > 2$) with pronounced negative Ce ($La/Ce \sim 700$) and Eu ($Sm/Eu \sim 20$) anomalies; (3) depleted LREE ($La/Sm \sim 1$), with a small Eu ($Sm/Eu \sim 3$) anomaly and a minimum Ce anomaly ($La/Ce \sim 0.5$), and (4) enriched LREE ($La/Sm \sim 6$) with a small Eu ($Sm/Eu \sim 2$) and a minimal to nonexistent Ce ($La/Ce \sim 1.5$) anomaly.

The authors concluded that the REE features distinguish the vadose zone deposits from those in the phreatic zone. Specifically, the vadose zone deposits were shown to be associated with a prominent double negative (Ce and Eu) anomaly, whereas those from the phreatic zone were mainly characterized by a single (Eu) negative anomaly.

* The anomalies may be quantified by comparing measured concentrations of Ce and Eu with expected concentrations obtained by interpolating between the normalized values of the "neighbor" elements (La and Pr for Ce or Sm and Gd for Eu). The value of the Ce/Ce^* or Eu/Eu^* (where the asterisk denotes an interpolated value) ratio > 1 indicates a positive anomaly, while the value < 1 is a negative anomaly. Sometimes, when data on the immediately following elements are not available, Nd and Tb are used in calculations instead of Pr and Gd. A somewhat more ambiguous method is the calculation of the La/Ce and Sm/Eu ratios. For some types of REE patterns this may lead to the appearance of "false" anomalies.

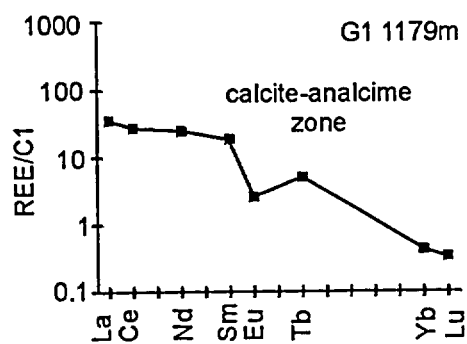
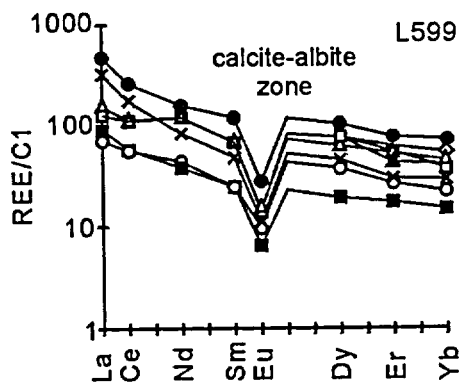
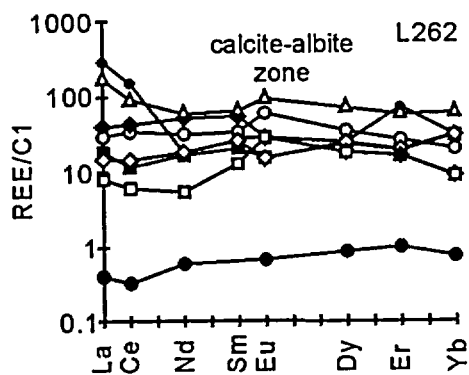
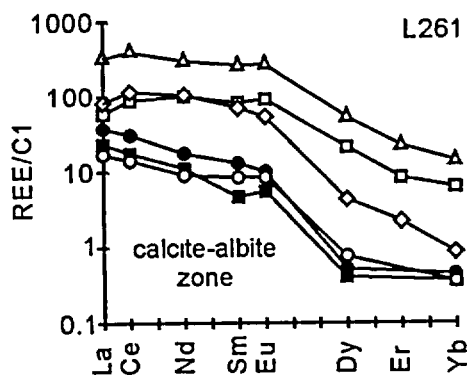


Figure 3-4-34. REE patterns of calcite from the phreatic zone of Yucca Mountain. The sample, G1 1179m, is from the shallower calcite-analcime alteration zone (by Vaniman and Chipera, 1996). Samples L261, L262 and L599 are from the deeper calcite-albite alteration zone (by Denniston et al., 1996).



Examples of the type-1 pattern of Vaniman and Chipera (patterns type-3 and type-4 of Denniston et al.) are shown in Figure 3-4-34. The pattern is believed to be characteristic of the deep-seated calcites from the “carbonate-altered zone”. Denniston et al. (1997) applied the latter term to the zone of carbonate mineralization of tuffs located deep in the phreatic zone (>1 km). The alteration is believed to be related to the Timber Mountain Caldera hydrothermal event (~10.4 Ma; Bish and Aronson, 1993). According to Bish and Chipera (1989) the shallower part of this zone is characterized by analcime + calcite assemblages, while albite + calcite predominates at greater depths. It is apparent from the figure that calcites from this deep-seated zone do not show the Ce anomaly. The negative Eu anomaly may or may not be present in different samples (some samples, in fact, show slight positive Eu anomaly).

Examples of the type-2 pattern of Vaniman and Chipera (patterns type-1 and type-2 of Denniston et al.) are shown in Figure 3-4-35. Distributions exhibit two pronounced negative anomalies – Eu and Ce.

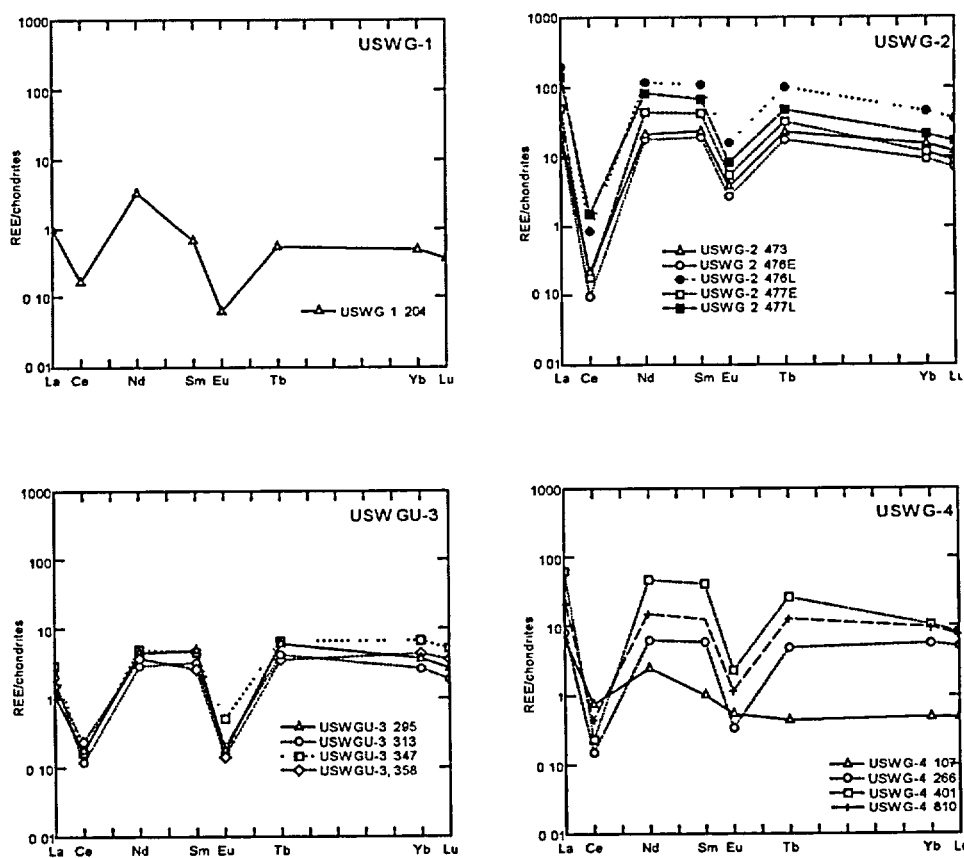


Figure 3-4-35. REE patterns of calcite from the present-day vadose zone and upper part of the phreatic zone (USW G-4, 810 m) of Yucca Mountain sampled in four boreholes. Note that pronounced negative Ce anomaly is present in all samples. Based on Vaniman (1993) and Vaniman and Chipera (1996).

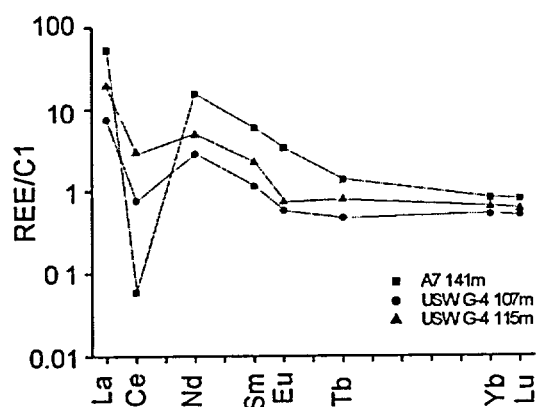


Figure 3-4-36. REE patterns displaying small or absent Eu minima. These patterns have been obtained from three samples, located beneath the quartz-latite horizon in drill holes A-7 and USW G-4. Data by Vaniman and Chipera (1996).

Such patterns were argued to be characteristic of calcites from the vadose zone, as well as from the upper part of the phreatic zone (see sample from depth 810 m in borehole USW G-4 in Figure 3-4-35). All samples of calcites with the type-2 pattern were from locations above the "carbonate-altered zone".

In addition, Vaniman and Chipera (1996) reported REE patterns of the three vadose-zone samples collected from drill holes A7 (141 m) and G-4 (107 and 115 m), which showed a pattern, different from the major pattern types (Figure 3-4-36). Specifically, distributions showed very small to

non-existent Eu minima, while preserving the pronounced Ce minima.

The database, examples from which were presented in the Figures 3-4-34 through 3-4-36, served as a basis for interpretation of the REE transport and redistribution in the Yucca Mountain vadose zone by the Yucca Mountain Project researchers. The interpretation includes the following points.

- Deposition of calcite from downward percolating rainwater (a postulate).
- The water acquired REE's through interaction with the bedrock tuff. As a consequence, the waters carried REE patterns characteristic of the Yucca Mountain rhyolites and, in some locations, quartz latites.
- Characteristic features of these "background" trends are: for quartz latites – strong LREE enrichment (high La/Sm ratios) and moderate negative to weak positive Eu anomaly; for rhyolites – moderate to weak LREE enrichment and strong negative Eu anomaly.
- Calcites depositing from percolating waters thus inherit the REE patterns of the local bedrock tuff, particularly the pronounced negative Eu anomaly, as well as characteristic slopes of the LREE distributions.
- Rare finds of calcites with the "quartz latite" patterns (e.g., Figure 3-4-36) are explained by location of these samples beneath possible perched water bodies in rocks of the quartz latitic composition (Vaniman and Chipera, 1996). These percolating waters resided for time periods sufficient to acquire the appropriate REE signature before being flushed by fresh waters during periods of increased recharge.

- Three mechanisms (models) are proposed to explain the conspicuous negative Ce anomaly in the calcite from the vadose-zone. They are discussed below (based on Denniston et al. 1997).
- **Model 1.** In an oxidizing environment Ce^{3+} may transform to Ce^{4+} , which ion has a small ionic radius. As a consequence, Ce may be excluded from the vadose zone calcite's lattice. Deep-seated calcite, which has formed in a more reducing environment, has Ce that remains in the 3+ state and is incorporated in the calcite along with other REE. It should be noted that the differences in ionic radii and valences do not readily address other chemical variations within individual calcite samples.
- **Model 2.** The vadose-zone calcite inherited its Ce anomaly from the source rock(s). The model is rejected on the ground that if this were the case (i.e., if the source of the vadose-zone calcite were eolian dust and calcretes on the topographic surface), the decrease in REE abundances with depth from surface would be expected. Such a decrease was not observed.
- **Model 3 (favored).** Because Ce^{4+} has an ionic radius similar to Mn^{2+} , the manganese oxides, co-precipitating with calcite may "scavenge" cerium from solution. Alternatively, Ce^{3+} may oxidize to Ce^{4+} on the surface of the Mn-oxide minerals and the Ce^{4+} may then be incorporated into the minerals through cation exchange (Vaniman and Chipera, 1996, p. 4430). Manganese oxide phases from fractures in Yucca Mountain yielded a wide range of REE patterns. One sample of rancieite was found to carry the REE pattern with a strong positive Ce anomaly, lithiophorite have shown a weak positive anomaly, and cryptomelane showed no noticeable Ce enrichment (Table 3-4-3).

Table 3-4-3.

Ce abundances in Mn-oxide minerals and Ce anomaly.
Data by Vaniman and Chipera (1996)

Mineral	Concentrations, ppm			C1-normalized concentrations			
	La	Ce	Nd	La _N	Ce _N	Nd _N	C _N
Rancieite (Ca,Mn ²⁺)Mn ₄ O ₉ ·3H ₂ O	94	2100	190	285	2386	317	
Lithiophorite (Al,Li)Mn ⁴⁺ O ₂ (OH) ₂	1700	6000	2500	5152	6818	4167	
Cryptomelane K ₂ (Mn ⁴⁺ , Mn ²⁺) ₈ O ₁₆	590	1100	440	1788	1250	733	

Note: subscript N indicates C1 chondrite-normalized values. Ce anomalies are calculated from the normalized concentrations.

Although the reasoning presented above appears to be plausible, it is also apparent that it is strictly model-dependent. Since the formation of calcite from descending meteoric waters is postulated, the bedrock tuffs along with eolian deposits and calcretes at the surface remain the only sources of the REE s admissible within the model.

In order to test the REE data for compatibility with the competing, hydrothermal upwelling concept, other potential sources must be considered. For example, within the concept, upwelling waters could have acquired their REE signatures from the rocks, occurring in their flow path, e.g., Paleozoic and Proterozoic sedimentary carbonate and clastic rocks underlying Yucca Mountain, silicic volcanic tuffs and their igneous counterparts. The REE signatures of all these rocks must hence be examined.

Waters rising up through the rhyolitic volcanic tuff "pile" would interact with these rocks. Before entering the tuffs, however, the waters would already carry the REE "signal" acquired from the underlying rocks. The final REE pattern of the fluids, which the minerals depositing from these waters would, in turn, inherit, should reflect a mixing of REE compositions derived from different sources.

It is apparent from examination of the data discussed above (Figures 3-4-34 and 3-4-35) that three features of the REE patterns are potentially informative. These are: (1) the presence or absence of the negative Eu anomaly; (2) the presence or absence of the negative Ce anomaly; and (3) the slope of the LREE distribution.

Eu anomaly

Inheritance of Eu

The Eu anomaly in secondary minerals is believed to be inherited from the source rock. This contention is based on the notion that although Eu may exist in two oxidation states, in the temperature interval relevant to the Yucca Mountain secondary minerals (25-100 °C), Eu maintains the 3+ valence state within the whole range of realistic Eh (Sverjensky, 1984).

A negative Eu anomaly is typical of many continental rocks and sediments. This stems from the fact that many crustal igneous silicic rocks were produced by intracrustal partial melting. The residues of these melts were enriched in plagioclase, which tends to retain elevated amounts of Eu. When granitic and granodioritic magmas made their way up and into the upper crust or to the Earth surface, Eu was left behind in the lower crust, thus leading to the Eu-depletion of the upper crust. Sediments derived from the continental upper crustal rocks inherit this anomaly.

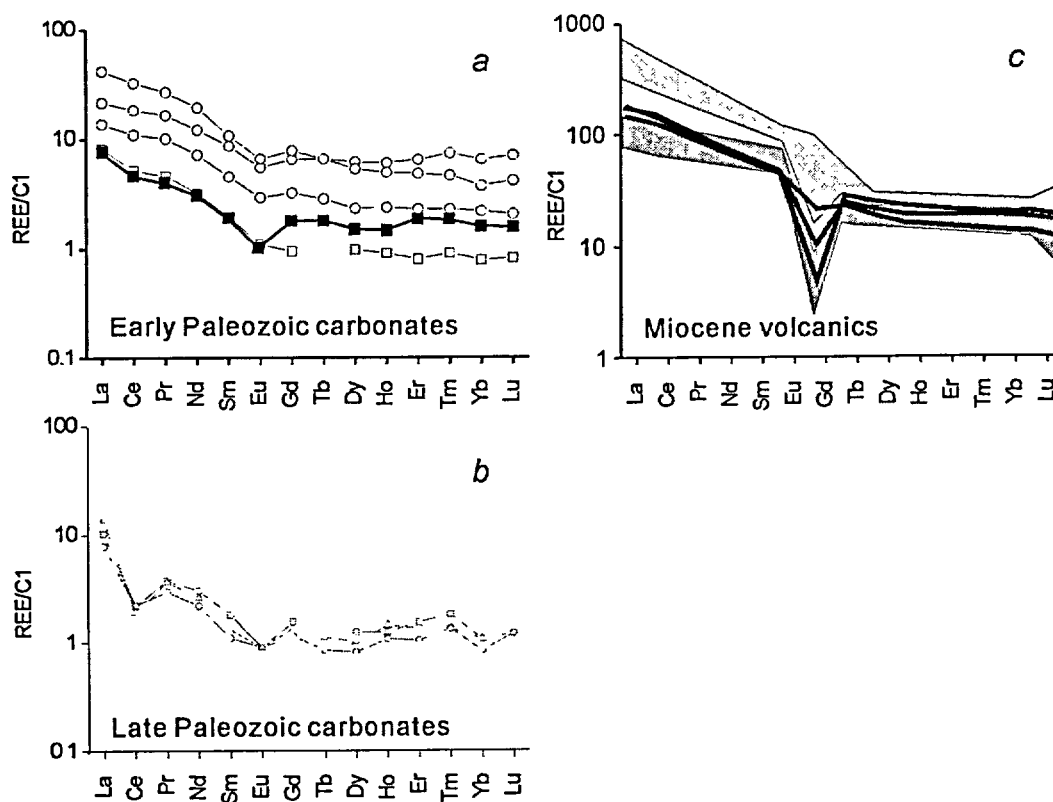


Figure 3-4-37. REE patterns of the Early Paleozoic (a) and Late Paleozoic (b) limestone and dolostone in southern Nevada and silicic Miocene volcanic rocks of Yucca Mountain (c).

a - Open circles - Frenchman Mountain, open squares - Fossil Ridge, filled squares - Bonanza King limestone (Early Cambrian). b - All symbols - Frenchman Mountain. Data from Johansson et al. (2000). c - Ranges in chondrite-normalized REE patterns for upper (light shading; quartz latites) and lower (heavy shading, rhyolites) portions of the Topopah Spring Tuff (after Schuraytz et al., 1989 and Broxton et al., 1989 as reported in Denniston et al., 1997), and average values (of four samples each) of the Tram, Bullfrog and Crater Flat ignimbrites (solid lines; from Scott and Castellanos, 1984).

This consideration is illustrated in Figure 3-4-37. It shows that many Paleozoic carbonate rocks in southern Nevada do show the negative Eu anomaly. This anomaly is also prominent in the rhyolitic tuffs of Yucca Mountain (Figure 3-4-37-c). The anomaly is less pronounced or non-existent in units of the quartz latite composition, which may be explained by a higher content of plagioclase, characteristic of these rocks (Slate et al., 1999). Unfortunately, the data on the REE patterns of clastic sedimentary rocks underlying Yucca Mountain are absent. It is most likely, however, that these rocks also carry a negative Eu anomaly.

Ground waters equilibrated with the bedrock are expected to inherit the REE patterns from them. An example from carbonate aquifers sampled in the vicinity of Yucca Mountain is shown in Figure 3-4-38. REE patterns shown in the Figure bear a striking similarity to the patterns of Early Paleozoic rocks shown in Figure 3-4-37-a. Apparently, waters equilibrated with volcanic rocks must also acquire REE patterns similar to those shown in Figure 3-4-37-c.

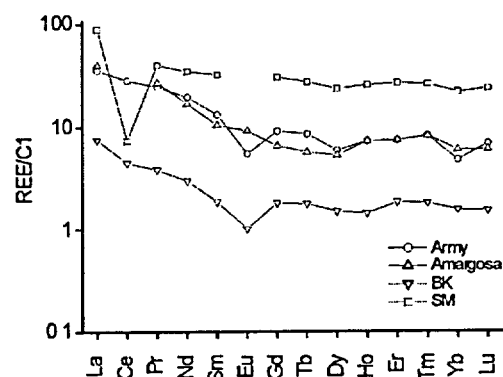


Figure 3-4-38. Chondrite-normalized REE patterns of groundwaters of the carbonate aquifers in the vicinity of Yucca Mountain. *Army* – South Nevada Test Site, *Amargosa* – Amargosa wells south and north of Bare Mountain, *BK* – Bonanza King, and *SM* – Spring Mountain. Compiled from Johannesson et al. (2000).

Summarizing, the data presented in Figures 3-4-37 and 3-4-38 demonstrate that the negative Eu anomaly may be acquired by waters from virtually any type of rocks, present in the vicinity of Yucca Mountain. Thus, the Eu anomaly is not helpful in discriminating between sources or in defining peculiarities of processes responsible for deposition of secondary minerals.

Exclusion of Eu from calcite

The inheritance of the negative Eu anomaly is not the only plausible mechanism for the deep-seated Timber Mountain calcite that has likely formed at high temperature (up to 250 °C according to Bish and Aronson, 1993). At such temperatures the oxidation state of Eu may become Eh-pH dependent. For example, Figure 3-4-34 shows two samples (L 261 and L 262) of this calcite, which are devoid of the negative Eu anomaly. Evidently, in these two cases, either the fluid was depleted in Eu or this element was being excluded from the calcite structure.

The presence of a negative Eu anomaly in some deep-seated samples and the absence in others suggests that the oxidation state of the Timber Mountain hydrothermal fluids varied between strongly reducing and near neutral. Consequently, some parts of the hydrothermal system contained trivalent Eu ions with ionic radii of 0.95 Å, which is very close to the optimal site characteristic (0.96 Å; Smyth and Bish, 1988) and these ions were being incorporated into the calcite structure. However, in some other parts of this system, the conditions seem to have been reducing enough to form Eu^{2+} with ionic radius of 1.17 Å, which is more than 15 % larger than the optimal site characteristic. The reduced Eu ions were therefore being excluded from the calcite structure creating a negative Eu anomaly in the latter. The presence of epigenetic pyrite (Weiss et al. 1994) and the local absence of a negative Eu anomaly, in

association with the Timber Mountain alteration aureole, both strongly suggest that the fluids at this stage did not inherit the Eu anomaly from the host tuffs. Instead, this anomaly is directly attributable to preferential exclusion of the reduced Eu^{2+} ions from the calcite structure.

Ce anomaly

There are three mechanisms that may be responsible for negative Ce anomaly in calcite.

Exclusion of Ce from calcite

Cerium is the only element in the lanthanide series that may change valence in the near-surface environments. Depending on the redox conditions, it may have a 3+-oxidation state (in reducing environments) or a 4+-state (in oxidizing environments). The presence of the negative Ce anomaly in the REE trends is commonly taken as an indication of near-surface oxidizing processes, which stems from the fact that Ce^{4+} is much less soluble than Ce^{3+} (Sholkovitz et al., 1994).

Ce^{3+} and Ca^{2+} in the VI-fold coordination have ionic radii of 1.034 Å and 1.00 Å, respectively (Shannon and Prewitt, 1969). Therefore, in a reducing environment Ce^{3+} readily substitutes Ca in calcite and other trigonal carbonates (Rimstidt et al, 1998). Because of its smaller ionic radius (0.80 Å), Ce^{4+} does not substitute Ca in the calcite lattice. Cerium is thus being excluded from the calcite lattice and the calcite depositing in an oxidizing environment may develop the negative Ce anomaly.

Inheritance of Ce

A pronounced Ce-anomaly is characteristic of seawater and the sediments deposited from them. For example, Johannesson et al. (2000) demonstrated that the Late Paleozoic (Pennsylvanian – Permian) carbonates in southern Nevada have REE patterns characterized by a clear negative Ce anomaly and by a somewhat less pronounced negative Eu minimum (see Figure 3-4-37-b). Late Paleozoic carbonates are not known in the immediate vicinity of Yucca Mountain (the closest outcrop is located some 33 km to the north-west in the Mid Valley area). Taking into account the fact that the character of rocks underlying the Yucca Mountain tuffs are not well known (carbonate rocks of the basement were reached by only one deep borehole, UE 25 p#1) Late Paleozoic rocks cannot be excluded from the list of potential sources of dissolved calcium carbonate and REE in the mineral-forming solutions. An example of groundwater possessing a prominent Ce anomaly is shown in figure 3-4-38.

Scavenging of Ce

The preferential uptake of Ce may be caused by the oxidation and cation exchange reactions occurring at the surfaces of some minerals, notably Mn oxides. The latter minerals are present in the Yucca Mountain secondary deposits and, as was shown by Denniston et al. (1997), they commonly contain elevated amounts of Ce. Carlos et al. (1993) demonstrated that in most cases calcite overgrows the

Mn-oxide minerals, although pyrolusite intergrown with calcite has been found as well, Vaniman and Chipera (1996). Therefore, Vaniman (1993), Vaniman and Chipera (1996) and Denniston et al. (1997) argued that Mn-oxide minerals may have removed Ce from waters moving through the vadose zone of Yucca Mountain. Minerals, deposited from these waters would thus acquire a negative Ce anomaly in the REE pattern. A similar effect would be caused by co-precipitation of Mn-oxides with other minerals.

Although the question was not exhaustively studied, preliminary information exists that suggests zeolites may selectively uptake LREE, and Ce in particular (see below). Passage of water through zeolitized tuff strata may thus produce Ce-depleted waters, and this anomaly may further be inherited by depositing minerals.

None of the mechanisms discussed above can be excluded from consideration as a possible cause of the Ce anomaly in the studied minerals. It is important to recognize that all three mechanisms fit into both competing concepts (rainwater and hydrothermal upwelling). For example, rainwater and upwelling hydrothermal fluids would acquire their dissolved calcite load through the dissolution of carbonate rocks of the basement (directly or in the form of carbonaceous dust deposited on the surface). Thus, inheritance of the REE signal may be expected for both. As we have shown in Figures 3-4-37, some carbonate rocks of the basement do carry a pronounced negative Ce-anomaly. We will see below that some waters from the carbonate aquifer also exhibit the anomaly.

The water equilibrated at depth (i.e., in a reducing environment) with rocks that do not possess the Ce-anomaly, may acquire it if it is transferred into the oxidizing environment. Water, circulating through the vadose zone would have been oxidizing, whether it was rainwater percolating down from the surface or hydrothermal fluid injected into the vadose zone (early portions of such water could have been reducing, but it could not have remained in this state in the vadose zone for any extended period of time). Therefore, the exclusion of Ce from the calcite lattice due to the oxidizing character of the environment is expected for both models. Finally, waters circulating through the vadose zone would interact with preexisting Mn-oxide minerals notwithstanding the origin of fluids and the direction of flow.

REE in ground waters

Johannesson et al. (2000) reported data on the REE contents in ground waters and the host aquifer rocks, volcanic and carbonate, from southwestern Nevada. The data show that the negative Eu anomaly is characteristic of water from not only volcanic, but also some carbonate aquifers (Figure 3-4-38). For example, waters from the Army well (southern part of the Nevada Test Site) and from the Bonanza King carbonates (30 km to the south of the Nevada Test Site) have a pronounced Eu anomaly, whereas waters from Amargosa wells do not have it. Important information presented by Johannesson et al. (2000) is that the negative Ce-anomaly might be characteristic of the deep Late Paleozoic carbonate aquifers.

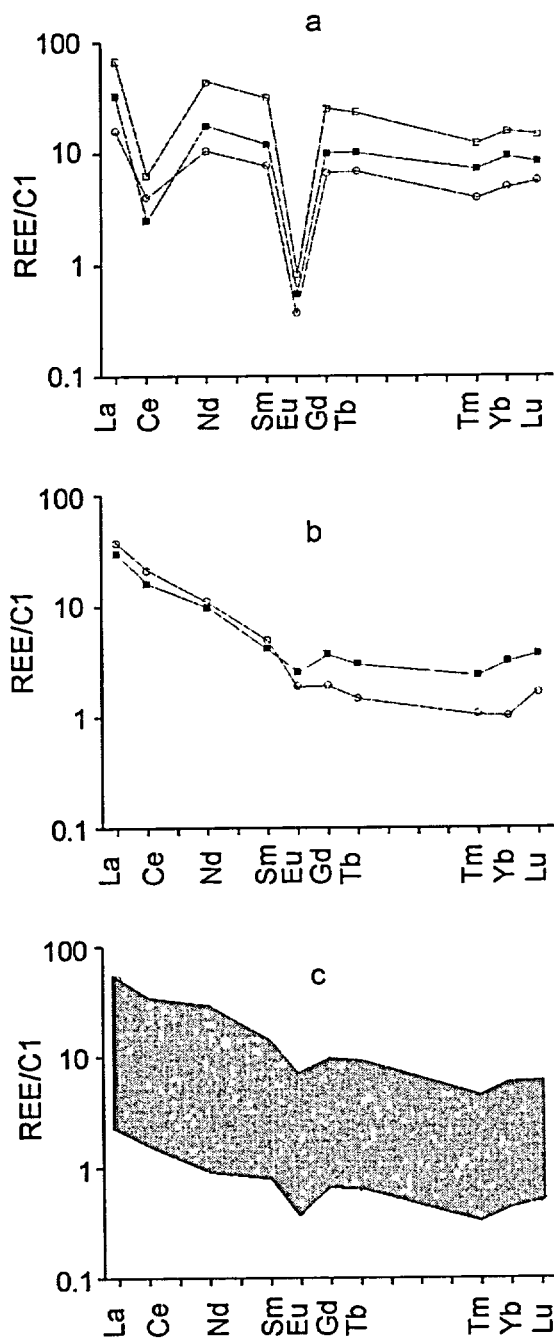


Figure 3-4-39. REE patterns of the secondary fluorite from the ESF (*a* and *b*) and from two industrial epithermal fluorspar deposits, Daisy Mine and Diamond Queen Mine, at Bare Mountain (*c*).

a - fluorite from the carbonate assemblage; fracture, ESF Station 52+43; *b* - fluorite from the silica assemblage; fracture, ESF station 16+08; *c* - range of REE patterns for fluorite from Bare Mountain fluorspar deposits. INAA analyses performed at the United Institute of Geology, Geophysics and Mineralogy SB RAS, Novosibirsk. Analysts M. Melgunov and E. Melgunova.

For example, groundwater from the Spring Mountain carbonate aquifers (50 km to the southeast of Yucca Mountain) exhibits a pronounced Ce-minimum (see Figure 3-4-38).

The data by Johannesson et al. (2000) clearly demonstrate that ground waters carrying either the Ce or Eu minima are present in carbonate aquifers in the vicinity of Yucca Mountain. Although Late Paleozoic carbonates have not been found directly beneath the Yucca Mountain, their outcropping at Mid Valley suggests that waters carrying both the Ce and Eu minima could also enter the vadose zone. If these waters did enter the vadose zone of Yucca Mountain, they may oxidize or interact with Mn-oxide minerals, rhyolite or quartz-latitude tuffs and even with meteoric waters to obtain or enhance the Ce and Eu minima and form REE pattern of the second type.

Unfortunately, we do not have the data on the REE geochemistry of the Precambrian clastic rocks of the basement. It is known that clastic rocks commonly have the Eu-anomaly. Since rhyolitic volcanic rocks of Yucca Mountain may be viewed as derivatives of the basement rocks, and these volcanics do have the Eu anomaly, it is reasonable to expect that waters, equilibrated with the clastic rocks of the basement would also carry the Eu-anomaly.

REE composition of minerals other than calcite

The available REE database mostly consists of analyses of secondary calcites. The complete geochemical analysis would require additional data on the REE distribution in other minerals, co-genetic with minerals of the secondary carbonate and the silica assemblages. The most promising subject for study, in this regard, is fluorite – a mineral with an unquestionable hydrothermal nature, which cannot, thermodynamically, form through the interaction of meteoric waters with Yucca Mountain rhyolitic tuffs (Palyanova et al., 2002). We have obtained multiple REE abundance patterns for two fluorite separates from the ESF (stations 16+08 and 52+43; Figure 3-4-39). The first fluorite belongs to the silica assemblage and occurs as overgrowths on the euhedral quartz crystals. The second one occurs as crystals and spherulites intergrown with calcite of the carbonate assemblage.

The figure shows that the fluorite from the carbonate assemblage is tagged by a double Ce and Eu anomaly (pattern of the *second type*) whereas the fluorite of silica assemblage is associated with a moderate single negative Eu anomaly (pattern of the *first type*). Importantly, the station 16+08 is located within the quartz-latitude horizon of the Topopah Spring tuff and we can see that fluorite deposited in the fracture does not inherit the specific quartz-latitude pattern (i.e., a zero or positive Eu anomaly). Both ESF specimens in Figure 3-4-39 represent the secondary calcite-silica deposits from the present-day vadose zone, and both were precipitated from thermal fluids (see Chapter 3-6). The two completely different REE patterns, determined for the same mineral found in the same setting (deposition in a fracture) indicate that two different chemical environments have likely existed in the past in what is now the vadose zone of Yucca Mountain. Importantly, the REE patterns of fluorite from the silica assemblage are very similar to the pattern of fluorite from the epithermal fluorspar deposits from Bare Mountain (Figure 3-4-39-c).

Calculated values of the Eu and Ce anomalies for fluorite samples are shown in Figure 3-4-40. There, the values of 1 on both axes correspond to the "no anomaly" situation, whereas all values less than unity reflect the degree of depletion of a mineral in Eu and Ce. Two interesting features are immediately apparent from the figure. First, two fluorite samples from the ESF (i.e., from the vadose zone) reveal two dramatically different REE patterns, in terms of the Eu and Ce anomalies. Fluorite from the carbonate assemblage has pronounced Eu and Ce negative anomalies, whereas these anomalies in fluorite from the silica assemblage are minor. In terms of the parameters of the Eu and Ce anomalies, as well as the overall REE pattern, the latter fluorite is statistically indistinguishable from the fluorite collected at two epithermal fluorspar deposits at Bare Mountain – Diamond Queen/Goldspar and Daisy. It must be noted that the latter deposits, hosted by the Early Paleozoic carbonate rocks and representative of the shallow (several hundred meters from surface) fluorite-Au-Hg type of mineralization formed around 12.9 Ma (K/Ar ages on the replacement adularia; Noble et al., 1991); before the emplacement of the Paintbrush Tuff that hosts the fluorite sampled in the ESF (12.7-18.8 Ma). Nevertheless, the parameters of the fluids from which the fluorite was deposited, as reflected by the REE geochemistry, are virtually identical. Having in mind dramatic difference in REE patterns between two temporally similar fluorites Smirnov et al (2002) suggested that formation of fluorite mineralization involved multiple sources of matter that include Pleozoic carbonate hosted fluorite deposits of Yucca Mountain basement and deep-seated clastic Proterozoic rocks.

Second, one fluorite sample studied by Vaniman and Chipera (1996) from the phreatic zone (approximately 175 m below the modern water table) in borehole USW G-2 had Eu and Ce anomalies identical to those characteristic of the vadose-zone calcite collected from the ESF (approximately 370 m above the modern water table).

Figure 3-4-40 shows chondrite-normalized patterns for the three most important secondary minerals of Yucca Mountain – fluorite, opal-A and zeolites reported by Vaniman and Chipera (1996). It is obvious that opal and fluorite carry flat patterns tagged by Ce and Eu minima (*second type*). The pattern of the zeolites is more similar to rhyolitic or early Paleozoic carbonate (*first type*)

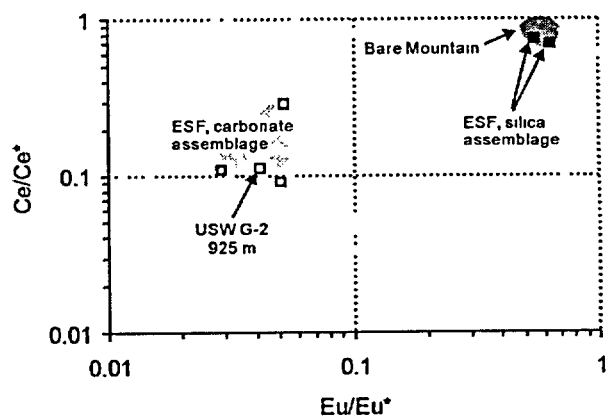


Figure 3-4-40. Ce and Eu anomalies in fluorite calculated on the basis of the data presented in Figure MIN-17REE. Tight gray field denoted "Fluorspar, Bare Mountain" envelops 10 individual data points. The datum point USW G-2 925 m is from Vaniman and Chipera (1996). Note that this sample is located some 175 m below the modern water table.

and contains a slight, yet distinctly positive Ce anomaly. It thus becomes apparent that the Mn-oxide minerals are not the only potential "sink" for Ce. Zeolites are known for their ability to sieve out large cations like REE's and Sr from water solutions. Therefore, they could prevent Ce from being incorporated into the co-genetic calcite or other secondary minerals.

Discussion

The database of the REE properties of minerals from the vadose zone and from the deep phreatic zone of Yucca Mountain does show that, as a rule, there is a pronounced difference between these two sets of minerals. The most important question that needs to be answered is:

Does this feature, indeed, reflect the difference between the two hydrological settings (phreatic vs. vadose) or it may reflect the different physicochemical parameters of the processes of mineral precipitation that both occurred under hydrologically saturated (phreatic) environments at different stages of the geological history of Yucca Mountain? In addressing this question, samples having uncharacteristic REE patterns ("exceptions to the rule") may provide important information.

"Vadose-zone" REE patterns in the phreatic minerals

Two calcite samples and one fluorite sample from borehole, USW G-3, collected at depths of 898, 917, and 925 m demonstrated the REE patterns possessing pronounced negative Ce and Eu anomalies (Figure 3-4-42). Thus, minerals with the REE properties ascribed to the vadose zone setting occur at depths of 150 to 175 m below the water table. One way of explaining these anomalies would be to invoke the high-amplitude fluctuations of the water table (approximately 300 m, from -180 m to +120 m; the later number is from U.S. DOE, 2001, p. 1-30). This unlikely scenario becomes even more problematic if one considers the stable isotope data from the calcites below the water table. Whelan et al. (1998) reported that the $\delta^{13}\text{C}$ of calcite collected up to 300 m below the water table range between -10 and +5 ‰ PDB, which spans almost the entire range of values measured in the vadose zone calcite. Taking into account that $\delta^{13}\text{C}$ isotopic ratios show a systematic pattern of decrease from the early parts of calcite to its late parts (see Section 3.5.2. for details), in the framework of the "rainwater concept", the data must be interpreted as indicating that the water table resided at a depth some 300 m greater than it is today for

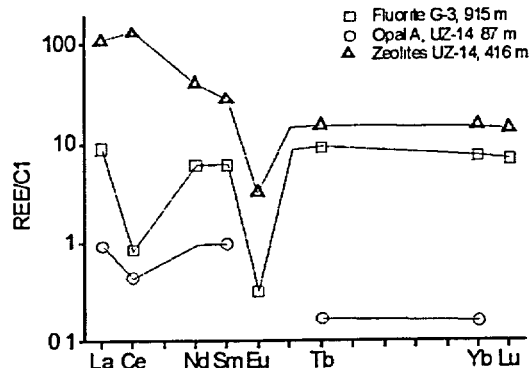


Figure 3-4-41. REE patterns of some secondary minerals deposited in rhyolitic tuffs of Yucca Mountain. Note slight Ce maximum in composition of zeolites and pronounced Ce minima in compositions of fluorite and opal-A. Concentration of Eu is not shown for opal-A because it was less than detection limit (<0.1 ppm). Data by Vaniman and Chipera (1996).

most of the calcite growth history. At the same time, the surface exposures of the spring deposits indicate that on a number of occasions, the water table was in fact substantially higher (up to 120 m; U.S. DOE, 2001) than it is today.

If the hydrothermal upwelling interpretation is accepted, however, the contradiction disappears. Calcite and fluorite from the "shallow phreatic" zone may be interpreted as part of the alkali-earth alteration aureole (see Chapter 3-1 for details), genetically identical to the mineralization in the vadose zone sampled in boreholes and in the ESF.

"Phreatic zone" REE patterns in the vadose zone minerals

Some samples (calcite and fluorite) from the ESF, as well as from the topographic surface (e.g., calcite from Trench 14) yielded REE patterns that appear to be characteristic of the deep-seated phreatic minerals rather than those of the vadose-zone. Figure 3-4-43 shows a series of samples that show clear Eu minima but no Ce minima. Apparently, in this case, no processes providing for Ce depletion in calcite and fluorite

(e.g., inheritance of the Ce anomaly, exclusion of Ce from mineral structure due to inappropriate ionic sizes, or scavenging by pre-existing or co-precipitating minerals) were operational during the formation of these deposits.

It is noteworthy that the unusual REE-patterns for the vadose-zone mineralization all occur in locations in the vicinity of the horst-bounding Bow Ridge–Paintbrush fault system (ESF samples are collected from near the North Portal (calcite) and in the North Ramp (fluorite); Trench 14 is excavated across the Bow Ridge fault at the surface). We note with respect to this connection, that this part of the repository block is characterized by the anomalous properties of secondary mineralization, including the dominant role of the silica mineral assemblage (discussed in this Chapter), the anomalously light values of $\delta^{18}\text{O}$ in calcite (Section 3.5.2.), and the highest fluid inclusion temperatures (Chapter 3-6). We relate

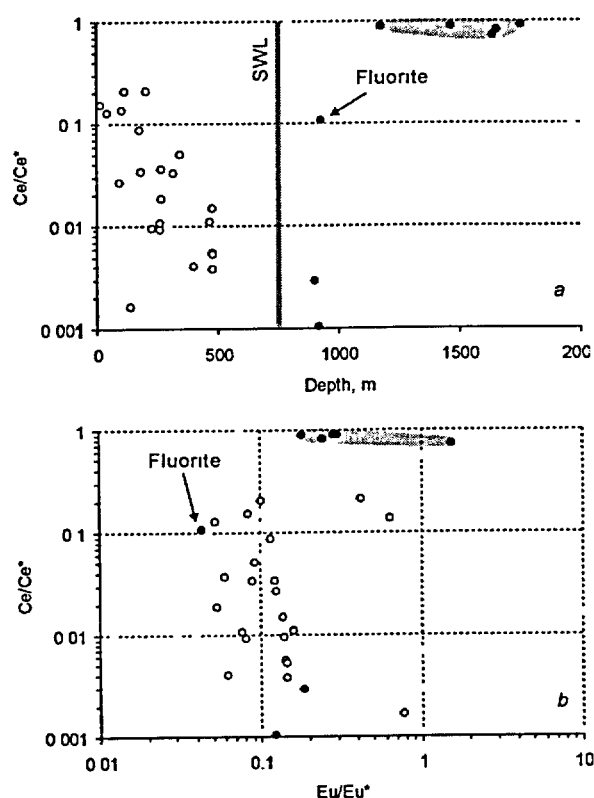


Figure 3-4-42. Values of negative Ce anomaly vs. depth (a) and Eu anomaly vs. Ce anomaly (b) for borehole samples (Vaniman and Chipera, 1996). Filled circles – calcite and fluorite from phreatic zone; open circles – calcite from vadose zone; shaded area – field of characteristic values for Timber Mountain calcite. All of the three "anomalous" data are from the USW G-3 borehole. SWL – modern static water table.

these features to the role that the deep-seated horst-bounding fault must have played in channeling the movement of the hydrothermal upwelling fluids. Such fluids would have carried geochemical (including REE) signatures characteristic of the deep subsurface.

Summary

Our analysis shows that the concept explaining the migration of the REE's and their specific patterns in the vadose-zone and phreatic-zone minerals, developed by the Yucca Mountain Project researchers, is based on the *a priori* assumption of the rainwater origin for the migrating water. The rainwater origin, however, is not unique.

We have demonstrated that the volcanic rock sequence interacting with rainwater at Yucca Mountain is not the only mechanism that may have produced the REE patterns observed in secondary minerals (e.g., enrichment in LREE and Eu minimum). We have discussed a number of mechanisms that may be responsible for the appearance of the negative Ce anomaly; these mechanisms, however, are equally

plausible within both the "rainwater" and the hydrothermal upwelling models. Some features of the REE record, notably the "vadose-zone" patterns of samples collected almost 180 m below the modern water table, are difficult to reconcile with the hypothetical "rainwater" origin of the minerals. REE geochemistry of secondary fluorite strongly suggests the multiple sources for fluids deposited secondary minerals in fractures and lithophysaes of Yucca Mountain.

The REE and trace element studies are potentially a powerful tool for deciphering origins and environments accomodating the deposition of minerals. Application of this tool to the Yucca Mountain mineralization is hindered by substantial gaps in the database. For instance, more detailed studies of different minerals from the vadose zone, as well as of minerals and rocks underlying the Miocene

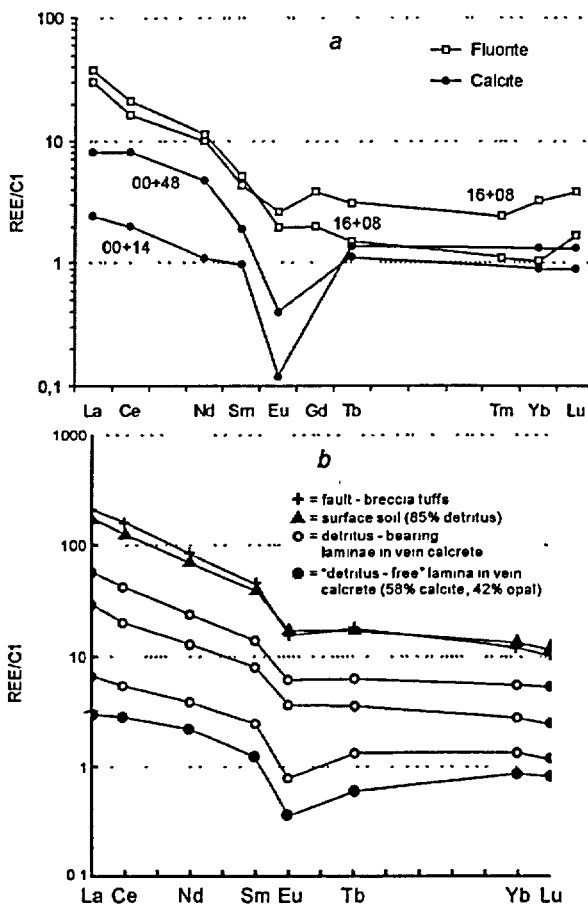


Figure 3-4-43. REE patterns of minerals from the vicinity of the Bow Ridge fault. *a* – calcite and fluorite from the North ramp of the ESF (ESF stations are shown); *b* – calcrites from Trench 14. Data sources: calcite from ESF – Vaniman and Chipera (1996); fluorite from ESF – this study; calcrites from Trench 14 – U.S. DOE (1993).

volcanic tuffs are warranted. Also necessary are studies of REE patterns in local waters (pore waters and perched waters in the vadose zone and waters from both rhyolite and carbonate aquifers underlying the repository zone).

3.4.6.4.7. Uranium in the silica minerals

One important geochemical feature requires additional discussion. This feature is the conspicuous enrichment of opals, and in some cases chalcedonies, sampled in the ESF, with uranium. In the course of the detailed work related to the U-Th and U-Pb dating effort (e.g. Paces et al, 1996 and 2001, Neymark et al. 2000 and 2002), the greatest content of U measured in secondary opal was 789 ppm, and values between 50 and 200 ppm comprised 77% of the database (see Appendices 3-7-1 and 3-7-2 in Chapter 3-7 for detailed discussion of the U data). Thus, the subject opal may be defined as uraniferous and the mode of its formation deserves close attention.

Uraniferous opals are known in association with both sedimentary and vein-type hydrothermal uranium deposits. They were also reported from areas, where no commercial deposits have been discovered. There, too, they may be related either to percolation of meteoric waters through U-rich sediments (e.g., Shirley Basin, Wyoming; Zielinski, 1980), or to the upwelling of thermalized ground waters along normal faults (e.g., Virgin Valley, Nevada; Zielinski, 1982). In all cases, uraniferous opals are believed to be the result of the interplay between the two governing parameters: elevated U contents in ancient ground water and high adsorptive properties of the silica-gel parent of the opal.

The most common source rocks for U in groundwater are silicic tuffaceous sediments or igneous rocks. The potential source rocks are present at Yucca Mountain in abundance. These are the Miocene rhyolitic tuffs and lava flows, as well as their igneous counterparts. It is known with certainty that uranium-enriched solutions, presumably of the deep-seated origin, did circulate through the rocks just 10-12 km west of Yucca Mountain approximately 13 Ma ago during the formation of the economic epithermal fluorspar deposits at Bare Mountain. Samples of fluorspar collected from Daisy mine contained from 0.002 to 0.015 equiv.% of U (Lovering, 1954), and fluorite from the Goldspar/Diamond Queen mine contained up to 50.7 ppm U (this study). By contrast, the contents of U in fluorites from the ESF do not exceed 19.3 ppm (this study).

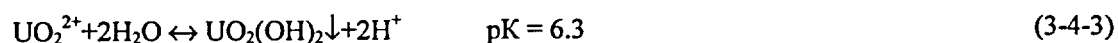
Silica and U geochemistry

Uranium cannot isomorphically substitute silicon in the silica-oxygen compounds. The Si^{4+} has an ionic radius of 0.39, whereas the smallest uranium ion, U^{6+} , has a radius of 0.83 Å (Sherbina and Naumov, 1963) and the radius of U^{4+} is 0.93 Å (Green, 1959). In addition, uranium in aqueous solutions is typically present in the form of the stable uranyl ion, which has sizes 6.04-6.84 Å along its long axis

and 2.64 Å along the short axis. Thus, the uptake of U by silica minerals must have a non-isomorphic character.

Uranium in nature is mostly transported in the form of the U^{4+} or U^{6+} compounds. U^{4+} is more typical of the magmatic processes, whereas U^{6+} is predominant in the hydrothermal solutions as well as in ground waters. This stems from the higher solubility of U^{6+} relative to U^{4+} (Garrels and Christ, 1965). In aqueous solutions uranium forms complexes containing uranyl-ion UO_2^{2+} . Reduction of U^{6+} to U^{4+} leads to formation of poorly soluble UO_2 и $U(OH)_4$, which leads to the removal of uranium from solution. The presence of the carbonate-ion, as well as the weakly alkaline character of the typical ground waters enhances the solubility of uranium due to formation of negatively charged uranyl carbonate complexes $UO_2(CO_3)_2(H_2O)_2^{2-}$ and $UO_2(CO_3)_3^{4-}$. The complexes are stable over a broad range of temperatures. In acidic solutions, uranium forms hydroxyl complexes and also migrates as free uranyl. In the presence of fluorine, uranyl fluoride complexes appear. Although fluorine complexes typically form in the acidic environment ($pH < 4$), at high concentrations of F the stability field of these complexes expands to encompass neutral and weakly alkaline areas also (Sherbina and Naumov, 1963). Taking into account the ubiquitous character of accessory fluorite in secondary mineralization from the ESF, fluoride complexes of U must be considered among the possible forms of uranium migration at Yucca Mountain.

The possibility of U migration in the form of the silicate complexes has been examined by Ermolaev et al. (1965), Truesdell and Jones (1974) and Langmuir (1978). It has been concluded that this form plays a minor role in U migration. This stems from the fact that the dissociation of the polysilicon acids is negligible (reaction constant on the order of $1 \cdot 10^{-21}$) and it occurs only at high pH (about 9 and higher; Sherbina and Naumov, 1963). Under such conditions uranyl is readily hydrolyzed and precipitates in the form of uranyl hydroxide:



In alkaline carbonate-bearing solutions uranyl will tend to form complexes with the carbonate rather than with the poorly dissociated polysilicon acids.

Uptake of uranium by silica minerals

So far the only concept explaining the mode of formation of uraniferous silica minerals envisages an uptake of uranium via the adsorption on and co-precipitation with colloidal silica. Zielinski (1980 and 1982) argued that in silica-supersaturated solutions silica gel precipitates could effectively compete with carbonate-rich solutions for dissolved uranium. The concept seems to be directly applicable to Yucca Mountain, where both carbonate- and silica-bearing waters circulated, and opal, chalcedony and fluorite

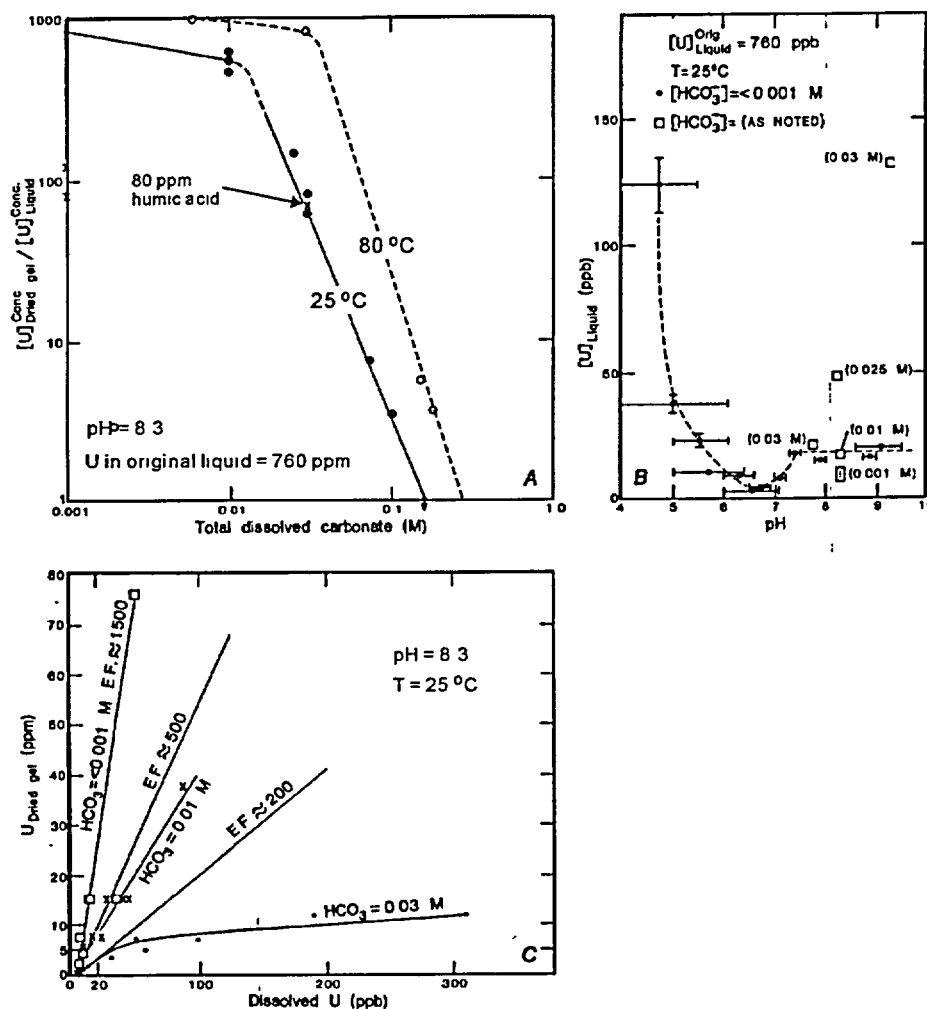


Figure 3-4-44. Experimental results of uranium partitioning between solution and silica gel. *A* – The concentration of uranium of separated, dried silica gel plotted versus the total dissolved-carbonate content of the liquid. *B* – The uranium concentrations of liquid in equilibrium with freshly precipitated silica gel, plotted versus pH. *C* – The concentration of uranium of separated, dried silica gel and coexisting liquid as a function of total uranium content and calculated enrichment factors (E.F.). From Zielinski (1980).

commonly formed from or in the presence of colloids. (The evidence regarding the role of colloidal solutions in the deposition of secondary minerals from the ESF was discussed in Section 3.4.5.5.).

The ability of colloidal silica to adsorb radioactive matter was first experimentally demonstrated by Ebler (1911). Later Zielinski (1980) demonstrated that opal formed through precipitation of silica gel may adsorb significant amounts of uranium, and that the efficiency of adsorption is strongly influenced by the content of the dissolved carbonate, the temperature and the pH. Experiments have demonstrated that for water with pH 7.0 to 8.5, total dissolved carbonate of 0.001 to 0.01 mole, and $T = 25\text{--}80^\circ\text{C}$, the dried silica gel precipitates may have about 400 to 1,500 times the uranium concentration of the original

coexisting solutions (see Figure 3-4-44). Greater concentrations of dissolved carbonate reduce the efficiency of uranium incorporation in silica gel. Zielinski (1980) noted that the carbonate concentration of typical ground waters might partially be buffered by the precipitation of calcite. This would definitely be the case at Yucca Mountain, where silica minerals are commonly co-precipitated or are intercalated with calcite. Limited experimental data suggest that the efficiency of uranium uptake may be greater at 80 °C than it is at 25 °C (Figure 3-4-44-a).

Adsorption on colloidal particles of silica is controlled by the presence of the negatively charged hydroxyl groups on the surface of the silica micelles. Therefore, direct adsorption of the negatively charged uranyl carbonate or most uranyl fluoride complexes is not electrostatically favored. Formation of the positively charged hydroxyl complex or free uranyl requires an acidic environment ($\text{pH} < 5$; Garrels and Christ, 1965), which is not feasible for the Yucca Mountain geochemical system. Nevertheless, Zielinski (1980) hypothesized that uranyl-hydroxyl complexation was the major factor controlling adsorption of uranium on silica gels:

One possible mechanism involves sorption of positively charged uranyl complexes such as uranyl-silica-hydroxyl or uranyl-hydroxyl, which are present as minor dissolved species (Langmuir, 1978; Truesdell and Jones, 1974). Such complexes should be strongly attracted to the negatively charged surfaces of silica gel and could be adsorbed via formation of hydrogen bonds with the hydroxylated surfaces of the gel (Iler, 1955). As positively charged complexes are selectively removed from solution, new amounts of the same complexes are regenerated from the remaining dissolved uranium species in response to the prevailing solution equilibria. The result is major sorption of uranium via a minor dissolved species. (p. 599-600).

Another potential mechanism of uranium uptake is adsorption of uranyl bicarbonate through an intermediary cation, which partly neutralizes the negative surface charge of the silica gel. Such partial charge neutralization is possible in solutions with high concentrations of cations (Iler, 1955). Although this mechanism seemed to be a less likely explanation of experimental results by Zielinski (1980), where carbonate was added to solutions in the form of NaHCO_3 , it might be more realistic for the specific environment of Yucca Mountain. There, solutions contained substantial amounts of Ca^{2+} , and, in the late stages of mineral deposition, Mg^{2+} . Magnesium, introduced in the calcium-bearing solutions, increases the ionic strength and stabilizes the colloids. These divalent alkaline-earth cations adsorbed on the micelle's surfaces could have served as intermediaries promoting adsorption of the negatively charged uranyl carbonate complexes.

Summarizing, the enrichment of opals and chalcedony from the Yucca Mountain vadose zone in uranium is related, most likely, to the sorption on the silica colloids. The details of the process (e.g., the nature of the uranium species involved in the adsorption, controlling parameters, etc.) are presently not well understood. Substantial variability of U-abundances reported from the Yucca Mountain samples suggests that the process was complex and its outcome was controlled by the interplay of a number of

parameters of fluids. One of those parameters is the chemistry of fluids. Variability of this parameter is apparent from the alternating deposition of the silica and the carbonate assemblages and the appearance of fluorite, strontianite, and zeolites. It is apparent that the activities of carbonate, fluorine and, possibly, minor sulfate and phosphate ions varied in the course of mineral deposition. All of these ions are capable of forming ligands with uranyl ions; therefore their changing activities should have influenced the behavior of U in solution.

An additional controlling parameter would be the time available for adsorption, or the time between the formation of colloidal particles and their coagulation and precipitation. These processes will be discussed in more details in Chapter 3-7. Here we will note that the coagulation of colloids is a strong function of the temperature (T^5).

Finally, the uranium content in mineral-forming solutions should also be an important factor controlling the amount of uranium incorporated in silica minerals.

Zielinski (1980) noted: "*Whatever the adsorption mechanism, adsorption continues until equilibrium between sorption ↔ desorption is established at the given set of environmental conditions. The experimental results indicate that ion exchange by sorption-desorption ceases or is greatly slowed by drying of the gel. Drying results in irreversible gel compaction and the closing of the interparticle pores once accessible to coexisting solution (Iller, 1965).*" (p. 600).

U-contents in the mineral-forming fluids

Experiments carried out by Zielinski (1980) and presented in Figure 3-4-44 had parameters fairly similar to the parameters of ancient fluids, which circulated through Yucca Mountain. The temperature range of mineral deposition at Yucca Mountain, established by fluid inclusions, is 85 to less than 35-50 °C, salinities (TDS) less than 21,000 ppm NaCl equiv., contents of dissolved carbonate buffered by precipitation of calcite (Dublyansky et al., 2001). Silica colloids in Zielinski's experiments equilibrated with solution for 7 days, which is close to our assessment of the time necessary for water exchange in the mineralized cavities at Yucca Mountain (1-10 days; see Chapter 3-7 for details). The results of Zielinski's experiments may thus be used to assess the contents of uranium dissolved in mineral forming fluids at Yucca Mountain.

We estimate the minimum HCO_3^- content in the Yucca Mountain paleofluids to be about 0.002 M (this corresponds to the HCO_3^- contents in modern groundwaters of volcanic aquifers underlying Yucca Mountain sampled in USW G-4 well). For colloidal opals precipitated from such waters, enrichment factors as high as ~800 to 1,100 are predicted (Zielinski, 1980). Assuming that these enrichment factors are realistic, waters that deposited opals containing the amounts of U similar to the average values

measured at Yucca Mountain (i.e., 20 to 200 ppm), must have been carrying from ~20 to 200 ppb of dissolved U. The enrichment factor decreases sharply with increasing dissolved carbonate content; hence substantially higher concentrations of U, from ~50 to 500 ppb, would be required to deposit uraniferous opals from groundwater with parameters similar to those of waters from the Yucca Mountain carbonate aquifer (~0.009 M HCO₃⁻; data from well UE25 p#1; Ebinger, 1992). Precipitation of opal with the highest measured U content (780 ppm) would require fluid containing between approximately 800 and 2,000 ppb of dissolved uranium.

These estimated values are well above the typical values characteristic of the low-temperature ground water (<1-20 ppb; Zielinski, 1982). They are also above the values typical of waters from the Yucca Mountain area, which include saturated-zone ground waters from 0.5 to 4.0 ppb U and vadose zone waters (sampled in the course of the Single and the Drift-Scale heater tests) from 0.05 to 0.01 ppb U (Fabryka-Martin et al., 2000).

Studying the uraniferous opals from Virgin Valley, Nevada, Zielinski (1982) estimated the uranium concentrations in ancient fluids there as between 5 and 800 ppb. He concluded: "*Such high values require an anomalously efficient process of uranium uptake and/or a U-rich source to provide dissolved uranium.*" (p. 208). This conclusion equally applies to Yucca Mountain uraniferous opals. Taking into account the specifics of the geochemistry of the mineral-forming fluid at Yucca Mountain, the efficiency of U uptake is unlikely to have been abnormally high there. In contrast to Virgin Valley, we can see from the mineralogic record that both "competitors" of silica gels, carbonate and (at times) fluorine ions, were present in the opal-precipitating solutions. This would tend to decrease rather than increase the efficiency of the uranium uptake by silica colloids.

Summary on U in silica minerals

Formation of uraniferous opals among the Yucca Mountain secondary minerals requires at least two conditions:

- Opals and chalcedonies should have formed from colloidal solutions; and
- The mineral-forming fluids must have carried elevated amounts of uranium (5 to 100,000 times the content of U in modern waters from the Yucca Mountain region).

3.4.6.5. Summary on mineralogy and geochemistry

The complex chemistry of fluids and the deposited mineral assemblages, such as was described for the Yucca Mountain vadose-zone secondary mineralization is atypical of the supergene deposits, in which meteoric waters play the major role as the mineralizing agent. On the other hand, such chemistry is typical of the low-temperature hydrothermal (epithermal) deposits (Lebedev, 1979; Stankeev, 1986).

The association of Ca-Sr-Mg requires a carbonate rock source. The most logical carbonate source is the limestone and dolomite rock of the Paleozoic carbonate formations, underlying the Yucca Mountain rhyolites. Waters of the carbonate aquifer, tapped by drill hole UE-25 p#1 are mineralized and contain substantial quantities of Ca (up to 100 mg·l⁻¹), Mg (up to 39 mg·l⁻¹) and Sr (up to 450 µg·l⁻¹) (Benson and McKinley, 1985). In the outcrops of Bare Mountain (tectonically an uplifted block of the Nopah formation some 15 km to the west of Yucca Mountain), Paleozoic carbonates host numerous hydrothermal ore deposits (including economic fluorspar and uranium deposits). Similar rocks underlie the Yucca Mountain rhyolites. The waters passing through such rocks could easily have acquired all the elements that were found in the secondary minerals at Yucca Mountain.

3.4.6.6. Textures of secondary deposits

3.4.6.6.1. Geopetal appearance of the crusts

One of the most striking features of the calcite-silica deposits in the ESF is their occurrence at the floors of cavities and footwalls of fractures, which suggests that deposition of the minerals was strongly affected by the force of gravity. The Yucca Mountain Project researchers interpret this feature as an indication of crystallization in the vadose zone from gravity-driven films or sheets of water (e.g., Paces et al., 1996; 2001). Even though a number of occurrences of secondary silica and calcite along the North ramp of the ESF were found to be non-geopetal (see Figures 3-4-4 and 3-4-14), we agree that most of the mineral crusts in the ESF do show gravity-controlled textures. Does this mean, however, that these deposits crystallized from gravity driven films of waters? Such a claim cannot be substantiated in our opinion.

Calcite at Yucca Mountain crystallized from solutions through chemical reactions. The reactions themselves are not subject to the control of gravity. The force of gravity, however, may control places where crystal growth begins and continues. If crystallization begins due to the abrupt change of the saturation state of the fluid (for calcite this may be caused, for example, by degassing of dissolved CO₂ caused by a rapid pressure drop during an earthquake), tiny crystal nuclei may form in the bulk of the fluid (so-called homogeneous nucleation). If degassing is vigorous, these nuclei may become large enough so that they sedimentate under the force of gravity and, upon settling on the cavity floors, serve as "seeds" for further crystal growth. This mechanism of producing crystal linings of cavity floors is well known in natural hydrothermal and phreatic mineral deposits (e.g., Grigoriev and Zhabin 1975). Textbook examples of such linings are shown in Figure 3-4-45.

One complication to the proposed scheme of the initiation of crystal growth is that the work required to form a nucleus on the interface between the two phases (for example, a cavity wall) is smaller than that required to support homogeneous nucleation in the bulk of the solution (Chernov et al., 1980). Thus, if the cavity had been filled with water during nucleation, some crystals would be expected to have nucleated on the cavity walls even if the majority of nuclei formed through homogeneous nucleation. This does not fit the pattern of cavity linings observed at Yucca Mountain, where most cavities have barren ceilings and hanging walls.

A number of mechanisms working in conjunction may be responsible. One reason could be that bubbles of gases expelled from the fluid during a seismic event, which triggers supersaturation, would move to the cavity ceilings due to buoyancy, where they would form gas pockets preventing nucleation there. Another possible reason is the effect of elastic vibrations associated with earthquakes. The latter are known to produce broadband vibrations (0.1 Hz to 10-30 kHz). Such vibrations of the rock at the time of nucleation would strip the forming nuclei from the walls (an effect similar to the ultrasonic cleaner). It must be stressed that the operation of such mechanisms does not have to be long. It would be sufficient to "protect" ceilings from nucleation during the first, very short period of vigorous nucleation; after that enough seeds would be present in the bulk of the fluid and at the cavity floor to ensure further preferential crystallization there.

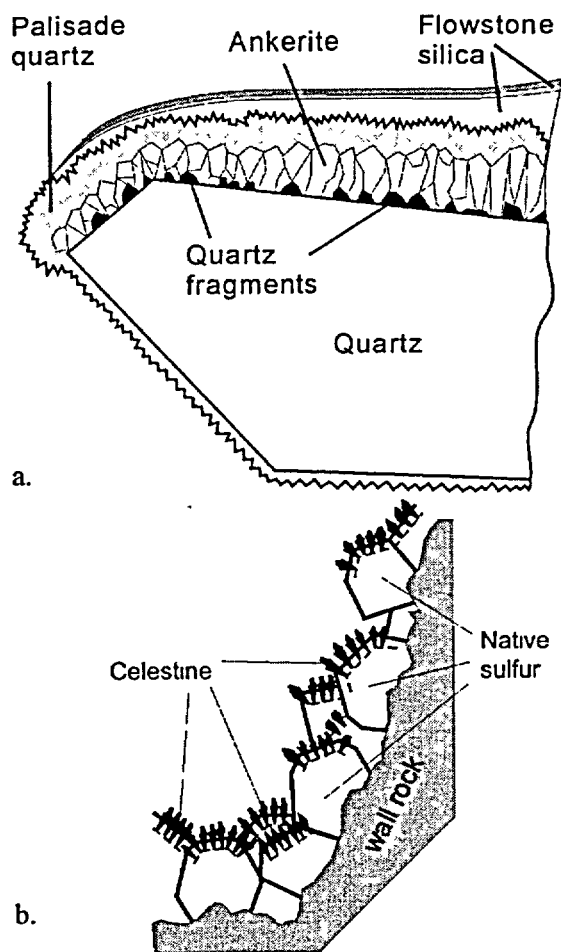


Figure 3-4-45. Examples of gravity-controlled crystal growth in the hydrothermal and low-temperature phreatic (saturated) environment. *a* - Hydrothermal quartz-ankerite assemblage, Urals, Russia and *b* - low temperature gypsum-sulfur deposit Shor-Su, Turkmenistan. Note that ankerite (*a*) and celestite crystals (*b*) grow on the upward-oriented surfaces of earlier crystals of quartz and native sulfur. Palisade quartz, although growing on all surfaces, also exhibits pronounced growth asymmetry (*a*). From Grigoriev and Zhabin (1975) and Yushkin (1966).

Gravity may also control the location of chemically grown deposits by controlling the availability of the mineral-forming fluid. If local accumulations of water were present at the bottoms of cavities, crystallization would preferentially occur in such micro-ponds, similar to pool spar found in caves (Hill and Forti 1997, p. 102). The absence of standing watermarks in the Yucca Mountain cavities (e.g., Paces et al. 2001) might be caused by water bodies that were transient in their character where the water level did not stay at the same place for an extended period of time sufficient to create deposits like shelfstones of folia (see Hill and Forti 1997 for description).

Overall, the gravity-related asymmetry is a common feature in speleothems that are formed from water films. It would be quite unusual for speleothems, however, to precipitate exclusively at the floors of caves, leaving walls and ceilings bare. This is because water films or sheets moving downward under the force of gravity must inevitably wet all surfaces. Consider a hypothetical water film that, moving down along the open fracture wall enters a lithophysal cavity. To get to the floor of the cavity, the film would have to flow first along the cavity walls. The velocity of the water film flow would be variable and quite irregular due to the varying roughness of the surface (for example, the surface of lithophysal cavities is typically lined with a "palisade" of 0.3-1.0 mm-long vapor-phase minerals, whereas surfaces of fractures are commonly smooth), and due to the variable slopes of the surface (from near horizontal at the top of the cavity to near vertical at the sides). Why then does this fluid, carrying dissolved calcite and silica, never leave any precipitate on the walls? It might be argued that the water accumulated at the cavity floors and subsequently reached supersaturation via evaporation. Such a hypothetical mechanism would still fail to explain the geopetal character of deposits in steep fractures, where "ponding" is impossible. In addition, as was mentioned above, no indications of local water ponding, such as watermarks were ever reported at Yucca Mountain.

Importantly, the common telltale textures of vadose (i.e., involving water films) cementation as meniscus and pendant textures are totally absent from the Yucca Mountain deposits. None of the several hundreds of samples studied by different groups of researchers have revealed these textures. Given that the vapor-phase minerals and the calcite crystals create quite "rugged" micro-relief with abundant and deep "valleys" between adjacent crystals, the appearance of the meniscus textures would seem to be inevitable if films of water were indeed involved in crystallization.

To summarize the discussion of the geopetal appearance of the Yucca Mountain secondary minerals:

- Geopetal occurrences are generally known to develop in both the vadose and the phreatic environments. Both settings offer a number of physical mechanisms that would force minerals to reflect gravity control.

- Since more than one mechanism may explain the geopetal appearance of the mineralization, the geopetal appearance, alone, cannot be used to discriminate between the vadose and phreatic environments. An examination of the more fine-scale features of the deposits is required to determine the environment of mineral growth.
- Textural evidence of the crystallization from water films (such as pendant and meniscus textures of cement) is absent from the Yucca Mountain secondary deposits.
- Crystallization of the secondary calcite and silica minerals from water films as postulated by the Yucca Mountain Project researchers implicitly invoke a number of mechanisms, the physical nature of which remains unknown.

3.4.6.6.2. Euhedral crystals

The "rainwater" concept, which envisages the formation of secondary minerals at Yucca Mountain via the growth of crystals from gravity-driven water films, contains a number of implicit (unstated) assumptions. The primary assumption is that a physical mechanism exists that allows for large, centimeter-scale, crystals of calcite and quartz to crystallize from thin films of water. From the standpoint of the theory of crystal growth this does not seem to be possible. For minerals with relatively low solubilities, such as calcite and quartz, growth of large euhedral crystals may only occur in a submerged state from slightly supersaturated fluid, because molecules that build the crystal lattice must be supplied uniformly to all crystal faces at a steady low rate (Sunagawa, 1982). An irregular supply of matter inevitably leads to a distortion of the crystal habit and to the preferential development of selected growth directions.

Highly soluble minerals, such as gypsum for example, may form large euhedral crystals in the subaerial setting (e.g. gypsum "needles" found in caves; Hill and Forti, 1997-b); this mechanism, however, does not apply to calcite and quartz. Describing the characteristic textures of calcite deposits formed from water films (speleothems), Kendall and Broughton (1978) provided a simple and logical explanation why the crystals formed through this mechanism necessarily have very small sizes: "*... distinctive fabrics of palisade calcite are formed because precipitation usually occurs from thin water films that flow over the growing speleothem surfaces. Large crystal terminations do not form on the speleothem surface because they form projections that disturb the water flow away from the projections which, as a consequence, are gradually eliminated*" (p. 519).

The proponents of the "rainwater" concept do not offer any coherent explanation of how the hypothetical process of crystal growth could be realized. They do note, however, that at Yucca Mountain "*... mineral growth commonly occurs at the tips of calcite blades...*" and that "*... a mechanism is required*

to transport dissolved ions to these sites ...". (Fabryka-Martin et al., 2000). So, what process would be capable of taking a hypothetical mineral-laden water sitting as a film on the cavity floor and transporting it all the way up to the top of a 2-3 cm-tall crystal? The proponents of the concept speculate: "Once water has been transported into a cavity, it then must reach the actual sites of mineral precipitation. In the case of the elongated calcite blades, water must be transported to crystal extremities up to 1 to 2 cm above the base of the blades. Because the cavities show no evidence of local water ponding, water films likely reach the blade tips by capillary forces up their outer surfaces." (Paces et al. 2001, p. 67, emphasis added)

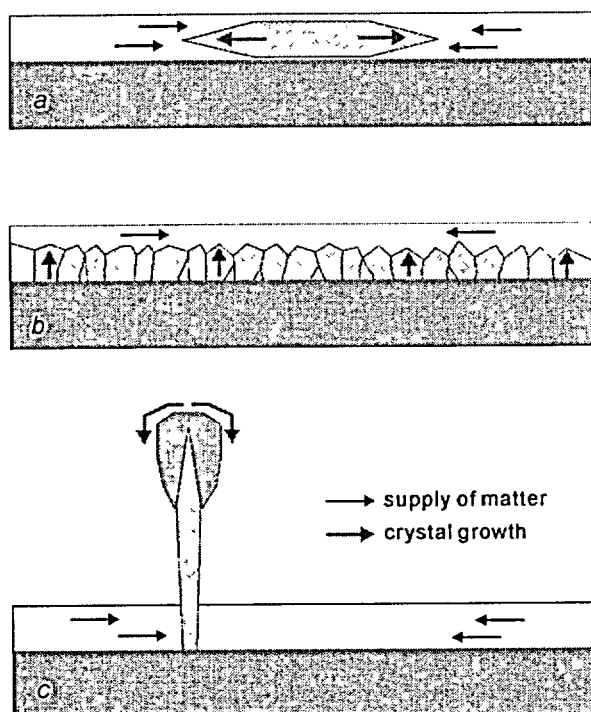


Figure 3-4-46. Examples of crystal growth from water films (white; thickness exaggerated). a – growth of single euhedral crystal; b – growth of palisade aggregate (typical of speleothems); c – Yucca Mountain scepter calcite. Note that drawing c combines the observed (inferred from physical evidence) directions of crystal growth with the hypothetical supply of matter by water films.

This statement seems to be in conflict with basic principles of physics. Capillary forces can only be effective in lifting up liquids if they operate in thin channels or pores. In geological objects, the size range in which capillary forces play the role is defined as 0.0002 to 0.5 mm for cylindrical channels and 0.0001 to 0.25 mm for slot-shaped channels (Chukhrov, 1955). In wider channels capillary forces are insignificant and do not produce any substantial lifting of water. It is easy to demonstrate that under the most conservative assumptions, the water film rise along a flat crystal surface cannot be greater than $\cong 2$ mm. Simple experiments with actual Yucca Mountain crystals partly immersed in waters with different salinities have shown that the water meniscus "climbs" up the crystal surface for approximately 1.5 mm. Thus, the proposed mechanism of capillary supply of the mineral-forming solutions to the tips of bladed crystals,

suggested by the Yucca Mountain Project researchers represents a physical impossibility.

Above we discussed how to supply the mineral-forming fluid to the top of the elongated (bladed) crystal. By doing so we implicitly assumed that the crystal already exists. Now, we need to discuss the problem of how this crystal was created in the first place. Let us assume that a single crystal grows in the water film (the thickness of which is significantly smaller than the surface area) wetting the surface of the

cavity. The preferential flux of the matter to the crystal will be directed parallel to the film surface. As was demonstrated by Shafranovsky (1968), in accordance with Curie's principle of symmetry, the direction of the fastest growth in such a system will also be oriented parallel to the film surface (i.e., parallel to the cavity surface). Therefore the single crystal growing within a film should grow by enlargement parallel to the cavity surface. In striking contrast, at Yucca Mountain bladed crystals are almost invariably oriented roughly perpendicularly to the cavity floors (Figure 3-4-46).

We contend that the growth of large euhedral crystals and aggregates similar to those found at Yucca Mountain is only possible in the submerged state and cannot occur from films of water. The morphology of crystals provides a very strong argument in favor of the phreatic setting during the growth of crystals.

Scepter morphology of calcite and quartz crystals indicates that growth layers propagate from the tips of the crystals toward their bases (i.e., toward cavity walls). Clear evidence of that was obtained by means of the scanning electron microscopy. Thus, a hypothetical water film contemplated by the "rainwater" concept must somehow have maintained equilibrium with respect to calcite and/or quartz while climbing up the crystal surface. The film must not have deposited its mineral load when it entered the cavity from an intersecting fracture, when it flowed down the cavity walls, when it moved along the cavity floor toward the crystal base, and when it climbed up the crystal surface. And only at the very top of the crystal it must have reached supersaturation and started depositing a mineral. In addition, such a truly remarkable chain of events would have to repeat itself throughout a substantial part of the repository zone in hundreds of cavities having different shapes and sizes.

As it was pointed out above, the late-stage opals in the scepter heads of calcite crystals have been deposited with the involvement of colloidal solutions. So, yet another question arises: how would the hypothetical films of water transport to the tips of crystals not only the ions of dissolved calcite but also colloidal particles of silica? Again, no physically plausible mechanism has been proposed to explain this.

Summarizing the discussion above we conclude that:

- The "rainwater" concept fails to explain the morphologic and textural features observed in the Yucca Mountain secondary mineralization, and
- Mechanisms of crystal growth involving capillary movement of the water films up the crystal surfaces (as proposed by Paces et al. 2001) appear to be physically unfounded.

3.4.6.7. Summary on the mineral textures

The "rainwater" concept rests heavily on an interpretation of the geopetal appearance of secondary minerals in the Yucca Mountain unsaturated zone. The proponents of the concept treat this feature as

undeniable evidence of mineral growth occurring in the unsaturated environment. This is one of the cornerstones of the "rainwater" concept, and most of the fine details of the concept are derived from this interpretation.

The major shortcoming of the approach adopted by the proponents of the concept is that they consider a general characteristic – geopetal appearance – and fail to consider the details of the textures of the real deposits. Our analysis has demonstrated that secondary minerals lining fractures and cavities in the rhyolitic tuff at Yucca Mountain have a number of characteristic features (e.g., large euhedral crystals, granular and drusy aggregates, etc.) that are atypical of the minerals forming in the vadose zone. The diversity of morphologies exhibited by major and accessory minerals indicates a substantial variability in the conditions during the crystal growth. These conditions evolved in a systematic manner: the sequence of crystallographic shapes found in the Yucca Mountain minerals indicates mineral deposition from the fluid with a decreasing overall supersaturation.

In discussing the morphology and textures of the Yucca Mountain secondary minerals we relied on general mineralogical knowledge, theory of crystal growth, and basic physics. We believe that our considerations have successfully demonstrated that the interpretation of the geopetal occurrence as being indicative of the deposition of minerals in the unsaturated environment is equivocal at best. In addition, specific textures and morphology of secondary minerals and aggregates found at Yucca Mountain make the proposed mechanism of crystal growth (from water films) physically impossible.

3.4.7. Summary

The data presented in Chapter 3-4 demonstrate that the deposition of the secondary minerals in open cavities in the rhyolite tuffs of the vadose zone at Yucca Mountain occurred when these cavities were filled, partly or entirely, with water. This environment should have persisted for the periods of time sufficient for crystallization of relatively large (centimeter-sized) crystals.

Critical evaluation of the competitive "rainwater" hypothesis, envisaging deposition of secondary minerals at Yucca Mountain from films of meteoric water percolating along the interconnected fractures in the vadose (unsaturated) zone (e.g., Paces et al. 1996 and 2001), as well as the ontogenetic analysis of different features of the mineralization have led us to the conclusion, that the hypothesis does not withstand scrutiny. Many processes that are postulated, explicitly or implicitly, to be operational in the "rainwater" model seem to be physically impossible (e.g., crystallization of large euhedral crystals and crystals with scepter morphology from water films).

The mineral compositions of crusts, particularly the presence of quartz, fluorite, heulandite and strontianite, are not compatible with the deposition of minerals from meteoric waters. Similarly

incompatible with the hypothetical mechanism of infiltrating rainwater is the geochemistry of minor elements (notably, elevated abundances of Mg, Sr, and As).

An environment entirely compatible with all of the features observed in the secondary minerals at Yucca Mountain is that of a short-lived low-temperature (~30 to 90°C) hydrothermal system. Upwelling waters in such a system would have acquired their mineral load mainly from within the Paleozoic carbonate sedimentary rocks underlying the Yucca Mountain rhyolitic tuffs and, partly, at deeper levels. Mineralogic features observed in the secondary mineralization in the vadose zone of Yucca Mountain are thus compatible with the conceptual model, presented in Parts I and II of this book.

In this Chapter 3-4 of Part III consideration was restricted to the mineralogical and selected geochemical features of secondary deposits sampled in the ESF tunnel. More evidence regarding the origin of these deposits have been obtained by means of the stable isotope and fluid inclusion studies. The results of these complementary studies will be discussed in subsequent chapters.

Appendix 3.4.1 Mineral species found as fracture and lithophysae coatings in the ESF and in the vadose zone of Yucca Mountain, Nevada

List of minerals

Mineral	Location	Origin	Reference
Oxides			
Tridymite	Ubiquitos	Vapor-phase alteration	Carlos, Chipera, Bish, 1995
Cristobalite		Vapor-phase alteration	Carlos, Chipera, Bish, 1995
Quartz	Ubiquitos	Secondary assemblages	Carlos, Chipera, Bish, 1995, Dublyansky et al., 1998
Hematite	Ubiquitos	Vapor-phase alteration assemblages	Carlos, Chipera, Bish, 1995
Goetite	Scarce, USW G-2	Occurs with hematite.	Carlos, Chipera, Bish, 1995
Ranceite (Ca, Mn ²⁺)Mn ₄ O ₉ ·3H ₂ O	USW G-2, USW G-4, not found in ESF	Secondary assemblages	Carlos, Chipera, Bish, 1995
Cryptomelane – hollandite K ₂ (Mn ⁴⁺ , Mn ²⁺) ₈ O ₁₆ Ba(Mn ⁴⁺ , Mn ²⁺) ₈ O ₁₆	Common below the SWL	Secondary assemblages	Carlos, Chipera, Bish, 1995
Pb-Hollandite			Carlos, Chipera, Bish, 1995
Lithiophorite (Al, Li)Mn ⁴⁺ O ₂ (OH) ₂		Secondary assemblages	Carlos, Chipera, Bish, 1995
Todorokite Manganese oxide blend			Carlos, Chipera, Bish, 1995
Pyrolusite MnO ₂			Carlos, Chipera, Bish, 1995
Auronte (Mn ²⁺ , Ag, Ca)Mn ⁴⁺ ₃ ·3H ₂ O			Carlos, Chipera, Bish, 1995
Phosphates			
Apatite	Rare, ESF, USW G-2	Secondary assemblages	Wilson, 2000 (pers. comm.) Carlos, Chipera, Bish, 1995
Sulphates			
Barite	ESF		Wilson, 2000 (pers. comm)
Gypsum	Scarce, ESF	Secondary assemblages	Smirnov and Dublyansky (2001)
Carbonates			
Calcite	Ubiquitos	Secondary assemblages	Carlos, Chipera, Bish, 1995; Whelan et al., 1996; Dublyansky et al., 1998; Smirnov and Dublyansky (2001)
K-carbonate	Scarce, ESF	Secondary assemblage	Smirnov and Dublyansky (2001)
Strontianite	Rare, ECRB	Secondary assemblage	Smirnov and Dublyansky (2001)

List of minerals (continued)

Silicates			
Ortosilicates			
Almandite	Scarce, ESF	Probably allogenic	Dublyansky et al, 1998
Band silicates			
Amphibole (?)	Scarce, ESF	Probably allogenic	Smirnov and Dublyansky (2001)
Sheet silicates			
Kenyaite (?) $\text{Na}_2\text{Si}_{22}\text{O}_{41}(\text{OH})_8 \cdot 6\text{H}_2\text{O}$	Scarce, GU-3	Unclear	Carlos, Chipera, Bish, 1995
Mica and clay minerals			
Smectite $(\text{Ca}, \text{Na})_0.33(\text{Al}, \text{Mg}, \text{Fe})_2\text{Si}_4\text{O}_{10}(\text{OH})_2 \cdot 4\text{H}_2\text{O}$	Sporadically occurs in wells	Secondary assemblage	Carlos, Chipera, Bish, 1995
Illite $(\text{K}, \text{H}_3\text{O})(\text{Al}, \text{Mg}, \text{Fe})_2(\text{Al}, \text{Si})_4\text{O}_{10}(\text{OH})_2 \cdot \text{H}_2\text{O}$	wells UE-25a#1, UE-25b#1	No information	Carlos, Chipera, Bish, 1995
Palygorskite $\text{Mg}_5\text{Si}_8\text{O}_{20}(\text{OH})_2(\text{OH}_2)_4 \cdot 4\text{H}_2\text{O}$	Rare, not deeper than 260 m in USW GU-3 and G-3	Secondary assemblage	Carlos, Chipera, Bish, 1995
Sepiolite $\text{Mg}_8\text{Si}_{12}\text{O}_{30}(\text{OH})_2(\text{OH}_2)_4 \cdot 8\text{H}_2\text{O}$	Rare, not deeper than 260 m in USW GU-3 and G-3.	Secondary assemblage	Carlos, Chipera, Bish, 1995
Kaolinite $\text{Al}_2\text{Si}_2\text{O}_5(\text{OH})_4$	Scarce, USW G-1 and G-2	Secondary assemblage	Carlos, Chipera, Bish, 1995
Zeolites			
Heulandite/Clynoptiolite $\text{Ca}_4[\text{Al}_8\text{Si}_{28}\text{O}_{72}] \cdot 24\text{H}_2\text{O}$	Abundant Appears below and over SWL	Secondary assemblage	Carlos, Chipera, Bish, 1995, Dublyansky et al., 1998; Feng et al, 1999, This study
Mordenite $\text{Na}_8[\text{Al}_8\text{Si}_{40}\text{O}_{96}] \cdot 24\text{H}_2\text{O}$	Abundant, ESF	Secondary assemblage	Carlos, Chipera, Bish, 1995
Stellerite $\text{CaAl}_2\text{Si}_7\text{O}_{18} \cdot 7(\text{H}_2\text{O})$	Abundant, ESF, UE-25, UZ-16 (Paintbrush Group only)	Secondary assemblage	Carlos, Chipera, Bish, 1995
Phillipsite $\text{K}_2(\text{Ca}, \text{Na}_2)_2[\text{Al}_6\text{Si}_{10}\text{O}_{32}] \cdot 12\text{H}_2\text{O}$	Rare, basal vitrophyre of Topopah Tuff USW GU-3, UE-25a#1	Secondary assemblage	Carlos, Chipera, Bish, 1995

List of minerals (continued)

Erionite (Na ₂ , Ca .) ₃ 5K ₂ [Al ₉ Si ₁₇ O ₇₂] 27H ₂ O	Rare, vicinity of basal vitrophyre of Topopah Tuff. ESF,	Secondary assemblage	Carlos, Chipera, Bish, 1995
Chabazite Ca ₆ [Al ₁₂ Si ₁₄ O ₇₂] 40 H ₂ O	Scarce, UE- 25a#1 (Crater Flat Group)	Secondary assemblage	Carlos, Chipera, Bish, 1995
Analcime NaAl(Si ₂ O ₆) (H ₂ O)	Unclear, USW G-2, Crater Flat, Zone III only	Secondary assemblage	Carlos, Chipera, Bish, 1995
Other tectosilicates			
Sanidine KAISi ₃ O ₈	Rare, ESF	Unclear. Probably authigenic	Smimov and Dublyansky (2001)
Halides			
Fluorite	Ubiquitous	Secondary assemblage	Vaniman, 1993; Carlos, Chipera, Bish, 1995, Whelan et al , 1996, Dublyansky et al, 1998, Smimov and Dublyansky (2001)

Chapter 3-5. Stable Isotope Geochemistry of Calcites from the Yucca Mountain Vadose Zone

By Y.V. Dublyansky and J.S. Szymanski

Table of contents

Chapter 3-5. Stable Isotope Geochemistry of Calcites from the Yucca Mountain Vadose Zone	277
3.5.1. Isotopic facies of calcite in the Yucca Mountain subsurface	277
3.5.1.1. Isotope facies of subsurface calcite studied in boreholes	279
3.5.1.2. Refinement of isotope properties of "shallow" calcite facies by ESF samples	283
3.5.1.2.1. Isotopes of strontium	283
3.5.1.2.2. Isotopes of oxygen	284
3.5.1.2.3. Isotopes of carbon	286
3.5.2. Isotope properties of the vadose zone calcite studied from ESF	287
3.5.3. Discussion	292
3.5.3.1. Significance of the heavy $\delta^{13}\text{C}$ values in calcite	292
3.5.3.1.1. Methanogenesis	293
3.5.3.1.2. Anoxic environment	294
3.5.3.2. Interpretation of the negative correlation of $\delta^{13}\text{C}$ and $\delta^{18}\text{O}$	297

Chapter 3-5. Stable Isotope Geochemistry of Calcites from the Yucca Mountain Vadose Zone

By Y.V. Dublyansky and J.S. Szymanski

3.5.1. Isotopic facies of calcite in the Yucca Mountain subsurface

Exploratory drilling, carried out during the DOE's Yucca Mountain site characterization activities, demonstrated that authigenic (secondary) mineralization, dominated by calcite and silica minerals, are present in the tuffs of Yucca Mountain to a depth of at least 2 km. Near the ground surface, the deposits are texturally similar (micritic) to the calcite-opal deposits at the topographic surface. Below a depth of about 15 m, however, the calcite becomes sparry and in addition to opal, crystalline forms of silica, chalcedony and quartz, appear.

Early studies of the drill core demonstrated that the calcite-silica minerals in the Yucca Mountain subsurface occur in the form of two distinct isotopic facies, and that the vadose-zone deposits differ from those in the phreatic zone in terms of their textures, trace element compositions, and isotope properties. The Yucca Mountain Project researchers (see Whelan et al., 1994 and Paces et al., 1996) attach a great deal of significance to this fact. Roedder et al. (1994) pointed out that, below the present-day "water table, calcite occurs as veins, often with chlorite and quartz or chalcedony, and as replacement cement of altered tuffs. This calcite is part of an alteration mineralogy formed during a low-temperature event that occurred ~10.4 Ma at temperatures up to 250 °C, based on earlier fluid inclusion studies." (p. 1854). The elevated fluid inclusion, homogenization temperatures and ages referred to in the cited passage were reported by Bish and Aronson (1993).

The "shallow" calcite is different. Denniston et al. (1997) provided the following description of it: "Coarser-grained calcite spar, often associated with opal and/or zeolites and less commonly with other minerals (manganese oxides, chain-structure clays, kaolinite, and fluorite) occurs from ~15 m throughout deeper tuffs of the upper unsaturated zone (UUZ), down to 500 m. Here calcite is found in open and closed fractures, breccia zones, lithophysal cavities, and penetrating the tuff matrix".

The isotopic constituents ($\delta^{18}\text{O}$, $\delta^{13}\text{C}$ and $^{87}\text{Sr}/^{86}\text{Sr}$) in calcite from the present-day vadose zone are different from those in the calcite from the phreatic zone, although there are certain exceptions. The limited depth of occurrence together with the distinct isotope and trace element contents, relative to the

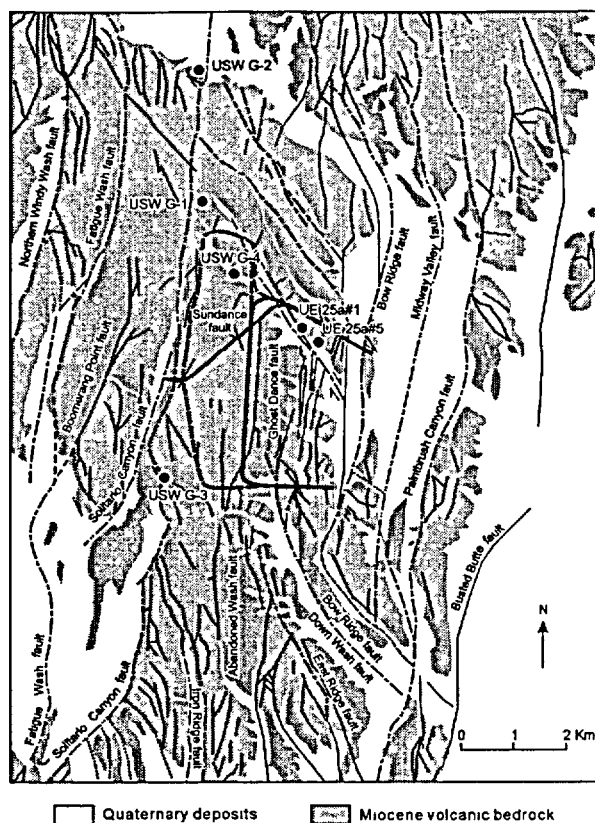


Figure 3-5-1. Location of boreholes for which an isotopic record for calcite is available.

hydrothermal calcite below, were taken by the Yucca Mountain Project scientists to indicate that both the vadose zone calcite and the surface calcite-silica deposits are products of infiltrating rainwater.

We, on the other hand, are of the opinion that in addressing the differences between the vadose zone calcite and the deeper hydrothermal calcite it is necessary to keep two points firmly in mind. First, the presumed pedogenic origin of the surface calcite-silica deposits is contradicted and invalidated, in our opinion, by several independent lines of evidence (see Chapter 3-3). Second, the spatial distribution of the isotopic properties of calcite from the present-day vadose zone is based on samples from only five drill holes, USW G-2, G-1, G-3/GU-3, G-4, and UE-25a#1. As shown on Figure 3-5-1, all of these drill holes are situated to the south of the NW-SE trending shear zone and to the west of the

Paintbrush fault zone.

In other words, the spatial distribution is known mainly in the central and western sectors of Yucca Mountain. It may be recalled (see Sections 3.1.4 and 3.1.5 on zeolite alteration and K/Ar ages) that, in these sectors, the alkaline earth alteration aureole is relatively thin and shallow. The bottom of this aureole occurs at a depth that diminishes to the south from about 900 m (top of T_{cp}), in USW G-2, to about 550 m (top of T_{pt}) in USW G-3/GU-3 (see Figures 3-1-30 through 3-1-34). Similarly, this depth diminishes to the northwest, from about 850 m (T_{cb}) in USW G-4 to about 500 m (T_{ht}) in USW G-1. Water level data from Robison (1984) indicate that the thickness of the present-day vadose zone, in the central and western sectors of Yucca Mountain, ranges between 524.9 m in USW G-2 and 750.0 m in USW G-3. This thickness is comparable to the thickness of the alkaline earth alteration aureole in these sectors. Thus, although it is, technically, correct to refer to the "shallow" calcite as "*upper unsaturated zone*" calcite (Denniston et al., 1997), it is also correct to refer to it as the one associated with the alkaline earth

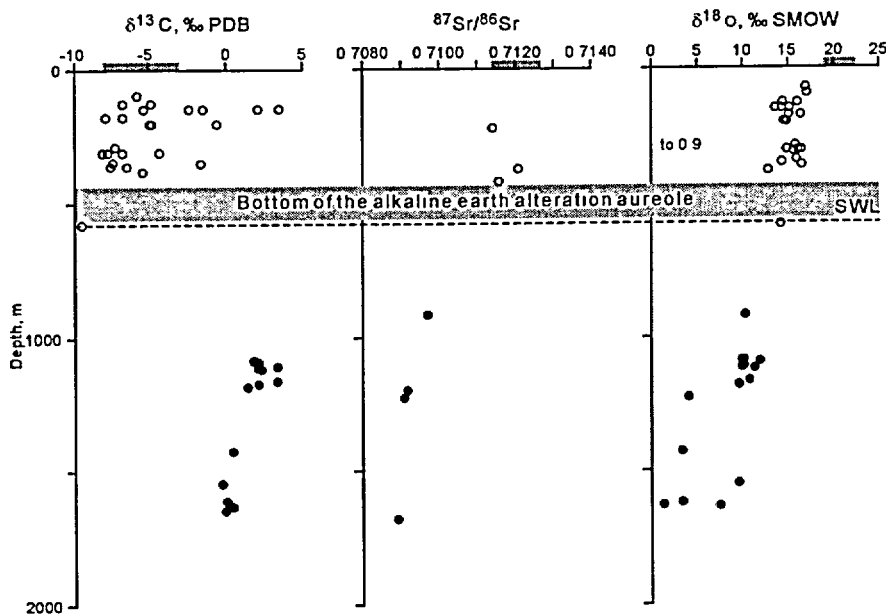


Figure 3-5-2. Isotopic character of carbon, strontium and oxygen incorporated in calcite deposits in the interior of Yucca Mountain. Borehole USW G-1. K/Ar ages (see Figure 3-1-38) suggest that the base of the alkaline-earth alteration aureole extends into the Tuff of Calico Hills to a depth of about 500 m. Stable isotope data are from U.S. DOE (1993); strontium isotopic data are from Marshall et al. (1993). SWL – position of the contemporary static water table. Isotopic values characteristic of the surface carbonate deposits are shown as gray bars ($\delta^{13}\text{C} = -3$ to -8 ‰ PDB, $^{87}\text{Sr}/^{86}\text{Sr} = 0.7114$ to 0.7127 ; and $\delta^{18}\text{O} = 19$ to 22.5 ‰ SMOW).

alteration aureole. The presence of such minerals as heulandite and stellerite and the asymmetry of the major cation alteration imply a hydrothermal origin for this aureole (see Section 3.1.4.9 for discussion).

3.5.1.1. Isotope facies of subsurface calcite studied in boreholes

The depth distribution of the subsurface calcite-silica deposits is known, in the interior of Yucca Mountain, based on rock cores extracted in five drill holes, which are USW G-1, G-2, G-3/GU-3, G-4, and UE-25a#1 and a#5 (see Figure 3-5-1). These deposits occur between the topographic surface and a depth of at least 2 km. Many samples have been analyzed for $\delta^{13}\text{C}$, $\delta^{18}\text{O}$, and $^{87}\text{Sr}/^{86}\text{Sr}$ isotope signatures (Whelan and Stuckless, 1991; U.S. DOE, 1993; Marshall et al., 1993). The entire database, which has been made available to us, is presented in Figures 3-5-2 through 3-5-6.

The figures show that the *deep-seated facies* deposits occur at a depth of more than 850 m. These deposits are developed as milky veins and replacement cements in the host tuffs and typically exhibit elevated abundances of Sc, Fe, and Mn (Vaniman and Whelan, 1994). They carry "heavy" carbon ($\delta^{13}\text{C}$ between -1.6 and 3.3 ‰ PDB), "light" oxygen ($\delta^{18}\text{O}$ between 1.3 and 12.9 ‰ SMOW), and primary marine Sr-isotope values ($^{87}\text{Sr}/^{86}\text{Sr}$ between 0.7086 and 0.7097). The deep-seated calcite-silica deposits are spatially associated with the orderly-interstratified clays (alleverdite, kalkberg, and illite) and alteration minerals from the alkali zeolite series, such as clinoptilolite, mordenite, analcime, and albite

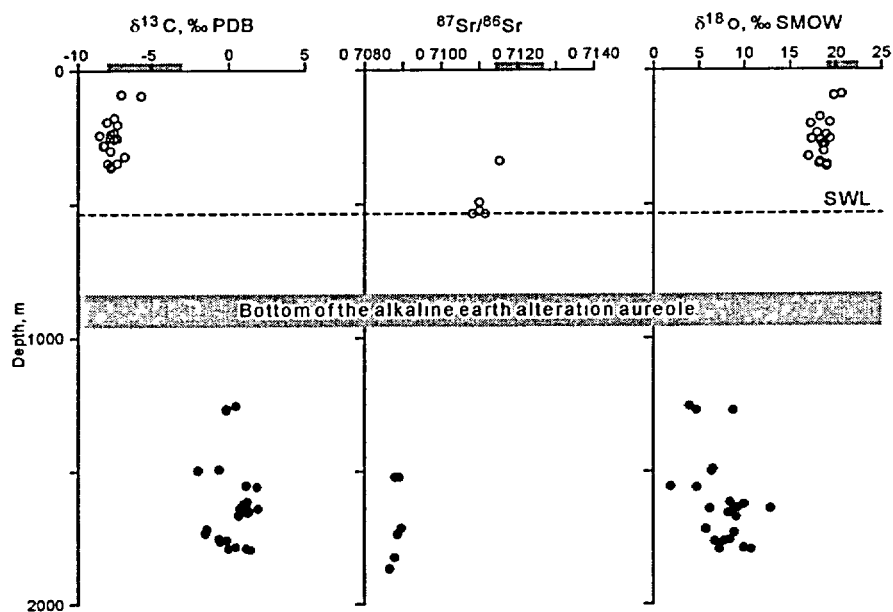


Figure 3-5-3. Isotopic character of carbon, strontium and oxygen incorporated in calcite-silica deposits in the interior of Yucca Mountain. Borehole USW G-2. K/Ar ages (see Figure 3-1-39) suggest that the base of the alkaline-earth alteration aureole extends to the top of Prow Pass Tuff or a depth of about 900 m. Stable isotope data are from U.S. DOE (1993); strontium isotopic data are from Marshall et al. (1993). SWL – position of the contemporary static water table. Isotopic values characteristic of the surface carbonate deposits are shown as gray bars ($\delta^{13}\text{C} = -3$ to -8 ‰ PDB, $^{87}\text{Sr}/^{86}\text{Sr} = 0.7114$ to 0.7127 ; and $\delta^{18}\text{O} = 19$ to 22.5 ‰ SMOW).

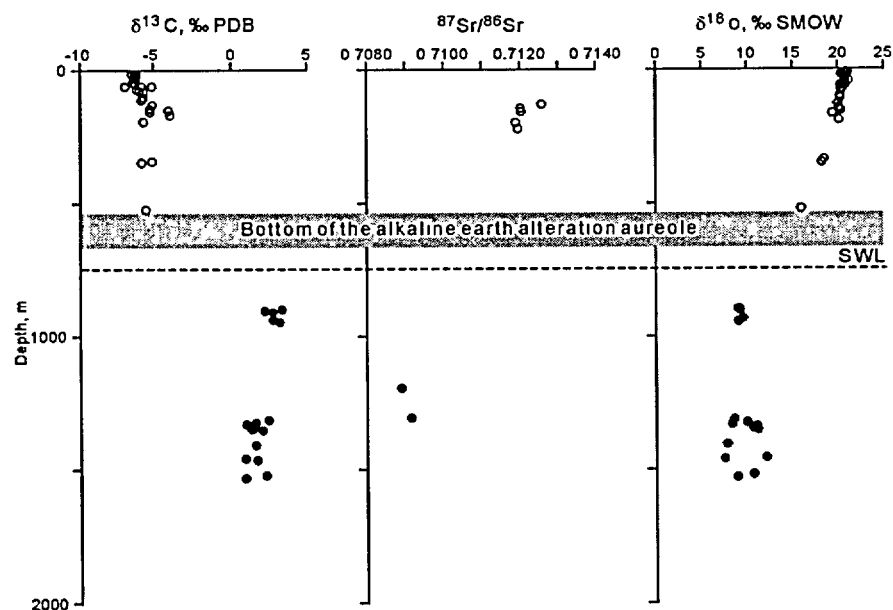


Figure 3-5-4. Isotopic character of carbon, strontium and oxygen incorporated in calcite-silica deposits in the interior of Yucca Mountain. Borehole USW G-3/GU-3. K/Ar ages (see Figure 3-1-40) suggest that the base of the alkaline-earth alteration aureole extends into the upper parts of the Prow Pass Tuff or a depth of about 600 m. Stable isotope data are from U.S. DOE (1993); strontium isotopic data are from Marshall et al. (1993). SWL – position of the contemporary static water table. Isotopic values characteristic of the surface carbonate deposits are shown as gray bars ($\delta^{13}\text{C} = -3$ to -8 ‰ PDB, $^{87}\text{Sr}/^{86}\text{Sr} = 0.7114$ to 0.7127 ; and $\delta^{18}\text{O} = 19$ to 22.5 ‰ SMOW).

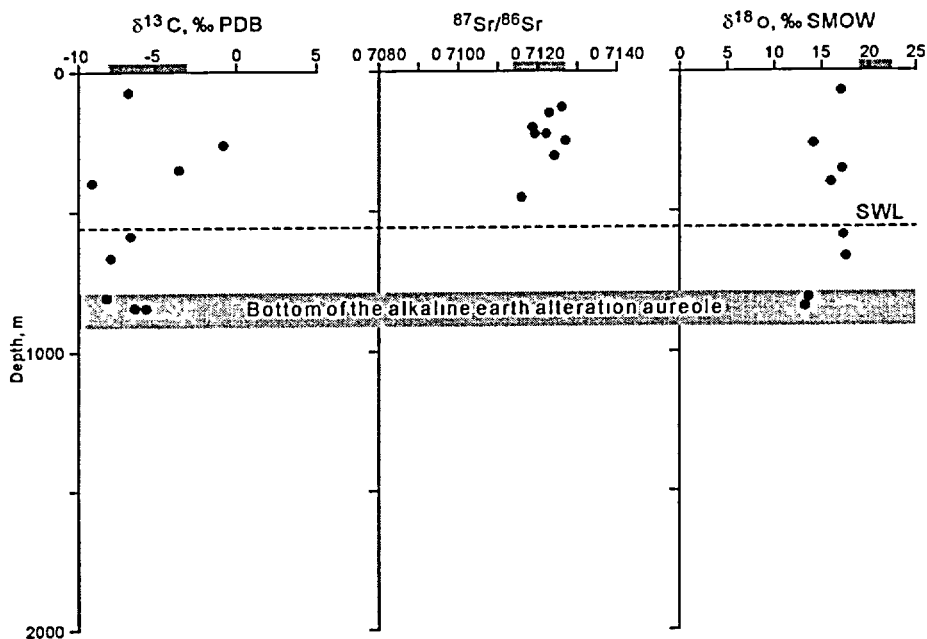


Figure 3-5-5. Isotopic character of carbon, strontium and oxygen incorporated in calcite-silica deposits in the interior of Yucca Mountain. Borehole USW G-4. Chemistry (see Figure 3-5-41) suggests that the base of the alkaline-earth alteration aureole extends down to the base of the Bullfrog Tuff or a depth of about 850 m. Stable isotope data are from U.S. DOE (1993); strontium isotopic data are from Marshall et al. (1993). SWL – position of the contemporary static water table. Isotopic values characteristic of the surface carbonate deposits are shown as gray bars ($\delta^{13}\text{C} = -3$ to -8 ‰ PDB, $^{87}\text{Sr}/^{86}\text{Sr} = 0.7114$ to 0.7127 ; and $\delta^{18}\text{O} = 19$ to 22.5 ‰ SMOW).

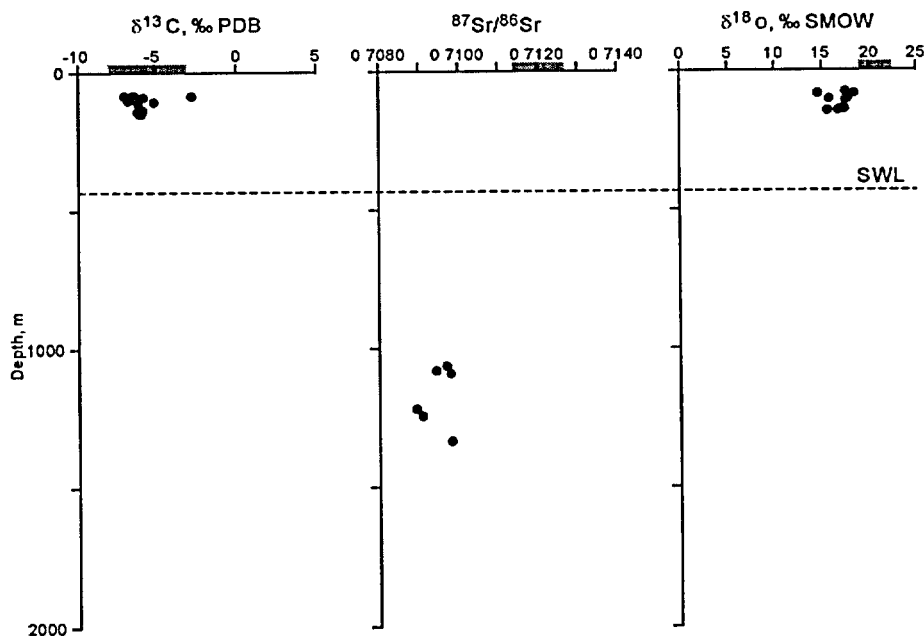


Figure 3-5-6. Isotopic character of carbon, strontium and oxygen incorporated in calcite-silica deposits in the interior of Yucca Mountain. Boreholes UE-25a#5 and UE-25a#1. Stable isotope data are from U.S. DOE (1993); strontium isotopic data are from Marshall et al. (1993). SWL – position of the contemporary static water table. Isotopic values characteristic of the surface carbonate deposits are shown as gray bars ($\delta^{13}\text{C} = -3$ to -8 ‰ PDB, $^{87}\text{Sr}/^{86}\text{Sr} = 0.7114$ to 0.7127 ; and $\delta^{18}\text{O} = 19$ to 22.5 ‰ SMOW).

(see Sections 3.1.3 and 3.1.4). The alteration minerals, from both the orderly-interstratified clays and the zeolite phases, carry the same K/Ar ages, between 9.5 and 11.0 Ma. Fluid inclusion temperatures as high as 78-260 °C were reported for calcites from the depth interval of 1268-1773 m in borehole USW G-2 (U.S. DOE, 1993). Thus, we may be reasonably certain that the deep-seated facies deposits represent the Timber Mountain hydrothermal metamorphism. We interpret this hydrothermal process as one, fueled by a "strong" heat source (see Part II of this report for discussion).

The *shallow facies* deposits were identified only in the upper tuffs at a depth of less than 850 m (see Figures 3-5-2 through 3-5-6). Isotopically, they differ from the underlying Timber Mountain deposits. These deposits generally contain "lighter" carbon isotopes ($\delta^{13}\text{C}$ between -9.5 and +4.5 ‰ PDB), "heavier" oxygen isotopes ($\delta^{18}\text{O}$ between 13.5 and 21.0 ‰ SMOW), and are enriched in radiogenic strontium ($^{87}\text{Sr}/^{86}\text{Sr}$ between 0.7114 and 0.7130). Spatially, the shallow facies deposits are associated with the whole-rock enrichment in alkaline earth elements and alkaline earth zeolites, such as heulandite and stellerite. The alteration minerals (clinoptilolite/heulandite) carry K/Ar ages (mixed), which range between 1.5 and about 9.0 Ma (see Section 3.1.5.). Scarce fluid inclusion data reported for calcite from 204 to 356 m in boreholes USW G-1 and G-2 range between 57 and 104°C (U.S. DOE, 1993).

Thus, we may be reasonably certain that the shallow facies deposits occur within the alkaline earth alteration aureole. Importantly, the occurrence of these deposits is not confined to the present-day vadose zone; they also occur in the phreatic zone, as shown in Figure 3-5-5. It is only in those sectors within which the alkaline earth alteration aureole is shallow (USW G-1 and G-3/GU-3, Figures 3-5-2 and 3-5-4, respectively) that the occurrence of the shallow facies deposits is restricted to the present-day vadose zone.

The database on the isotopic properties of the shallow facies of calcite-silica deposits has recently been updated by an extensive set of data obtained on samples from the ESF. The collection of this dataset began after the initiation of excavation in 1995. When analyzing and comparing the data from the borehole and the ESF studies, it must be kept in mind that the spatial resolution (and, therefore, quality) of the analyses differs between these two data sets.

The analyses of calcite removed from boreholes typically exhibit a lower spatial resolution. Although analytical procedures were not described in documents available to us, it may safely be assumed that "*a few milligrams to tens of milligrams*" samples were used in isotopic analyses of the subsurface samples, as specified in U.S. DOE (1993) for analyses of the surface calcretes. The ability to trace the data presents a separate issue. For example, if more than one analysis is reported from the same sample, locations of subsamples within the analyzed sample are not identified in the documents available to us. This is not a trivial issue, because later, more fine-scale studies have demonstrated that isotopic properties

of calcite from the Yucca Mountain vadose zone may vary dramatically over very short distances. For example, a variation in $\delta^{13}\text{C}$ of 17 ‰ across a 1.5 mm-thick sample of mineral crust was documented by Dublyansky (2001). Thus, two major shortcomings of the early (borehole) dataset is the comparatively large size of samples, likely resulting in severe and indiscriminate averaging of carbonates with widely variable isotopic compositions and, in most instances, an unknown location of the analyzed sample within the mineral crusts or crystals.

Samples from the ESF were studied at substantially finer scales. The sample sizes remained substantial (about 10 mg) for Sr-isotope analyses; nevertheless isotopic transects across the crusts (along the inferred growth direction) have been performed (e.g., Paces et al., 1996). Although the spatial resolution of stable C and O isotope analyses has improved greatly later in the Yucca Mountain characterization program, the description of the results in most cases remains vague, with samples from mineral crusts broadly classed in three categories, "early", "late" and "intermediate" or "other" (Paces et al., 1996, 2001). The first three categories are determined on the basis of visual observations (i.e., samples are collected at the base and at the top of mineral crusts, as well as in between) and are not keyed to the specific calcite crystal morphology. Category "other" commonly lumps together samples collected from intermediate positions in crusts, as well as samples, whose position or genetic relationships to the rest of the sample could not be determined.

Fine-scale, stable isotope research was performed by Dublyansky (2001) by employing an *in situ* GC-IRMS technique in which the analytical volume of the CO_2 gas is produced from calcite by impact of the laser beam. The size of the analytical spot varied from 90 to 300 μm , and the method allowed, in a number of cases, construction of stable isotope "maps" of the studied samples. These results will be discussed in more detail later in this Chapter.

3.5.1.2. Refinement of isotope properties of "shallow" calcite facies by ESF samples

Figures 3-5-7 through 3-5-9 summarize the distribution of the isotopic properties of the calcites collected at different depths in boreholes and compare them with the data from the ESF calcites. The data from the carbonate deposits that were suggested as the source-rocks for the subsurface calcites are shown for comparison. When analyzing the data presented on the figures, it should be recognized that the ESF calcite, according to its position in the vadose zone, as well as its petrographic features, belongs to the "shallow" calcite facies studied from the boreholes.

3.5.1.2.1. Isotopes of strontium

It is apparent from Figure 3-5-7-a that the data from boreholes and from the ESF are very consistent. The deep-seated calcite facies has substantially less radiogenic values than the shallow facies one. It is noteworthy that although the borehole calcites seem to show some correlation with depth from

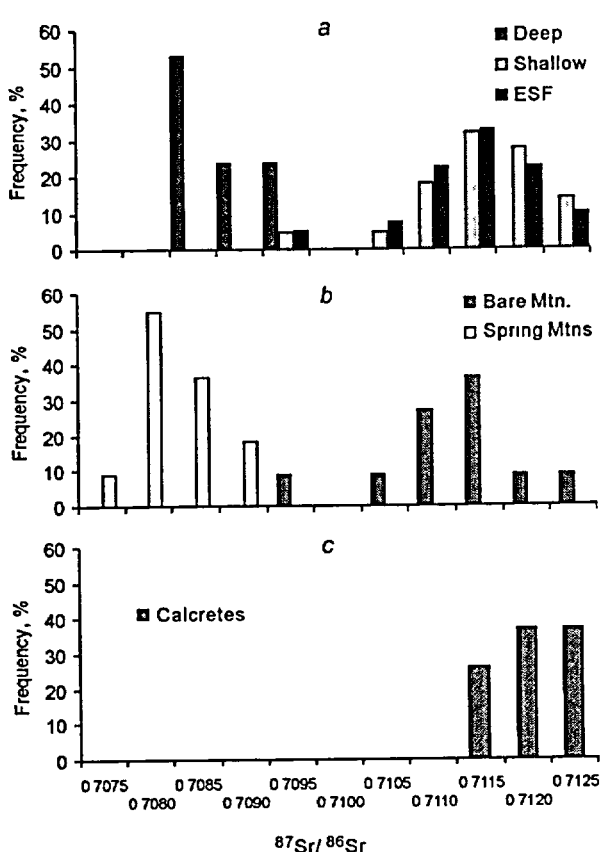


Figure 3-5-7. Isotopic character of strontium incorporated in calcite from the interior of Yucca Mountain (a) compared with hypothetical source-rocks of the shallow calcite: Paleozoic-Proterozoic carbonate rocks (b) and surface calcretes (c). Data sources and number of measurements in the database: deep-seated and shallow calcite - Marshall et al., 1993 (n = 39); ESF calcite - Paces et al., 1994 (n = 40); carbonate rocks from Bare mountain and Spring Mountains - U.S. DOE, 1993 and Zartman and Kwak 1993-a (n = 25), and slope calcretes - U.S. DOE, 1993 (n = 27).

the surface (decreasing $^{87}\text{Sr}/^{86}\text{Sr}$ values; see Figures 3-5-2 through -6, and Figure 3-4-30 in Chapter 3.4), the $^{87}\text{Sr}/^{86}\text{Sr}$ ratios of the calcite from the ESF span the whole range of values measured throughout the vadose zone.

Figure 3-5-7-b clearly shows that the Paleozoic and Proterozoic carbonate sedimentary rocks of the basement are legitimate candidates for the role of parents of both facies of calcite from the Yucca Mountain subsurface. It is to be noted that the carbonate rocks at Bare Mountain have experienced epigenetic mineralization, thought connected to the Timber Mountain Caldera hydrothermal circulation. Severely altered carbonate rocks may have $^{87}\text{Sr}/^{86}\text{Sr}$ values much more radiogenic than those shown in the figure (above 0.7142; Peterman et al., 1994). It is also noteworthy that the surface calcretes, which in the framework of the "rainwater" concept are believed to be the source-term of the subsurface carbonates, tend to have more-radiogenic $^{87}\text{Sr}/^{86}\text{Sr}$ values than the latter (Figure 3-5-7-c).

3.5.1.2.2. Isotopes of oxygen

Figure 3-5-8-a shows that based on the results from boreholes, the two spatial facies of calcite have quite distinct oxygen-isotope properties. The distribution is clearly bi-modal with the deep-seated calcite having "lighter" $\delta^{18}\text{O}$ values and the shallow vadose-zone calcite having "heavier" $\delta^{18}\text{O}$ values. There is, however, some overlap in the area of $\delta^{18}\text{O} = 12$ to 13 ‰ SMOW; in addition, several analyses of the deep-seated calcite yielded $\delta^{18}\text{O}$ values typical of the "shallow" calcite ($\delta^{18}\text{O}$ about 17 ‰ SMOW). The currently accepted interpretation of the data is that deep-seated calcite is the product of the Timber Mountain Caldera hydrothermal episode, while the shallow facies was deposited from meteoric waters (U.S. DOE, 1998 and 2001). Occasional "heavy" values of $\delta^{18}\text{O}$ in calcite from the deep-seated zone are attributed to "deeper infiltration of meteoric waters at a point when groundwater levels were

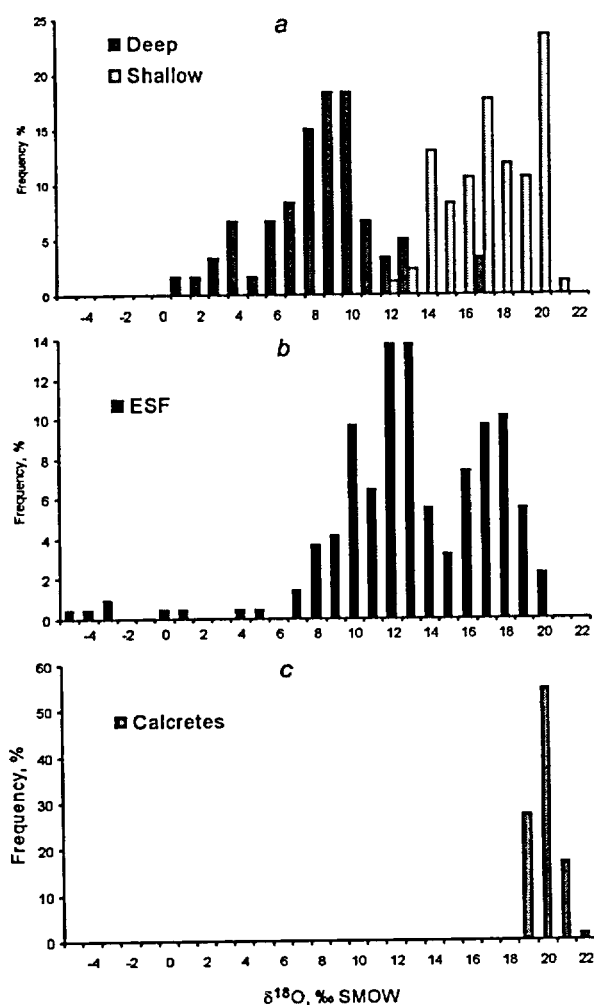


Figure 3-5-8. Isotopic character of oxygen incorporated in calcite from boreholes (a) and ESF (b) compared with the hypothetical source-rock ("rainwater hypothesis"), surface calcretes (c). Data sources and number of measurements in the database: deep-seated and shallow calcite from boreholes – U.S. DOE, 1993 (n = 145); ESF calcite – Dublyansky, 2001-a (n = 218); and surface calcretes – DOE, 1993 and Dublyansky, 2001-b (n = 77).

lower than present" (Denniston et al., 1997). The apparent gradual decrease of the $\delta^{18}\text{O}$ values with depth, in the "shallow" calcite (see, e.g., Figures 3-5-2 and 3-5-4) is interpreted, by the Yucca Mountain Project researchers, as a reflection of the gradually increasing temperature in accord with the "normal" geothermal gradient of 3- to 40° C·km⁻¹ (e.g., Szabo and Kyser, 1990; Fabryka-Martin et al., 2000).

The data obtained from the ESF calcites have virtually eliminated this simple conceptual explanation of the $\delta^{18}\text{O}$ value. Figure 3-5-8-b demonstrates that O-isotope values of the ESF calcite substantially overlap the values of both the shallow and the deep-seated calcite facies studied in boreholes. In a number of ESF samples, the isotope values measured in the earliest layers turned out to be "lighter" than the lightest values reported from the deep-seated calcite.

The obvious discrepancy in the results of the isotope studies of the vadose-zone calcite from boreholes and from the ESF may presently be explained in a number of ways. The discrepancy might be due to the poorer spatial resolution and lower density of sampling during the early stages of isotope studies (boreholes).

Thus, it might be presumed that if the borehole samples were studied by means of modern high-resolution techniques, the results for the borehole samples would be similar to the ESF results. (An important question is: What would be the change in the isotope distribution for the deep-seated samples?) Alternatively, the discrepancy might reflect a true spatial variability of the stable isotope record across the repository block. This question cannot be answered without additional studies.

The surface calcretes have the "heaviest" and the most uniformly distributed O-isotope values of all the carbonate lithofacies discussed above. They plot within a tight 3 ‰-interval (19 to 21 ‰ SMOW). It is

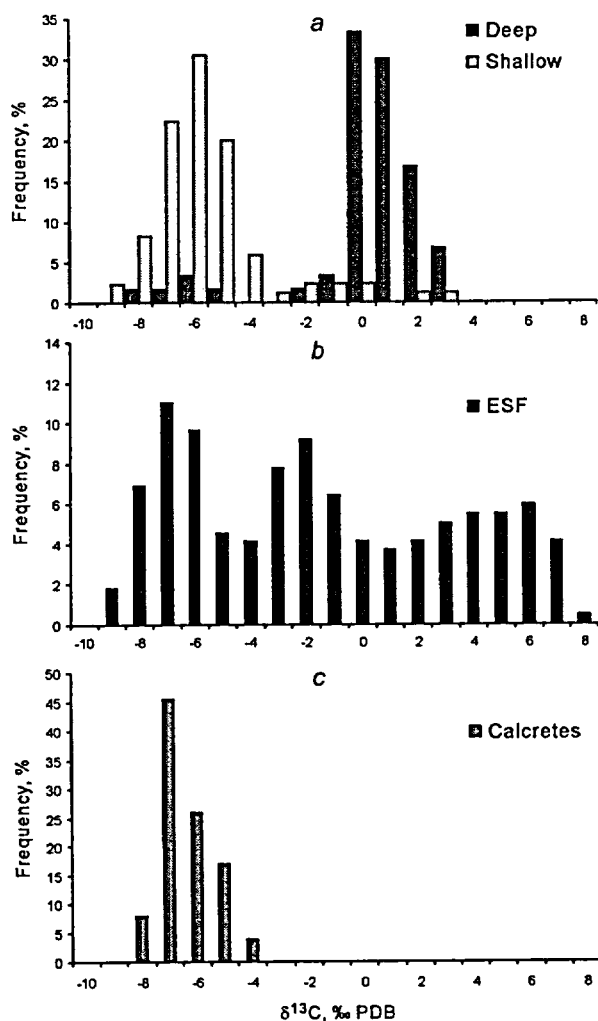


Figure 3-5-9. Isotopic character of carbon incorporated in calcite from the boreholes (a) and ESF (b) compared with the hypothetical source-rock ("rainwater hypothesis"), surface calcretes (c). Data sources and number of measurements in the database: deep-seated and shallow calcite – U.S. DOE, 1993 (n = 145); ESF calcite – Dublyansky, 2001-a (n = 218); and surface calcretes – U.S. DOE, 1993 and Dublyansky, 2001-b (n = 77).

striking that the massive (sometimes several meter-thick) surface deposits show so little variability in the $\delta^{18}\text{O}$ contents, whereas the range of values say, from 8 to 20 ‰ SMOW, is commonly found in just a several mm-thick crust of calcite from the vadose zone.

3.5.1.2.3. Isotopes of carbon

Like the O-isotopes, in the borehole samples, the isotopes of carbon split in two distinct populations (Figure 3-5-9-a). Two prominent modes at about +1 ‰ (deep-seated facies) and -6 ‰ PDB (shallow facies) are accompanied by "tails" that penetrate deep into the "light carbon" area for the deep-seated calcite and into the "heavy carbon" area for the shallow calcite. Again, the distinction between these two isotope facies disappears when more finely resolved results from the ESF calcites are considered (Figure 3-5-9-b). Importantly, virtually the whole range of isotopic values shown in the figure may be present in a single sample with "heavy" values typically associated with the early stages of mineral growth and "light" values occurring at the late stages (this subject will be discussed in more detail later in this Chapter).

Although the $\delta^{13}\text{C}$ values measured in surface calcretes displayed an almost-perfect match with the "shallow" borehole calcites (which was used as an argument to claim their genetic relationships), they show a reasonable match only with the latest portions of the ESF calcite (Figure 3-5-9-c).

The preceding considerations reveal that the subsurface tuffs of Yucca Mountain do indeed host two distinct generations of the calcite-silica deposits, which is the point made by the Yucca Mountain Project scientists. Relative to the Timber Mountain deposits, the subsequent deposits are enriched in the

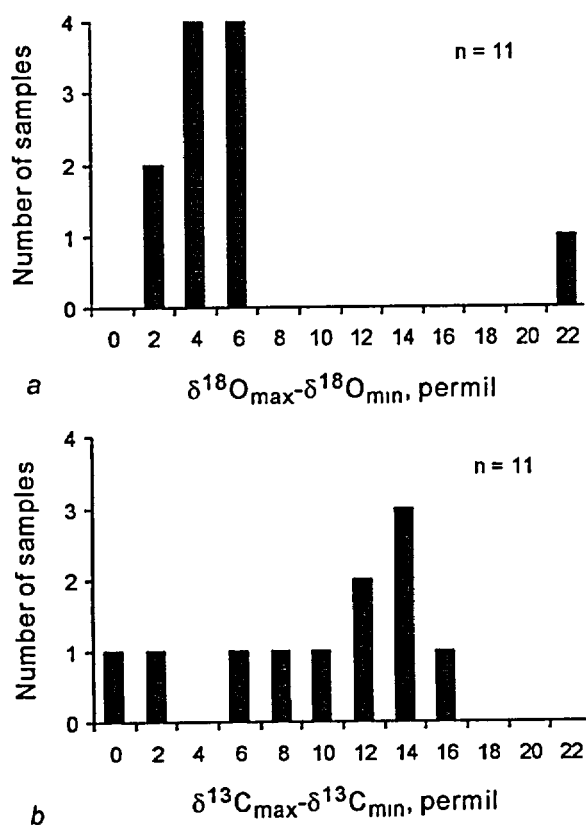


Figure 3-5-10. Variability of isotopic values in individual calcite samples from ESF. *a* – oxygen; *b* – carbon. Each of 11 samples was characterized by 10 to 45 *in situ* measurements of $\delta^{13}\text{C}$ and $\delta^{18}\text{O}$ with the analytical spot size ranging from 90 to 300 μm .

radiogenic strontium (^{87}Sr) and in the "heavy" isotope of oxygen (^{18}O). The differing Sr-isotope signatures indicate that the respective fluids acquired their dissolved strontium from different sources. In the case of the Timber Mountain fluid, it is clear that the dissolved Sr was acquired from the marine carbonates of the basement, which, before the outset of the Timber Mountain hydrothermal circulation, were unaltered (compare Figure 3-5-7-*a* and *b*). Substantial amounts of radiogenic ^{87}Sr isotope that was derived, most likely, from the clastic rocks of the basement, were introduced into the Paleozoic carbonates by the Timber Mountain fluids. For subsequent generations, however, the sources of more-radiogenic Sr were, most likely, clastic rocks and, in part, hydrothermally altered (mineralized) Paleozoic/Proterozoic carbonate rocks of the basement. This two-member pattern bears a striking similarity to the isotopic record obtained from calcretes from the USW VH-2 drill core (see Figure 2-16).

The fact that at least the latest part of the second-generation calcite exhibits isotopic affinity with the surface calcite-silica deposits is important. This is because this affinity establishes the fact that the formation of ^{87}Sr , ^{18}O and ^{12}C -enriched deposits has continued into late Quaternary.

3.5.2. Isotope properties of the vadose zone calcite studied from ESF

The analyses of stable isotopes became a very powerful tool in the Yucca Mountain studies when micro sampling techniques were employed instead of less discriminating techniques, and a more detailed record was obtained from different parts of the mineral crusts. Two remarkable features of the Yucca Mountain calcite became apparent. First, the isotopic properties of calcite were found to be variable, and the extent of these variations, in some samples, was extreme: 4-6 ‰ for $\delta^{18}\text{O}$ and 14-16 ‰ for $\delta^{13}\text{C}$. In one sample a $\delta^{18}\text{O}$ variation as great as 22 ‰ was measured (Figure 3-5-10).

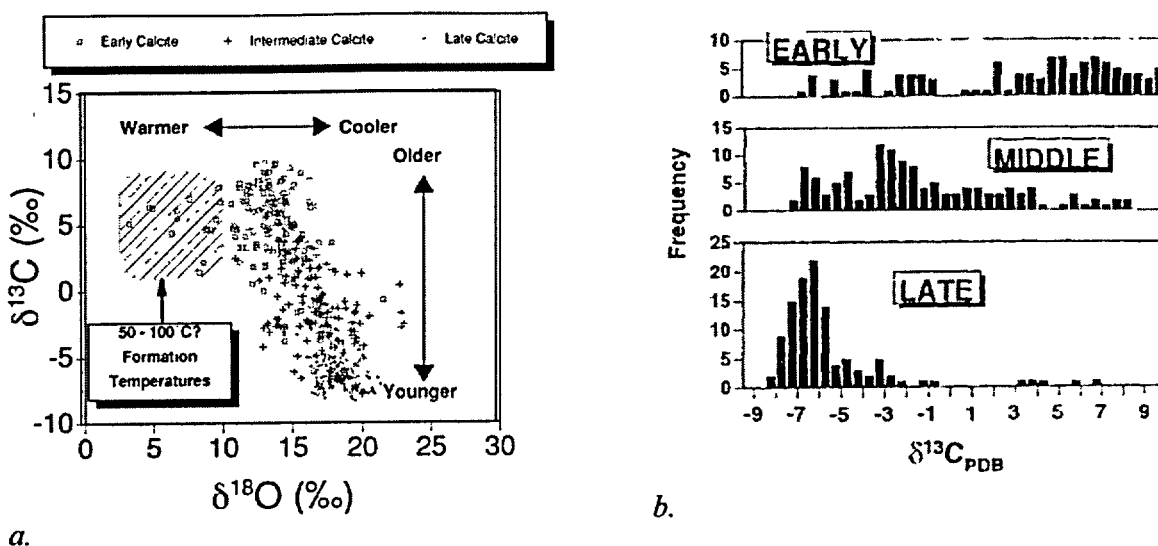


Figure 3-5-11. Summary of the USGS stable isotope data (from Whelan et al. 2001): *a* – $\delta^{18}\text{O}$ vs. $\delta^{13}\text{C}$ cross-plot, *b* – frequency distribution of carbon isotope values from "Early", "Middle" and "Late" calcites as defined in the USGS studies (from Whelan and Moscati, 1998).

Second, the isotopic properties of calcites were found to change in a systematic way, for many samples with the overall behavior of the isotopes of oxygen and carbon showing a prominent inverse correlation. These isotopic trends will be discussed in detail below.

In the Yucca Mountain Project isotopic studies, individual samples were subdivided into three zones: "Samples were classified as early, intermediate or late based on their relative positions in the observed microstratigraphy of each sampled thin section. These groupings are determined by visual observations ... Comparisons between classifications are subject to some misrepresentation because not all depositional stages are present in every sample, and because boundaries between groups are artificially assigned. Nonetheless, this simple-minded approach was taken to ensure that no subjective bias was introduced in the grouping process." (Paces et al., 1996, p. 30).

It was found that the $\delta^{13}\text{C}$ in the Yucca Mountain calcite systematically decreases from the deepest (earliest) parts of coatings toward the outer (latest) parts, whereas $\delta^{18}\text{O}$ does the opposite (Figure 3-5-11-*a*). The Yucca Mountain Project researchers used this trend to define three isotopic "stages" of calcite growth, with each stage being associated with a peak or mode on the frequency distribution of the isotopic values: "Samples classified as early-calcite have $\delta^{13}\text{C}$ values that tend to cluster between about +5 to +8‰ on a frequency distribution plot ..., whereas analyses of late-calcite form well-defined peak between -5 and -8 ‰ The latter groups of subsamples were obtained from outer layers of coatings and are generally represented by the age distributions over the last several hundred thousand years The

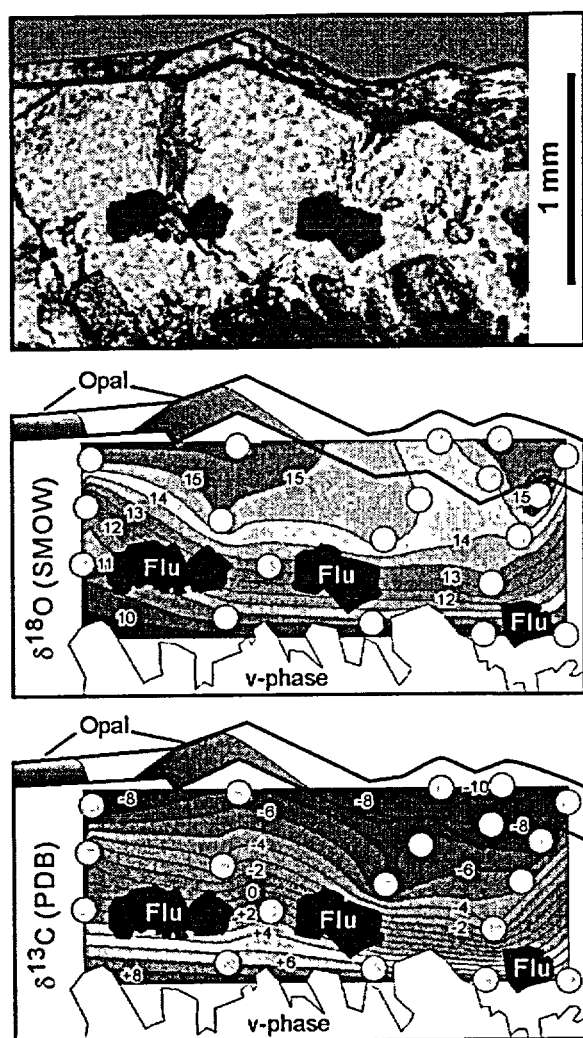


Figure 3-5-12. Stable isotope data from 1.4 mm-thick calcite (with fluorite and opal) crust from lithophysal cavity. ESF station 38+80. Note extreme and systematic variation of $\delta^{13}\text{C}$ (from +8 to -10 ‰ PDB) and $\delta^{18}\text{O}$ (from 10 to 15 ‰ SMOW).

Sample was studied by *in situ* GC-IRMS method (locations and approximate size of analytical spots are shown as yellow circles). Interpolation of isotope values was done using *Matchcad 6 0 PLUS* software.

frequency distribution plot also indicates a third mode, between -3 and 0 ‰" (Paces et al., 1996, p. 30). The trend is illustrated in Figure 3-5-11-b.

In order to further refine the isotopic record and minimize any "noise" related to random sampling of a number of crystal individuals, we attempted to study the stable isotopic properties of calcite within mineral individuals, paying special attention to different calcite morphologies, defined in the course of the mineralogic studies (see Sections 3.4.3.1.1 and 3.4.5.1 for calcite morphology discussion). We employed a method of Gas Chromatography – Isotope Ratio Mass Spectrometry (GC-IRMS). This *in situ* technique, allowing spatial resolution of about 90-200 μm , was described by Sharp (1992) and Sharp and Cerling (1996). Employed in combination with the appropriate software, this fine-resolution method allowed, in a number of cases, to perform an "isotopic mapping" of samples.

An example of such mapping is given in Figure 3-5-12. The figure shows that $\delta^{13}\text{C}$ changes from +8 to -9 ‰ across a 1.4 mm-thick calcite crust in a very systematic manner. Oxygen shows a similar, but inverse pattern. It is apparent from the figure that isotopic properties of the mineral-forming fluid were evolving, and the depositing calcite recorded the continuity of the evolution.

In Figure 3-5-13, we present a summary of stable isotopic properties for four calcite samples, showing a variety of crystal morphologies.

Each sample in Figure 3-5-13 exhibits a certain evolution of crystal morphology. Early calcite is represented by granular, platelet, platelet+scepter, or blocky morphologies (see Section 3.4.5.1 and Figure 3-4-23 for discussion of calcite morphology). In all four samples, the latest in the sequence is the blocky

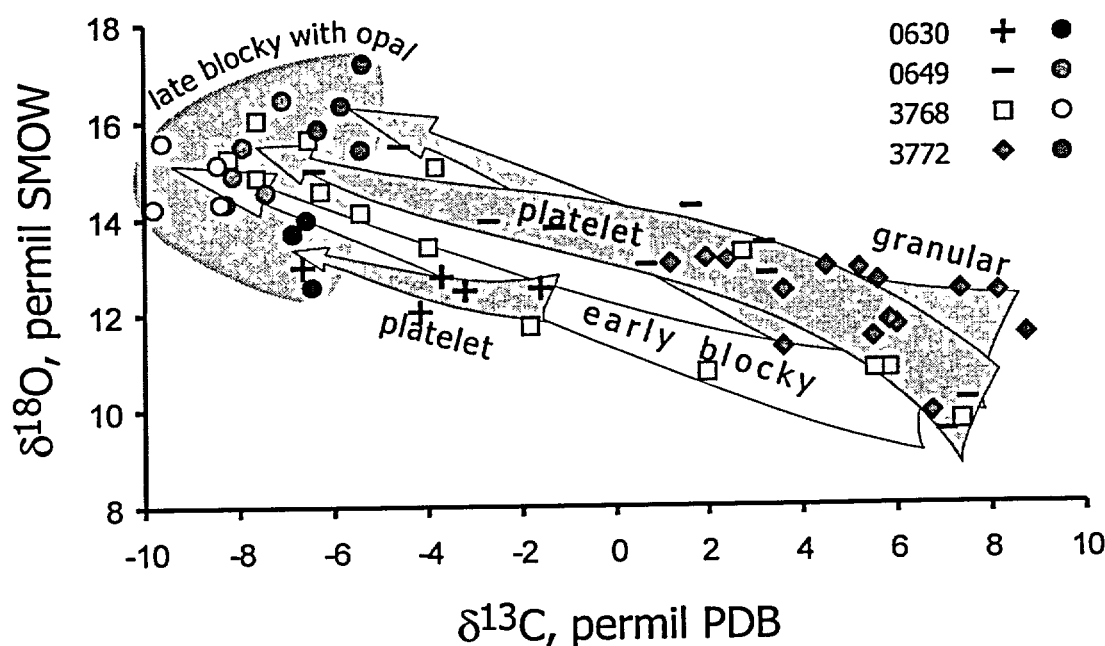


Figure 3-5-13. Systematic change of stable isotopic properties in calcite with different morphologies. Four individual calcite samples were studied by means of the *in situ* GC-IRMS technique along crystallographically defined directions (across mineral crusts). Overall direction of growth is shown by arrows. The latest morphologic variety for all four samples is blocky calcite with opal (circles).

calcite associated with opal—universally recognized as the latest member of the mineral paragenesis at Yucca Mountain.

As is apparent from Figure 3-5-13, the four samples taken from different parts of the repository block and from different types of occurrences (fracture and lithophysal cavities) exhibit remarkably similar behavior. In all samples, $\delta^{13}\text{C}$ gradually decreases and $\delta^{18}\text{O}$ increases as crystals grow. Slopes of the linear regression for all four samples range between -0.29 to -0.35, and coefficients of correlation between values of $\delta^{13}\text{C}$ and $\delta^{18}\text{O}$ range between 0.7 and 0.9. In the process of mineral growth, $\delta^{13}\text{C}$ in calcite has experienced a dramatic unidirectional shift from values as heavy as +8 to +9 to -5 to -10 ‰ PDB. Importantly, calcite with different crystal morphologies, i.e., granular, platelet or bladed, and blocky (without opal) may incorporate "heavy" $\delta^{13}\text{C}$ (+4 to +8 ‰) at early stages of growth and "light" $\delta^{13}\text{C}$ (-4 to -8 ‰) at late stages. Analyzed in only one sample, granular calcite contained only positive $\delta^{13}\text{C}$ (+1 to +9 ‰ PDB); thus, at this point, we cannot say whether granular calcite incorporating "light" carbon exists. The latest end-member in all growth sequences—blocky calcite associated with opal—has a characteristic $\delta^{13}\text{C}$ of -5 to -10 ‰ PDB. The $\delta^{18}\text{O}$ evolves in the opposite direction to $\delta^{13}\text{C}$; that is, it increases relative to time. In most samples from the central part of the repository block, the extent of the $\delta^{18}\text{O}$ variations (4-7 ‰) is almost 3 times smaller than that of the $\delta^{13}\text{C}$ (12-16 ‰).

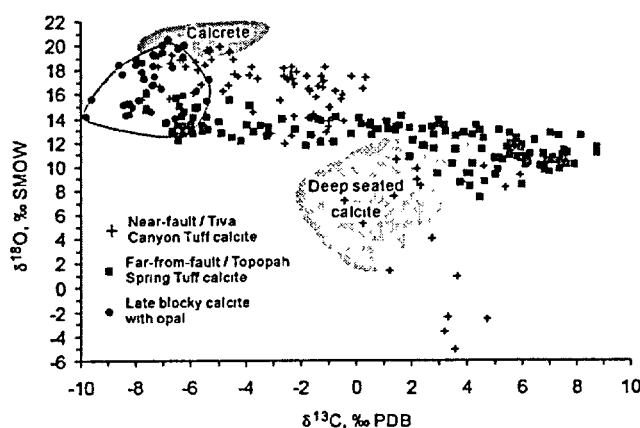


Figure 3-5-14. Summary of isotopic data for calcites from ESF. *Crosses* show the data from calcite collected in the North Ramp in the vicinity of the horst-bounding fault. *Squares* and *circles* represent data from calcites from the central part of the ESF. *Circles* show the data from the latest morphologic variety of blocky calcite associated with opal. Fields of surface calcretes and deep-seated calcite (studied from boreholes) are shown for comparison.

Database: ESF calcites (n = 272; Dublyansky, 2001). Field of calcretes based on 40 measurements (Dublyansky, 2001). Field of deep-seated calcites based on the data for USW G-1, G-2 and G-3/GU3 boreholes (U.S. DOE, 1993).

Several samples have shown a substantial deviation from the pattern illustrated in Figure 3-5-13. Specifically, samples taken in the vicinity of the North Portal exhibit a much wider variability of the $\delta^{18}\text{O}$ with the "lightest" values as light as -5 ‰ SMOW (Figure 3-5-14). The negative correlation between $\delta^{13}\text{C}$ and $\delta^{18}\text{O}$ persists in these samples.

There are at least two ways of interpreting the variability at the North Portal. On one hand, the samples from the vicinity of the North Portal are located close to the Earth's surface, in the stratigraphically higher Tiva Canyon tuff unit. Thus, some sort of stratigraphic control might be suspected, although the nature of this control is unclear. On another hand, these samples are the

closest to the horst-bounding Paintbrush fault – an area where the highest fluid inclusion temperatures have been reported (Dublyansky et al., 2001; see also Chapter 3-6). Thus, lateral zonation of isotopic properties seems to offer a reasonable explanation.

Another noteworthy feature is that the latest in the Yucca Mountain paragenetic sequence variety of calcite – blocky calcite with opal – seems to be a partial exception from the established isotopic trends. As a group, it occupies the "low $\delta^{13}\text{C}$ -high $\delta^{18}\text{O}$ " corner of the $\delta^{13}\text{C}$ vs. $\delta^{18}\text{O}$ cross-plot and by doing so, conforms to the trend. Within the group, however, a negative correlation between carbon and oxygen isotopes is absent (see Figures 3-5-13 and 3-5-14). There seem to have been a dramatic change in the physico-chemistry of mineral growth at this time.

The stable isotopic properties of calcite studied in the ESF may be summarized as follows:

1. The heavy $\delta^{13}\text{C}$ -light $\delta^{18}\text{O}$ values ($\delta^{13}\text{C}$ of 8 to 10 ‰ PDB and $\delta^{18}\text{O}$ of 9 to 10 ‰ SMOW) are typical of the earliest parts of the calcite from the central part of the repository block. These values, however, are not uniquely related to a specific morphologic type of calcite but are found in granular, platelet-bladed, and blocky (without opal) calcite.

2. The heavy $\delta^{13}\text{C}$ -light $\delta^{18}\text{O}$ calcite does not represent a specific mineral-deposition event; rather, it is one end-member of a continuum, evolving, as crystals grew, toward the light $\delta^{13}\text{C}$ -heavy $\delta^{18}\text{O}$ ($\delta^{13}\text{C}$ of -5 to -8 ‰ PDB and $\delta^{18}\text{O}$ of 13 to 17 ‰ SMOW) end-member. This resulted in a prominent negative correlation between $\delta^{13}\text{C}$ and $\delta^{18}\text{O}$.

3. The spatial scale of the isotopic evolution described above varies within at least one order of magnitude. Complete transitions from heavy $\delta^{13}\text{C}$ -light $\delta^{18}\text{O}$ to light $\delta^{13}\text{C}$ -heavy $\delta^{18}\text{O}$ calcite were documented in a 1.2 mm-thick mineral crust (sample 3768) as well as across a 1.4 cm-thick crust (sample 0649) (see Figure 3-5-13).

4. The latest, in the paragenetic sense, blocky calcite with opal has characteristically light $\delta^{13}\text{C}$ -heavy $\delta^{18}\text{O}$ properties. Inside this group, however, a negative correlation between $\delta^{13}\text{C}$ and $\delta^{18}\text{O}$ is absent.

5. The variability of isotopic values within individual samples is, generally, quite large (see Figure 3-5-10). The variability of $\delta^{18}\text{O}$ ranges between 2 to 6 ‰ (with one outlier showing as much as 22 ‰ variation), whereas for $\delta^{13}\text{C}$ the range of variations may be as large as 12-16 ‰.

6. The variability of $\delta^{18}\text{O}$ is greater in samples from the North and South Ramps, and smaller in samples from the Main Drift of the ESF. The variability of $\delta^{13}\text{C}$ does not show any discernible spatial pattern.

3.5.3. Discussion

The stable isotope data obtained from the secondary minerals have been used by the Yucca Mountain Project researchers to infer environmental changes in vegetation at the Yucca Mountain surface in the past (carbon; Marshal et al., 1998), and to assess the paleo temperatures of the mineral forming fluids (oxygen; Whelan et al., 2001). Since another, direct and more precise method of paleo temperature measurement by fluid inclusions is now available, we will discuss the "oxygen isotope temperatures" along with the fluid inclusion data in Chapter 3-6. Below we discuss some aspects of the carbon isotope record.

3.5.3.1. Significance of the heavy $\delta^{13}\text{C}$ values in calcite

As we have demonstrated above, $\delta^{13}\text{C}$ values as "heavy" as +5 to +10 ‰ PDB are not uncommon for the early parts of the Yucca Mountain vadose zone calcite. Meanwhile, calcites with such heavy positive values of $\delta^{13}\text{C}$ are not common in terrestrial environments (Figure 3-5-15). The reason for that is that all carbon bearing compounds typically present in the near-surface environment have light (mostly,

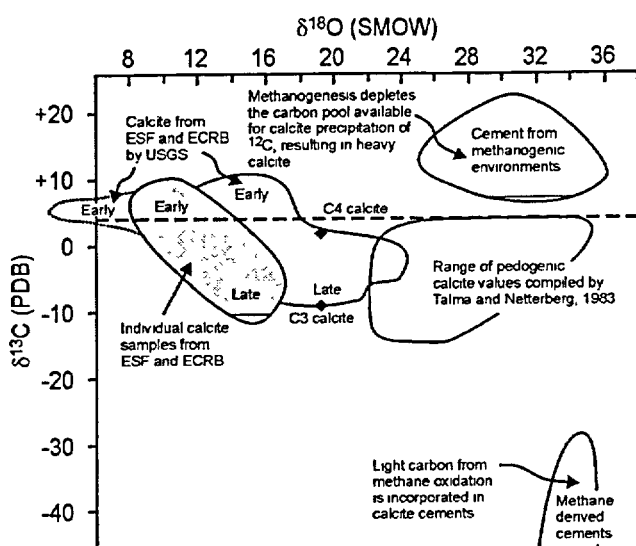


Figure 3-5-15. $\delta^{18}\text{O}$ vs. $\delta^{13}\text{C}$ plot for calcites precipitated in different environments. The average range of pedogenic calcites compiled by Talma and Netterberg (1983) is shown along with the range of values measured in calcites from ESF and ECRB. Values denoted "by USGS" are from Whelan and Moscati (1998); values denoted as individual calcite samples" are from Dublyansky (2001). Diamonds represent the $\delta^{13}\text{C}$ values of C3 and C4 plant-derived calcites. Dashed horizontal line shows the highest value of $\delta^{13}\text{C}$ expected for the Yucca Mountain calcites if no "exotic" mechanisms were involved. Modified from Newman et al. (1997).

negative) values of $\delta^{13}\text{C}$ (Figure 3-5-16). In order to precipitate calcite with a $\delta^{13}\text{C} = +5$ to $+10$ ‰, some uncommon settings or processes are required.

$\delta^{13}\text{C}$ values as heavy as $+7.5$ ‰ were reported from calcite of some thermal spring travertines in Italy (Gonfiantini et al., 1968). Such heavy values are believed to be caused by intense kinetic fractionation associated with the degassing of CO_2 from thermal fluids that, upon discharge at the Earth's surface, already carried relatively "heavy" dissolved carbon. The latter owes its "heaviness" to the thermal decarbonation of carbonate sedimentary rocks by igneous rocks via contact metamorphism.

In most other environments, the formation of the "heavy carbon" calcites require a preferential enrichment of dissolved carbon species that take part in the

precipitation of calcite with the "heavy" carbon isotope (^{13}C) as contrasted with a concentration of "light" isotopes (^{12}C) in those species that do not participate in the precipitation of calcite. Most commonly, this happens through the partition of carbon isotopes between dissolved oxidized (CO_2) and reduced (CH_4) species of carbon. The latter species has a strong tendency for the preferential accumulation of ^{12}C . There are two settings that are known to favor such partitioning: methanogenesis and residence in an anoxic reducing environment.

3.5.3.1.1. Methanogenesis

Bacteria-assisted methanogenesis may deplete the carbon pool available for calcite precipitation of ^{12}C , resulting in heavy calcite (see Figure 3-5-15). Biogenic methane is produced by strictly anaerobic Archaea, called methanogens, through reduction of CO_2 using H_2 as an electron donor:



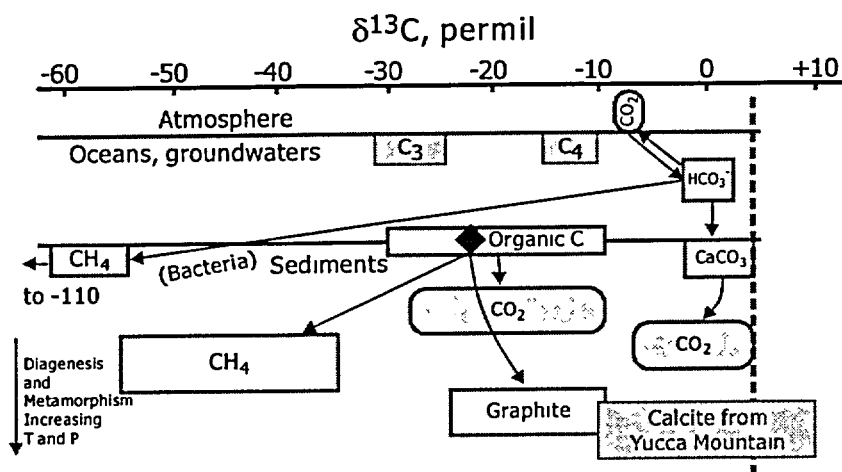


Figure 3-5-16. Schematic diagram showing $\delta^{13}\text{C}$ values of carbon-bearing compounds in near-surface environments (slightly modified from Ohmoto, 1986), as well as data for secondary calcite from Yucca Mountain. Vertical dashed line at +4 ‰ cuts $\delta^{13}\text{C}$ values that are anomalous for the near-surface environment. C_3 and C_2 boxes indicate isotopic values of carbon produced by plants with C_3 and C_2 metabolic pathways.

The most typical habitats of methanogens in nature are either anoxic sediments, such as marsh or swamp, or geothermal sources of H_2 and CO_2 (Brock..., 2000).

The existence of a strictly anoxic environment within the thick unsaturated zone of Yucca Mountain in the past is highly improbable. In this regard, examination of the modern-day

underground air chemistry is quite revealing. The air sampled from the Yucca Mountain instrumented boreholes contains oxygen and nitrogen in "atmospheric" proportions (i.e., ~20 vol. % O_2 and ~80 vol. % N_2) and slightly elevated concentrations of CO_2 (up to 0.13 vol. %). Importantly, underground air is depleted in methane: 0.05 to 0.2 ppmv as opposed to 1.7 ppmv in the outside atmospheric air (Thorstenson et al., 1989). Also depleted in methane are gases from the Yucca Mountain soils: 0.5 to <1.7 ppmv.

Microbiological studies of several calcite samples from the ESF have revealed the presence of viable, moderately thermophilic ($\leq 41^\circ\text{C}$), calcite-precipitating bacteria (Else et al., 1999). This, along with the known elevated temperatures of deposition of the host calcite (85 to $<35^\circ\text{C}$; Dublyansky et al., 2001) strongly suggests a geothermal source habitat. It is not known at present whether or not the thermophilic bacterial communities established by Else et al. (1999) contain methanogens. In geothermal systems, however, the same isotope partitioning processes may occur without bacterial involvement.

3.5.3.1.2. Anoxic environment

Carbonate minerals with strongly positive $\delta^{13}\text{C}$ were reported in association with hydrothermal ore deposits. For example, in the Pine Point hydrothermal, Pb-Zn deposit (Canada) $\delta^{13}\text{C}$ increases from -10 - 0 ‰ in early-stage gangue calcite to +1 - +11 ‰ PDB in late calcite. Ohmoto (1986) has interpreted this trend as indicating the evolution of the mineral-forming fluids from a high to a very low (reducing) oxidation state. By analogy, the isotopic record shown for the example in Figure 3-5-12 may be

interpreted as reflecting an evolution of the mineral-forming fluid from a low to high oxidation state (i.e., from reducing to oxidizing).

Of the different carbonate species dissolved in aqueous fluids, only oxidized ones participate in precipitation of calcite. Reduced carbon species, such as $\text{CH}_4(\text{aq})$, if present, may, through fractionation, affect the isotopic properties of oxidized species and hence, of depositing calcite. The oxidation states of carbon species are strongly affected by the fugacity of oxygen (Ohmoto, 1972 and Ohmoto and Rye, 1979). Faure (1986) stated: *“If the oxygen fugacity is about 10^{-38} atmospheres, most of the carbon is oxidized and $\text{CH}_4(\text{aq})$ is negligible. At lower oxygen fugacities $\text{CH}_4(\text{aq})$ rapidly increases in abundance. Changes in the abundance of $\text{CH}_4(\text{aq})$ have dramatic effect on the $\delta^{13}\text{C}$ values of the coexisting carbonate species because CH_4 is strongly enriched in ^{12}C ... The enrichment of the oxidized carbon species in ^{13}C is due to the preferential partitioning of ^{12}C into $\text{CH}_4(\text{aq})$ which becomes important at low oxygen fugacities.”* (p. 505).

The isotope fractionation factor between CO_2 and CH_4 and calcite is large and temperature-dependent (Figure 3-5-17-a). Studies of natural hydrothermal systems, however, show that complete isotope equilibration is rarely attained, so that the fractionation between reduced and oxidized species of carbon is typically smaller than the calculated equilibrium values (Figure 3-5-17-b). In addition to a strongly reducing (anoxic) environment, isotopic exchange between dissolved CO_2 and CH_4 is favored by a long length of time available for reaction and elevated temperatures (Ohmoto, 1972; 1986). These parameters are directly opposite to what would be expected for meteoric waters percolating through the vadose zone (“rainwater” concept), where oxygen is abundant, methane is scarce, the temperature is low, and the residence time of waters is relatively short. In the context of the conceptual model of the hydrothermal upwelling, however, such parameters are expected for the early portions of the fluid that, prior to coming into the vadose zone, resided for a long time in the deep (anoxic) parts of the Earth's crust (see Parts One and Two for discussion). It is noteworthy, therefore, that a substantial number of calcite samples studied from the ESF contain calcite with $\delta^{13}\text{C} > +4$ ‰ PBD (see Figure 3-5-9). For example, of the 11 ESF samples studied by the GC-IRMS method, 7 were found to contain heavy-carbon calcite (Dublyansky, 2001).

The position of the Yucca Mountain Project researchers as to the meaning of the carbon isotopic properties of calcite was summarized as follows: *“Carbon isotopes in unsaturated zone calcite are consistent with the carbon isotopic signature acquired in the soil zone by downward percolating water...”* (U.S. DOE, 2001, p. 4-404). According to the USGS researches, *“Isotopic studies of secondary calcite and opal in the UZ [= unsaturated zone]... demonstrate that they precipitated from meteoric waters with pedogenic signatures. These waters percolated along fractures through the UZ tuffs.... As such,*

"rainwater" concept fails to coherently explain the observed isotopic properties of secondary calcite from the vadose zone of Yucca Mountain.

The invalidity of the "rainwater" concept becomes even more apparent when the stable isotope and fluid inclusion data from secondary minerals are considered together as a single coherent record. This will be done in Chapter 3-6.

3.5.3.2. Interpretation of the negative correlation of $\delta^{13}\text{C}$ and $\delta^{18}\text{O}$

The Yucca Mountain Project scientists interpret the evolving $\delta^{18}\text{O}$ properties of secondary calcite from the vadose zone as reflecting an increasing temperature with depth from the surface and, at a given depth, a decreasing temperature as a function of time. They interpret the evolving $\delta^{13}\text{C}$ properties as reflecting changes in the vegetation at the mountain's surface.

We are of the opinion that $\delta^{18}\text{O}$ may, indeed, be reflecting the changing temperatures of the mineral-forming fluids; at least for some of the morphologic types of calcite. The $\delta^{18}\text{O}$, most likely, is not a function of the temperature in the latest morphologic type – blocky calcite with opal (the matter will be discussed further in Chapter 3-6). As was shown above, the changing vegetation does not seem to be capable of providing an explanation of the $\delta^{13}\text{C}$ pattern. We interpret the decreasing $\delta^{13}\text{C}$ values of calcite with time as reflecting the overall change of the redox properties of fluids. Early fluids injected into the vadose zone came from the deep anoxic parts of the Earth's crust where they resided for substantial periods of time. In such an environment, the isotopic fractionation and enrichment of the dissolved oxidized carbon ($\text{CO}_2\text{ aq}$) with "heavy" carbon isotopes may have reached advanced stages. These fluids, upon reaching supersaturation with respect to calcite, deposited CaCO_3 with heavy positive $\delta^{13}\text{C}$ values. The conceptual model developed in Parts I and II of this report requires that the initial "injection" of the deep-seated fluids is followed by a more-prolonged circulation of fluids, which inevitably involves the oxidized waters of the upper part of the hydrosphere. The increasing role of such oxidized waters, which would carry "lighter" $\delta^{13}\text{C}$ values, we believe, are responsible for the gradual decrease in $\delta^{13}\text{C}$ of the calcite, deposited by such waters.

Chapter 3-6. Fluid inclusion studies

By Y.V. Dublyansky

Table of Contents

Chapter 3-6. Fluid inclusion studies	300
3.6.1. Applicability and limitations of the fluid inclusion method in paleo-hydrogeological studies	300
3.6.2. History of fluid inclusion research on secondary minerals from the unsaturated zone at Yucca Mountain	302
3.6.2.1. Work by the Yucca Mountain Project scientists	302
3.6.2.2. Work by State of Nevada scientists	304
3.6.2.3. Clash of opinions, evaluation and resolution process	305
3.6.3. Types of fluid inclusions in the Yucca Mountain secondary minerals	307
3.6.4. Fluid inclusion thermometry	309
3.6.4.1. Calcite	309
3.6.4.2. Fluorite and quartz	311
3.6.4.2. Fluorite and quartz	312
3.6.4.3. Summary of the thermometric data	312
3.6.4.4. Salinity of the mineral-forming fluids	313
3.6.4.5. Spatial distribution of the fluid inclusion homogenization temperature in the ESF	314
3.6.5. Interpretation of the thermometric data	316
3.6.5.1. UNLV and U.S. DOE interpretation of a thermometric significance of the all-liquid inclusions	317
3.6.5.2. USGS interpretation of a genetic significance of two-phase liquid-vapor inclusions with variable vapor-to-liquid ratios	319
3.6.5.3. Heat flow indicated by the paleo-thermometric data	321
3.6.6. Gases in inclusions hosted by the ESF secondary minerals	324
3.6.6.1. Results of Quadrupole mass spectrometric analyses of the entrapped gases at Yucca Mountain	325
3.6.6.2. Results of gas chromatographic analyses of the ESF minerals	330
3.6.6.3. All-gas inclusions in the ESF secondary minerals	332
3.6.6.4. Significance of the all-gas inclusions	334
3.6.6.5. Chemistry of all-gas inclusions	335
Crushing	335
Raman spectrometry	336

Gas chromatographic analysis of gas from individual inclusion _____	337
3.6.7. Interpretation of the data on gases in inclusions _____	337
3.6.7.1. Natural gas flow system and gas chemistry at Yucca Mountain _____	337
3.6.7.2. Gases trapped in inclusions _____	339
3.6.7.3. Suggested origin of hydrocarbon gases _____	340
3.6.8. Interpretation of the combined $\delta^{18}\text{O}$ and fluid inclusion data _____	340
3.6.8.1. Geothermal reconstructions based on $\delta^{18}\text{O}$ values _____	340
3.6.8.2. Timing of the entrapment of two-phase inclusions relative to "stable isotope stages" of the mineral growth _____	345
3.6.9. Summary _____	349

Chapter 3-6. Fluid inclusion studies

By Y.V. Dublyansky

An adequate understanding of the paleo-hydrogeology at the potential nuclear waste repository site is absolutely necessary for making reliable forecasts of hydrogeologic phenomena that may be expected to affect the long-term repository performance. Ancient waters moving through the rocks commonly leave "footprints" in the form of secondary minerals and zones of chemical rock alteration. Integrated mineralogic, fluid inclusion and isotope studies of secondary minerals are important, because they provide direct information regarding the paleo-hydrogeology of the site. Such studies play a central role in many national programs dealing with the siting of facilities for the geological disposal of nuclear waste. Pertinent examples are Chalk River Site in Canada (Bukata et al., 1998) and Olkiluoto Site in Finland (Blyth et al., 1998). In France, an investigation of fluid inclusions in secondary minerals was used to study paleo-fluid migration in the Charroux-Cirway (Vienne) crystalline basement and sedimentary cover in an effort to characterize the potential ANDRA (Agence Nationale pour la gestion des Dechets Radioactifs) site for an underground research laboratory on nuclear waste storage. Cathlineau et al. (1999) remarked: *"Fluid inclusions can be considered as the most sensitive markers of the fluid migration at several scales, and much more discriminant than the mineral assemblages"* (p. 64). Studies of fluid inclusions are recommended for use in site characterization for disposition of excess weapon plutonium. According to Heiken et al., (1996, p. 22): *"Fluid inclusions provide insightful tool for interpreting the fluid history of geologic systems. They are presently the only direct evidence available for characterizing past fluid events in a rock."*

It is unfortunate that the results of fluid inclusion studies were not timely recognized and considered during the site characterization activities at Yucca Mountain. Early fluid inclusion results have been largely ignored and, on a number of occasions, inadequately presented.

3.6.1. Applicability and limitations of the fluid inclusion method in paleo-hydrogeological studies

Fluid inclusions are microscopic cavities in the minerals, containing remnants of fluids from and in the presence of which minerals were formed (primary inclusions), or with which they were in contact at later stages (secondary inclusions). The fluid inclusion method is widely used for reconstructing temperatures, chemical compositions and salinities of fluids that deposited the hydrothermal (Roedder,

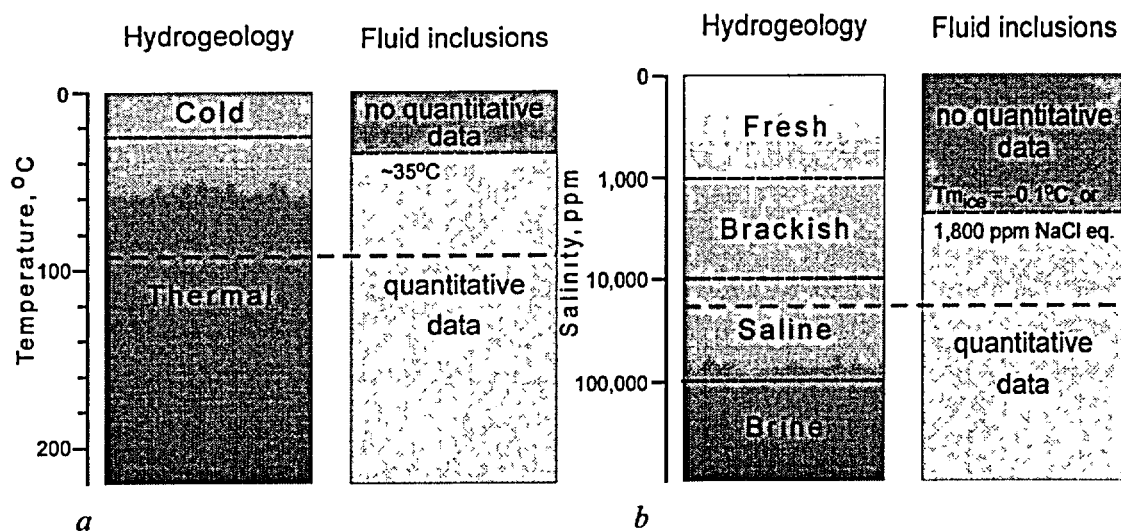


Figure 3-6-1. Data obtainable by the fluid inclusion method in the context of the hydrogeological classification of waters (by Davis & De Wiest, 1966). *a* – classification according to the temperature *b* - classification according to the salinity. Dashed red lines indicate the highest fluid inclusion temperature and salinity measured in calcite from ESF (85°C and 21,000 ppm; Dublyansky et al., 2001).

1984) and diagenetic minerals (Goldstein and Reynolds, 1994). Commonly, fluid inclusions are used to address paleo-hydrological problems (Shepherd et al., 2000).

When evaluating the results of fluid inclusion studies, it is important to keep in mind the limitations of the method. The fluid inclusion method does not provide numeric information on the temperature of fluids if aqueous inclusions in minerals do not contain shrinkage bubbles. Monophase, all-liquid inclusions are interpreted as an indication that the mineral-forming fluids were "low-temperature" ones. In most cases it is not possible to specify the lowest entrapment temperature, below which a shrinkage bubble does not nucleate in the inclusion. Therefore, all-liquid inclusions are regarded as being trapped in the temperature range, which is less than *approximately* 50 °C (Goldstein, 2001). In some cases, it might be argued (but not proved) that the upper limit is lower (say, 35°C). In the near-surface environment, however, a temperature of less than 35-50°C may equally indicate the "ambient-temperature" and "thermal" water (Figure 3-6-1).

In freezing experiments the salinity of fluids is assessed on the basis of the freezing depression temperature. The accuracy of measurement for an ice-melting temperature depends largely on the quality of the equipment used. For the best commercially available equipment, a final melting temperature as close to zero as -0.1°C can be measured. In terms of the salinity, this translates into 1,800 ppm (NaCl equivalent). This means that fluid inclusions with a reported ice melting temperature of 0°C, which in most fluid inclusion studies would be interpreted as "fresh water" inclusions, may in fact have a salinity

ranging from ~0 to ~1,800 mg·l⁻¹. In hydrology such waters are classed as either fresh (0-1000 ppm) or brackish (1000-2000 ppm) as shown in Figure 3-6-1.

3.6.2. History of fluid inclusion research on secondary minerals from the unsaturated zone at Yucca Mountain

3.6.2.1. Work by the Yucca Mountain Project scientists

The earliest fluid inclusion data obtained from the Yucca Mountain minerals date back to 1984. After studying secondary deposits at Trench 14 on the west side of Exile Hill Vaniman et al. (1984) reported: "*The drusy quartz crystals that occur in altered tuff also are poor in large inclusions, but the small inclusions, which occur in abundance, contain visible bubbles. The largest inclusion found so far (8 μm) yielded a homogenization temperature of 145°C. ... This preliminary datum plus the textural evidence for early growth of the drusy quartz suggest that some form of hydrothermal event preceded the calcite – opal CT – sepiolite – palygorskite (?) – amorphous silica crystallization along the fault*" (p. 5). A higher-than-boiling temperature reported for a mineral collected at land surface argues against *in situ* crystallization (a pressure of ~5 bar, equivalent of ~50 m of hydrostatic pressure is needed to keep water from boiling at this temperature).

In 1992, a Panel of the National Academy of Sciences/National Research Council evaluated the hydrothermal upwelling concept that was identified in 1989 by a U.S. DOE scientist, Jerry S. Szymanski, as a potential site suitability issue. The review was requested by the DOE to obtain input into the decision whether or not to proceed with the site characterization at Yucca Mountain. Even though the NAS/NRC Panel disputed the hydrothermal upwelling hypothesis, it did recommend that fluid inclusion research needed to be carried out (NAS/NRC, 1992).

The first fluid inclusion data for calcite from the vadose zone of Yucca Mountain were reported by Bish (1989). Samples for this study were collected from cores of two drill holes, USW G-2 and USW G-3/GU-3. Later these data were reported in a paper by Bish and Aronson (1993): "*Homogenization temperatures in calcite from USW GU-3/G-3 were 101° to 227°C at 31 m, 125° to 170°C at 130.8 m...*" (p. 152). The authors studied the ancient magma chamber-based, hydrothermal alteration system related to silicic volcanism that was active approximately 11 Ma ago (the so called Timber Mountain Caldera hydrothermal event). They immediately recognized that such high homogenization temperatures at such low depth are difficult to attribute to the Timber Mountain hydrothermal episode, which, in this part of Yucca Mountain, supposedly affected only the deep (deeper than ~1000 m) part of the tuff sequence. The authors suggested that the high temperatures either reflect an initial cooling of the tuffs, or were artifacts related to the determination of homogenization temperatures of unsuitable re-equilibrated inclusions.

More homogenization temperatures obtained by Prof. Edwin Roedder were reported in the U.S. Geological Survey's "Monthly Report of Ongoing Work" in January 1993 (USGS, 1993). By request, these data were transmitted by the U.S. DOE Yucca Mountain Site Characterization Office to the State of Nevada Agency for Nuclear Projects (U.S. DOE, 1993-b). Homogenization temperatures of 74 to 104°C were measured in calcite from borehole USW G-1 at depths from 129.7 to 313.6 m (i.e., within the vadose zone of Yucca Mountain). These early results were not mentioned in subsequent publications between 1993 and 2000 and were ignored in paleo-hydrological reconstructions done by the Yucca Mountain Project researchers during this period of time.

Roedder, with co-authors (1994), described the two-phase, liquid+vapor inclusions in calcite from four depths: 130, 204, 292 and 314 m in core of borehole USW G-1: "...inclusions occurred in groups, with an apparently uniform and small V/L ratio, which visually indicated that the inclusions had formed at low temperatures, probably $\leq 100^{\circ}\text{C}$ " (p.1858) Surprisingly, the authors did not report any measurements of the homogenization temperatures. Instead, they asserted: "...these calcites have formed at low temperatures, $< 100^{\circ}\text{C}$, possibly comparable to modern ambient temperatures." (p.1859). The later conclusion appears clearly unwarranted. The presence of the two-phase inclusions with consistent liquid-to-vapor ratios indicates that the temperature of the paleofluids was higher than *approximately* 50 °C (at lower temperatures the shrinkage vapor bubbles do not normally nucleate; see Roedder, 1984, Goldstein and Reynolds, 1994, and Goldstein, 2001 for discussion). Therefore, in order to produce two-phase liquid-vapor inclusions, temperatures of mineral-forming waters must have been higher than the "modern ambient temperatures" (20 to 25°C at a depth of the sample collection; Sass et al., 1987). In their paper Roedder with co-workers did not mention either the fluid inclusion temperatures published earlier (e.g., Bish and Aronson, 1993) or homogenization temperatures obtained by the senior author in 1993 (see above). If the temperatures of 74 to 104 °C, which were measured by Roedder and reported in USGS (1993) and U.S. DOE (1993-b), were acknowledged a central conclusion of the paper, regarding the depositional temperature being "*possibly comparable to modern ambient temperature*" in vadose zone of Yucca Mountain, could not possibly have been made.

In 1995 a group of researchers from LANL reported their analyses of the fluid inclusion gas chemistry in calcites from the ESF obtained by Quadrupole mass spectrometry (Levy et al., 1995). They determined the contents of H₂O, CH₄, N₂, O₂, Ar, and CO₂ in two samples collected in the vicinity of the Bow Ridge Fault. The authors reported that the fluid inclusions contain proportions of water, which are uncharacteristically high compared to vadose zone calcite studied elsewhere; but are typical of phreatic-zone calcite. (The data will be discussed in detail in section 3.6.6.1 below.)

In 1998, results of new fluid inclusion studies in the Yucca Mountain unsaturated zone calcite were presented by Roedder and Whelan (1998) at the 7th Pan-American Conference on Current Research on Fluid Inclusions. The authors stated: "*We have studied the fluid inclusions in vein and vug calcite from the tuffs and find that all unsaturated zone calcite contains abundant inclusions that are full of liquid, and lesser numbers of inclusions that are full of gas mixtures of atmosphere-like composition at about one atmosphere pressure.*" (p. 56; emphasis by authors). The authors' statement not only refuted their earlier claim quoted above ("*...inclusions occurred in groups, with an apparently uniform and small V/L ratio...*" Roedder et al., 1994), from which it is apparent that, besides all-liquid inclusions, the studied samples do contain two-phase liquid-vapor inclusions, which are suitable for the paleo-temperature studies. They again failed to mention homogenization temperatures of 75 to 104°C measured by Roedder earlier (USGS, 1993; U.S. DOE, 1993-b). Obviously, had they acknowledged these observations and measurements, they would not be able to draw the conclusion: "*Our fluid inclusion studies of numerous samples from the underground workings of the Exploratory Studies Facility and from Yucca Mountain boreholes have revealed no evidence of either hydrothermal activity or ascending fluids during formation of unsaturated-zone secondary minerals, but have instead confirmed our earlier conclusions that these minerals formed from descending cool waters, above the level of water table*" (Roedder and Whelan, 1998, p. 56; emphasis by authors)

Summary. As it is apparent from the record of publications presented above, limited studies of fluid inclusions have been carried out by the Yucca Mountain Project researchers, and preliminary results produced by two different organizations (LANL and USGS) have been available to the Yucca Mountain Site Characterization Project Office as early as 1989-1995. These early results, albeit preliminary in character, clearly presented the possibility that (a) some secondary minerals from the Yucca Mountain vadose zone could record circulation of hot waters (74 to >100°C) and (b) the deposition of minerals likely occurred in the saturated environment. Arguably, a prudent approach for the Yucca Mountain Project management in such circumstances would be to initiate a focused research project and perform a comprehensive study of fluid inclusions in minerals recovered from drill cores and, upon completion of the ESF, to perform the same studies of minerals exposed in the tunnel. Such research was recommended in 1992 by the National Academy of Sciences/National Research Council panel. Nevertheless, no research was carried out by the Yucca Mountain Project researchers until as late as 1999.

3.6.2.2. Work by State of Nevada scientists

In 1993, several samples collected in surface outcrops near Yucca Mountain were examined for the presence of fluid inclusions (Harmon, 1993). Fluid inclusions were found in quartz from mixed carbonate-silica samples collected at the Wailing Wall (south of Yucca Mountain) and Pull Apart fault

(approximately 20 m-wide fault gap in the Paleozoic limestone filled with micritic calcite-silica deposits some 10 km to the south of Yucca Mountain. At the Wailing Wall, quartz contained two types of inclusions: monophasic gaseous and two-phase liquid-vapor with high vapor-to-liquid (V:L) ratio of about 0.9. The two-phase inclusions were too small for thermometric studies. Inclusions from vug-filling quartz from Pull Apart fault yielded 21 homogenization temperatures ranging from 118 to 195 °C. Two measurement of the melting temperatures of ice yielded salinities of 1,000 and 5,000 ppm (NaCl-equiv.).

These results are consistent with a single datum of 145°C reported by Vaniman et al. (1984) for a quartz crystal, collected in a similar setting of the mixed carbonate-silica fault material at Bow Ridge fault. The reported temperatures require a depth of formation of at least 150 m (to prevent boiling). Similarly to Vaniman et al. (1984), Harmon concluded: "*Thus, the vug-filling quartz in sample 4d [from Pull-Apart fault] appears to have been deposited from a moderate-temperature, low-salinity fluid or, at least, was subjected to an episode of interaction with such a fluid some time after its formation. These facts, together with the presence of microbreccia veinlets and sulfides in the Yucca Mountain samples, point to a hydrothermal environment with a low-temperature character (i.e. epithermal origin)*" (Harmon, 1993, p. 26).

In 1995 Dublyansky and Reutsky (1995) reported the results of the pilot fluid inclusion study on a set of samples from the first 300 m of the ESF, which have been completed at that time. Homogenization temperatures ranging from 34 to 75°C were measured in six samples of calcite. In 1996, these data were reported at the Annual Meeting of the Geological Society of America and of the 6th Pan-American Conference on Current Research on Fluid Inclusions (Dublyansky et al., 1996-a, and -b). Results of additional studies carried out in 1998-1999 were reported at the Meeting of the American Geophysical Union (Dublyansky, 1999). In the course of this research, homogenization temperatures of 35 to 85°C and salinities from ~0 to 21,000 ppm NaCl-equiv. were measured in a number of calcite samples. The overall conclusion regarding the origin of secondary minerals at Yucca Mountain was formulated in Dublyansky et al. (2001) as follows: "*Our data indicate that the calcite-opal-quartz (with minor fluorite) crusts from the presently unsaturated (vadose) zone of Yucca Mountain were formed from low-temperature hydrothermal aqueous fluids in the saturated (phreatic) environment.*" (p. 125).

3.6.2.3. Clash of opinions, evaluation and resolution process

Public clash of opinions regarding the properties of the fluid inclusions in the Yucca Mountain secondary minerals and, more generally, the origin of these minerals took place in 1998 at the 7th Pan-American Conference on Current Research on Fluid Inclusions in Las Vegas, Nevada. The U.S. Geological Survey researchers, Edwin Roedder and Joseph Whelan, went on record with strong statements that the calcite from Yucca Mountain unsaturated zone contains no two-phase fluid inclusions suitable for

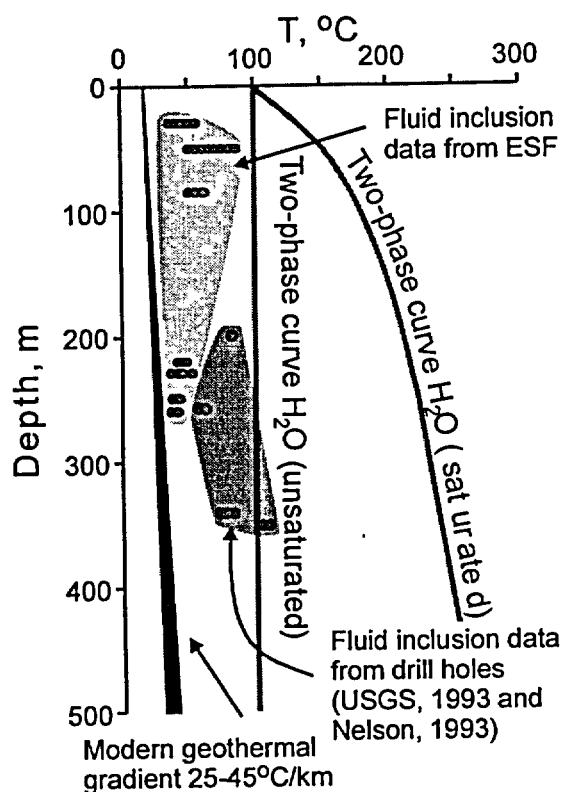


Figure 3-6-2. Fluid inclusion data obtained on secondary minerals from the Yucca Mountain vadose zone available by 1998. All inclusion data plot to the right of the modern geothermal gradient line, indicate paleo-temperatures higher than can be related to "normal" conductive geothermal gradient. Most homogenization temperatures lie within the liquid field (i.e., to the left of the two-phase curve). Two measurements from boreholes plot right of the vadose-zone boiling curve, which make them incompatible with the vadose-zone setting.

thermometric studies, and that this calcite, therefore, was formed in the vadose zone environment from descending cool waters (see above). Yuri Dublyansky of Russian Academy of Sciences presented the data showing that the two-phase fluid inclusions do exist in calcite from the ESF and that these inclusions indicate a saturated (phreatic) environment and depositional temperatures of up to 75°C (Dublyansky, 1998-a). Later in 1998, the U.S. Nuclear Waste Technical Review Board (NWTRB) completed the review of several reports submitted for evaluation by the State of Nevada. Among those was one report on fluid inclusions (Dublyansky and Reutsky, 1995). The consultant to NWTRB Robert Bodnar of Virginia Technological Institute and State University concluded: "...fluid inclusions found in mineral deposits at Yucca Mountain do provide direct evidence of the past presence of fluids at elevated temperatures ... in the vicinity of the proposed repository" (Cohon, 1998, p. 2), based on which the NWTRB recommended further studies aimed at resolving the fluid inclusion issue. In December 1998, the Institute of Energy

and Environmental Research (USA) released a report describing new results of the fluid inclusion studies at a press conference in Washington, DC (Dublyansky, 1998-b). In this report more fluid inclusion results were presented.

A summary of the data on fluid inclusions in the Yucca Mountain vadose zone, available by 1998, is shown in Figure 3-6-2.

Discrepancies in reported observations and an intense and unyielding disagreement in the interpretations of the data between scientists representing the Yucca Mountain Project and the State of Nevada eventually led the U.S. DOE to launch a verification project for the fluid inclusion issue. In April 1999, a 2-year research project "Thermochronology of the Yucca Mountain secondary minerals" was

started at the University of Nevada at Las Vegas (UNLV). Upon initiation of this project, the U.S. Geological Survey and the State of Nevada have elected to carry out “parallel” fluid inclusion research, including sharing samples and discussing the results as well as the emerging interpretations.

After studying large number of samples, both UNLV and USGS teams obtained the homogenization temperatures and salinity of the fluids, as well as the spatial distribution of paleo temperatures in the ESF, all of which were similar to those reported earlier by Dublyansky and Reutski (1995) and Dublyansky (1998). The presence of waters with elevated temperatures at the repository horizon in the past has been, therefore, confirmed. The early contention of the Yucca Mountain Project researchers, in regard to the absence of such waters (Roedder et al., 1998), was demonstrated to be fallacious.

The UNLV researchers reported that fluids with elevated temperatures (up to 75 °C) did pass through the planned repository horizon more than 1.9 Ma ago (Wilson and Cline, 2001). Thus far, however, the UNLV researchers did not propose any model that would explain such properties of the secondary minerals as stable isotope signatures (including their spatial and temporal variability), crystallographic forms and mineralogical types (including their spatial and temporal variability), salinity of the entrapped fluids, chemistry of the entrapped gases, spatial variability of the homogenization temperatures, etc.

The USGS researchers reported that they have made more than 2000 determinations of the homogenization temperatures ranging up to ≥ 85 °C (Whelan et al., 2001). In order to account for these elevated temperatures, the USGS researchers now speculate that rainwater, which they still maintain deposited the secondary minerals, percolated through the mountain that has been heated (conductively) by a magmatic body underneath the Timber Mountain Caldera, which is situated some 5-8 km to the north of Yucca Mountain (Marshall et al., 2000). Alternatively, they attribute the elevated depositional temperatures to the heating of rocks in the vadose zone by heated waters that circulated at a depth > 1000 m under Yucca Mountain during the Timber Mountain Caldera hydrothermal event 10.5-11.0 Ma ago (Whelan et al., 2001). Even though the results of their own thermal modeling fail to explain the highest temperatures observed in the fluid inclusions, as well as the spatial distribution of these temperatures, they nevertheless refuse to consider the hydrothermal upwelling as a possibility.

3.6.3. Types of fluid inclusions in the Yucca Mountain secondary minerals

In modern fluid inclusion research, the thermometric analyses are typically carried out on so-called fluid inclusion assemblages, or FIA's. This term is used to denote petrographically defined groups of inclusions trapped contemporaneously (Goldstein and Reynolds, 1994). At Yucca Mountain, calcite is a

mineral that contains most of the fluid inclusions. Typically, this mineral hosts a number of different inclusion types.

The most abundant inclusions, which are present practically in all samples, belong to a monophasic *all-liquid inclusion* type. In fluid inclusion research, all-liquid FIA's are typically interpreted as indicating that the depositional temperature was less than *approximately* 50 °C (Goldstein, 2001). In addition to forming homogeneous FIA's, all-liquid inclusions are commonly present in those FIA's that contain two-phase liquid-vapor inclusions.

FIA's composed of *two-phase liquid-vapor inclusions with consistent liquid-to-vapor ratio* are usually scarcer, including in the ESF. Nevertheless, they were found in approximately 50 % of calcite samples from the ESF and ECRB (Dublyansky et al., 2001; Wilson and Cline, 2001). In many instances primary character of these inclusions has been established, because many of them were found to be developed along the crystallographically defined mineral growth zones. This type of inclusions is most important from the perspective of thermometric analyses. This is because it allows for direct determination of temperature of the mineral growth by measuring the inclusion homogenization temperature, or T_h .

Two-phase liquid-vapor inclusions with variable liquid-to-vapor ratios are common but not abundant. Such inclusions may be produced by a number of processes and mechanisms. They may be a result of so-called heterogeneous entrapment, which means that the two phases – liquid and vapor – co-existed during the mineral crystallization. Examples of situations in which the heterogeneous entrapment may occur are: (a) boiling fluid (vapor phase is composed of water vapor); (b) effervescing fluid (vapor phase is composed of effervescing gas); and (c) fluid in the vadose zone (the vapor phase contains air). Another mechanism that may produce such liquid-vapor inclusions is necking-down (see Roedder, 1984 for details). In addition, such inclusions may be produced through a post-entrapment damage, which causes that the inclusion vacuoles either increase in volume (stretching) or partially lose their content (leakage). Both stretching and leakage may occur naturally (e.g., due to heating of the sample during burial or mechanical damage caused by tectonic movements) and artificially (e.g., due to inadvertent overheating or mechanical damage during sample collection, handling and preparation for analysis). Caveats of interpretation of the two-phase inclusions with variable vapor-to-liquid ratios are discussed in detail in section 3.6.5.2.

The last type, *monophasic all-gas inclusions* are present in ~70 % of mineral samples from the ESF and ECRB, and such inclusions were observed to be present in all morphological varieties of calcite. They were also found in some fluorite and quartz samples. The presence of all-gas inclusions constitutes unequivocal evidence of the heterogeneity of the mineral-forming fluid during crystal growth.

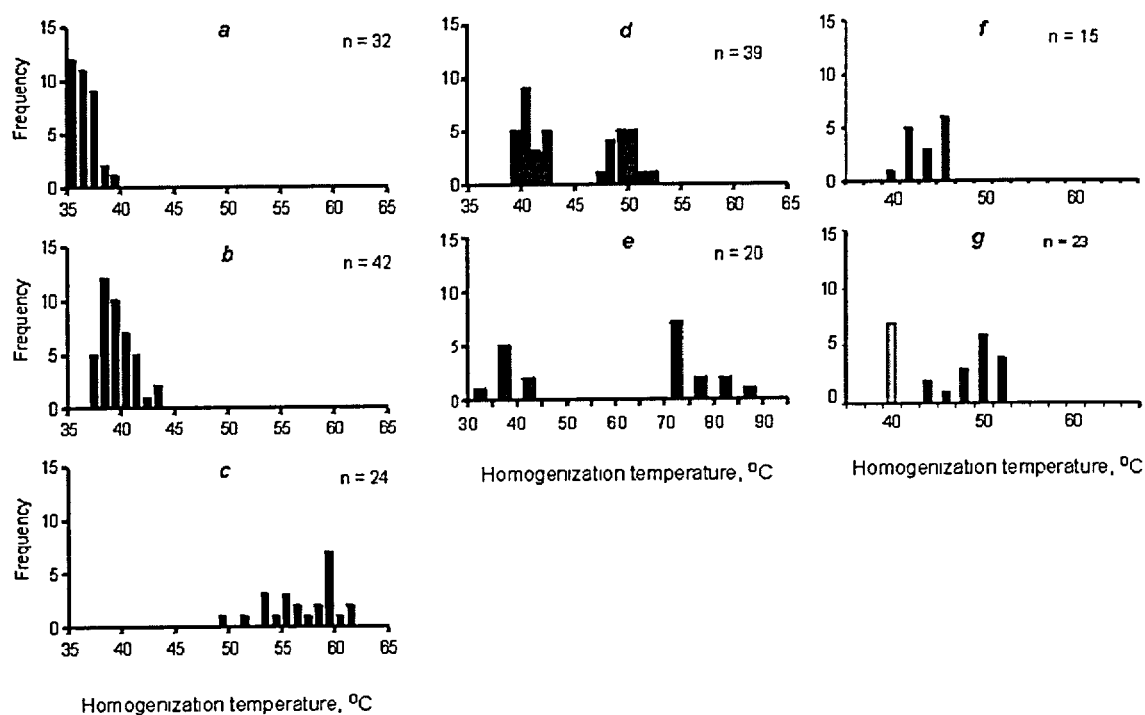


Figure 3-6-3. Patterns of distributions of the homogenization temperatures measured in fluid inclusions: *a* through *c* – single event; *d* and *e* – two events; *f* and *g* – two mineral deposition events and one post-depositional event (these two diagrams are from the base (*g*) and outer blocky part (*f*) of the same sample). *Black* - primary inclusions; *gray* – secondary or pseudo-secondary inclusions.

Stations in the ESF: *a* – 37+38; *b* – 28+00; *c* – 76+00.6; *d* – 28+81; *e* – 01+62.3; *f* and *g* – 52+43 (*f* – outer part of the crust, and *g* – middle part of the crust).

3.6.4. Fluid inclusion thermometry

3.6.4.1. Calcite

Most of depositional temperatures for the Yucca Mountain secondary minerals were inferred based on fluid inclusion homogenization experiments carried out on samples of calcite (Dublyansky et al., 2001). A characteristic feature of the Yucca Mountain results is that the homogenization temperatures (T_h s), which were obtained from the same FIA's, typically plot within quite narrow intervals. It is not uncommon, for example, for T_h s, measured in as many as 20 to 40 individual inclusions from the same FIA, to fall within a 5 °C-interval. Goldstein and Reynolds (1994) recommended that a FIA in which 90% of inclusions homogenize within a 10–15 °C-interval should be considered as showing consistent result (which means that the homogenization temperatures, most probably, accurately reflect paleo-temperatures of the entrapped fluids).

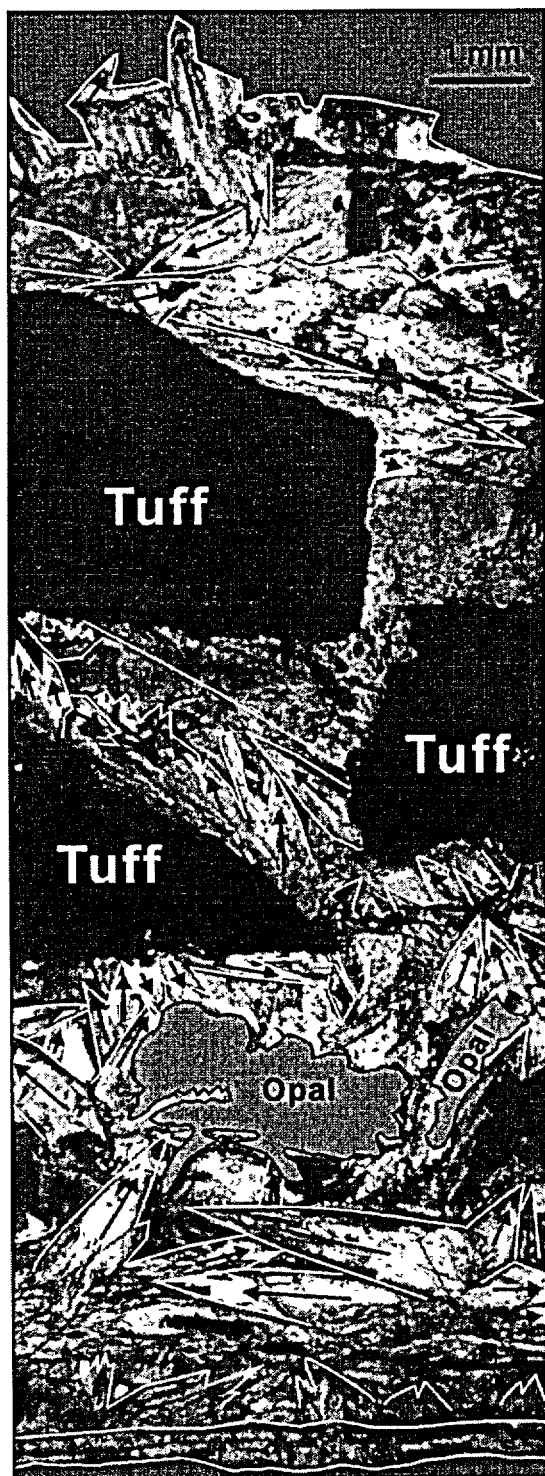
One question that might be addressed through fluid inclusion studies is whether the mineral growth was a single continuous event, or whether it happened as a number of "pulses" each with a distinct temperature. Typical distribution patterns for the Yucca Mountain T_h s are shown in Figure 3-6-3.

Homogenization temperatures shown in Figure 3-6-3-*a* through -*c* have unimodal distributions. The calcite in these samples likely formed through a single event in which waters with elevated temperature played a role. Histograms in Figure 3-6-3-*d* and -*e* show two distinct thermal episodes.

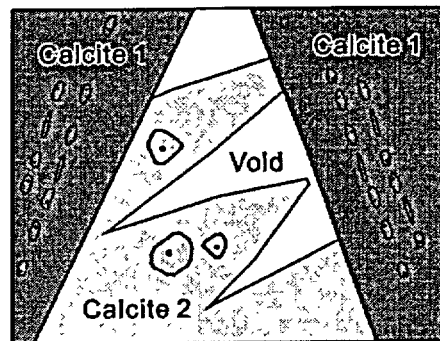
Another type of the T_h distribution is shown in Figure 3-6-3-*f* and -*g*. The sample for both (f) and (g), taken from station ESF 52+43, is composed of two distinct morphologic varieties of calcite. Older granular calcite (g) was formed at a temperature slightly higher than that for the late blocky calcite (f). In this case, gradual cooling of the mineral-forming fluid, rather than the presence of two temporarily distinct thermal episodes, appears more likely. Basal granular calcite also hosts secondary (or pseudo-secondary) inclusions with temperatures similar to the "coolest" part of the fluid, from which late blocky calcite crystallized. These secondary or pseudo-secondary inclusions yielded homogenization temperatures of 40-41 °C.

It should be noted that, in all samples, populations of all-liquid inclusions are present. These all-liquid inclusions may record one or several depositional events, but these events cannot be resolved by the fluid inclusion method alone.

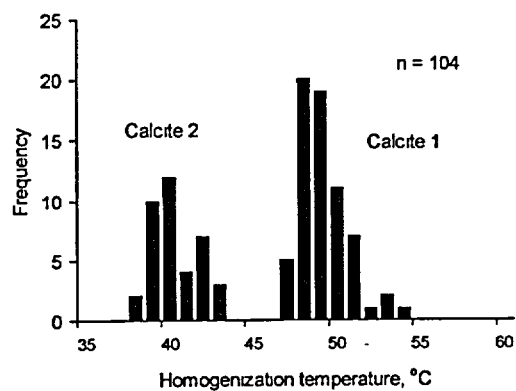
Sample shown in Figure 3-6-3-*d* is examined in a greater detail in Figure 3-6-4. This sample represents a 1.5 cm-thick crust, built up of blade-shaped calcite crystals, 0.3 to 3.0 mm in size. The crust contains irregular patches of co-genetic opal as well as fragments of bedrock tuff. Petrographic observations coupled with fluid inclusion studies reveal that the bulk of the crust most likely formed with a relatively rapid crystallization of calcite from an aqueous fluid with $T \cong 47$ to 54 °C. At some point in time, opal was deposited and became overgrown by bladed calcite. Fragments of bedrock tuff fell on the surface of the growing crust and became overgrown by it. Because of the fast growth, the crust acquired a porous character with a significant amount of free space left between adjacent irregularly oriented crystals. Later, cooler fluids ($T \cong 38$ to 43 °C) deposited calcite crystals in the interstices between the early calcite (see Figure 3-6-4-*b*). Similarly to the early calcite, the late calcite has bladed morphology.



a.



b.



c.

Figure 3-6-4. Mineral crust from the ESF station 12+81. *a* – Section view showing outlines of individual crystals (yellow), projections of vectors of the fastest growth directions (red arrows), segregations of opal and fragments of tuff embedded in calcite. *b* – Line-drawing showing interrelationships between the two generations of the 2-phase inclusion-bearing calcite present in sample (Calcite 1 corresponds to the bladed crystals shown in *a*; Calcite 2 crystals are too small to be seen on the photograph). *c* – Fluid inclusion data: Calcite 1 crystallized at $T \cong 48-55$ and Calcite 2 at $\cong 38-44$. Calcite 2 – at $T \cong 39-44$ °C. Separate fluid inclusion analyses performed on the basal, intermediate and outer parts of the crust produced bi-modal distributions similar to those shown in *c*.

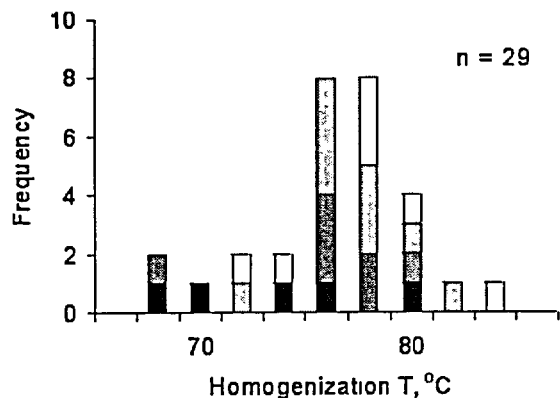


Figure 3-4-5. Homogenization temperatures measured in fluorite (station ESF 05+57). Different FIAs are shown as shades of gray.

3.6.4.2. Fluorite and quartz

Fluorite from the Yucca Mountain vadose zone also contains two-phase fluid inclusions that are suitable for thermometric analyses. These inclusions have more or less equilibrated shapes, consistent V:L ratios, and commonly occur in the form of three-dimensional clusters (FIA's). An example of the T_h s distribution in fluorite is shown in Figure 3-6-5.

This sample was collected from a sub-vertical zone of crushed tuff, which locally contains unfilled

voids. Within this zone, a wedge-shaped tuff fragment has been found to be coated by minerals of the silica assemblage. Chalcedony, quartz and fluorite occur on both hanging- and footwalls. On a microscopic scale, the sample represents a complex crust composed of rhythmic alternation of fluorite and quartz+chalcedony layers. The latest chalcedony layer is overgrown by calcite.

Two-phase inclusions in quartz are extremely rare in the Yucca Mountain samples. One sample was collected from a vertical fracture in the crystal-rich non-lithophysal Topopah Spring tuff at station ESF 12+12.5. This sample belongs to the silica assemblage and represents a crust composed of opal, chalcedony and quartz with accessory fluorite. The opal-chalcedony groundmass contains voids which host white translucent cubic crystals of fluorite. The silica assemblage is overgrown by a thick crust of blocky calcite (the carbonate assemblage). Overall the crystallization sequence is: opal – chalcedony – fluorite – quartz – calcite.

A grouping of 4 small (less than 8 μm) inclusions with nearly isometric shapes was found in one of the quartz crystals. Of the four inclusions only one contained a vapor bubble. This inclusion yielded a homogenization temperature of 59°C. Other inclusions in this FIA did not contain bubbles, which reflect, most probably, metastability (failure to nucleate a bubble) resulting from the low entrapment temperature compounded by small size of the inclusions. Inclusions in quartz are much less susceptible to stretching or leakage than those in calcite; therefore it is unlikely that the measured homogenization temperature reflects a post-entrapment alteration of the inclusion volume.

3.6.4.3. Summary of the thermometric data

As of now, crystalline calcite species, from the ESF, are associated with extensive thermometric record. This record consists of thousands of measurements of the homogenization temperature obtained

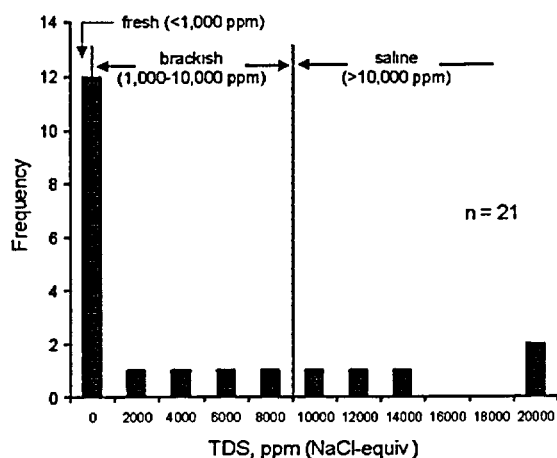


Figure 3-4-6. Salinities of waters trapped in the liquid-vapor inclusions in calcite from ESF (plotted by data of Dublyansky et al., 2001). The waters may be classified as fresh, brackish, and saline, according to Davis and De Wiest (1966).

from several tens of the specimens by three different research teams, which represent the State of Nevada and the Russian Academy of Sciences (Dublyansky and Reutsky, 1995; Dublyansky 1998; 2001; and Dublyansky et al. 2001), U.S. DOE's Yucca Mountain Project and U.S. Geological Survey (Whelan et al. 2000; 2001) and the University of Nevada, Las Vegas (Wilson et al, 2000 and Wilson and Cline, 2001).

By contrast, the record representing the silica minerals is extremely scarce. The homogenization temperature, which has been reported above, is the first and likely the only paleo-temperature datum

obtained from a quartz specimen representing the interior of Yucca Mountain. A 59 °C homogenization temperature, which has been obtained from a quartz specimen at station ESF 12+12.5, is consistent with homogenization temperatures (~35 to 85 °C) representing the calcite specimens. This temperature is not consistent, however, with homogenization temperatures that have been reported from quartz specimens at the ground surface near Yucca Mountain (i.e., 145 °C in Vaniman et al., 1984, and 118 to 195 °C in Harmon, 1993). The discord suggests that Yucca Mountain hosts, at least, two different generations of quartz, possibly, representing two distinct episodes of deposition of the secondary minerals.

Homogenization temperatures, which have been derived from the quartz and fluorite specimens, are generally consistent with those from the calcite specimens. This consistency suggests that the two major assemblages found in the Yucca Mountain vadose zone, the silica and carbonate assemblages, were formed by fluids that had similar temperatures. This and the mineralogical data discussed in Chapter 3-3, in turn, strongly suggest that the both assemblages may have formed through chemical evolution of the same fluid, rather than through incursions of fluids having differing chemistries.

3.6.4.4. Salinity of the mineral-forming fluids

Data on salinity of mineral-forming fluids at Yucca Mountain are scarce. Some 21 measurements of the freezing depression temperatures were reported by Dublyansky (1998) and Dublyansky et al. (2001). The salinity, calculated from these data ranged from ~0 to 21,500 ppm NaCl equivalent, as shown in Figure 3-6-6.

The figure shows that the entrapped fluids belong to three broad hydrogeological categories: fresh, brackish and saline waters, with fresh and slightly brackish being the dominant type. Other researchers

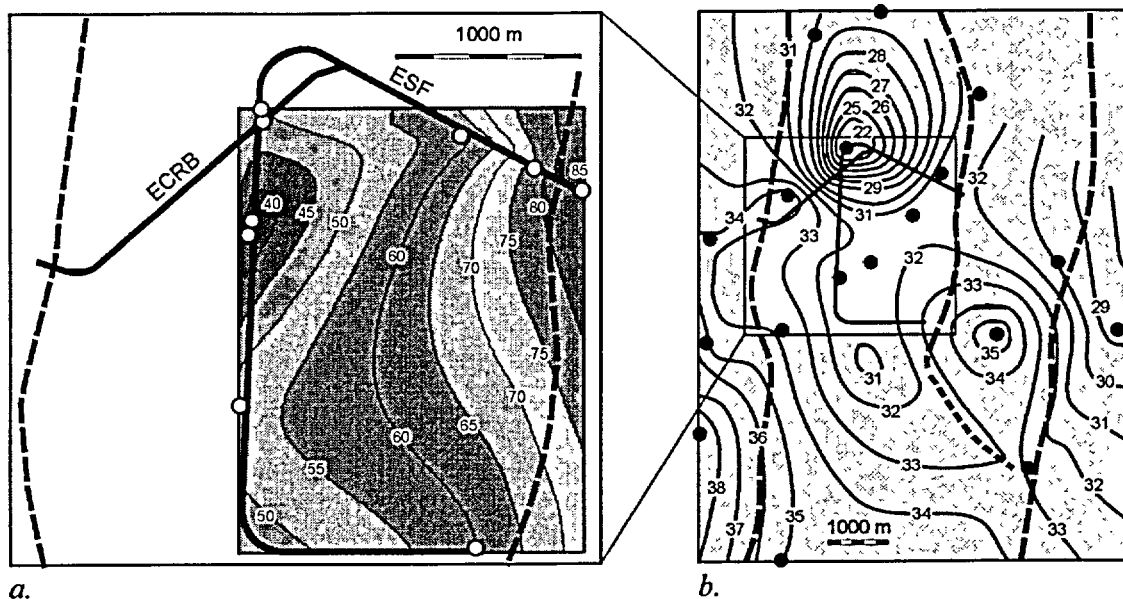


Figure 3-6-7. Structural similarity in paleo- and modern temperature fields in the Yucca Mountain area. *a* - Reconstructed field of maximum paleo temperatures (°C) in the ESF area, by fluid inclusions. White circles indicate locations of samples (Dublyansky et al., 2001 and Dublyansky, 2001). Note that the temperatures of fluids in eastern part of the repository block were substantially higher than in its central part. *b* - Present-day temperatures at the water table (°C) in the vicinity of the proposed repository (based on data of Sass et al., 1987). Boreholes are shown as filled circles. Note two maxima indicating hydrothermal circulation along the horst-bounding fault zones. Dashed lines indicate faults: Solitario Canyon (west), Bow Ridge (middle), and Paintbrush (east). Graphical interpolation was done with *Machcad PLUS 6 0* software.

obtained similar results. For example, Wilson et al. (2000) reported that the salinity ranges from 0.9 to 1.9 wt. %, which corresponds to 900 to 19,000 ppm NaCl equivalent, respectively.

3.6.4.5. Spatial distribution of the fluid inclusion homogenization temperature in the ESF

Even at early stages of the fluid inclusion research at Yucca Mountain (see Dublyansky, 1998-a), it has been recognized that the homogenization temperatures are highest near the north and south portals, and that they gradually decrease to the west. This important pattern has been later confirmed in the course of the UNLV "Yucca Mountain Thermochronology Project" and parallel USGS studies. It is shown in Figure 3-6-7-a, wherein the maximum homogenization temperatures have been recalculated, by the means of *Machcad 6.0 PLUS* software, to depict the paleo-geothermal field. The figure, therefore, depicts the highest fluid temperatures that were present in the ESF block at a time of deposition of the secondary minerals.

The figure shows that the depositional temperatures decrease systematically from the east to the west, with the lateral gradient being $dT/dx,y \cong 25^{\circ}\text{C}\cdot\text{km}^{-1}$. We interpret this gradient as expressing a

genetic linkage between the secondary minerals and the horst-bounding Paintbrush fault, including the Bow Ridge fault.

Importantly, the observed westward decline of the maximum depositional temperature is also reflected by the systematic change of composition of the secondary minerals. Silica assemblage is the most abundant near the north and south portals where the depositional temperatures are highest, whereas carbonate assemblage dominates in the western ESF, where the depositional temperatures are lowest (see Figures 3-4-13 and 3-4-14 in Chapter 3-4). The controlling role of the eastern horst-bounding fault zone is further emphasized by the fact, that, near the north portal (between ESF stations 0+00 and 16+08), silica minerals (quartz) but also rarely calcite occur on both floors and ceilings of lithophysal cavities, which is in contrast to the western ESF wherein the minerals are restricted to floors of the cavities.

From the hydrological perspective, the preceding interpretation seems to be both logical and non-equivocal. In particular this is true because the controlling influence of the Paintbrush fault zone is also indicated by both the present-day distribution of temperature at the water table and the distribution of contemporary heat flow, as respectively shown in Figures 1-21 and 1-28 (Part One) and 3-6-7-b.

Although the lateral paleo-geothermal gradient (see Figure 3-6-7-a) and the similarity between this gradient and the contemporary lateral geothermal gradient (see Figure 1-31) are both striking and revealing, the proponents of the rainwater hypothesis either ignore these important trends or construct nonsensical explanations for them. In this regard, the position of the USGS researchers is that the highest homogenization temperatures near the north and south ESF portals, for example, express a “stratigraphic control” of the paleo-*in situ* temperature (Whelan, pers. comm., 2000 and 2001). No reasonable explanation has been offered, however, as to why the stratigraphically higher Tiva Canyon tuff (which contains the north ESF portal and is situated nearer to the land surface) would host those secondary minerals that yield the highest homogenization temperatures.

Alternatively, the USGS researchers (see Whelan et al., 2001) speculate that the highest temperature (85-89 °C) yielding calcite (specifically the specimen from the ESF station 1+62.3) expresses deuteric fumarolic alteration, which affected the tuffs in-between the ESF stations 10+25 and 10+45 in late Miocene. Here again, no reasonable explanation has been offered as to why the fumarolic activity would be expressed at a location (station 1+62.3) some 860-880 m to the east of the alteration center without being expressed elsewhere closer to the center. Also, the purported fumarolic activity fails to explain the systematic eastward increase of the homogenization temperatures, which is also observed near the south ESF portal wherein the fumarolic alteration is absent; nor this activity explains the observed systematic change in mineralogy of the secondary minerals, from the quartz-dominated assemblage (to the east of the alteration center) to the one dominated by calcite (to the west of this center). Furthermore, the calcite-

bearing deposit at the ESF station 1+62.3 is indistinguishable in terms of its mineralogy (calcite + accessory fluorite and zeolite) and textures (translucent blocky calcite lining and cementing broken fragments of tuff in near-vertical fractures) from many other deposits occurring throughout the ESF.

3.6.5. Interpretation of the thermometric data

In a classic paper "Thermal waters of volcanic origin" Donald White introduced the following definitions:

Thermal Spring. G.K. Gilbert (1875, p. 149) considered springs thermal if their temperatures were higher than 10°F above the mean annual temperature of the area. A temperature significantly above the mean annual temperature of the region generally characterizes springs as thermal. For the characterization, 5°C to 10°F is considered significant.

Hydrothermal. Any water that is appreciably warmer (5°C or more) than the surrounding environment is considered hydrothermal. According to Holmes (1928, p. 121) the term refers to "*magmatic emanations rich in water*". The same view is held by many geologists, but this was clearly not the intent of Morey and Niggli, (1913, p. 186-188), who first brought the term into popular use. It should refer to any water that is warm or hot relative to its surrounding environment, and it should have no genetic implications. (White, 1957, p. 1638; emphasis added).

A somewhat more conservative criterion, for distinguishing thermal waters from non-thermal waters, has been recently adopted by the Nevada Bureau of Mines and Geology for the purposes of assessing geothermal resources of the State of Nevada. In accordance with this criterion (see Garside, 1994), geothermal or low-temperature hydrothermal spring-waters are those whose temperature is 10°C above the mean annual temperature.

Figure 3-6-8 is a histogram showing frequency of occurrence of geothermal spring-waters in Nevada as a function of their temperature. Range of the homogenization temperatures from the ESF secondary minerals and range of the depositional temperatures, which is implied by the complete absence of two-phase liquid-vapor FIAs are also shown for purposes of the comparison.

The figure shows that parental fluids of the ESF secondary minerals had unambiguously thermal character. In addition, the figure emphasizes that, based solely on the fact that minerals are completely devoid of the two-phase FIA's, it is not possible to ascertain whether or not their parental fluid have had a thermal character.

Prior to presenting our interpretation of the ESF thermometric data, we wish to evaluate merits of the two interpretations, which recently have been advanced by other researchers involved in fluid

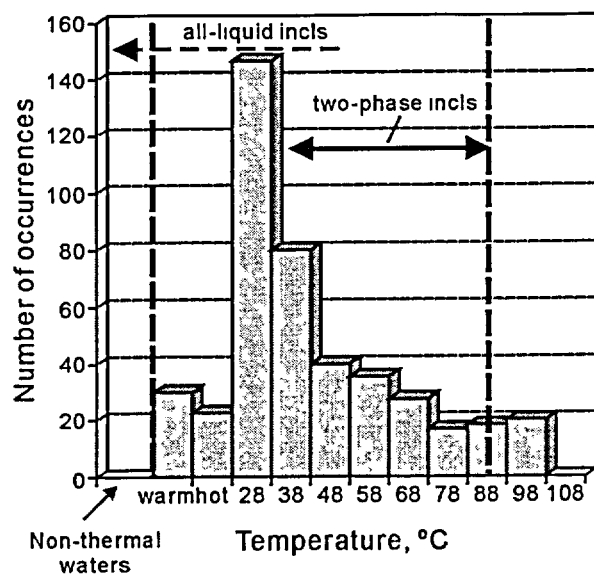


Figure 3-6-8. Temperatures of the low-temperature geothermal occurrences in Nevada (by Garside, 1994) compared with the fluid inclusion temperatures obtained from the ESF minerals. *Solid arrow* – interval of measured homogenization temperatures; *dashed arrow* – temperatures, suggested by all-liquid inclusions.

Note that all fluid inclusion data are from shallow depths (30 to 300 m), which means that the increase of the temperature due to the "normal" conductive geothermal gradient is small (maximum, 10°C).

inclusion studies of the ESF secondary minerals (Wilson et al., 2000; Wilson and Cline, 2001; and Whelan et al., 2000 and 2001). The contentious issues are: (1) UNLV and USGS/U.S. DOE interpretation of a thermometric significance of the all-liquid inclusions and (2) USGS interpretation of a genetic significance of the two-phase liquid-vapor inclusions with variable vapor-to-liquid ratios. Both of these interpretations constitute a foundation upon which the concept envisaging rainwater infiltrating through the warm (cooling) mountain and depositing the secondary minerals has been constructed. Below we will demonstrate that these interpretations are devoid of scientific merits, which makes the whole concept unacceptable to us.

3.6.5.1. UNLV and U.S. DOE interpretation of a thermometric significance of the all-liquid inclusions

The UNLV researchers observed that the latest calcite, which is associated with a characteristic oscillatory zoning involving fine alternating layers of Mg-enriched and Mg-depleted calcite, is totally devoid of the two-phase fluid inclusions. In this regard, they concluded: "...*FIA's with 2-phase fluid inclusions are not present in outermost Mg-enriched calcite that begun precipitating in the LCZ [lithophysal cavity zone in the ESF] between 3.8 and 1.9 Ma*", (Wilson et al., 2000). These observations led the authors to further conclude: "*Therefore, passage of fluids with elevated temperatures in this part of the repository site occurred prior to 1.9 Ma*" (Wilson et al., 2000; emphasis added) and later "*These results indicate that fluids with elevated temperatures were not present in the recent past (i.e., < 1.5 Ma), but moved through the site more than 1.9 to ~2.8 Ma*" (Wilson and Cline, 2001; emphasis added). We regard these conclusions as ambiguous, because they contain a vague (undefined) phrase "*fluids with elevated temperatures*".

The preceding ambiguous conclusions were stretched further by the U.S. DOE researchers. In their Yucca Mountain Science and Engineering Report – Technical Information Supporting Site Recommendation Consideration they conclude: “...*this calcite lacks two-phase inclusions, thereby indicating precipitation at ambient temperatures (Wilson, Cline, and Amelin 2001)* (U.S. DOE, 2001, p. 4-402; emphasis added). This conclusion is not ambiguous, but it is erroneous. Below, we attempt to justify this statement and, to this end, the following two issues are considered.

The first issue is: what can be inferred about a temperature of the parent fluid if only all-liquid inclusions are present in the daughter mineral? In this regard, Goldstein and Reynolds (1994) recommend: “*Upon identification of all-liquid aqueous fluid inclusions, one must determine their significance as records of low entrapment temperature. ... Their usefulness as records of low temperature can only be established if other mechanisms of all-liquid inclusion formation can be ruled out.*” (p. 78, emphasis added).

The nucleation of the vapor bubbles upon cooling is controlled by a number of factors, such as difference between the entrapment temperature and the present-day temperature, size of the inclusions and their composition, the presence of dissolved gases and particulate matter, etc. Roedder (1984), for example, noted that among aqueous inclusions, which were trapped at a temperature of less than about 100 °C, many do not nucleate shrinkage bubble upon cooling to room temperature, and that such inclusions may remain in the metastable all-liquid state for millions of years. In applied fluid inclusion research, it is assumed that: “...*the presence of all-liquid fluid inclusions, that are in the same size range as two-phase inclusions, suggests that the all-liquid fluid inclusions were trapped at a temperature below about 50°C.*” (Goldstein, 2001, p. 166).

The UNLV researchers (Cline, 2001, pers. com.) consider that, because the lowest homogenization temperature actually measured in specimens of the ESF calcite is about 35 °C, the sole presence of all-liquid inclusions in a mineral indicates that this mineral was formed at a temperature of less than about 35 °C. We fail to see the logic that justifies this point of view. For example, it is commonly observed at Yucca Mountain and elsewhere that the FIA’s containing two-phase inclusions also contain numerous monophase all-liquid inclusions. In this regard, Whelan et al. (2001) noted that, in various FIA’s, the two-phase variety comprises between less than 10 and nearly 100 % of the total fluid inclusion population. If the UNLV logic were applied to such FIA’s then an erroneous conclusion would be drawn that these FIA’s (by definition formed at the same time), trapped fluids with two different temperatures, one ranging from 35 to 85 °C and the other less than 35 °C.

In summary, the sole presence of monophase all-liquid inclusions can only be taken to indicate that the host calcite specimen was formed at a temperature of less than approximately 35-50 °C, but how much

less cannot be specified with any degree of certainty. This does not mean, of course, that calcite specimens that are devoid of two-phase inclusions must have been formed at “ambient temperatures”, which at the level of the ESF do not exceed 25 °C.

The second issue is: what can be inferred about an origin (i.e., geothermal or otherwise) of a shallow (less than say 250 m) fluid if all that is known about it is that its temperature was less than approximately 35-50 °C? Simple calculation demonstrates that even the 35-50 °C-temperature range, which, in the case of all-liquid inclusions, cannot be resolved by the fluid inclusion method, may indicate the presence of geothermal waters provided, of course, they occur at a shallow depth. For example, a calcite specimen deposited at a depth of 50 m and at a temperature of 35 °C would indicate heat flow as high as about 16 HFU, which is possible but only in a hydrothermal setting.

It thus appears that the sole presence of monophasic all-liquid inclusions in specimens of the Mg-enriched calcite is telling us no more but that this calcite has been precipitated either under the ambient temperature or under a somewhat (by up to 15-30 °C) higher temperature. Figure 3-6-8 illustrates this ambiguity quite well and, in addition, emphasizes that the 20-50 °C range falls in a “gray area” within which the fluid inclusion thermometry does not allow for unequivocally establishing whether or not the corresponding minerals are of a thermal origin.

In summary, the sole presence of monophasic all-liquid inclusion is not sufficient for unequivocally establishing that the latest Mg-enriched calcite at Yucca Mountain precipitated under a temperature similar to the present-day ambient temperature. Therefore, the conclusion (Wilson et al., 2000; Wilson and Cline, 2001; U.S. DOE, 2001) regarding a non-thermal character of fluids, which resided in the interior of Yucca Mountain during deposition of the latest Mg-enriched calcite, does not withstand scientific scrutiny and must be rejected.

3.6.5.2. USGS interpretation of a genetic significance of two-phase liquid-vapor inclusions with variable vapor-to-liquid ratios

Some specimens of the ESF calcite contain two-phase liquid-vapor inclusions, within which the vapor-to-liquid ratios lack consistency and are sometimes quite large. The USGS researchers consider such inclusions as indicative of a supergene origin of parent fluids for the host calcite. Specifically, they regard them (inclusions) as being a result of the heterogeneous entrapment of infiltrating rainwater and air and thus indicative of the mineral deposition in a vadose environment. In this regard, Whelan et al. (2000) reasoned: “Assuming that the type 2 and 3 FI’s [all-vapor inclusions and inclusions with large and variable V/L ratio, respectively] record vadose zone heterogeneous trapping, the observed FI assemblages are inconsistent with phreatic conditions.”

The preceding quotation is a good example of circular reasoning, wherein the authors assume that the inclusions were entrapped in a vadose environment, based on which they conclude that these inclusions were not formed in a phreatic environment. Putting aside the unacceptable circular logic, an attempt to infer an environment of deposition (vadose or otherwise) of a mineral specimen, based solely on the fact that it contains the subject inclusions, is an exercise in futility. This is because two-phase inclusions with variable V/L ratios express a number of processes, such as heterogeneous entrapment, necking-down, stretching and re-equilibration, and leakage.

The heterogeneous entrapment, or entrapment of co-existing aqueous and gaseous phases, may occur in a phreatic environment as well as in a vadose environment. In the former the entrapment expresses either boiling of the fluid or its effervescence, whereas in the latter it is a result of entrapping of water together with bubbles of air. The necking-down, or splitting of a single large vacuole into two or more smaller ones after nucleation of the shrinkage bubble, may produce two-phase inclusions with variable L/V ratios. Such inclusions may also be a result of the stretching, with or without a partial opening of pre-existing inclusions and the resulting leakage. Often the stretching is accompanied by thermal re-equilibration of the inclusions. For example, if a low-temperature mineral, which contains all-liquid inclusions, is introduced into a higher temperature environment, such as during burial or magmatic intrusion, some of the inclusions may stretch and re-equilibrate with the new environment. Inclusions may also be mechanically damaged as a result of tectonic deformation. Similar effects may be produced by the accidental overheating during sample collection and transport or during preparation of the doubly polished wafers for fluid inclusion studies. Inclusions hosted by cleavable minerals, calcite for example, are particularly susceptible to mechanical and thermal damage.

Whilst evaluating the origin of two-phase liquid-vapor inclusions with variable vapor-to-liquid ratios, it is extremely difficult or downright impossible, in most cases, to identify a process that is being expressed by them. Because of this insurmountable ambiguity, these inclusions are usually ignored in fluid inclusion studies, unless they display some additional features that would allow for determination of their origin.

Typically, minerals formed in a vadose environment are characterized by the presence of all-liquid and liquid-vapor inclusions with highly variable V:L ratios, which expresses the entrapment of random amounts of liquid and air (Goldstein and Reynolds, 1994). Partial losses of the entrapped fluid are also common (Schwartz et al., 1976). A characteristic feature of calcite deposited in a vadose environment is the presence of inclusion-rich layers, within which elongation of the vacuoles is parallel to c-axis of the host crystal. Kendall and Broughton (1978, p.526) noted that inclusions trapped in the vadose-zone carbonate cements typically exhibit "*...marked growth anisotropism because they are thorn-shaped, with*

abrupt constrictions, bulbous origins and taper to fine points in the direction of growth of the host carbonate crystal. A complete gradation apparently exists between this type and the more common small, linear spindle-shaped inclusions.” Importantly, none of these diagnostic features has been observed in association with the ESF secondary minerals. In addition, chemistry of gases that are entrapped in these minerals (see section 3.5.6.5) is characterized by high abundance of methane and carbon dioxide with virtual absence of oxygen, which precludes the entrapment in a vadose environment.

In summary, the presence of two-phase liquid-vapor inclusions with variable V:L ratios alone cannot be regarded as an unequivocal evidence for a vadose environment of deposition of the ESF secondary minerals. The USGS/U.S. DOE conclusion in that regard (Whelan et al., 2000 and U.S. DOE, 2001) lacks a proper foundation.

3.6.5.3. Heat flow indicated by the paleo-thermometric data

Because water has a very high heat capacity, it plays important role in the dissipation of heat in the Earth’s crust, and hydrologists have long recognized it. In this regard, Sass (1998) remarked “...*careful measurements of temperature and heat flow can provide important constrains on hydrologic models.*” Fluid inclusion thermometry allows for applying this concept to studies of fossil hydrologic systems.

Data that are required for reconstruction of heat flow at Yucca Mountain in the past include: temperatures of parent fluids for the ESF secondary minerals, depth at which these minerals occur, and thermal conductivity of the host tuffs. Temperature of the parent fluids can be inferred based on the fluid inclusion homogenization temperatures. Erosion at Yucca Mountain is believed to be insignificant, of the order of 0.1 to 1.1 cm per thousand years (U.S. DOE, 1998). Reconstructed values of the paleo-geothermal gradient (dT/dz), therefore, can be bounded by the values calculated using present-day depths to the fluid inclusion samples (upper bound) and the values calculated using the depths that are approximately 100 m greater than those at the present-day (lower bound), which presumes the most intense erosion rates (1.1 cm per thousand years) operating over the past 9-10 Ma. Values of the thermal conductivity are given in Sass et al. (1987).

Spatial distribution of the highest homogenization temperatures in the ESF block is shown in Figure 3-6-7 above. We regard the westward systematic decrease of the homogenization temperatures, which is apparent in this figure, as expressing a cause-effect relationship between the Paintbrush heat-dominated dissipative structure (cause) and the ESF secondary minerals, as the proposed conceptual model implies. In addition, we regard “smoothness” of the east-west lateral paleo-geothermal gradient, which is shown in Figure 3-6-7, as an evidence for a broadly contemporaneous entrapment of the corresponding fluid inclusions.

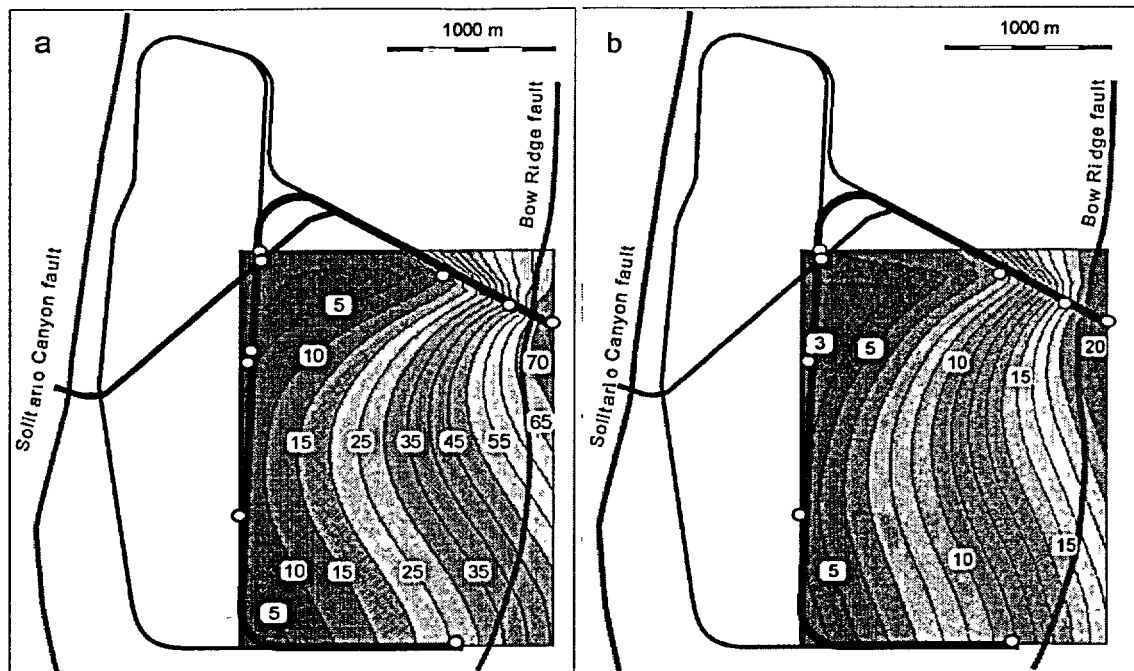


Figure 3-6-9. Paleo-heat flow at Yucca Mountain by fluid inclusions. *a* – paleo heat flow (in HFU) calculated using modern-day topography (i.e., no erosion); *b* – paleo heat flow calculated assuming additional uniform 100 m-thick overburden. Fluid inclusion data for calculations were taken from Dublyansky et al. (2001). Calculations of the paleo heat flow are based on the known depth of the sample location (thermal gradient is assumed to be linear). Average thermal conductivity of the Yucca Mountain tuffs is assumed to be $1.74 \text{ W}\cdot\text{m}^{-1}\cdot\text{K}^{-1}$ (Sass et al., 1987), and mean temperature at the ground surface 15°C . Graphical interpolation was done with *Mathcad PLUS 6 0* software.

We reconstructed the spatial distribution of heat flow in the ESF block at a time when the fluid temperature, which was inferred based on the homogenization temperatures, was at its maximum. This reconstruction has been made based on two assumptions. The first is that those of the ESF calcite specimens, which yielded the highest homogenization temperatures, were deposited at approximately the same time. The second assumption (conservative) is that transport of heat through a section of tuff, which is situated between the specimen sampling sites and the ground surface, involved only conduction. In addition, two cases were considered in reconstructing the paleo heat flow. The first case involves assuming that the specimens (which yielded the highest homogenization temperatures) were formed at the same depth (below the ground surface) as they occur today, which implies either negligible erosion or very young age of the specimens. The second case is most conservative because it has been constructed assuming that the erosion rate was at its maximum (about 1 cm per thousand years) and that the homogenization temperatures were derived from about 10 Ma-old specimens, which implies that a section of tuff about 100 m thick was removed by erosion. Both of the reconstructed cases are shown in Figure 3-6-9.

The figure shows that the reconstructed intensities of heat flow are very high, particularly in northeast part of the ESF block where they reach between 20 and 70 HFU (compare with the range of 0.5 to 3.0 HFU representing the variability of conductive heat flow in the continents). Nevertheless, the reconstructed intensities are similar to those that are observed in association with active geothermal fields. For example, heat flow in Yellowstone Park may reach intensities as high as 30 HFU, and in the northern Nevada there are "...hydrothermal convection systems where q locally exceeds 1000 mW m^{-2} , [= 24 HFU] many of which support geothermal power plants and non-electrical geothermal applications." (Sass, 1999).

Another noteworthy feature of the heat flow field, which is shown in Figure 3-6-9, is a strong lateral gradient of the reconstructed intensities of heat flow. Magnitudes of this gradient are very large ranging from $dq/dx = 40 \text{ HFU}\cdot\text{km}^{-1}$, for the case of unchanged depth of the overburden, to $dq/dx = 10 \text{ HFU}\cdot\text{km}^{-1}$, for the case of a hypothetical removal of the 100-m thick overburden section. For comparison, magnitude of the corresponding present-day gradient is only about $0.4 \text{ HFU}\cdot\text{km}^{-1}$.

The reconstructed structure of the paleo-heat flow field implies the past presence of a linear heat source along eastern margin of the ESF block. This heat source have had intensity in excess of approximately 20-70 HFU, it seems to have been elongated in an approximately north-south direction, and it could have been operating within the Paintbrush fault zone. These inferences, in turn, entail the following three implications.

First, neither the reconstructed intensities of heat flow (q) nor the reconstructed lateral gradient (dq/dx) could have been maintained near the Earth's surface for time spans measured in term of millions of years. This implies a fairly short life span for the heat source. Even over time spans measured in terms of hundreds or thousands of years, the reconstructed intensities of heat flow and the resulting magnitude of the lateral gradient could have been maintained but only through a continuous and localized supply of heat into the system.

Second, the reconstructed structure of the heat flow field, which is characterized by north-south trending isothermal lines and east-west oriented lateral geothermal gradient, cannot be accounted for by a model which calls for involvement of the cooling Timber Mountain magma chamber, located in 7-10 km to the north of Yucca Mountain, as a heat source. If such were the case, east-west trending isothermal lines, and a north-south oriented lateral geothermal gradient, would be expected. The expected (i.e., north-south oriented) lateral geothermal gradient is, in fact, expressed at Yucca Mountain in the deep-seated sections of tuffs in the form of Timber Mountain montmorillonitic alteration. In this regard, Bish and Aronson reported: "... it is apparent that a significant thermal event has occurred in the northern end of

Yucca Mountain but has not significantly affected the southern end." (p.153). This north-south oriented lateral geothermal gradient, however, is absent from the ESF thermometric data.

Third, the reconstructed structure of the heat flow field points out towards the Paintbrush fault zone as a structure which, in the past, has controlled flow of heat through the ESF block. Importantly, the present-day distribution of temperature and heat flow inside and through Yucca Mountain also points out towards the controlling role of fault structures, including the Paintbrush fault zone. Most researchers attribute the observed temperature and heat flow distribution patterns (see Figures 1-28 in Part One and 3-6-7-b) to upwelling of hot water along the fault-based enhanced conductivity channels. Sass et al. (1983) concluded that the Paintbrush thermal anomaly expresses "*a complex hydrothermal circulation system*". Bredehoeft (1997) provided the following description of the temperature distribution pattern: "*The higher water temperatures are associated with the series of faults in Midway Valley: Paintbrush and Bow Ridge faults. The Solitario Canyon fault to the west of Yucca Mountain also has a higher temperature anomaly associated with it. There is a temperature low directly beneath Yucca Mountain.*" (p.2462). In regard to the phenomenology involved, Lehman and Brown (1995) noted: "*The temperature distributions suggest localized recharge or an area of relatively high permeability along strike of the Ghost Dance Fault and a thermal hot spot along the western flank of Yucca Mountain. This information may indicate that faults serve as pathways for both cool water from the surface as well as warm water upwelling from depth.*"

We conclude, therefore, that the Paintbrush fault zone served, in the past, as it continues to serve today, as a pathway for hot waters. The difference indicated by the fluid inclusion record from the ESF secondary minerals is that in the past the zone may have hosted larger-amplitude upwellings, resulted in incursions of hot waters into what is now the vadose zone.

3.6.6. Gases in inclusions hosted by the ESF secondary minerals

The chemical composition of gases trapped in fluid inclusions can provide valuable information regarding the origin of fluids trapped in the inclusions and the crystal growth environment. It is typical of the minerals formed in the near-surface environment that the amount of gases trapped in inclusions are so tiny that the chemistry of these fluids cannot be analyzed on an individual inclusion basis. Analyses may become possible only when gases from many inclusions are released. The obvious shortcoming of the bulk-analysis approach is that the contents of inclusions trapped at different times and, possibly, hosting different fluids, are mixed in unknown proportions but lumped together for analysis.

More complications may be caused by the methods of gas release from the inclusions. Two methods are used in fluid inclusion research: thermal decrepitation and mechanical crushing. The thermal

decrepitation involves heating of the sample, which leads to an increase in the internal pressure in the inclusion vacuoles. At a certain temperature, the internal pressure exceeds the mechanical strength of the host mineral and the inclusions "explode" – decrepitate. This method has a number of disadvantages: - it is ineffective in releasing the contents of low-density gaseous inclusions (the pressure in such inclusions increases little with increasing temperature); - elevated temperatures further reactions between gases, so that the gas composition of the mixture changes; - heating may affect organic matter contained in the mineral and generate gases that have nothing to do with fluid trapped in the inclusions.

The second method employs a mechanical crushing of the sample either in a vacuum or in the continuous flow of a gas-carrier. While this method is free of the problems mentioned above, it has an inherent disadvantage, however, because crushing increases the specific surface of the sample, which in turn increases the sorption of gases on the "fresh" mineral surface. Since the sorptive properties of gases differ, the gas transferred from crusher to the analytical equipment may also be altered relative to its original composition.

3.6.6.1. Results of Quadrupole mass spectrometric analyses of the entrapped gases at Yucca Mountain

As of now, little information on the bulk composition of gases trapped in inclusions from Yucca Mountain minerals is available. In addition, some of the information was published in such an abbreviated form, that any evaluation of its reliability is difficult, if not impossible. For instance Roedder et al. (1994; p. 1859) reported the following: *"...we have obtained preliminary qualitative Quadrupole™ mass spectrometer analyses of the gases in the inclusions in these samples ... These analyses show that the gases are mixtures of nitrogen and oxygen (at near "air" ratios), CO₂, and methane."* No information was provided in the quoted paper regarding the method of gas extraction, amount of material analyzed, character of sample from which these data were obtained, etc. This is in striking contrast with the strong statement made by the senior author of the paper earlier: *"Although it might seem extreme, I believe that the possibilities of major errors in inclusion analyses are sufficiently numerous that one should simply discount all analytical reports that do not give details on sample size, and selection, cleaning, and extraction procedures used, as well as the usual statements of analytical methods, sensitivity, accuracy, precision, blanks, standardization, etc."* (Roedder, 1984, p. 110).

More disappointing, however, is the absence of the numeric data. General descriptive characteristics like *"major methane"* and *"nitrogen and oxygen at near "air" ratios"* are about all of the information on the composition of gases in the Yucca Mountain calcites that Roedder et al. (1994) made available. Since the "near air" N₂/O₂ ratios might be interpreted by some as evidence supporting the model of calcite deposition in the vadose setting from rainwater, we evaluate the true meaning of it in the discussion,

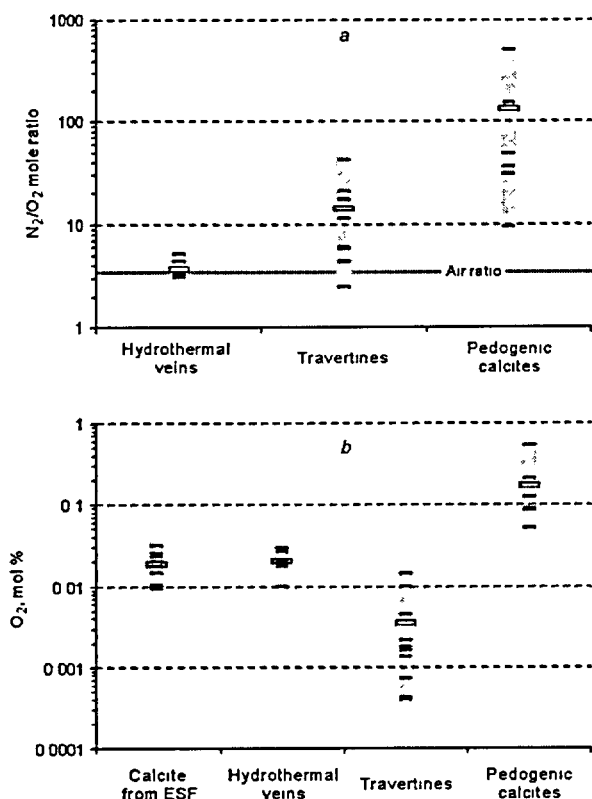


Figure 3-6-10. Chemistry of gases trapped in inclusions. *a* - N₂/O₂ mole ratios in samples from hydrothermal calcite veins, modern and ancient travertines, and pedogenic calcites compared with the atmospheric air ratio (3.3); *b* - contents of O₂ in calcite from ESF compared with contents in hydrothermal veins, travertines and pedogenic calcites from New Mexico.

Calcite from ESF: average O₂ = 0.019, σ = 0.008 (n = 8) (by Levy, 2001, pers. com.). Hydrothermal vein calcite: average N₂/O₂ = 3.7, σ = 0.8, O₂ = 0.0020, σ = 0.007 (n = 6); travertine: average N₂/O₂ = 13.8, σ = 11.6, O₂ = 0.0035, σ = 0.0045 (n = 11); and pedogenic calcite: average N₂/O₂ = 129.2, σ = 188.6, O₂ = 0.18, σ = 0.18 (n = 6) (by Newman et al., 1996). Average values are shown by horizontal bar. Note that (a) hydrothermal calcite gives the closest match to the atmospheric N₂/O₂ ratio and (b) O₂-contents in calcite from ESF give the closest match with the hydrothermal vein calcite.

which follows. Figure 3-6-10-*a* shows calculated N₂/O₂ ratios (Quadrupole MS) of gases trapped in calcites with different origins: hydrothermal vein, travertine and pedogenic (based on the data of Newman et al., 1996). It is apparent from the figure that of the three categories, hydrothermal calcite shows the closest match with the "air" N₂/O₂ mole ratio of 3.3, whereas all pedogenic carbonates yield substantially greater ratios (more than one order of magnitude).

It is to be noted that one genetic category of calcite relevant to the discussion is missing from this consideration. This is speleotemic or flowstone calcite that is formed in caves from water films percolating through the vadose zone. Conceivably, gases trapped in inclusions in such calcite would also show a N₂/O₂ ratio close to the "air" value. In the absence of the numeric data it would be prudent to conclude that the N₂/O₂ ratios reported by Roedder et al. (1994), for calcite specimens from the vadose zone at Yucca Mountain, can be interpreted as evidence, suggestive of or, at a minimum, perfectly compatible with the hydrothermal origin of the Yucca Mountain calcites.

Further corroboration of this conclusion comes from the data presented in Figure 3-6-10-*b*, which compares the contents of O₂ determined in two calcite samples from the ESF (Levy, 2001,

pers. com.) with the contents, measured in hydrothermal calcite veins, modern and ancient travertines and the vadose pedogenic calcites of New Mexico (data of Newman et al., 1996). It is apparent that the O₂-contents of the ESF calcites show an almost perfect match with the hydrothermal calcite and differ substantially (orders of magnitude) from both travertines and pedogenic calcites.

Levy et al. (1995) reported some numerical data on fluid inclusion gas chemistry for Yucca Mountain calcites obtained by Quadrupole mass spectrometry. The authors determined the contents of H₂O, CH₄, N₂, O₂, Ar, and CO₂ in three samples collected in the vicinity of the Bow Ridge Fault: *"Fluid inclusions from two samples of calcite closest to the fault in the ESF were analyzed. One is laminated deposit from a small fault in pre-Rainier Mesa bedded tuff 8 m west of the fault zone, and other is coarse sparry calcite from a fracture within breccia in the Tiva Canyon Tuff 38 m east of the fault. Pedogenic calcite from a fracture within the Bow Ridge fault in densely welded Tiva Canyon Tuff near the surface of Exile Hill was analyzed for comparison with the ESF calcites."*

The approach adopted whilst interpreting the data presented in the quoted paper involved comparison of chemistry of the gases entrapped in the Yucca Mountain samples with the chemistry of gases in calcite specimens from New Mexico whose origin (i.e., hydrothermal vein, travertine, and pedogenic) was presumed to be known. The rationale for adopting this approach was given as follows: *"Calcites formed under saturated conditions (e.g., hydrothermal veins and spring-deposited travertines) have H₂O-rich inclusions with a narrow range of N₂/Ar values, reflecting equilibrium with air, and either CO₂ or N₂ as the dominant inclusion gas. Pedogenic calcites have gas-rich (H₂O-poor) inclusions with high CH₄, and variable N₂/Ar ratios. The high CH₄ content is a by-product of anaerobic bacterial and fungal process in the soil zone."*

A major flaw of the Levy et al. rationale is that methane is uniquely attributed to the *"anaerobic bacterial and fungal processes in soil zone"*, so that the methane is considered as a "fingerprint" of the pedogenic environment. Arguably, such an attribution is groundless. Methane is intrinsically associated with many endogene processes, and thus it is a common constituent of the deep-seated ground waters, including those discharging from thermal springs. For example the textbook entitled "Principles of Hydrogeology" (1982; p.104-105) contains the following remark: *"Even if the content of organic matter in the rock is as low as 1-2 %, methane and other hydrocarbons are able to segregate into the free phase. If oxidizers (oxygen and sulfate-ion) are absent, methane becomes a dominant component in the gas phase. Therefore, groundwaters from the deep-seated horizons are preferentially methane-rich, even when the host rocks are poor in organic matter"*. In addition, methane is an ubiquitous component of fluids trapped in inclusions in a variety of minerals of different origins, from sedimentary to hydrothermal and metamorphic (see e.g., Carbon..., 1978). Finally, it has been demonstrated that soils in the Yucca Mountain area are, in fact, depleted in methane relative to the normal atmospheric air content of 1.7 ppmv: *"All soil gases sampled on and near Yucca Mountain show CH₄ concentrations that are depleted relative to the air, but still greater than 0.5 ppmv."* (Thorstenson et al., 1989. p. 22)

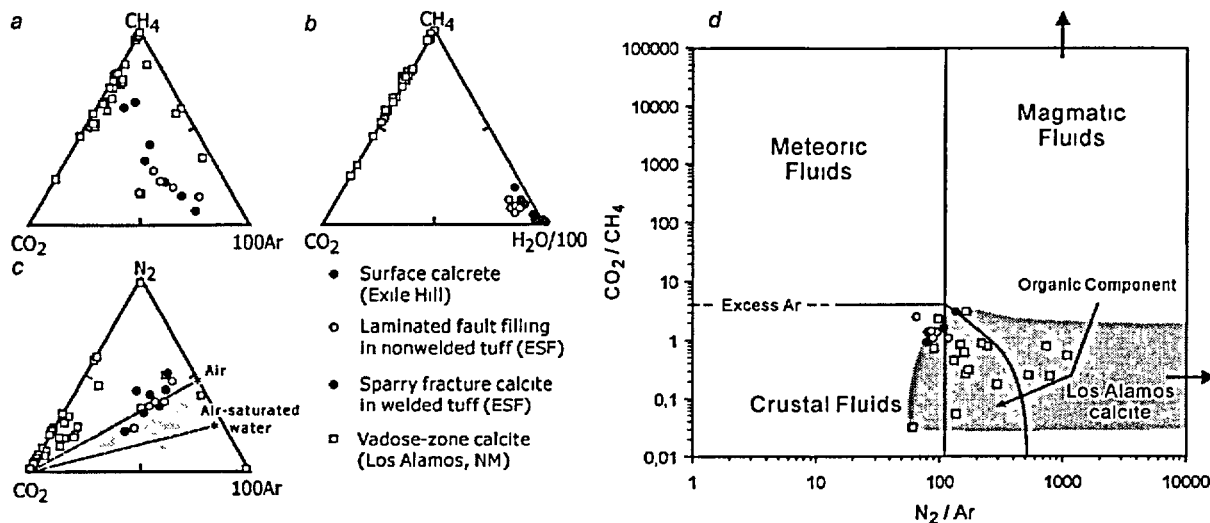


Figure 3-6-11. Comparison of the results of Quadrupole mass spectrometric analysis of surface calcrite and two calcite samples from the ESF (Levy et al., 1995) and of the pedogenic calcite fracture fillings from Los Alamos, New Mexico (Newman et al., 1997). Diagram *c* also shows typical values of gases trapped in inclusions in ancient and modern travertines (*gray field*, by Newman et al. 1996). Diagram *d* compares the Yucca Mountain and Los Alamos calcite data with the fields established for different types of terrestrial fluids. The boundaries of fields are by Norman and Moore (1999) as reported in Moore et al. (2001). Note that the gray field of the Los Alamos calcite must be extended to the right, because in 10 out of 28 samples no argon was detected by mass-spectrometric analysis (which results in the infinite N₂/Ar ratios).

The two samples from the ESF are NR-1-SSL (*red*) and NR-2-SSL (*yellow*) collected 38 m east and 8 m west of the Bow Ridge fault, approximately 40 m below land surface. The sample of the Yucca Mountain surface calcrite (identified in the original paper by Levy et al. (1995) as “pedogenic calcite”) is from a fracture within the Bow Ridge fault at Exile Hill.

The analytical results from Levy et al. (1995) are shown in Figure 3-6-11, where they are compared with the data from pedogenic carbonates from Los Alamos, New Mexico, as well as placed in the context of the gas chemistry determined in various types of terrestrial fluids, as given in Norman and Moore (1999).

The figure shows that the gases entrapped in the carbonates at Yucca Mountain, including those at the topographic surface as well as those in the ESF, differ significantly from the gases that are entrapped in the reference (pedogenic) carbonates from the Southwestern United States (Newman et al., 1996 and 1997). Relative to the latter, The Yucca Mountain calcites are significantly enriched in Ar, H₂O, and N₂. All of the considered carbonates, however, contain the entrapped gases that are broadly similar to those dissolved in crustal fluids, but in case of the reference pedogenic carbonates the N₂ abundance relative to the Ar abundance is noticeably increased, as shown in Figure 3-6-11-*d*.

Two additional observations can be made on the data shown in Figure 3-6-11. First, all of the Yucca Mountain samples yielded gases with CO₂-N₂-Ar ratios that fall near or within the field of ancient and contemporary travertine deposits, and with H₂O contents characteristic of the saturated-zone minerals.

According to Newman et al. (1996, p. 1790) "*Travertines and hydrothermal vein calcites have well constrained N_2/Ar ratios and plot between the boundaries defined by air and air-saturated water ... Gundimeda (1995) and Newman et al. (1996) showed that calcites with gas dominant inclusions have a vadose origin, while those with inclusions that contain over 98 mol% water form under saturated conditions.*"

Second, the high concentrations of CH_4 , in conjunction with the low concentrations of O_2 , indicate that the calcites were precipitated under reducing conditions (see e.g., Newman et al., 1996). Such low-Eh environment is not expected in the open fractures existing in a well-aerated vadose zone, such as the one at Yucca Mountain.

In spite the preceding considerations, Levy et al. (1995) keep insisting that origin of the Yucca Mountain carbonates is linked to rainwater, which resides at the topographic surface (surface calcretes) and descends through the vadose zone (sparry calcite in the ESF). Nevertheless, they do recognize some of the difference and state: "*Although the three samples are from the unsaturated zone, their fluid inclusions have water contents ≥ 99.2 mol % typical of saturated-zone calcite and much higher than the maximum of 86 % in pedogenic calcites from New Mexico...*". Notwithstanding this observation which, according to the authors' own rationale, contemplates a saturated environment for calcite deposition, they attempt to force-fit their results to a preconceived pedogenic origin for the calcite in question: "*In the drier climate of Yucca Mountain, calcite precipitation and recrystallization and carbonate transport may occur mostly when major meteoric recharge events create transient saturated conditions in the shallow subsurface. This may be especially true for pedogenic calcite within fractures in densely welded rock because the low-permeability fracture walls promote impoundment of water*" (emphasis added).

This interpretation is not only ambiguous *per se*, but it is also in conflict with conclusions reached by other Yucca Mountain Project scientists who studied the same secondary minerals from the ESF. For instance, Roedder et al. (1994) concluded: "*...the above arguments seem to establish that the calcite crystallized from a descending film of water on the walls of a vein that was open to the atmosphere ...*" (p. 1860), and Paces et al. (1998) stated "*A depositional environment consistent with observed textures involves water moving down connected fractures as sheets or films where it can enter intersected rock cavities.*" (p. 38; emphasis added).

The model advanced by Levy et al. (1995) envisages crystals that grew in locally saturated environments created by impoundment of waters in fractures during major meteoric recharge events. Since such an impoundment cannot exist as a lasting state of the fractures in the vadose zone; the mineral deposition events must have been rapid and intermittent. By contrast, the model favored by Roedder et al. (1994), Paces et al. (1998) and Neymark et al. (2001) calls for a continuous, on a million-year scale,

crystal growth in the unsaturated environment from gravitation-driven films of water. These two models are mutually exclusive.

The chemistry of gases trapped in fluid inclusions, therefore, appears to be incompatible with the postulated rainwater origin of solutions that deposited secondary minerals in the Yucca Mountain vadose zone. In addition, both models, which envisage the deposition of calcite in the vadose zone either from descending films of water or from water residing in a locally saturated environment created by an increased meteoric recharge, are in direct conflict with the fluid inclusion data obtained from the ESF secondary minerals. One sample analyzed by Levy et al. (1995), NR-1-SSL, was collected 38 m to the east of the Bow Ridge Fault, which means the sample location corresponds approximately to ESF station 01+62. We have collected and analyzed a sample of the sparry fracture filling at ESF station 01+62.3. It yielded homogenization temperatures of up to 85°C (see Figure 3-6-3-e). Recent results of the UNLV and the USGS researchers agree very well in that fluid inclusion temperatures measured in the vicinity of the Bow Ridge fault are among the highest in the entire ESF (75 to 89°C). These near-boiling temperatures are clearly outside the "pedogenic realm". For instance, meteoric water that would have filled the fracture during the increased recharge (e.g., a heavy precipitation event) would have to be heated somehow from ~15 °C (temperature of the rain water) to 85-89 °C after infiltrating through a section of tuff that is only 35-40 m thick.

Summarizing our analysis, we conclude that the contents and ratios of the most important gases trapped in inclusions in two calcite samples from the ESF are strikingly dissimilar from the typical vadose zone pedogenic values. The ESF inclusions contain too much water (99.2 to 99.9 mol %) and such amounts are greater than the maximum values of 98 mol % reported for the vadose calcites from the Southwestern United States (Newman et al., 1996). They also contain too little oxygen ($9.6 \cdot 10^{-3}$ to $3.2 \cdot 10^{-2}$ mol %, as opposed to $5 \cdot 10^{-2}$ to $5 \cdot 10^{-1}$ mol %, characteristic of the vadose zone pedogenic calcites; Newman et al., 1996). Both O₂ contents and O₂/N₂ ratios are similar to those of the hydrothermal carbonates and dissimilar, by as much as 1 to 2 orders of magnitude, from the vadose zone pedogenic carbonates. We conclude, therefore, that the interpretation of this type of calcite as "pedogenic" is clearly unwarranted. The data reported by Levy et al. (1995) may, in fact, be interpreted as suggesting the same hydrothermal (or travertine) origin for both the calcite from the ESF and the near-surface micritic calcite in the Bow Ridge Fault (see Chapter 3-3, Figures 3-3-22 and 3-3-23). If the gas chemistry data is considered in conjunction with the elevated fluid inclusion temperatures, the inference regarding the phreatic hydrothermal origin of the minerals, becomes compelling in our opinion.

3.6.6.2. Results of gas chromatographic analyses of the ESF minerals

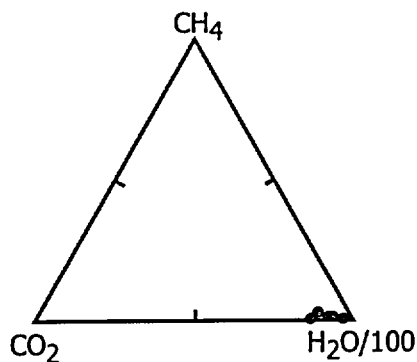


Figure 3-6-12. Results of gas chromatographic analyses of four samples of sparry calcite from the first 170 m of the ESF, east of the Bow Ridge fault (see caption for Figure 3-6-11 for details on sample locations).

During early stages of the fluid inclusion research at Yucca Mountain, Dublyansky and Reutsky (1995) extracted and performed chromatographic studies of gases entrapped in inclusions from four specimens of the ESF sparry calcite. These specimens were collected within the 170 m-interval east of Bow Ridge fault. The results are presented in Figure 3-6-12.

The figure shows that the chromatographic analyses yielded results generally consistent with those reported by Levy et al. (1995). The dominant gas detected was H₂O; minor gases were CO₂ and CH₄ (Figure 3-6-12; compare with Figure 3-6-11-b). Oxygen was not detected in all four analyzed samples (10 runs with varying gas-extraction temperatures). In view of the Quadrupole MS data discussed in the previous section, this is not surprising, since the O₂ contents appear to be too small to be detectable by the gas chromatographic method.

Gases for chromatographic analysis were extracted by thermal decrepitation. This method of extraction is inefficient for the low-density gas-filled inclusions, which explains why lower quantities of methane (compared with the mass-spectrometric analyses) were detected by gas chromatography. It is likely that the gas extraction was biased in favor of gases (predominantly H₂O) contained in high-density vapor-liquid inclusions, but at the expense of gases (CH₄ and CO₂) residing in low-density all-gas inclusions. Further studies demonstrated that methane is commonly a major component of the all-gas inclusions in the Yucca Mountain secondary minerals.

The results of the microthermometric studies of the four samples analyzed by gas chromatography are shown in Figure 3-6-13.

It can be seen from the figure that the subject minerals were precipitated from fluids whose temperature ranged between 35 and 87 °C, which demonstrates their low-temperature hydrothermal character. Needless to say that such temperatures are not expected in association with minerals precipitated from infiltrating rainwater.

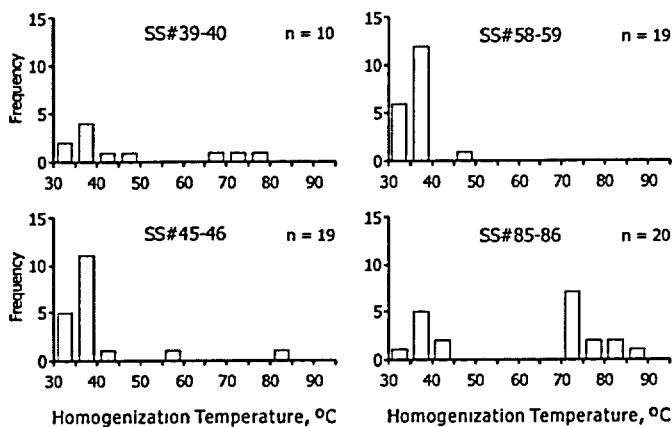


Figure 3-6-13. Homogenization temperatures measured in calcite samples for which GC analyses are presented in Figure 3-6-12. Locations: SS#39-40 – station ESF 01+03.4, SS#45-46 – station ESF 01+12.7, SS#58-59 – station ESF 01+28.5, and SS#85-86 – station ESF 01+62.3. From Dublyansky et al. (1995; 2001).

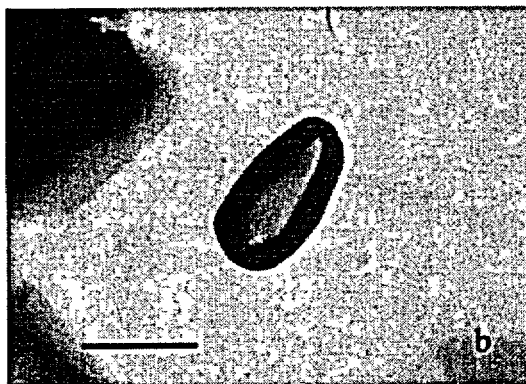
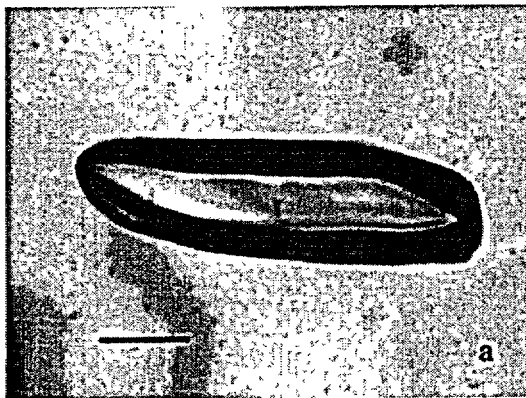
3.6.6.3. All-gas inclusions in the ESF secondary minerals

All gas inclusions, while not generally common in minerals, are abundant in secondary minerals (calcite, quartz, and fluorite) from the ESF and ECRB. These inclusions are particularly noteworthy, because they indicate the presence of two immiscible phases, aqueous and gaseous. Overall, all-gas inclusions were present in approximately 70% of the calcite samples, which were studied. Their abundance in different

samples showed significant variation. For some samples only 1 or 2 such inclusions were found in the entire standard-size fluid inclusion slide; other samples were "packed" with all-gas inclusions. Examples of all-gas inclusions from the ESF minerals are shown in Figure 3-6-14.

Inclusions are rounded, sometimes with elements of negative faceting. Most commonly they are nearly isometric, but elongated shapes also occur. Typical sizes are 20-120 μm , although both smaller and larger inclusions exist. In many instances, the primary origin of these inclusions may be ascertained. For example, in granular variety of calcite, three-dimensional all-gas inclusions commonly have sizes comparable with the sizes of the host mineral grains (an indication of the primary character of inclusions according to Roedder, 1984 and Goldstein and Reynolds, 1994). In a number of samples, all-gas inclusions were found to be restricted to 80–100 μm -thick growth zones delineated by trapped impurities, which also indicates the primary character of the inclusions. In some samples all-gas inclusions seem to be associated with all-liquid and liquid-vapor inclusions ($T_h = 35\text{--}65^\circ\text{C}$), but most commonly occur individually.

All-gas inclusions are also present in euhedral quartz crystals from the silica assemblage. There, they commonly occur along the axial part of crystals and are sometimes quite large (up to 2-3 mm in size). This, according to the criteria used in fluid inclusion research (Roedder, 1984; Goldstein and Reynolds, 1994), provides a clear indication of their primary origin. All-gas inclusions were also found in granular fluorite (Figure 3-6-14) where they, too, may be classified as primary.



↑

All-gas inclusions in calcite. Top: Sample 2226, station ESF 28+00 (Alcove 5, station AL5 0+28.5) scale bar is 25 μm . Bottom: Sample 2217, station ESF 38+64.0; scale bar is 100 μm .



↑

Primary all-gas inclusions in quartz. Top: SEM-photograph of euhedral quartz crystal with a cavity along the 2-fold axis. If such cavity is sealed in the course of crystal growth, it forms all-gas inclusion, similar to the one shown in bottom photograph (transmitted light). Sample 3727, station ESF 16+02; scale bar is 1 mm. Bottom: Sample SS#27-28, station ESF (approximate) 00+79; scale bar is 0.1 mm.

⇐ Primary all-gas inclusion (dark) in granular fluorite. Sample 3719, station ESF 05+56.9. Scale bar is 20 μm .

Figure 3-6-14. Examples of all-gas inclusions in calcite, quartz and fluorite from the ESF.

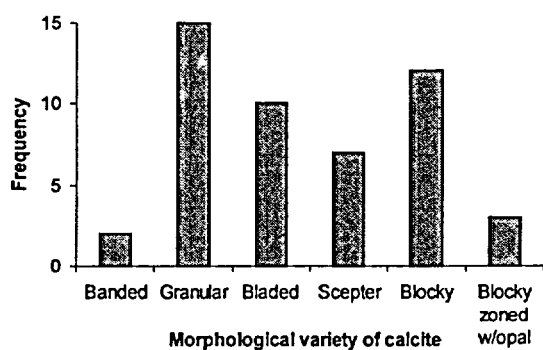


Figure 3-6-15. Abundance of all-gas inclusions in different morphological varieties of calcite. Varieties are arranged in a sequence, approximately reflecting overall sequence of calcite crystallization in the Yucca Mountain paragenesis. Histogram is based on observations from 47 samples. More than one variety of calcite was typically present in each sample.

Different morphologic varieties of calcite reflect different environments of crystal growth and may be related to different temporal stages of crystallization. It is important to discern, therefore, whether the immiscibility indicated by entrapment of all-gas inclusions might be related to a specific crystal morphology (i.e., environment of growth or temporal stage) or whether it is a universal property of the mineral-forming system at Yucca Mountain. It is apparent from Figure 3-6-15 that immiscibility seems to have existed during the formation of all morphological varieties of calcite at Yucca Mountain.

3.6.6.4. Significance of the all-gas inclusions

The presence of all-gas inclusions indicates that crystal growth occurred from a heterogeneous fluid, composed of (at least) two immiscible phases – liquid (water) and vapor (some gas and/or water vapor). Two major processes that may lead to the appearance of vapor bubbles (and, subsequently, to the entrapment of all-gas inclusions) are boiling and effervescence. To-date, no homogenization temperature exceeding boiling temperatures has been measured in secondary minerals from ESF. True boiling, therefore, may safely be ruled out as a possible mechanism for the formation of all-gas inclusions in the Yucca Mountain secondary minerals.

Another process of potential relevance is the entrapment of bubbles of underground air. Such a process is typical of the vadose-zone environment and is known to produce inclusions with erratic and typically high vapor-to-liquid ratios. In other words, such inclusions always contain a clearly recognizable aqueous phase (see e.g., Goldstein and Reynolds, 1994). We are not aware of any reported examples where entrapment of air bubbles would create single-phase all-gas inclusions.

The absolute number of all-gas inclusions in a given section provides an indication of how apparent and readily recognizable immiscibility is, but it does not provide information as to the relative abundance of the immiscible vapor phase in the mineral-forming fluid. As Roedder (1994) noted: "*Incorrect inferences are frequently drawn in the inclusion literature that the amount of vapor phase trapped, or the ratio of the number of inclusions of vapor to those of liquid phase, give an indication of the relative amounts of these two phases present in the original heterogeneous system. A single tiny inclusion of a gas phase indicates gas saturation just as well as a million of such inclusions, but the amount and number of*

such inclusions in a sample are merely a result of the vagaries of the inclusion-trapping process ... and do not give any valid indication of the phase ratios in the original two-fluid system at any given time." (p. 23).

3.6.6.5. Chemistry of all-gas inclusions

Bulk techniques of chemical analysis employed in fluid inclusion research, such as mass spectrometry and gas chromatography integrate the chemistry of fluids present in the studied mineral in the form of predominantly liquid and predominantly gaseous inclusions. In most Yucca Mountain minerals, the number of liquid inclusions is much greater than that of the gas-dominated ones. The former also have higher densities. Bulk analyses, therefore, are biased toward the chemical compositions of the liquid inclusions. Compositions of the low-density all-gas inclusions, therefore, must be studied on the scale of individual inclusions.

Crushing

Results of studies of individual fluid inclusions in calcite by crushing were reported by Roedder et al. (1994) and Dublyansky et al. (1996-a and -b). Based on the apparent contraction of the gas phase of inclusions crushed in oil and the absence of contraction for inclusions crushed in glycerol, Roedder et al. (1994) inferred the presence of methane in all-gas inclusions: "*Methane is highly soluble in the immersion oil used, and we now believe that most or even all of the collapse of the gas inclusions that was found on crushing stems from dissolution of methane. ... Some corroboration of this interpretation was obtained by crushing additional vapor inclusions in glycerol, a fluid that is not a good solvent for methane. Neither collapse nor expansion occurred in glycerol...*" (p. 1859). This interpretation is now moot, because Roedder and Whelan have recently found that many all-gas inclusions in the Yucca Mountain calcite do contract after crushing in glycerol and reported a volumetric decrease of up to 30% (Whelan and Roedder, pers. comm. 2001).

Dublyansky et al. (1996-a, and -b) performed a semi-quantitative assessment of the gas chemistry in several gas-rich and all-gas inclusions in a calcite sample from station ESF 01+62.3 (in this sample the highest so far T_h s = 85°C were measured) by employing the selective absorption method. In this method, gas bubbles released from an inclusion by crushing into the non-reactive media (typically, dehydrated LiCl-doped glycerol) are sequentially transferred into batches of glycerol doped with reagents, which are reactive with regard to different gases. The amount of gas removed by a reagent is determined by comparing the volume of a bubble before and after the reaction. Analyses revealed the presence of major methane and/or other hydrocarbons (80-85 vol. %), some non-reactive gases (presumably, nitrogen; 5-18 vol. %), and variable amounts of CO₂ (0-15 vol. %). No oxygen was detected.

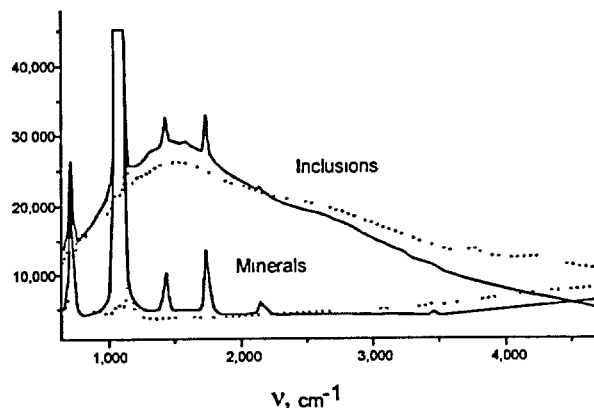


Figure 3-6-16. Raman spectra of the two all-gas inclusions and their host minerals. *Solid lines* – calcite; *dotted lines* – quartz. Station ESF 16+08. Note that inclusions in two different minerals exhibit similar luminescence patterns

Raman spectrometry

Results of Raman-spectrometric studies of the all-gas inclusions from the Yucca Mountain secondary minerals were reported by Dublyansky (1998-a; 2001-a and -b). Some 24 all-gas and gas-rich inclusions in five samples of calcite, one sample of quartz and one sample of fluorite were analyzed using a *Dilor* Raman spectrometer with Ar laser.

In most instances, inclusion gases yielded broad humps on Raman spectra (400 to 4500 cm^{-1}) characteristic of fluorescence. In only one sample of granular calcite, were all-gas inclusions

found not to fluoresce. By contrast, host calcite and quartz did not normally fluoresce (Figure 3-6-16).

Several attempts to exhaust fluorescence of the inclusion fill by prolonged exposure to a laser beam (6-12 hours) failed. Even though the intensity of fluorescence decreased with time following the power law, residual fluorescence remained sufficiently high to mask any possible peaks on Raman spectra.

In Figure 3-6-17 we show a typical result obtained from quartz. In this sample a euhedral crystal of quartz overgrows calcite and chalcedony. Quartz contains some dark condensed matter, most probably organic, associated with the growth zones. One gas-rich inclusion (V:L=0.9) was found in the crystal, for which separate Raman spectra were obtained from its gaseous and liquid parts (Figure 3-6-17-a). The gaseous phase of the inclusion yielded prominent fluorescence, expressed as a broad hump on the Raman spectrum. By contrast, the host quartz did not fluoresce. The liquid phase (water) in the inclusion showed some fluorescence with intensity lower than that of the co-existing gas. The dark condensed matter in the quartz growth zone yielded a fluorescence spectrum, virtually identical to that of the inclusion gas (Figure 3-6-17-b). The host quartz, again, did not exhibit any fluorescence.

Fluorescence of fluid inclusions in Raman studies is typically caused by the presence of cyclic and aromatic hydrocarbons (Burke, 2001). We infer, therefore, that the studied, all-gas inclusions may contain quantities of such aromatic hydrocarbons, most likely along with methane and possibly with other hydrocarbons. If this interpretation is correct, the results shown in Figure 3-6-17-a suggest that water, trapped simultaneously with gas bubbles may also contain aromatic hydrocarbons in the dissolved state.

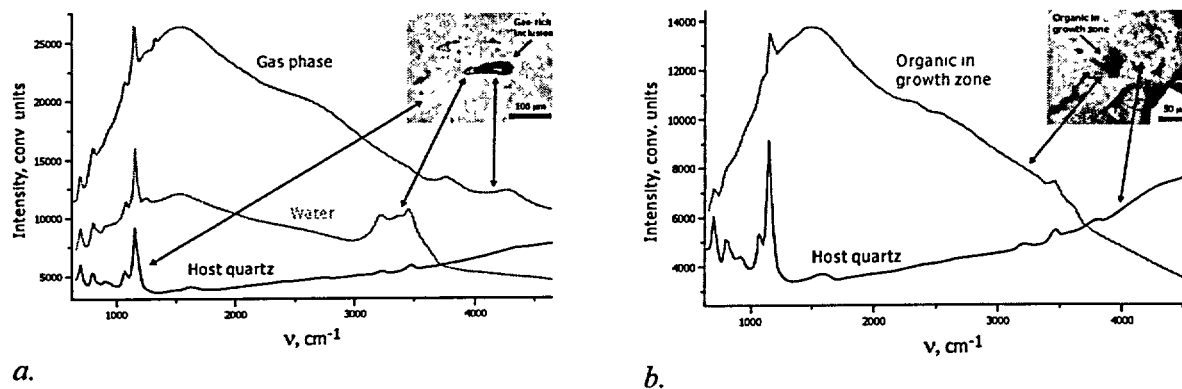


Figure 3-6-17. Results of the Raman spectrometry of the gas-rich inclusion and the organic-rich growth zone in quartz crystal from the ESF station 16+08.

a - Spectra of the gas and liquid phases of the gas-rich inclusion (inset) compared with the spectrum of the host quartz. Note strong luminescence of the gas phase, weaker luminescence of liquid phase (prominent peak of H₂O is present), and absence of luminescence of the host quartz. *b* - Spectrum of the dark organic matter in the quartz growth zone (inset) compared with the spectrum of the host quartz.

Gas chromatographic analysis of gas from individual inclusion

One large primary all-gas inclusion in a quartz crystal from station ESF 16+08 was subjected to gas chromatographic (GC) analysis. The crystal was mechanically broken in a special chamber in a continuous flow of helium and analyzed on a setup consisting of two gas chromatographs. The amount of gas contained in the inclusion was too small to allow quantitative determinations. Two gases: CO₂ and N₂ yielded clearly discernible peaks with roughly similar size. A signal of O₂ was not detected.

3.6.7. Interpretation of the data on gases in inclusions

3.6.7.1. Natural gas flow system and gas chemistry at Yucca Mountain

Since the Yucca Mountain Project "rainwater" concept contemplates secondary minerals crystallizing from films of water in the air-filled (open to atmosphere) fractures of the vadose (unsaturated) zone, it is important to evaluate what gases, and in what quantities, are present in the vadose zone of Yucca Mountain today. Arguably, if the overall topography of the mountain remained unchanged and the 300-700 m-thick vadose zone existed at Yucca Mountain at all times over the last 10 million years or so, as it is believed by the Yucca Mountain Project researchers, the physical processes controlling the migration of gases through the mountain may be expected to persist throughout its history. The present-day data, thus, may be used as a baseline for assessing the nature and quantities of gases trapped in

inclusions. The similarity between the fluid inclusion gases and gases from the present-day underground atmosphere would confirm the "rainwater" concept, whereas the substantial dissimilarity would demonstrate its fallacy

Sullivan and Pescatore (1994) summarized the knowledge on the gas flow system at Yucca Mountain as follows:

Near the surface of Yucca Mountain gas flow is strongly influenced by atmospheric pressure, temperature, wind velocity, and topography. ... the flow in and out of Yucca Mountain due to seasonal temperature variations was modeled numerically by the USGS (Kipp, 1987). Their predictions indicate that in summer, air enters the mountain near the crest and exits along the lower half of the valley wall. In winter, the flow is reversed. Maximum pore velocities are near five m/day (Kipp, 1987). Within the mountain, responses to changes in the surface conditions influenced flow to a depth of 50 – 100 meters.

...

More recent work (Weeks, 1991) indicates that wind flow is an important mechanism for moving air into the mountain. ... Weeks estimates that wind pumping is responsible for approximately 30% of the flow through the mountain. With 70% being due to thermal effects. (pp. 19-20).

It is apparent from the quotation above that Yucca Mountain seems to be a well-ventilated and aerated geological structure, which is consistent with the chemistry of gases analyzed from the underground atmosphere.

According to Thorstenson et al. (1990), all gas samples from boreholes collected to date show concentrations of O₂ and N₂ that are identical to the concentrations of these gases in atmospheric air to the limits of analytical precision. According to the U.S. DOE (2001) "*The oxygen concentration throughout the unsaturated zone is apparently close to atmospheric, indicating there are no natural processes that consume oxygen at rates nearing the rate of potential supply from the ground surface.*" (p. 4-160). Gases sampled in instrumented boreholes generally showed methane concentrations near zero, ranging up to a maximum value of 0.5 (±0.1) ppmv (Thorstenson et al., 1990).

In addition, all soil gases sampled on and near Yucca Mountain showed methane concentrations that were depleted relative to the atmospheric value of about 1.7 ppmv, but still greater than 0.5 ppmv. Thorstenson et al. (1990).

A hypothetical mineral crystallizing in the vadose zone of Yucca Mountain would be expected to carry (in fluid inclusions) gas chemistry generally corresponding to the chemistry of the underground air. The latter, as the preceding discussion implies, has O₂ and N₂ contents identical to the atmospheric air and is somewhat depleted in methane.

Table 3-6-1

Summary on composition of gases in secondary minerals from Yucca Mountain
determined by different methods

Method	G a s e s					Mineral	Extraction method	Note
	CO ₂	CH ₄	Other hydro- carbons	O ₂	N ₂			
Bulk compositions								
Quadrupole MS	yes	yes	n/a	yes (?)	yes	calcite	crushing	
GC	yes	yes	yes (C ₂ -C ₆)	no	n/a	calcite	thermal decrepita- tion	Hydrocarbons heavier than C ₆ were detected, may be due to thermal cracking of condensed organic matter
Individual inclusions								
GC	yes	no	no	no	yes	quartz	crushing	Number of studied inclusions – 1.
Selective adsorption	yes	yes (up to 80%)	yes	no	no	calcite	crushing	CH ₄ and other hydrocarbons are summed. Number of studied inclusions – 8
Raman spectrometry	no	no	yes (aromati c/cyclic)	no	n/a	calcite, quartz, fluorite	laser, non- destructiv e	Signals of other gases are masked by fluorescence Number of studied inclusions – 24.

Notes: MS – mass-spectrometry; GC – gas chromatography; yes – detected; no – not detected; n/a – cannot be detected by this method.

3.6.7.2. Gases trapped in inclusions

Data on gases identified by different methods in the Yucca Mountain secondary minerals are summarized in Table 3-6-1. It is apparent from the Table that chemistry of the gases actually entrapped in the ESF secondary minerals differs considerably from that which would be expected for the gases entrapped in the vadose zone of Yucca Mountain.

The characteristic feature of the analyses discussed above is the presence of methane. Roedder et al. (1994) reported “*major methane*”; Levy et al. (1995) measured methane in proportions similar to that of CO₂. Our GC analyses also revealed the presence of CO₂ and CH₄. The presence of methane and carbon dioxide as major constituents of the gas mix is conspicuous and makes the gases trapped in secondary minerals at Yucca Mountain look quite dissimilar from the present-day gases of the underground atmosphere.

Semi-quantitative selective absorption and gas chromatographic analyses of individual gas-filled inclusions reinforce this conclusion. Gases trapped in all-gas inclusions contain CO₂ in amounts of three orders of magnitude, and CH₄ in amounts of six orders of magnitude greater than the contents in the underground air at Yucca Mountain. Ratios of CH₄/CO₂ and CO₂/N₂ range from 1 to 10 (as compared to the typical atmospheric values of ~0.05 and ~0.0005, respectively). The absence or very low contents of O₂ in inclusions is also conspicuous. Thus, the chemistry of fluid inclusion gases seems to be incompatible with the aerated vadose-zone environment in which, according to the Yucca Mountain Project's "rainwater" hypothesis, the secondary minerals have formed. The presence of gaseous aromatic hydrocarbons is also difficult to reconcile with the aerated vadose zone setting.

3.6.7.3. Suggested origin of hydrocarbon gases

The most logical source of gaseous hydrocarbons in inclusions (as well as condensed organic matter found in some samples; see Figure 3-6-17) is the early Paleozoic carbonate complex underlying the Yucca Mountain rhyolitic tuffs. Thermal history of this marine complex indicates that the rocks are over mature from the standpoint of oil generation, but do have thermal potential for gas generation (Grow et al., 1994; French, 2000). On their way to the surface, upwelling waters would pass through the Paleozoic rocks and acquire (dissolve) hydrocarbon gases. Closer to the surface, because of an overall decrease in hydrostatic pressure and temperature, these waters would likely become supersaturated relative to these gases, which would lead to exsolution (effervescence) of the latter into a vapor phase. The gas bubbles would be transported along with the fluid and move independently upward due to buoyancy.

The process of exsolution must have been most efficient in the zones, where the temperatures were between 70 and 90°C, because at these temperatures the solubility of methane is at a minimum: "*Segregation of a gas from saturated waters may occur during upwelling of waters and during the passage of the gas-saturated waters through the temperature zone in which the solubility of hydrocarbon gases is minimal (for methane, these temperatures are 70-90°C)*" (Principles of Hydrogeology, 1982. p. 148). Judging from the fluid inclusion thermometry, paleo waters that circulated through Yucca Mountain and deposited secondary minerals had temperature that would favor exsolution of methane.

3.6.8. Interpretation of the combined $\delta^{18}\text{O}$ and fluid inclusion data

3.6.8.1. Geothermal reconstructions based on $\delta^{18}\text{O}$ values

The $\delta^{18}\text{O}$ values measured in calcite have been used to estimate the formation temperatures. The rationale of the method was formulated as follows: "*The fractionation of oxygen isotopes between calcite and water is temperature sensitive. Figure 69 plots this fractionation against temperature and shows, for*

low temperatures, a change of about 0.18‰/°C (O'Neil et al. 1969, p. 5552; Kim and O'Neil 1997, p. 3467). If any two of the variables— $\delta^{18}\text{O}$ of calcite, $\delta^{18}\text{O}$ of water, or temperature—are known, then the third can be estimated.” (Fabryka-Martin et al., 2000, p. 114).

The empirical equation relating the oxygen isotope properties of water with those of depositing calcite, at equilibrium, is:

$$\delta^{18}\text{O}_{\text{Cat}} = \delta^{18}\text{O}_{\text{water}} - A \cdot (10^6 \cdot T^{-2}) - B \quad (3-6-1)$$

where A and B are coefficients, and T is the temperature in K. The $\delta^{18}\text{O}_{\text{Cat}}$ is measured in the course of the isotopic studies; hence, in order to solve the equation and obtain the temperature, it is necessary to know the value of $\delta^{18}\text{O}_{\text{water}}$. Since the latter is not measurable, its value must be assumed. Another assumption that needs to be made when attempting to derive the temperature record from isotope data is that $\delta^{18}\text{O}_{\text{water}}$ does not change (or the function of the change is known) in the process of crystal growth. This caveat must be born in mind when assessing the reliability of the oxygen isotope temperatures.

Researchers associated with the Yucca Mountain Project interpret the $\delta^{18}\text{O}$ in calcite as recording “undisturbed” geothermal conditions in the Yucca Mountain vadose zone. A recent document prepared in support of the Yucca Mountain Site performance assessment entitled “Analysis of Geochemical Data from the Unsaturated Zone” (Fabryka-Martin et al., 2000) states: “Most of the reported $\delta^{18}\text{O}$ values vary systematically with depth from the surface (Figure 57) and are consistent with temperature-controlled water-calcite isotope fractionation factors responding to modern-day geothermal gradients of 30 to 40°C per kilometer measured at Yucca Mountain (Szabo and Kyser 1990, p. 1718).” (p. 103). The Figure 57 from the passage cited above is reproduced as Figure 3-6-18-a.

Isotopic values shown in Figure 3-6-18-a were obtained from comparatively large (a few mg) fragments of calcite removed from rock cores that were extracted from the vadose zone tuffs, at a depth ranging between 0 and 500 m (Szabo and Kyser, 1990). Later, when more discriminating methods of analysis were used calcite samples from the ESF provided an additional extensive isotope record, which represents the vadose zone at a depth between about 30 and 300 m. Figure 3-6-18-b shows that new results from the ESF tunnel exhibit a depth distribution virtually inverse to those obtained from boreholes. Thus, if $\delta^{18}\text{O}$ is any proxy of the change of the depositional temperature with depth, the ESF data reflect a paradoxically inverse geothermal gradient in which the temperatures near the surface are greater than those in the deeper parts of the mountain.

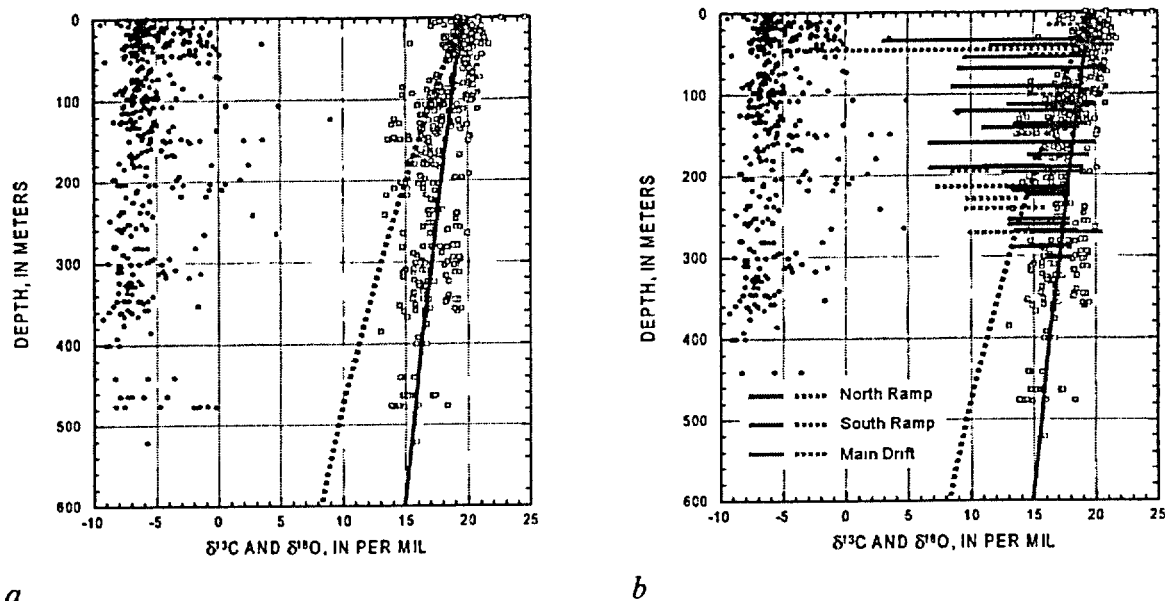


Figure 3-6-18. Stable carbon and oxygen compositions of unsaturated-zone calcite as a function of depth.

a – Isotope data on calcite from boreholes. The $\delta^{18}\text{O}$ values are interpreted as recording the increase of temperature within the vadose zone in accordance with the geothermal gradient. Solid gray line – calculated $\delta^{18}\text{O}$ values for calcite formed in equilibrium with water having $\delta^{18}\text{O} = -12.5$ ‰ SMOW, assuming a $10\text{ }^{\circ}\text{C}$ mean surface temperature and a geothermal gradient of $34\text{ }^{\circ}\text{C}\cdot\text{km}^{-1}$. Dotted line – the same, except geothermal gradient is taken to be $100\text{ }^{\circ}\text{C}\cdot\text{km}^{-1}$. Reproduced from Fabryka-Martin et al. (2000; Figure 57). *b* – Superimposed on previous graph are the $\delta^{18}\text{O}$ data from the ESF calcite. *Solid color lines* – data from Fabryka-Martin et al. (2000, Figure 75); *dotted color lines* – data from Dublyansky (2001).

The apparent discrepancy between the borehole and the ESF $\delta^{18}\text{O}$ data may be explained by taking into account lateral paleo-thermal gradients established by means of the fluid inclusion analysis (see Figure 3-6-7-a). Although substantially less steep, similar lateral geothermal gradient also exists in the present-day vadose zone, as shown in Figure 3-6-7-b. Most of the isotopic data presented in Figure 3-6-18 were obtained from boreholes USW-G-1, G-2, G-3/GU-3 and G-4 located to the west of the ESF, i.e., close to the central zone of the Yucca Mountain horst, in an area wherein the vertical geothermal gradient is at a minimum (see Figure 3-6-7-b). This gradient averages about $23\text{ }^{\circ}\text{C}\cdot\text{km}^{-1}$, which is substantially less than the $34\text{ }^{\circ}\text{C}\cdot\text{km}^{-1}$ depicted as solid line in Figure 3-6-18-a. It may be expected, on the basis of the fluid inclusion data presented in Figure 3-6-7-a, that calcite in this part of the block was deposited at lower temperatures than calcite precipitated in the vicinity of the horst-bounding fault. Hence, the apparent isotopic vertical gradients are expected to be less steep there.

Figure 3-6-19 compares $\delta^{18}\text{O}$ values and the homogenization temperature data for the ESF samples. The data clearly show that these two independent records are mutually consistent; thus, the hypothesis that

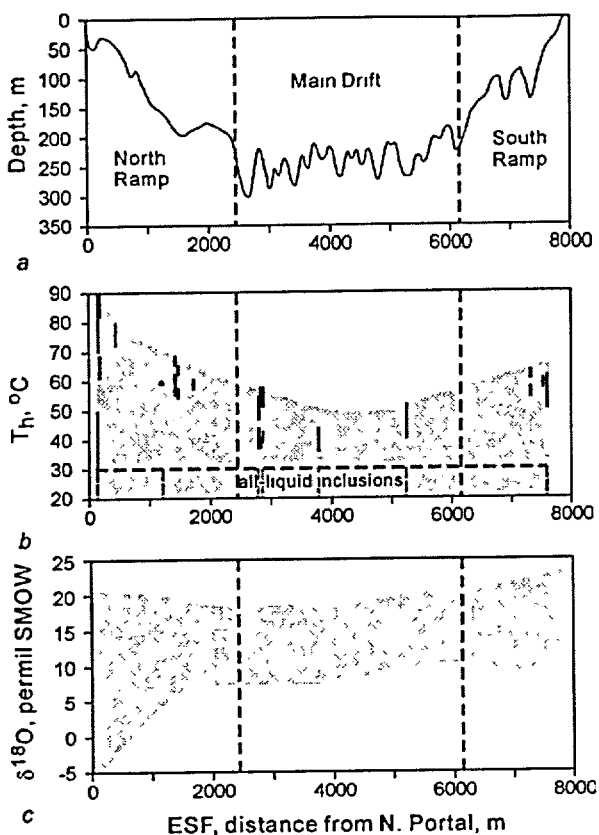


Figure 3-6-19. Comparison of the fluid inclusion and stable isotope ($\delta^{18}\text{O}$) record from the ESF.

a – Depth from the surface in the ESF (from Neymark et al., 1998). *b* – Homogenization temperatures measured in calcite, fluorite, and quartz (data from Dublyansky, 2001 and Whelan et al., 2001). Red lines show measured homogenization temperatures; blue lines indicate the presence of all-liquid fluid inclusions. Note that the low-temperature side of the temperature field is not constrained numerically (see discussion in section 3.6.5.1); *c* – Field of the $\delta^{18}\text{O}$ values in calcite (integrated data from Fabryka-Martin et al., 2000; and Dublyansky, 2001).

$\delta^{18}\text{O}$ values in calcite reflect the temperature of the mineral forming waters, with the lower $\delta^{18}\text{O}$ corresponding to higher temperatures, appears plausible. It is apparent that the seemingly “irrational” behavior of the ESF isotopic results ($\delta^{18}\text{O}$ values increasing with depth reflecting decreasing temperatures) expresses the fact that the deepest samples collected in the ESF north-south Main Drift are located further away from the heat source—the horst bounding fault (see Figure 3-6-7), which evidently acted as a pathway for the ascent of hot fluids.

Additionally, it seems to us that the very approach employed by the Yucca Mountain Project researchers, whereby mean isotopic values measured in fairly large (a few mg) samples obtained from widely-spaced boreholes are compared with the geothermal, constant gradient-based, calculated, isotopic values (see Figure 3-6-18-*a*) is inappropriate. Two established facts must be taken in consideration. First, detailed isotopic studies have demonstrated that, typically, the “lightest” $\delta^{18}\text{O}$ values are associated with the earliest calcite and the “heaviest” – with the latest; the $\delta^{18}\text{O}$ across individual crusts may change by as much as 6 ‰ (see Figures 3-5-10, 3-5-12 and 3-5-13 in Chapter

3-5). Second, fluid inclusion studies have demonstrated that, in most cases, the earliest calcite was formed from the hottest solutions and the temperature decreased as the minerals grew. Recognizing the preceding observations, the logical way to treat the isotopic data would be to consider the “lightest” $\delta^{18}\text{O}$ values as a proxy for the early stages of mineral growth, and the heaviest values, as reflecting the late stages. The shape of the early and the late $d\delta^{18}\text{O}/dz$ (proxy of dT/dz) gradients would best be approximated by two envelope curves constructed for the lightest and heaviest $\delta^{18}\text{O}$.

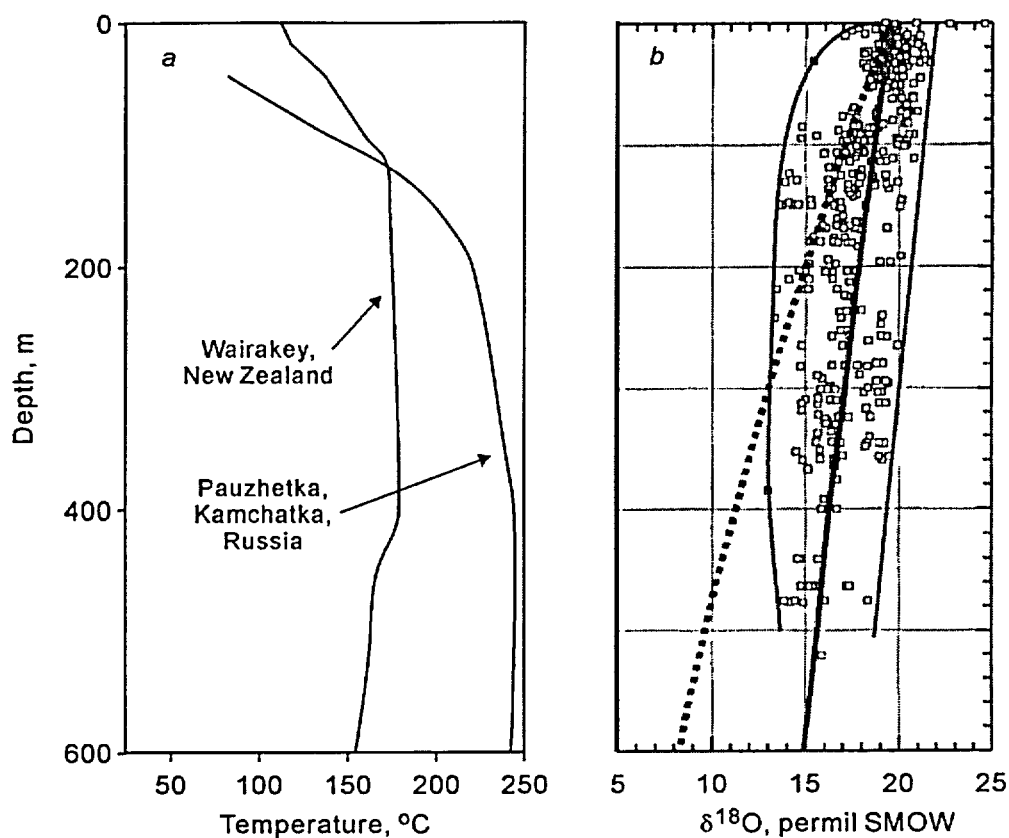


Figure 3-6-20. Thermal logs from boreholes drilled in two active geothermal areas (*a*; from Frolov, 1976) compared with the stable carbon and oxygen compositions of unsaturated-zone calcite as a function of depth (*b*; from Fabryka-Martin et al., 2000).

Different interpretations of the data: Solid gray line shows values of $\delta^{18}\text{O}$ in calcite formed in equilibrium assuming a geothermal gradient of $34\text{ }^{\circ}\text{C}\cdot\text{km}^{-1}$. Dotted line – the same, except the geothermal gradient is $100\text{ }^{\circ}\text{C}\cdot\text{km}^{-1}$ (the latter two lines are computed based on the assumption that mineral-forming water has $\delta^{18}\text{O} = -12.5\text{ }_{\text{‰}}\text{SMOW}$ and mean surface temperature is 10°C). Red line – envelope curve for the early-stage calcite. Blue line – envelope-curve for the late-stage calcite.

Note that the shape of the red line (early calcite) is similar to the thermal profiles characteristic of the advective geothermal systems (*a*) with a steep gradient near the surface and adiabatic or even negative gradient at depth. The blue line (late calcite) corresponds to the "normal" conductive geothermal gradient.

The shape of the envelope curves shown in Figure 3-6-20-*b* is quite revealing. While the latest-stage isotope gradient seems to be linear and consistent with the geothermal gradient of about $35\text{ }^{\circ}\text{C}\cdot\text{km}^{-1}$, the early-stage gradient is clearly non-linear. It is very steep near the surface, and becomes zero (adiabatic) or even negative at depth.

The adiabatic part of the earliest-stage gradient (red line in Figure 3-6-20-*b*) has profound implication for assessing validity of the latest interpretations of the ESF thermometric data by the Yucca Mountain Project researchers. To account for the elevated homogenization temperatures, they now

speculate that the rainwater responsible for deposition of the ESF secondary minerals was percolating through cooling yet hot tuffs, which then comprised the ever-present vadose zone. These tuffs would have been heated conductively either by the Timber Mountain magma chamber (Marshall et al., 2000) or, alternatively, by hot waters that circulated at a depth of more than 1 km in association with the Timber Mountain hydrothermal event (Whelan et al., 2001). However, an adiabatic temperature distribution, such as that suggested by Figure 3-6-20-b (red line), implies the dominant role of the advective transport of heat in the form of flow of hot water. Similar temperature distributions are commonly observed in association with modern geothermal systems, and two examples of such distributions are shown in Figure 3-6-20-a. The $\delta^{18}\text{O}$ data seem to directly contradict the "conductive heating" model proposed by the Yucca Mountain Project researchers.

The slope of the latest-stage $\delta^{18}\text{O}$ gradient (blue line in Figure 3-6-20-b) corresponds to a value of the geothermal gradient of about $35\text{ }^{\circ}\text{C}\cdot\text{km}^{-1}$, which is some 40% higher than the modern geothermal gradients in this part of the mountain (about $23\text{ }^{\circ}\text{C}\cdot\text{km}^{-1}$; Sass et al., 1987). This suggests that fluids with elevated (i.e., above the modern-day ambient temperature) may have been circulating through the Yucca Mountain vadose zone during the latest stages of deposition of the secondary calcite.

3.6.8.2. Timing of the entrapment of two-phase inclusions relative to "stable isotope stages" of the mineral growth

Since two-phase liquid-vapor inclusions provide direct evidence of elevated (i.e., in excess of 35-50 $^{\circ}\text{C}$) temperatures during crystal growth, distribution of such inclusions within calcite crystals may provide important information on the relative timing of the occurrence of hot waters. The Yucca Mountain Project researchers are of the opinion that only the earliest (and, on rare occasions, intermediate*) calcite hosts two-phase fluid inclusions: *"Most of the FIAs containing TPVL [two-phase liquid-vapor] inclusions are in early-stage calcite. Some samples from the north bend area, however, contain FIAs with TPVL inclusions in intermediate-stage calcite as well. Some of these display a range of T_h 50 to 60 $^{\circ}\text{C}$ to as low as 35 $^{\circ}\text{C}$ that correlates with deposition beginning in the early stage and extending into the early part of the intermediate stage.... Fluid inclusion assemblages containing TPLV inclusions have not been found in the late-stage calcite."* (Whelan et al. 2001; emphasis added).

Early, middle, and late stages of calcite deposition are defined by the Yucca Mountain Project researchers based on the relative position of the calcite in the sample (determined by visual observations) and on the $\delta^{13}\text{C}$ and $\delta^{18}\text{O}$ values. Characteristic values of the three calcite stages are: early stage $\delta^{13}\text{C}$ +5 to +8 ‰ PDB and $\delta^{18}\text{O}$ <16 ‰ SMOW; intermediate stage $\delta^{13}\text{C}$ -3 to 0 ‰ PDB; and late stage $\delta^{13}\text{C}$ -5 to -

* Discussion of the "stable isotope stages" can be found in section 3.5.2, Chapter 3-5.

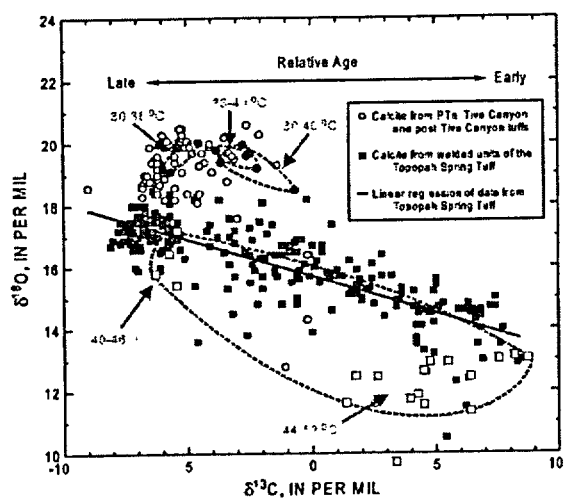


Figure 3-6-21. Isotopic composition of carbon and oxygen in subsamples of calcite from the ESF compared with coupled stable isotope – fluid inclusion results.

Circles – calcite from PTn, Tiva Canyon and post-Tiva Canyon tuffs; *squares* – calcite from welded units of the Topopah Spring Tuff. *Open circles* and *red squares* – data from Whelan et al. (1998), as presented in Fabryka-Martin et al. (2000), *blue circles* and *yellow squares* – data from Dublyansky (2001) and Dublyansky et al. (2001). *Dashed red lines* envelop data points obtained from individual mineral crusts.

8 ‰ PDB, $\delta^{18}\text{O}$ 18 to 21 (calcite from Tuff Tiva Canyon) and 16 to 18 (calcite from Tuff Topopah Spring) ‰ SMOW (Paces et al. 1996; Whelan et al. 1999; Fabryka-Martin et al. 2000). In Figure 3-6-21 we compare isotopic data for the ESF calcites obtained by the Yucca Mountain Project researchers (as summarized by Fabryka-Martin et al., 2000) with the coupled stable isotope-fluid inclusion results (Dublyansky 2001; Dublyansky et al., 2001). The data show that two-phase fluid inclusions, for which homogenization temperatures were determined, are present in calcite that has characteristic isotopic values of all three (i.e., early, intermediate, and late) stages of calcite deposition, as defined by the Yucca Mountain Project researchers. At least part of the data shown in Figure 3-6-21 was obtained from the latest blocky calcite. Thus, the contention that at Yucca Mountain the elevated temperatures are restricted to “*early stage and early part of the intermediate stage*” (as given by Whelan et al. 2001) is clearly contradicted by the data. To the contrary, the data presented in Figure 3-6-21 suggest that waters with elevated temperatures have deposited calcite with isotopic properties ranging from +8.7 to -6.3 ‰ PDB ($\delta^{13}\text{C}$) and from 9.9 to 20.0 ‰ SMOW ($\delta^{18}\text{O}$), i.e., almost the entire range of values reported for the ESF secondary calcite.

One example is shown in Figure 3-6-22. Sample 3772 (station ESF 52+43; fracture) represents a complex calcite-fluorite crust. The early part of the sample is built up of granular calcite intergrown with fluorite. Fluorite is zoned and commonly has a botrioidal core and crystalline outer rim. Many calcite grains contain large (comparable in size with the host grains) primary all-gas inclusions. Toward the rim of the crust, the granular calcite grades into a blocky variety (there is no apparent indication of a hiatus). Late blocky calcite also contains fluorite, which sometimes overgrows the latest calcite crystals. Primary two-phase FIAs were found in both the early granular and the late blocky calcite, so that the coupled stable isotope-homogenization temperature studies of the entire aggregate could be undertaken. The results of these studies are shown in Figure 3-6-22.

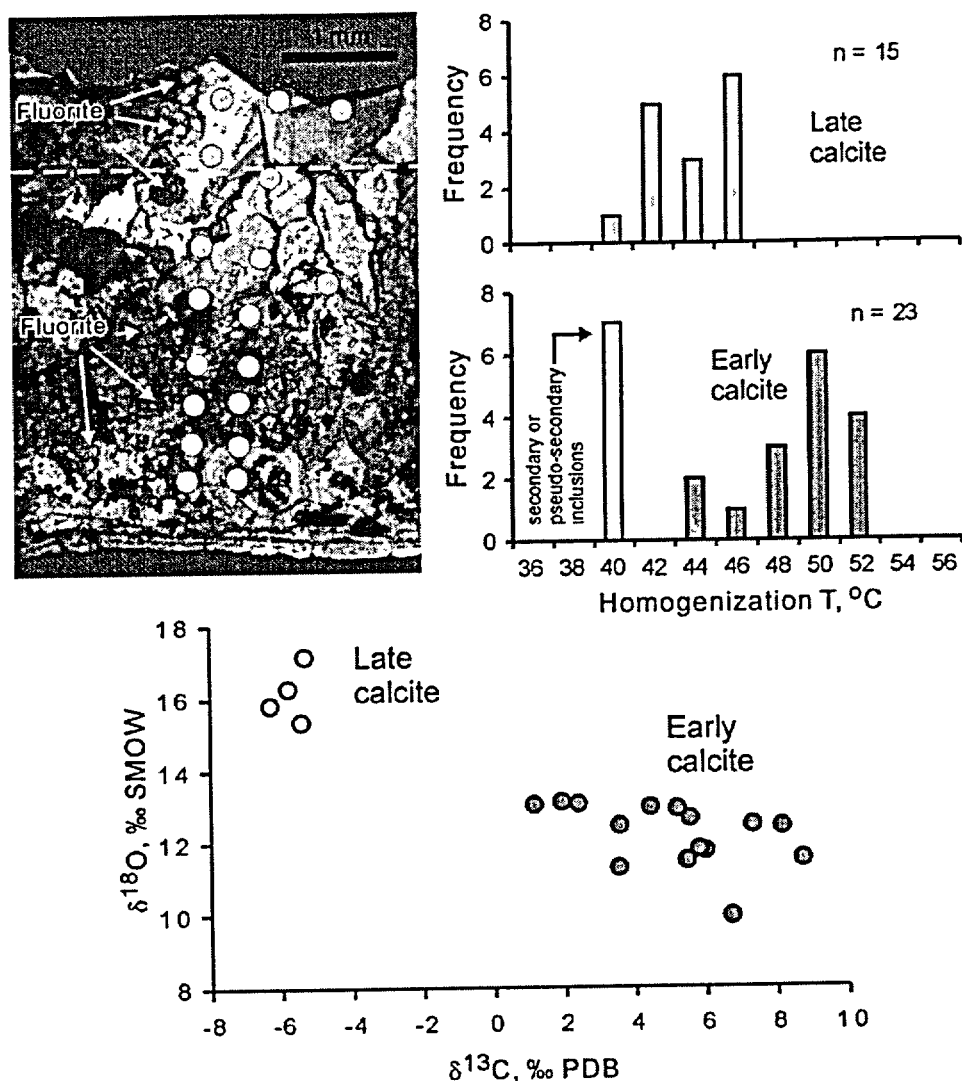


Figure 3-6-22. Coupled fluid inclusion and stable isotope data on sample 3772 (station ESF 52+43; fracture). A 4.5 mm-thick crust is built up of granular (early) and blocky (late) calcite. Both varieties contain fluorite and fluid inclusions. Homogenization temperatures measured in early granular calcite show mode at 50 °C, and in late blocky calcite – at 42–46 °C. Early calcite also contains secondary or pseudo-secondary inclusions that homogenize in a narrow 40–41 °C-interval. $\delta^{13}\text{C}$ vs. $\delta^{18}\text{O}$ cross-plot shows that notwithstanding seemingly gradual decrease of the temperature, isotopic properties of the mineral-forming fluid have changed abruptly.

Yellow circles on the photograph indicate locations and approximate size of the stable isotope measurements. Dashed line marks the transition between early and late calcite varieties.

Inclusions in granular calcite yielded homogenization temperatures from 44 to 52 °C with the mode at 50 °C. This calcite also contains secondary (or pseudo-secondary) inclusions homogenizing in a narrow 40–41 °C-interval. Fluid inclusions in late blocky calcite yielded somewhat lower homogenization temperatures of 42 to 46 °C (mode at 45 °C).

The fluid inclusion data demonstrate that the temperature of the waters, that deposited the calcite-fluorite aggregate decreased with time. Notwithstanding this seemingly gradual decrease, the $\delta^{13}\text{C}$ vs. $\delta^{18}\text{O}$ cross-plot shows that isotopic properties of the latter changed abruptly during the transition from a granular to blocky morphology: the late blocky calcite abruptly became enriched in the "light" isotope of carbon (^{13}C) and simultaneously in the "heavy" isotope of oxygen (^{18}O). Importantly, secondary or pseudo-secondary inclusions indicate that the waters remained heated to $\sim 40^\circ\text{C}$ even after the cessation of crystallization of the main part of the crust.

The late calcite in our sample 3772 has all attributes of the "late-stage" calcite as defined by the Yucca Mountain Project researchers (see Whelan et al., 2001). This calcite is clear (translucent) and contains little inclusions, it has a blocky texture and occupies the latest paragenetic position within the aggregate, and it overgrows the typical "early-stage" calcite represented by "*intergrowths or mosaics of semi-equant grains*" (Whelan et al., 2001). In addition, it has characteristic of the "late-stage" calcite $\delta^{13}\text{C}$ values of -5 to -7 ‰ PDB and $\delta^{18}\text{O}$ values of 15 to 17 ‰ SMOW. Nevertheless, this latest calcite was deposited from fluids with temperature of 42 - 45°C and further, the crust was washed in fluids with temperatures of 40 - 41°C at the very late stages or even after the cessation of mineral growth.

Another way of showing that calcite from all the stages (temporal or isotope) has precipitated from thermal waters, is to compare the $\delta^{13}\text{C}$ and $\delta^{18}\text{O}$ values of those calcite specimens which contain two-phase fluid inclusions with the stable isotope values characteristic of the three stages of the mineral growth. In Figure 3-6-23 we compare our stable isotopic-fluid inclusion results with the reported radiometric ($^{207}\text{Pb}/^{235}\text{U}$) ages* obtained from the ESF samples, correlated with the "isotopic stages".

The figure shows that the two-phase inclusion bearing calcite is associated with $\delta^{13}\text{C}$ and $\delta^{18}\text{O}$ values which span the entire range of values reported for the ESF secondary calcite.

* Figure 3-6-23 shows $^{206}\text{Pb}/^{235}\text{U}$ ages of specimens for which both the paragenetic position and the stable isotope values were determined independently. As explained in Chapter 3-7, the "conventional" Pb-U dating method, if applied to a mineral precipitation of which occurred in a large open cavity and involved colloidal solutions, are not reliable. A mineral sequences that has been precipitated over a fairly short (say, thousands of years) time-span may appear as having been precipitated over a much longer (millions of years) time-span.

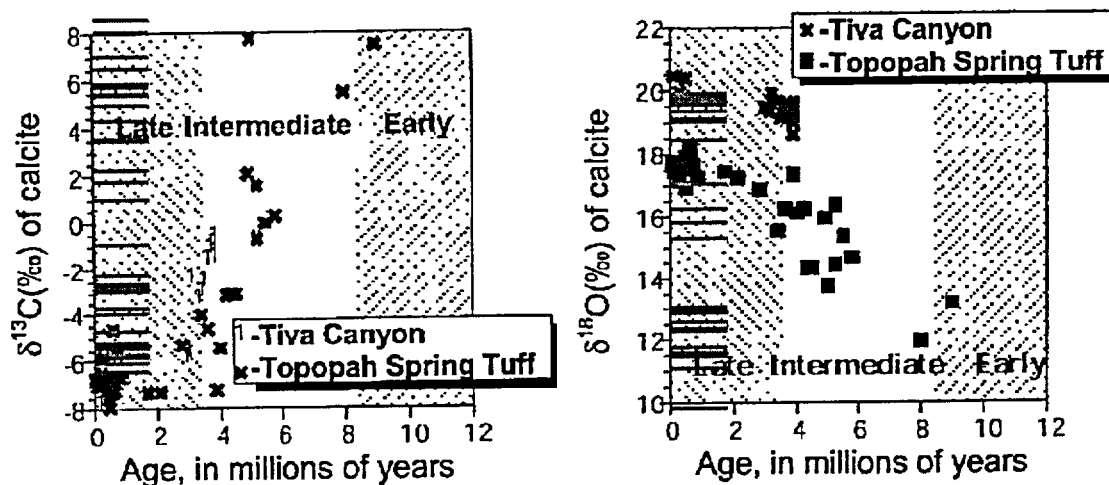


Figure 3-6-23. Persistence of the elevated temperatures through the isotopic record. $\delta^{13}\text{C}$ and $\delta^{18}\text{O}$ values of calcite versus its apparent radiometric $^{207}\text{Pb}/^{235}\text{U}$ age (from Fabryka Martin et al., 2000; Figures 70 and 72). Areas denoted "Late", "Intermediate" and "Early" reflect "isotopic stages" as defined by Yucca Mountain Project researchers (e.g. Paces et al., 2001).

Colored bars show isotopic values of calcite samples for which elevated temperatures of 30 to 52°C were determined by fluid inclusion method (see Figure 3-6-21; data from Dublyansky, 2001 and Dublyansky et al., 2001). *Blue bars* – calcite from Tiva Canyon Tuff, *red bars* – calcite from welded units of the Topopah Spring Tuff. Note that the bars show only isotopic values and do not show apparent radiometric ages.

3.6.9. Summary

Two-phase fluid inclusions suitable for determinations of the homogenization temperature were found in secondary calcite, fluorite and (rarely) quartz from the proposed repository horizon (ESF). Inclusions in all three minerals yielded consistent homogenization temperatures ranging from 85°C to as low as 35°C. Monophase all-liquid inclusions suggesting temperatures less than approximately 35-50°C were also found.

The fluid inclusion temperature record is not uniform within individual mineral crusts. Typically, the temperature decreases with the decreasing relative age of minerals (i.e., it is higher at the bases of crusts and lower at the tops, although somewhat more complex spatial relationships also exist). Typically, the minerals at and near top of the crusts host only monophase inclusions, which implies that these relatively young minerals were precipitated from fluids whose temperature was less than approximately 35-50 °C. Nevertheless, fluid inclusions with elevated homogenization temperatures have been found in the paragenetically latest variety of calcite (the clear blocky euhedral calcite characterized by "light" $\delta^{13}\text{C}$ and "heavy" $\delta^{18}\text{O}$ signatures).

The fluid inclusion temperature record is not uniform across the proposed repository horizon, as represented by the path of the Exploratory Studies Facility tunnel. The highest temperatures were found in its northeastern part (near the North portal and along the north ramp), as well as in the southeastern part (south ramp). The coolest temperatures were measured in samples from the area near the north bend (north central part of the ESF). We interpret the spatial zonation as reflecting the distance from the horst-bounding Paintbrush fault zone, which served as a pathway for the ascent of a hydrothermal plume.

The paleo temperatures measured in the fluid inclusions indicate the presence of very high paleo heat flows in the proposed repository area. Calculated values range from 5 to 70 HFU (as compared with the present-day values of less than 1.5 HFU), which is only possible in the setting of a hydrothermal system. Like the homogenization temperature lateral zonation, the calculated paleo heat flow field exhibits a strong east-west gradient with values increasing in the direction of the horst bounding Paintbrush fault.

The salinities of the mineral forming fluids determined by freezing experiments ranged from <1,800 ppm to 21,000 ppm, which encompasses the three categories – fresh, brackish and saline waters. This character of ancient waters is in contrast with that of the modern aquifer fluids, which invariably contain less than 1000 ppm of total dissolved solids and are classified as fresh waters.

Chemistry of gases trapped in inclusions was analyzed by means of bulk methods (mass spectrometry, gas chromatography) as well as in individual inclusions (crushing, selective adsorption, Raman spectrometry, gas chromatography). Inclusions were found to contain significant quantities of methane and, possibly, some quantities of heavy aromatic hydrocarbons (tentatively identified by Raman fluorescence). The high abundance of CH₄ in combination with the very low abundance of O₂ indicates reducing character of the mineral forming fluid. Contents of O₂ and O₂/N₂ ratios are similar to those of the hydrothermal carbonates and dissimilar, by as much as 1 to 2 orders of magnitude, from the vadose zone pedogenic carbonates.

Overall, the gas chemistry data are incompatible with entrapment in an aerated vadose zone. The data are readily explained within a context of the upwelling water hypothesis by a model whereby thermal fluids acquire dissolved hydrocarbons during their upwelling through the Paleozoic carbonate rocks underlying the Yucca Mountain rhyolitic tuffs. These carbonate rocks are known to have limited thermal potential for natural gas.

The $\delta^{18}\text{O}$ in calcite seems to represent a proxy for the paleo temperatures. There is an impressive match between the fluid inclusion homogenization temperatures and the $\delta^{18}\text{O}$ distributions in the ESF. Calcite with "light" $\delta^{18}\text{O}$ values, suggestive of elevated temperatures, tends to concentrate in the eastern part of the ESF. Pronounced lateral zonation and the occurrence of the higher temperatures and "lighter"

$\delta^{18}\text{O}$ values closer to the Earth's surface, argues strongly that the variability of these parameters has nothing to do neither with changing climate nor with the cooling of the conductively-heated rock mass of the vadose zone (e.g., Paces et al. 2001, Fabryka-Martin et al., 2000; Marshall and Whelan, 2000).

Finally, fluid inclusions with elevated homogenization temperatures (35 to 60 °C) were found in calcite with a variety of isotopic properties ($\delta^{13}\text{C}$ ranging from +8.7 to -6.3 ‰ PDB and $\delta^{18}\text{O}$ ranging from 9.9 to 20.0 ‰ SMOW). The fluid inclusion record, therefore, covers almost the entire range of isotope values reported for the Yucca Mountain calcite. Importantly, this range includes the signatures characteristic of the calcite-silica deposits at the topographic surface of Yucca Mountain. This partial overlap suggests a common origin. The presence of two-phase fluid inclusions, in turn, suggests a hydrothermal origin for both of the deposits.

The conceptual model proposed in Parts One and Two implies that Paintbrush and Solitario Canyon faults were associated, in the past, with transient incursions of the deep-seated water into the vadose zone and constitution of a hydraulic mound, in the manner shown in Figure 2-1 (Part Two). The field of the maximum homogenization temperatures shown in Figure 3-6-7-a represents a thermal "snapshot" of such a mound, which existed for some (geologically short) time in the vicinity of the proposed repository footprint, in the past. It thus appears that proposed conceptual model provides an adequate context for explaining, on the contradiction-free basis, both the structure of the heat flow field reconstructed based on the homogenization temperatures and the present-day structure of the heat flow field.